TID-7622

REACTOR TECHNOLOGY

NUCLEAR REACTOR CHEMISTRY

Second Conference
Gatlinburg, Tennessee
October 10-12, 1961

Issued: July 1962

Oak Ridge National Laboratory
Oak Ridge, Tennessee
operated by
Union Carbide Corporation
for the
U. S. Atomic Energy Commission

PREFACE

The 1961 Conference on Nuclear Reactor Chemistry was held in Gatlinburg, Tennessee on October 10-12, in conjunction with the Conference on Analytical Chemistry in Nuclear Reactor Technology. The two conferences were held jointly in order to afford the greatest possible opportunity for the dissemination and free exchange of ideas and information among scientists of different disciplines and locations who have common interests in the chemical aspects of nuclear reactors. Of particular importance were the many significant advances in knowledge and techniques which were discussed in the formal papers as well as in informal talks.

The Conference on Nuclear Reactor Chemistry dealt in general with various reactor materials and the effects on these materials of conditions arising during reactor operations. The conference was divided into five sessions. Fourteen papers were presented at the two sessions which dealt with Reactor Core and Coolant Materials, eleven at the two sessions on Behavior of Fission Products in Reactor Materials, and six at the session on The Effect of Radiation on Reactor Materials.

The 31 papers presented at the Nuclear Reactor Chemistry Conference comprised the work of 90 authors who represented the Harwell facility of the United Kingdom Atomic Energy Research Authority; the Dounreay (Scotland) facility of the UK Atomic Energy Authority; the Arnhem (Netherlands) facility, N.V. KEMA; the Saclay facility of the Commissariat a L'Energie Atomique; three USAEC national Laboratories; two research institutes; and nine industrial laboratories. The 321 registrants at the joint conferences included 24 from nine foreign countries (Australia, Belgium, Canada, England, France, Greece, Italy, the Netherlands, and Sweden), with the remainder coming from 24 states and the District of Columbia.

Twenty-three of the papers presented at the Nuclear Reactor Chemistry Conference are included in full in the Proceedings. Abstracts of the remainder are included with journal or other publication references where they are known. In several instances some editing was required in order to change an oral presentation to a written one. The editors, therefore, assume responsibility for any errors or omissions which may occur. The paper presented by Dr. L. Dolle, of Saclay, France, (No. 28, Study of the Formation and Distribution of Dissolved Gases and Hydrogen Peroxide in the Cooling Water of a Swimming Pool Reactor (Triton)), is included both in French and in English. The English translation was rendered by Mr. A. L. Monks, Oak Ridge National Laboratory, and the editors.

The primary success of this conference was due mainly to the speakers and authors who are listed in the Proceedings, and to the high quality and sustaining

interest of the papers they presented. In addition, however, a large number of people, many of whom must go unnamed, are deserving of credit, and we would like to take this opportunity to acknowledge some of their contributions to the success of the conference. First, we wish to thank Dr. A. M. Weinberg, Director of the Oak Ridge National Laboratory, and Mr. W. D. Manly, Director of the Gas-Cooled Reactor Project, ORNL, for their timely, interesting, and informative talks at the general sessions on Tuesday and Wednesday evenings, respectively; Dr. L. R. Zumwalt (General Atomic Division of General Dynamics Corporation), Dr. W. H. Denton (UK/AERE) and Mr. R. B. Briggs (ORNL) for their assistance in presiding at the various sessions; and Mr. D. D. Cowen, Director of the ORNL Public Relations Division, for his capable handling of general arrangements and publicity.

We also wish to thank Mr. C. D. Susano and the members of the ORNL Analytical Chemistry Division who handled arrangements for the Conference on Analytical Chemistry in Nuclear Technology for their experienced and invaluable assistance; Nuclear Reactor Chemistry Conference committee members Dr. F. F. Blankenship, G. C. Warlick, and Miss Carol Proaps for their assistance in planning and registration; Mr. J. R. Burkhart for his efforts in arranging travel reservations; Dr. R. B. Evans III for his assistance in reviewing the mathematical aspects of some of the papers; and Mrs. Dorothy Caldwell and Miss Proaps for typing the drafts of the papers and abstracts which appear in the Proceedings.

The 1962 joint conferences are tentatively scheduled for October 9-11, again at Gatlinburg, Tennessee. Participants in previous conferences and other interested persons are invited to attend and to consider submitting appropriate papers for possible presentation at the 1962 conference. Additional information and details will be distributed at a later date.

W. R. Grimes
C. J. Barton
J. P. Blakely

CONTENTS

EFFECTS OF RADIATION ON REACTOR MATERIALS

CARBON TRANSPORT PROBLEMS IN A HIGH TEMPERATURE GAS COOLED GRAPHITE REACTOR

By P. J. Bourke and W. H. Denton

Chemical Engineering Division
United Kingdom Atomic Energy Research Establishment
Harwell, England

INTRODUCTION

Helium is a favored inert gas coolant for a high temperature reactor with an outlet gas temperature approaching 900°C in which the moderator and the fuel elements are constructed from graphite. In this system carbon transport problems arise because of chemical reactions between gaseous impurities in the helium and the hot graphite core. Carbon can thus be removed from the core as gaseous reaction products. Such gaseous products can then cause deposition of carbon on the colder metal surfaces of the external coolant circuit by the reverse of the reactions occurring in the core. This leads to continuous carbon removal and deposition without the need for further admission of impurities. Gaseous impurities can appear in the otherwise chemically inert coolant both from out-gassing of graphite and from inleakage of steam into the coolant circuit through heat exchangers. Out-gassed impurities represent only an initial transient problem in reactor operation. In a power reactor employing a steam cycle the inleakage of steam is a permanent problem. Since the pressure of the steam in the steam producing heat exchangers is necessarily very much higher than the helium coolant pressure, inleakage of steam into the helium stream is expected to be responsible for the most serious graphite corrosion and it could be one of the limitations to the maximum surface temperature in the core. It will be necessary to provide a separate plant for the continuous purification of the helium coolant in order to reduce carbon transport rates to acceptable levels. Because of the very high graphite surface temperatures (up to 1000°C in a thermodynamically efficient reactor) and the very low graphite corrosion rates that are permitted in a power reactor, a special feature of this problem is the very low partial pressures (p.p.m.) of impurities which are likely to be permitted. Little experimental information exists on the reactions with graphite and on metal surfaces at these low partial pressures and high temperatures, and on the type of processes required for the efficient and economic purification of the helium coolant. This paper discusses the seriousness of the carbon transport problem and indicates the research required to assess its magnitude.

CHEMICAL COMPATIBILITY

A closed reactor coolant circuit, as shown diagrammatically in Fig. 4, consists of a graphite reactor core with surface temperatures (including the graphite reflector) from about 400°C to 1000°C and an external metal circuit, including a steam producing heat exchanger, with surface temperatures varying from 850°C to 350°C.

The steam which leaks into the helium circuit from the heat exchanger passes into the high temperature core and can react with the hot graphite according to the equation:

$$H_2O + C \rightleftharpoons CO + H_2 \qquad (1)$$

and remove one carbon atom in doing so. The CO product of this reaction passes into the lower temperature heat exchanger circuit where it can deposit carbon on metal surfaces according to either the reverse of reaction (1) or:

$$2CO \rightleftharpoons CO_2 + C \qquad (2)$$

The H_2O and CO_2 thus formed then pass into the high temperature core where they can react with the hot graphite to remove further carbon atoms according to reaction (1) and the reverse of reaction (2). Thus each oxygen atom, combined with the hydrogen as steam, which enters the coolant circuit can, firstly, remove one carbon atom from the core (according to reaction (1)) and can subsequently continue to transfer carbon atoms from the core to the heat exchanger by either of the H_2O-CO or CO_2-CO cycles in its subsequent circulation round the coolant circuit.

The extent to which these chemical reactions can proceed is dependent on the chemical equilibria. Fig. 1 is the ideal chemical equilibrium for C-O-H for the relevant case of H:O = 2:1. This has been calculated [1] from available thermodynamic data [2]. It shows that for the higher temperature range in the core the equilibrium is overwhelmingly in favor of excess H_2 and CO.

However, this equilibrium is very sensitive to temperature. At the lower temperatures in the heat exchanger and at the cold end of the core, H_2O and CO_2 can exist in comparable concentrations of H_2 and CO. Thus, the changes in the equilibria around this circuit provide appreciable chemical driving forces for the transport of carbon from the hot end of the core and deposition of carbon in the metal heat exchanger circuit and even at the cold end of the core.

Referring to the direct reactions with graphite of the H_2 product from reaction (1), Fig. 1 shows that it can react at temperatures below about 500°C and remove carbon to form methane according to:

$$2H_2 + C \rightleftharpoons CH_4$$

Fig. 1 also shows that this methane could then dissociate to hydrogen and carbon in passing through the higher temperatures in the core, when the carbon atom would either be re-deposited in the core or pass out of the core in the hot gas stream. This is another mechanism for removing carbon from the colder end of the core only. This reaction is not discussed further in this

paper because, since it can only proceed to an appreciable extent below about 500°C, the rates are likely to be much lower than the corresponding rates of the H_2O and CO_2 reactions (1) and (2) at the higher temperatures in the core.

THE ENGINEERING PROBLEM

There will be definite limits on the amount of carbon it will be permissible to remove from the exposed graphite surfaces of the fuel elements and the reflector in a high temperature power reactor. In particular, carbon removal from the fuel elements can adversely affect both the mechanical and gas permeability properties of the graphite and heat transfer characteristics (due to an increase in cooling channel dimensions). There will also be a limit to the amount of carbon that can be deposited in the heat exchanger circuit.

The problem considered here is that of carbon transport due to continuous steam inleakage into a reactor coolant circuit, as shown in Fig. 4. The local carbon removal and deposition rates in this circuit depend on the local partial pressures of H_2O, CO_2, H_2, and CO and the local chemical reaction and transfer kinetics. For given rates of inleakage of steam and removal of impurities (from the bi-pass purification stream, a in Fig. 4), mass balances for each element will result in a steady state dynamic equilibrium in the circuit. This will determine the impurity partial pressure distributions in the circuit. Hence, for given surface areas, temperatures and flow rates, the overall carbon removal and deposition rates will depend on:

1. Rate of inleakage of steam.

2. Rates of removal of steam and reaction products.

3. The chemical reaction and transfer kinetics with graphite and on metal surfaces.

Steam inleakage is obviously to be kept to a minimum by developing steel heat exchangers with a very high standard of leak tightness at relatively high temperatures and high pressure differences.

Since it would be neither practical nor economic to pass the whole of the coolant flow through the purification plant, the purification will need to be achieved by diverting only a small fraction (a) as a bi-pass stream.

The size of the plant will then be directly related to a. It will have to remove inleaking steam and reaction products from helium at partial pressures which will give acceptably low carbon transport rates. Therefore, the faster the kinetics (in (3) above), the lower will be the permissible partial pressures of H_2O, CO_2, H_2 and CO and the larger will be the purification bi-pass stream required.

Any analysis of the dynamic equilibria in this system must take account of the reversibility of the reactions and therefore of the chemical equilibrium data and of the dependence of reaction kinetics on the partial pressures of products as well as of reactants.

Data on the chemical equilibria are available, (Fig. 1), but the only experimental data on reaction kinetics with graphite and on steel surfaces, applicable to H.T.G.C.R. temperatures and impurity partial pressures in an inert gas, are those of Antill and Peakall [3]. In particular, their work showed that the kinetics of reactions of H_2O and CO_2 (separately) with graphite at 1000°C are markedly dependent on relatively low partial pressures of the products H_2 and CO, as shown in Figs. 7 and 8, but their data on this dependence were confined to only one value of the partial pressure of each reactant. The dependence on reactant partial pressures, for reactions with both graphite and metal surfaces, was only investigated in the absence of appreciable partial pressures of products. Therefore, because of the very limited data on the complicated dependence of reaction kinetics on temperature and on partial pressures for this system, it is not possible to set down analytical expressions which govern the dynamic equilibrium and hence the interdependences of:

(a) Water inleakage rate.

(b) Local carbon removal rates.

(c) Local carbon deposition rates.

(d) Impurity partial pressures.

(e) Purification bi-pass flowrate.

Summarizing, it is important to appreciate that, whereas estimates can be made of steam inleakage rates and permissible carbon transport rates in a high temperature helium cooled power reactor, no specification can yet be made for either the permissible partial pressures of chemical impurities in the coolant circuit or the specification for the size and type of helium purification plant. Such specifications require knowledge of the reaction and transfer kinetics.

It is most likely that these data can be obtained in out-of-pile experiments since the effect of the reactor radiations on the graphite reaction kinetics, at least for partial pressures of oxidizing gases of the order of one atmosphere, has been shown to be rapidly exceeded by the thermal reaction rates at temperatures above about 650°C.

SPECULATION ON MAGNITUDE OF PROBLEMS

Subject to the limitations of the data on carbon removal reaction and transfer kinetics mentioned above estimates of the impurity partial pressures and purification flow (a) required to give permissible corrosion rates in the core are made in this section, using the experimental results of Ref. 3. To do this it is necessary to assume that these results, obtained with low and uncertain gas flows over small specimens of graphite in a background of 1 atmosphere of argon, may be applied to high gas flows in reactor coolant channels with 20 atmosphere of helium. These assumptions may be seriously in error. The estimates based on them give, however, the best indication of the order of magnitude of the engineering problem possible with the available data.

The maximum permissible corrosion rate at any point on the cooled surface of the graphite in the core is considered to be 0.1 mm/year removal of carbon in a

reactor designed for a 20 year life. This carbon removal may occur at the outside surface of the graphite or from the bulk of the graphite leaving a porous structure of lower apparent density. Applying the results of Ref. 3 to Pile Grade A graphite at 1000°C, 0.1 millimeters of carbon can be removed per year by any of the following combination of mole fractions of impurities in 20 atmospheres of helium:

TABLE I. MOLE FRACTIONS (p.p.m.) IN 20 ATS. HELIUM

	H_2O	H_2	CO_2	CO
(1)	0.3	0	0	0
(2)	0	0	2	0
(3)	5	50	0	0
(4)	0	0	15	150

These figures are obtained by extrapolation of the experimental results to lower partial pressures, assuming all the reactions to be first order. Extrapolation over a range of nearly 100 is necessary for cases (1) and (2), for which the experimental results indicate first order dependence at the higher partial pressures.

From these figures it can be seen that in the absence of H_2 and CO products the H_2O reaction is faster than the CO_2 reaction. If, however, the partial pressures of the products are appreciable the rates of the reactions are much reduced.

To estimate the purification flow required, a typical 1000 MW (t) reactor design is considered in which the recirculation rate of helium coolant at 20 atm. is 4×10^6 lb/hr, the cooled graphite surface area is 3×10^7 cm^2 and the maximum graphite surface temperature is 1000°C. If we assume that the carbon removal rate from the hottest part of the core at 1000°C is the maximum permitted value of 0.1 mm per year, then the removal rate from the remainder of the core at lower surface temperatures (down to 400°C) would be substantially less because of the sensitivity of reaction rate to temperatures. (The resistance to transfer in the gas stream is small for these conditions - see next section.) We may therefore take as a rough approximation that the total carbon removal rate from the core is equivalent to 0.1 mm per year from (say) 10% of the core surface area. This can be expressed as the increase in the mole fraction of carbon in the coolant in passing through the core, namely:

$$\Delta C_o \simeq 0.0013 \text{ p.p.m.}$$

This is also the change in the mole fraction of the reactants in passing through the core, i. e.,

$$\Delta C_{H_2O} + \Delta C_{CO_2} \simeq 0.0013 \text{ p.p.m.}$$

Considering the steam inleakage rate, this can be expressed as the increase in mole fraction of H_2O in the coolant in passing through the heat exchanger and equals (x/F), where x is the molar H_2O inleakage and F is the helium flow rate. For steady state conditions the mass balance for H_2O in the circuit then requires that:

$$\alpha\left(C_{H_2O} + \frac{x}{F} + \Delta C'_{H_2O}\right) = \frac{x}{F} - \Delta C_{H_2O} + \Delta C'_{H_2O} \qquad (3)$$

where C_{H_2O} is the mole fraction of H_2O in the coolant at the core outlet and $\Delta C'_{H_2O}$ is the increase in mole fraction of H_2O due to the carbon deposition reaction in the heat exchanger circuit. Sufficient experimental data are not available to estimate $\Delta C'_{H_2O}$.

A lower limit to the required purification flow may however be determined without this data if the steam inleakage rate is large compared with the permissible carbon removal and deposition rates, i. e., when

$$\frac{x}{F} >> \Delta C_{H_2O}$$

and

$$\frac{x}{F} >> \Delta C'_{H_2O}$$

In this case most of the inleaking steam must be removed from the coolant as steam before it reacts with the graphite. For example, if heat exchangers are developed to reduce the steam inleakage rate to (say) 5 lbs per day for a 100 MW (t) reactor ($x/F = 0.009 \times 10^{-6}$) this will still be considerably bigger than the permissible carbon removal rate ($\Delta C_o = 0.0013 \times 10^{-6}$). Taking the permissible H_2O concentration in the core as 0.3×10^{-6} in the absence of products (Table I) the required purification flow expressed as a fraction α of the main flow considering only the H_2O reaction alone and not the CO_2 reaction is then given by equation (3) as

$$\alpha \simeq 0.03$$

From the economic standpoint this value of α is not small. It is however for the case of H_2O reaction with graphite in the absence of products. The presence of appreciable partial pressures of products (H_2 and CO) could allow a higher mole fraction of H_2O for the same carbon removal rate from the core (see Figs. 7 and 8 and above table). The required purification flow, α, could then be smaller. Some control of the relative mole fractions of reactants and products could be achieved by selective removal of the different impurities in the gas purification plant, i. e., α could be arranged to be different for reactants and products. There is a limit to the reduction of α which may be achieved in this way by increasing H_2 and CO partial pressures, because of possible excessive local carbon deposition in the heat exchanger circuit.

For steam inleakage rates appreciably smaller than considered above, when x/F is of the order $\Delta C'_{H_2O}$, the dependence of α on inleakage is seen, from equation (3), to be complicated. It becomes more dependent on the product mole fractions in the circuit as the inleakage rate is reduced, since increasing proportions of the inleaking steam may be allowed to react with the core and later be removed from the purification stream as products.

TRANSFER AND REACTION KINETICS IN THE GRAPHITE CORE

There are few relevant data on the kinetics of the carbon deposition reactions in the heat exchanger circuit and this section is restricted to a discussion of the carbon removal from the graphite core into the bulk of the coolant gas stream. Since the carbon is removed by the reaction of the gaseous impurities with the graphite throughout its porous structure the rate will depend on the molecular transfer rates through the porous structure as well as the chemical reaction rates on the internal surfaces of the graphite. Before impurity molecules can react with the internal surfaces they must:

(a) Be transferred from the bulk of the helium gas stream to the outside graphite surface, and

(b) diffuse through the pores of the graphite, reacting with the internal surfaces while doing so.

Similarly, the gaseous reaction products must diffuse in the opposite direction.

The first transfer process is well understood and depends on diffusion coefficients, the geometry of the coolant channel and turbulence in the gas stream. The second transfer process depends on the size, shape and distribution of the pores and the transfer mechanism, either molecular diffusion through the helium or molecular streaming (Knudsen) flow.

Considering the effect of the chemical reaction kinetics for the case of given partial pressures of reactants and products at the geometric surface of the graphite, if these reactions are slow then the carbon removal tends to be uniform throughout the graphite. If, on the other hand, the chemical reactions are fast then the carbon removal will tend to be concentrated closer to the geometric surface and the total carbon transfer rate will be higher. This is shown in Fig. 3, the reason being that the higher transfer rates result in steeper partial pressure gradients from the geometric surface.

Considering next the case of given partial pressures in the bulk of the gas stream flowing over the surface of the graphite, if the transfer resistance in the gas stream is appreciable then both the reactant partial pressure at the interface and the transfer rate will be reduced. Therefore, as the chemical reaction rates increase, the carbon transfer rate tends to increase and becomes more dependent on the resistance to transfer in the gas stream, as shown diagrammatically in Fig. 2. Since the transfer resistance in the gas stream is comparatively insensitive to temperature while reaction rates increase rapidly with temperature then, at sufficiently high temperatures, the transfer rate is mainly controlled by the gas stream and is much less

dependent on temperature. In this extreme case almost all the reactant partial pressure driving force is consumed across the Whitman gas film (see Fig. 2).

An indication of the importance of the gas stream resistance at 1000°C can be made for reactor conditions. If we take the maximum permitted carbon removal rate of 0.1 mm per year and a typical case of 20 atmospheres of helium flowing in a coolant channel with a Reynolds number of 10^4 and an equivalent channel diameter of 1 cm, the usual mass transfer calculation shows that either H_2O or CO_2 can be transferred at a rate equivalent to 0.1 mm per year graphite removal by a partial pressure difference of approximately 0.02 p.p.m. in 20 atmospheres. This figure can then be compared with the reactant partial pressure at the graphite surface corresponding to the above removal rate. This partial pressure can be obtained from the experimental data in Ref. 3, (assuming it to be independent of gas stream transfer resistance), and is given in Table I as 0.3 p.p.m. of H_2O or 2 p.p.m. of CO_2 for 1000°C. Thus, for H_2O reacting with pile grade A graphite at 1000°C in the absence of appreciable partial pressures of products, approximately 7% of the resistance to transfer is in the gas stream.

The effect of the gas stream resistance at higher temperatures can be appreciated if the H_2O partial pressures permitted at the graphite surface need to be halved for every (say) 25°C increase in temperature (i. e., activation energy = 40 k.cals per gm mole). Then, 90% of the resistance to transfer would be in the gas streams at 1500°C, and the permitted bulk partial pressure in the gas stream would be almost equal to the above figure of 0.02 p.p.m. Still higher graphite temperatures would require only a small reduction in this permitted bulk partial pressure.

HYPOTHETICAL ANALYSIS OF COMBINED REACTION AND DIFFUSION KINETICS IN A POROUS SOLID

The following is a hypothetical analysis of carbon transfer by gaseous reactions with graphite and its temperature dependence, treated as a combined diffusion and simplified reaction process in an idealized porous solid in the presence of an inert gas. This analysis is reported fully in Refs. 6 and 7. It is not concerned with transfer through an external gas stream and the impurity partial pressures at the outside surface of the solid are taken as a fixed boundary condition. Further, only the case where the partial pressure of the inert gas is high compared to the partial pressures of the impurities is considered.

Gaseous reactants from the outside surface pass through the inert gas in the pores of the solid and react with its internal surfaces. The gaseous products pass outwards in the opposite direction.

The following assumptions are made in this analysis:

(1) The porous solid consists of solid material containing uniform cross section pores of length L, long compared with their equivalent diameter d.

(2) The transfer of impurity molecules through the pores can be partly by molecular diffusion through the inert gas and partly by Knudsen streaming flow, when impurity molecules collide with the solid only.

(3) The impurities react with the solid surface of the pores which has a uniform chemical activity.

(4) The net rates of the forward and backward reactions of gases A and B with a unit area of solid surfaces, according to:

$$mA + C \rightleftharpoons nB \tag{4}$$

can be expressed by:

$$\frac{d(A)}{dt} = k_A P_A^m - \frac{m}{n} k_B P_B^n$$

and

$$\frac{d(B)}{dt} = k_B P_B^n - \frac{n}{m} k_A p_A^m \text{ (symbols defined below)}$$

Regarding assumption (2), the extent to which either of these transfer mechanisms predominates depends on the distribution of pore diameter and the mean free path of the impurity molecules. For diffusion flow the diffusion coefficient is inversely proportional to total pressure so that the resistance to transfer is proportional to total pressure. In contrast, for Knudsen flow, the resistance to transfer is independent of pressure.

Regarding assumption (4), it is realized that this is not justified for H_2O and CO_2 reactions with graphite. For example, in the case of CO_2 reacting according to:

$$CO_2 + C \rightleftharpoons 2CO$$

this assumption would lead to the back reaction being second order (n = 2), while experimental data shows that it can be close to first order for some ranges of partial pressures (see Ref. 3). This may be explained by the adsorption of CO on reacting sites and more appropriate kinetic relationships than those assumed above have been advanced by Hinshelwood.[5]

Considering a single representative pore with partial pressures of reactant A and product B maintained constant at the entrance to the pore and a uniform temperature throughout, the equations for steady state conditions over an element of pore of length dx are given from mass balances of A and B, by

$$\frac{\pi}{4} d^2 \frac{D_A}{RT} \frac{d^2 p_A}{dx^2} - \pi d \left(k_A p_A^m - \frac{m}{n} k_B p_B^n\right) = 0 \tag{5}$$

$$\frac{\pi}{4} d^2 \frac{D_B}{RT} \frac{d_B p_B}{dx^2} - \pi d \left(k_B p_B^m - \frac{n}{m} k_A p_A^m\right) = 0 \tag{6}$$

where

D = diffusion coefficient of A or B in the inert gas

p = partial pressure

k = reaction rate coefficient defined by $\frac{d(A)}{dt} = k_A p_A^m \ \frac{\text{moles}}{\text{cm}^2\text{sec}}$

x = distance into pore

d = pore diameter

R = universal gas constant

T = temperature

When the inert gas mean free path (M.F.P.) is small compared to pore diameter, d, the normal diffusion coefficient, D, can be used. When the M.F.P. is of the order of d and Knudsen flow occurs, an equivalent diffusion coefficient D^x can be used. This is given by:

$$D^x = \frac{2}{3}\sqrt{\frac{2}{\pi}}\, d\, \left(\frac{RT}{M_A}\right)^{1/2}$$

where M_A is molecular weight of A.

Solutions of equations (5) and (6) for various orders of the reactions of equation (4) may be used to show the effects of impurity penetration depth, temperature, equilibrium constant for equation (4) and corrosion rate suppression by excess products.

CASE I. IRREVERSIBLE FIRST ORDER REACTION

If the corrosion reaction A → B is assumed to be irreversible and first order with respect to A then the solution (Ref. 6) of equations (6) and (5) subject to:

m = 1

$k_B = 0$

gives the rate of A entering unit area of a pore mouth as

$$J_A^o = 2p_A^o \left(\frac{D_A k_A}{RTd}\right)^{1/2} \tanh(\alpha L) \qquad (7)$$

where

$$\alpha = 2\left(\frac{RTk_A}{D_A d}\right)^{1/2}$$

P_A^o = partial pressure at entry to pore (x = 0).

and

$$J_A^o = -D_A/RT\ (dp_A/dz)_{x=0} = \frac{\text{mole rate of transfer of A into graphite}}{\text{unit cross section of pore}}$$

This shows that the driving force for this combined diffusion and reaction may be simply expressed as the partial pressure of A at entry to the pore.

The dependence of equation (7) on temperature may be investigated if it is assumed that:

1. The chemical rate constant may be expressed in the usual Arrhenius form

$$k_A = k_O \exp\left(-\frac{E_A}{RT}\right) \tag{8}$$

2. The diffusion coefficient is given by

$$D_A = \frac{D_O T^{3/2}}{P} \tag{9}$$

where

E_A = the activation energy

P = total pressure

Substituting these expressions for k_A and D in terms of temperature into equation (7) and then differentiating this equation in logarithmic form with respect to the reciprocal of temperature gives:

$$\frac{d}{d(1/T)}\left[\ln\left(J_A^o/P_A^o\right)\right] = -\frac{T}{4} - \frac{E_A}{2R} + \left(\frac{T}{4} - \frac{E_A}{2R}\right)\frac{2\lambda T^{-1/4}\exp(u)}{\sinh\left(2\lambda T^{-1/4}\exp(u)\right)} \tag{10}$$

where

$$\lambda = 21\left(\frac{k_{A_o} RP}{D_o d}\right)^{1/2}; \qquad u = -E_A/2RT \tag{11}$$

P = total gas pressure

Equation (10) shows that, for the process of combined diffusion and irreversible first order reaction, the rate of transfer may be divided by the impurity partial pressure at the entry to the pore (driving force) to give an effective transfer coefficient which is a unique function of temperature for a given value of the non-dimensional λ group (which characterizes the graphite structure, its reactivity, and the reactant diffusivity). Hence the usual Arrhenius form of presenting the temperature variation of a chemical reaction by plotting

$$\ln\left(\frac{\text{Rate of reaction}}{\text{Driving force}}\right) \text{ against } \left(\frac{1}{\text{temperature}}\right)$$

may still be used for this combined diffusion and reaction regime.

From this equation (10) it may also be shown that for temperatures in the range

$$0 < T < 2\frac{E}{R} \tag{12}$$

and for all value of the λ group the slope of the Arrhenius plot (left hand side of Eq. 10) will lie in the range

$$-E/R < \text{slope} < -1/2\ E/R \qquad (13)$$

Most reactions have activation energies greater than 5000 cal/gm mole and R in these units is 1.98. Thus the upper temperature limit specified by inequality (12) will generally be above 5000°/abs. Hence the limits of the Arrhenius slope specified by inequality (13) will apply quite widely.

In Fig. 5 equation (10) has been plotted for the reaction

$$CO_2 + C \rightarrow 2CO$$

This reaction is known to be approximately first order and to have an activation energy about 80 Kcal/mole. It is assumed that the CO partial pressure is so low throughout the pore that the reaction is everywhere irreversible.

From Fig. 5 it may be seen that at lower temperatures the Arrhenius slope becomes asymptotic to E/R as the temperature approaches zero. The explanation for this is that both the chemical reaction rates and the total transfer rates become so slow that negligible partial pressure differences are required as driving forces for diffusion. These slow transfer rates then depend only on the chemical rate coefficient and have the same temperature dependence as this coefficient, i. e., -E/R.

At higher temperatures, the higher transfer rates require appreciable partial pressure differences for diffusion and the slope approximates to -E/2R. The reason for this may be found in equation (7) which, for high temperatures and therefore large values of the reaction coefficient, k_A, becomes:

$$J_A^o/p_A^o = \left(\frac{Dk}{RT}\right)^{1/2}$$

The rates of transfer are then equally dependent on both the diffusivity and reactivity. The temperature dependence of $\ln (dk)^{1/2}$ has a slope of -E/2R for the chemical rate coefficient (because of the form of equation (8)) less a small amount resulting from the smaller dependence on temperature of the diffusion coefficient divided by temperature.

Fig. 5 shows also that the temperature range in which the change in slope occurs depends on the λ group. For large values of λ the changes occur at lower temperatures and very critically with temperature. The change should show on the Arrhenius plot as a kink. For smaller values of λ the change occurs at higher temperatures and more gradually with temperature.

CASE 2. REVERSIBLE FIRST ORDER

If the corrosion reaction is reversible $A \rightleftharpoons B$ and first order with respect to both A and B the solution (Ref. 6) of equations (5) and (6) subject to m = n = 1 gives the mole rate of A entering unit area of the pore mouth as

$$J_A^o = (p_A^o - p_B^o/K)\left(\frac{D_A}{RTd}\right)^{1/2} \frac{2k_A}{(k_A + k_B)^{1/2}} \tanh(\gamma L) \qquad (14)$$

where $\gamma = (\alpha^2 + \beta^2)^{1/2}$

$$\alpha = 2\left(\frac{RTk_A}{Dd}\right)^{1/2}$$

$$\beta = 2\left(\frac{RTk_B}{Dd}\right)^{1/2}$$

K = equilibrium constant $(P_B/P_A)_{eq.}$

$D_A = D_B$

p^o = partial pressure at $x = 0$

Thus, in this case again, the rate of transfer may be divided by a partial pressure driving force for both diffusion and reaction (which may be simply expressed as the departure from chemical equilibrium at the entry to the pore) to give a transfer coefficient which is a unique function of temperature for a given value of the geometry group.

Elsewhere in this paper it has been suggested that in a reactor coolant the partial pressure of any products formed by reversible corrosion reactions should be deliberately maintained at a high value to suppress the amount of carbon removal by reducing the departure from chemical equilibrium at the graphite surface. The extent of this suppression in the first order reversible case is given by the L.H.S. denominator of equation (14) and is seen to be linear.

The temperature dependence of equation (14) has been derived but is not presented here because, as far as is known, none of the important corrosion reactions are in fact first order reversible.

CASE 3. REVERSIBLE FIRST ORDER FORWARD, SECOND ORDER BACKWARD

If the corrosion reaction is of the form $A \rightleftharpoons 2B$ and it is assumed that it is first order with respect to A and second order with respect to B, then equations (5) and (6) must be solved subject to $m = 1$ and $n = 2$. This solution is mathematically considerably more involved than the previous ones and is reported in Ref. 7. The solution of the particular case of capillaries assumed to be infinitely long and for equal diffusivities of A and B is:

$$J_A^o = \left[\left(\frac{32}{3}\right)\left(\frac{Dk_A}{RTd}\right)(p_B - p_A^o)\right]^{1/2} (p_A^o - p_1) \qquad (15)$$

where

$D_A = D_B$

$$p_1 = \frac{1}{3}\left[v - (v^2 - 3s)\right]$$

$$p_2 = \frac{1}{3}\left[v + 2(v^2 - 3s)\right]$$

$$v = \frac{3}{2}\frac{k_A}{k_B} + 3p_A^o + \frac{3}{2}p_B^o$$

$$s = 3(p_A^o)^2 + \frac{3}{4}(p_B^o)^2 + 3p_A^o p_B^o$$

Equation (15) is plotted on Fig. 6, which gives the rate of transfer as a function of K and p_B^o for an arbitrary value of p_A^o of unity. Fig. 6 shows the suppression of the transfer rate as the product partial pressure at the entrance to the pore is increased and also shows how this suppression depends on the equilibrium constant, K.

A point of interest arising from equation (15) is that it is now no longer possible to divide the transfer rate by the departure from equilibrium at the entrance to the pore to obtain a function for the transfer coefficient which is independent of the partial pressure as used in the Arrhenius plot. The reason for this is that while the driving force for diffusion is proportional to a partial pressure difference, the driving force for the reaction depends on the square of a partial pressure. An important consequence of this is that the effect of temperature on the transfer rate cannot be expressed in an Arrhenius form.

CONCLUSIONS AND RESEARCH REQUIRED

From the foregoing review of carbon transport problems in a high temperature reactor circuit caused by a continuous inleakage of steam, the conclusions are:

1. The extent of carbon removal and deposition will depend on the steady state dynamic equilibrium in the coolant circuit and therefore on the kinetics and the reversibility of the chemical reactions with graphite and on metal surfaces.

2. Carbon removal rates for the graphite core for temperatures up to at least 1000°C (in the range required for efficient power generation by steam), will depend on the chemical and physical properties of the graphite and to a much lesser extent on transfer in the coolant gas stream.

3. For probable permissible carbon removal rates from the core, the coolant gas will need to be maintained pure to p.p.m. impurity levels. Therefore, for suggested steam inleakage rates, a sizeable fraction of the coolant stream will need to be purified to below these low levels.

A proper assessment of the carbon removal, carbon deposition and gas purification problems requires very much more extensive data on kinetics than exists at present, both for reactions with graphite and on metal surfaces. Since both these reactions will take place in the presence of appreciable partial pressures of their respective products, it will be necessary to study the dependence of kinetics on both reactant and product partial pressures.

The foregoing theoretical analysis of reactions with a porous solid, although it is idealized, at least shows the importance of a knowledge of the following data for graphite:

1. The effect of pore structure on internal surface area and on transfer kinetics of gaseous reactants and products,

2. The effect of the pressure of the inert gas on transfer kinetics,

3. The chemical equilibrium between gaseous reactants, reaction products, and graphite, and

4. The dependence of chemical reaction kinetics on partial pressures of reactants, reaction products, and on temperature.

The reactions on metal surfaces may probably be treated as occurring on the surface of an impermeable solid and are therefore likely to be simpler to study than the graphite reactions.

REFERENCES

1. Mme. M. L. Pointud, private communication.

2. D. D. Wagman, Jour. Nat. Bur. Stds. 34, 143 (1945).

3. J. E. Antill and K. A. Peakall, GCM/UK/13, 1960 and J. E. Antill and P. Murray, Progress in Nuclear Energy, Series IV, 3, 81 (1960) Pergammon Press.

4. H. B. F. Gow and W. R. Marsh, GCM/UK/2, 1960.

5. C. Hinshelwood, "Structure of Physical Chemistry", British Report Chapter XIX, Clarendon Press (1951).

6. P. J. Bourke and W. H. Denton, British Report AERE-R-3853.

7. J. Woodrow, British Report AERE-R-3854.

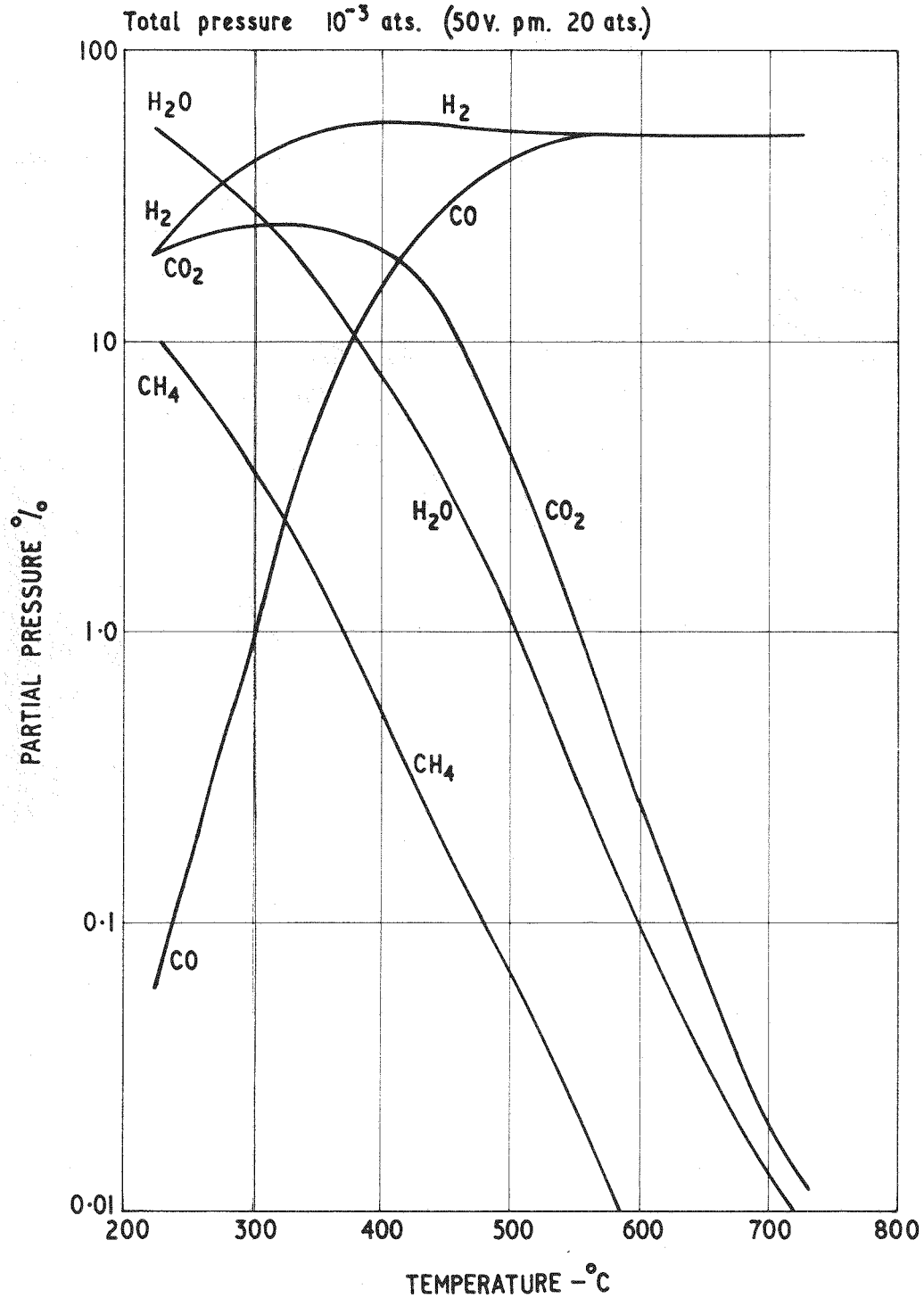

HYDROGEN – OXYGEN – CARBON EQUILIBRIUM FOR H:O = 2:1.

FIGURE 1.

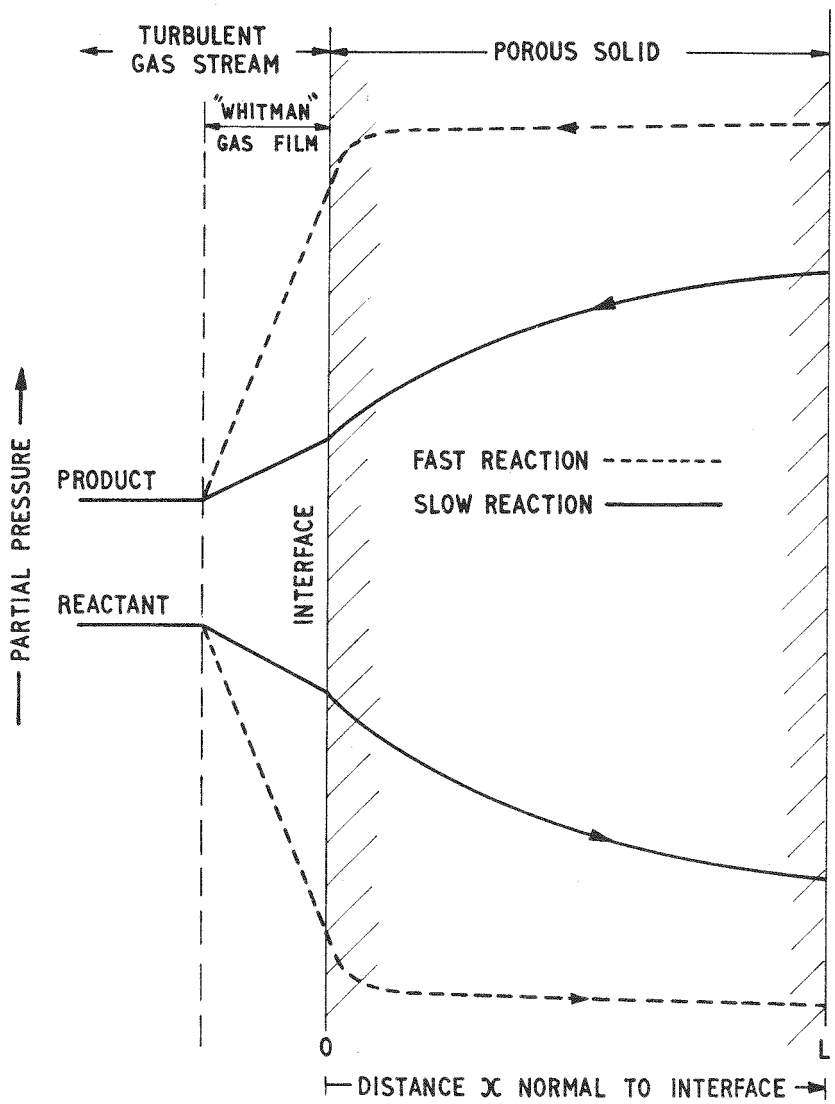

PARTIAL PRESSURE DISTRIBUTIONS FOR REACTION BETWEEN A GAS STREAM & A POROUS SOLID.

FIGURE 2.

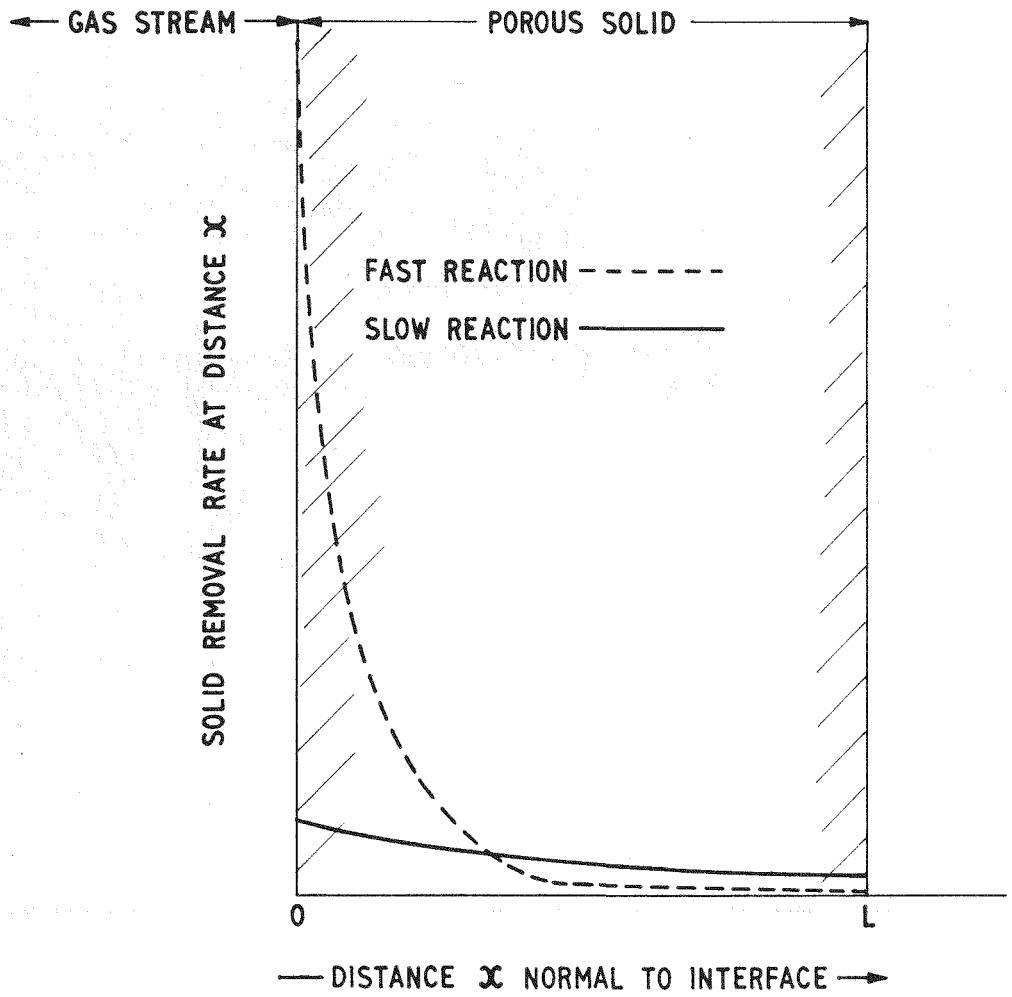

SOLID REMOVAL RATE FOR REACTION BETWEEN A GAS AND A POROUS SOLID FOR NEGLIGABLE RESISTANCE TO MASS TRANSFER IN GAS STREAM.

FIGURE 3.

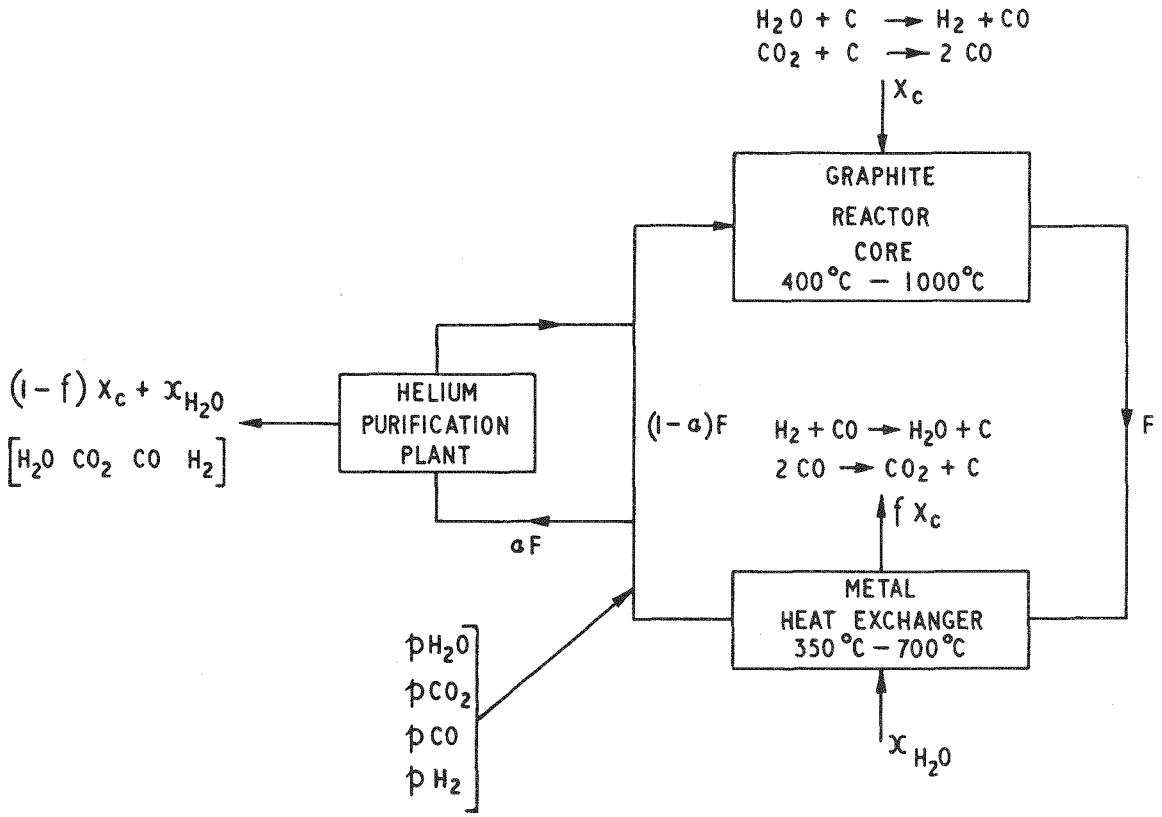

X_c – CARBON REMOVAL RATE FROM CORE – MOLES/SEC.

X_{H_2O} – WATER INLEAKAGE RATE – MOLES/SEC.

F – HELIUM COOLANT FLOW RATE – MOLES/SEC.

a – FRACTION OF COOLANT FLOW BI-PASSED THROUGH PURIFICATION PLANT.

f – FRACTION OF CARBON REMOVED WHICH IS DEPOSITED IN HEAT EXCHANGER.

$p H_2O$ $p CO_2$ $p CO$ $p H_2$ – PARTIAL PRESSURES.

CARBON TRANSPORT IN COOLANT CIRCUIT — METHANE REACTIONS NEGLECTED.

FIGURE 4.

G. 3/867

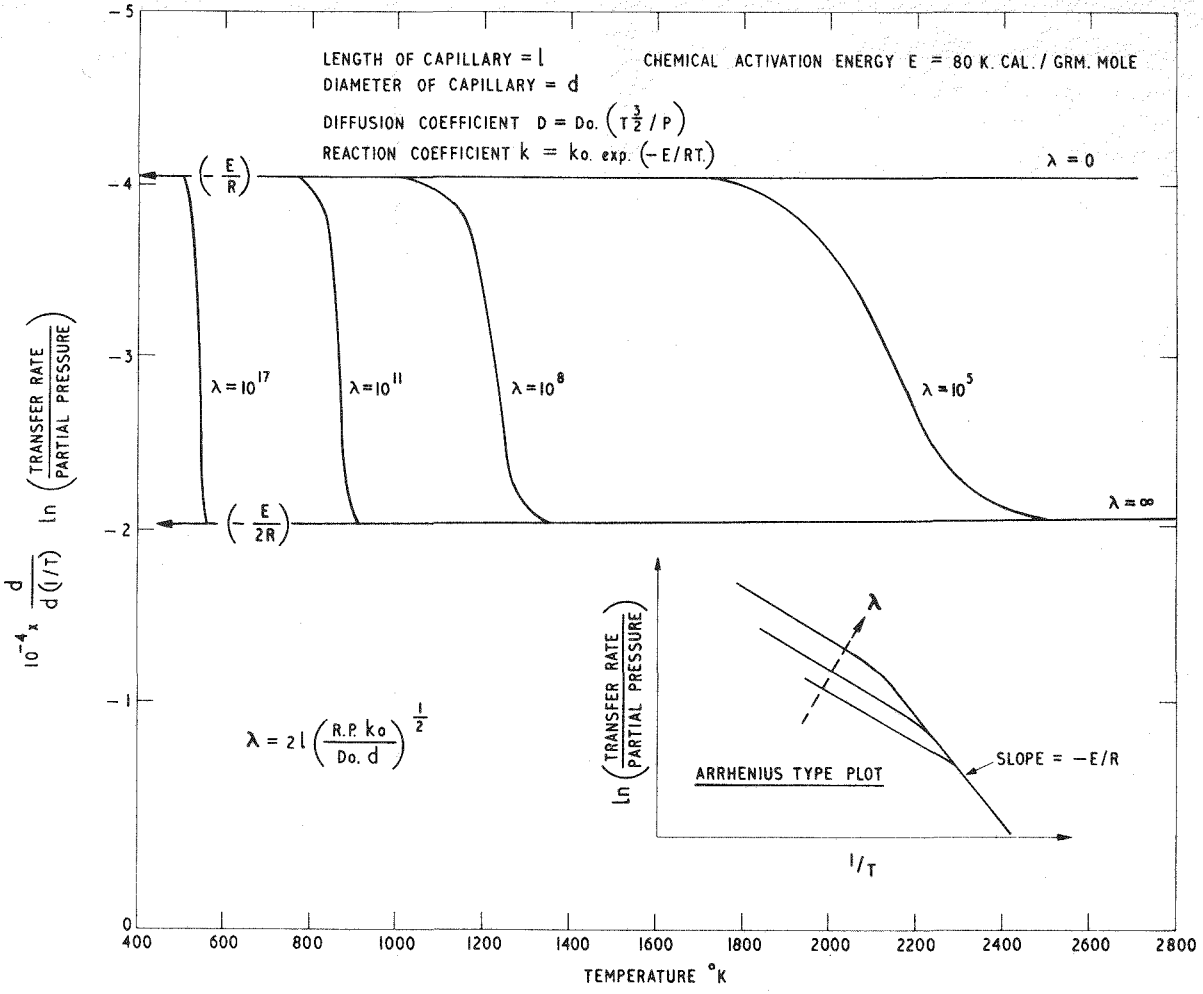

SLOPE OF ARRHENIUS TYPE PLOT OF TRANSFER RATE FROM A CAPILLARY BY GAS-SOLID CHEMICAL REACTION AND MOLECULAR DIFFUSION.

(IRREVERSIBLE FIRST ORDER REACTION.)

FIGURE 5.

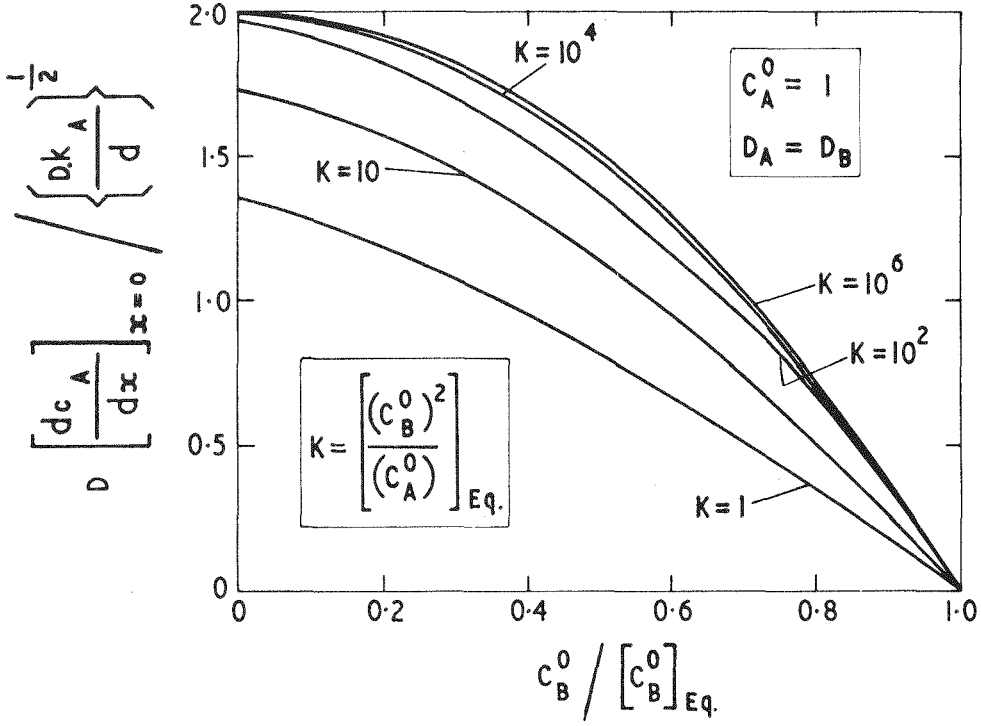

TRANSFER RATE FOR INFINITE CAPILLARY FOR FIRST ORDER FORWARD REACTION AND SECOND ORDER BACKWARD REACTION.

FIGURE 6.

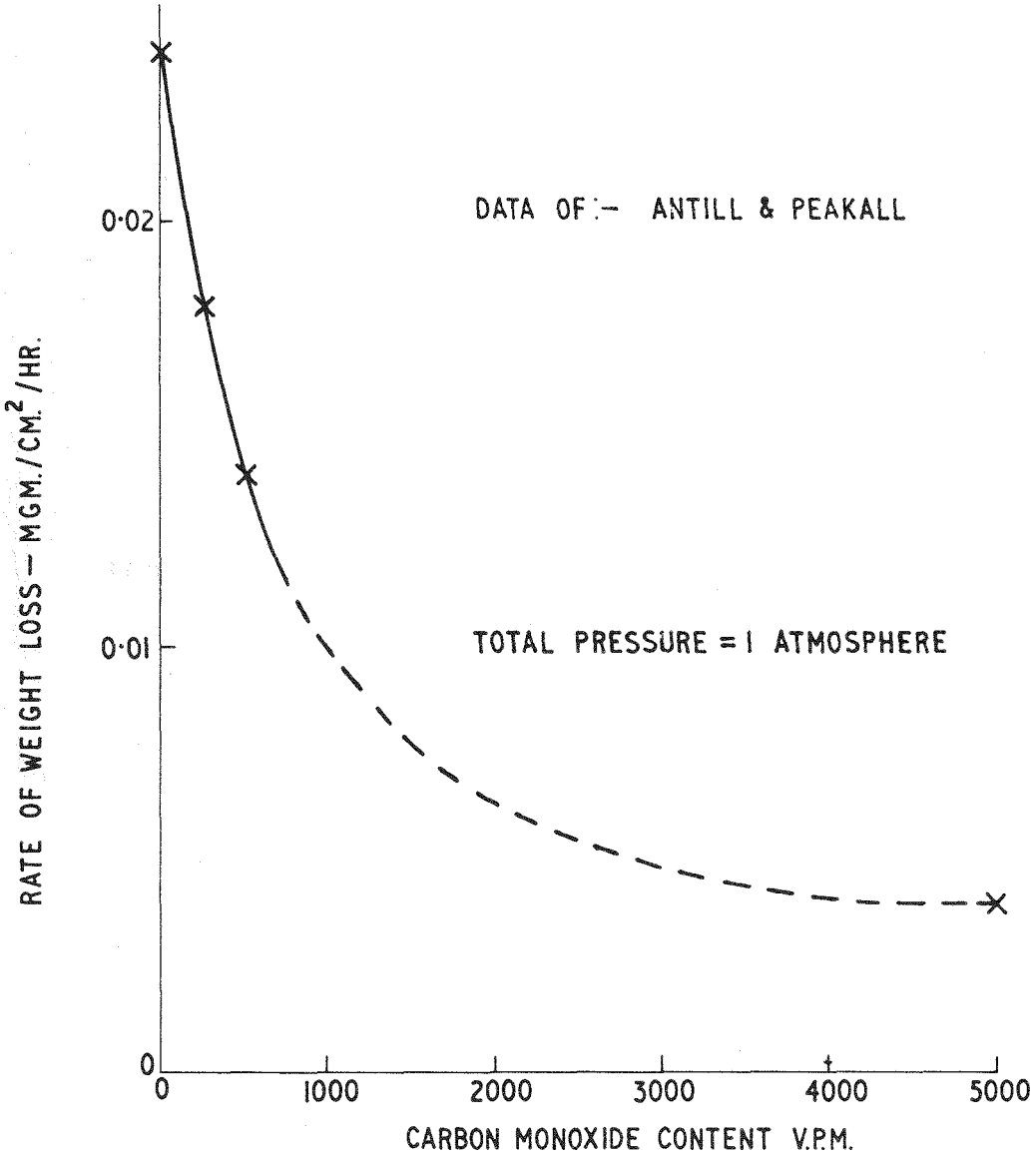

EFFECT OF CARBON MONOXIDE ON ATTACK OF PILE GRADE A.

BY 500 V.P.M. CARBON DIOXIDE AT 1000 °C.

FIGURE 7.

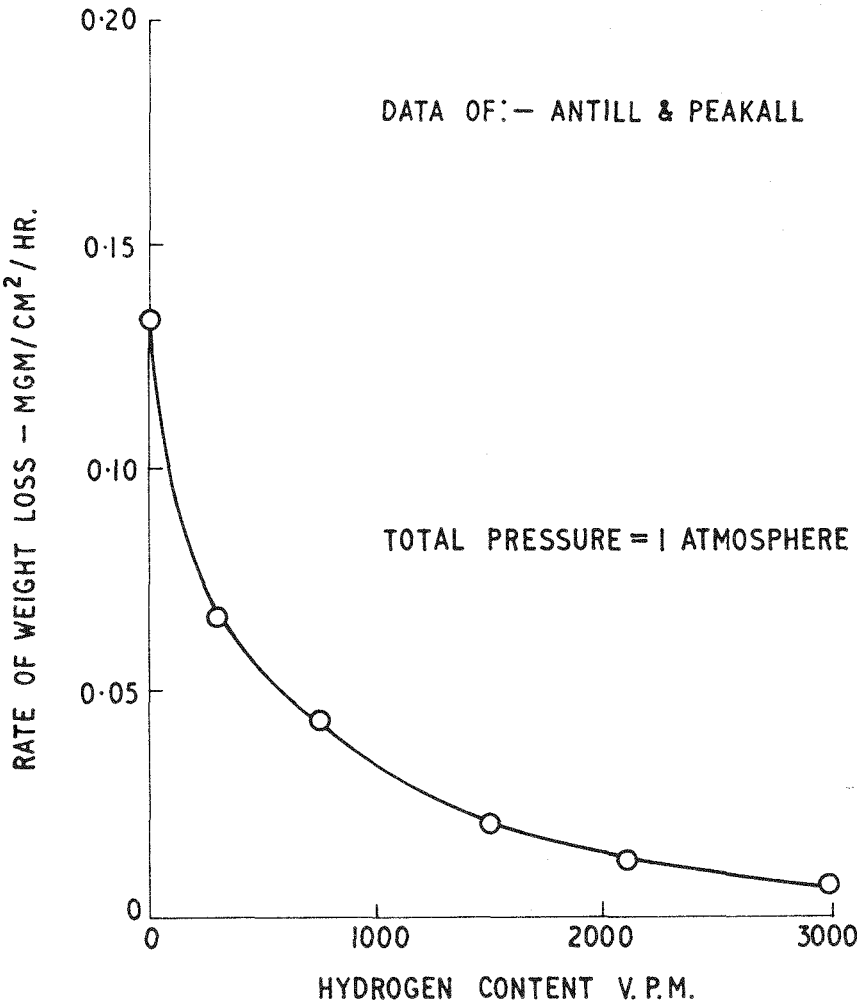

EFFECT OF HYDROGEN ON ATTACK OF PILE GRADE A.

BY 300 V.P.M. WATER VAPOUR AT 1000°C.

FIGURE 8.

EVOLUTION OF GAS FROM HIGH PURITY GRAPHITES

By L. G. Overholser and J. P. Blakely

Oak Ridge National Laboratory[a]
Oak Ridge, Tennessee

INTRODUCTION

Recent developments in the gas-cooled reactor concept entailing the use of graphite as moderator, cladding or canning material, and as matrix for the fuel elements at temperatures in the 1000°C range, have resulted in an increased interest in the compatibility problems associated with the circulation of contaminated helium in direct contact with the graphite. The reaction of water and of carbon dioxide with graphite at these temperatures may lead to serious burnout of the graphite and the resulting carbon monoxide may transport carbon to the cooler regions of the reactor. The presence of contaminants also may result in corrosive and/or embrittling attack of certain metallic components of the reactor. The outgassing behavior of the graphite is of considerable importance, since it may provide a significant amount of the impurities present in the coolant.

Early work on the degassing of graphite showed that desorption occurs over a wide temperature range and that temperatures of the order of 2000°C are required to effect an essentially complete removal of the adsorbed gas [1,2]. In more recent years, nuclear grades of graphite produced in the United States have been degassed and the results reported by a number of investigators [3-10]. Various English workers [11-14] also have presented data obtained from the degassing of several grades of British pile graphite.

The results of a number of these studies [3,6,8,9,10] show that a rather broad correlation exists between the ash and gas contents for many of the graphites examined. In general, graphites having an ash content above 400 ppm will evolve considerably more gas than will those having an ash content of 50 ppm or less. Furthermore, the ratio of H_2 to $CO + CO_2$ is larger in the gas released by the purer graphites. The presence of a high concentration of calcium also has been shown [10] to have a marked effect on the degassing behavior of several graphites. The desorbate obtained from these graphites at 600°C contains a large fraction of carbon dioxide which is released very rapidly. If the volume of desorbate is plotted against the log of time, a curve is obtained which has a large initial slope. The slope decreases rather markedly and for periods of time beyond about 6 hr a linear relationship prevails. The purer graphites evolve much smaller volumes of gas at 600°C containing very

[a]Operated for the U.S. Atomic Energy Commission by Union Carbide Corporation.

little carbon dioxide. A corresponding plot of volume and log of time results in a linear relationship from the early stages of degassing to periods of time in excess of 50 hr.

The ash content of graphite is influenced by a number of factors during the manufacturing process. Relatively pure petroleum coke is generally used for the nuclear grades of graphite. The coke is not sufficiently pure, however, to produce high purity graphite using the common graphitization conditions. A graphitization temperature of ~ 2800°C is commonly used to obtain the desired degree of crystallization of the carbon and effect some purification. Limited data[9] indicate that increasing the graphitization temperature decreases the ash and gas content of graphite in the temperature range 2600 to 3000°C. A more pronounced effect of furnace temperature probably would be found at lower temperatures. A purification process is required to produce high purity graphite (ash content < 30 ppm). This may be thermal purification utilizing temperatures above 3000°C or more commonly a gas purification employing halogens to remove the metals as volatile halides.

Following the purification step, the graphite is usually let down in an inert atmosphere to a sufficiently low temperature to prevent a rapid reaction with moist air to which it is finally exposed. The gas purification process not only reduces the ash content to a low level, but also limits the chemisorption of oxygen thereby yielding a graphite with a low gas content. The standard graphitization process allows exposure of the graphite to reactive gas during the let down, as well as being less effective in removing the impurities. As a result, it is difficult to separate the effect of ash content and of conditions of let down on the gas content of commercial graphites. Another variable affecting the gas content is the exposure experienced by the graphite between the time of removal from the graphitization or purification furnace and its ultimate application. Unfortunately, it is very difficult to define the exposure conditions for commercial graphites. The data available[4, 8, 14, 15] indicate that high purity graphites adsorb water vapor and possibly oxygen rather slowly at room temperature, and that complete removal of the adsorbed gas may be achieved only by high temperature degassing. The data are incomplete, however, and of little value for predicting the rate of adsorption under various conditions.

Data obtained from the degassing studies of 12 high purity graphites (ash content < 30 ppm) are presented in this paper. Three of the graphites are commercial grade materials while the others are experimental lots. Different sources of coke, different methods of purification, and fillers consisting of coke having various particle sizes were employed in the manufacture of these graphites. Since none of these variables has shown any consistent effect on the degassing behavior, they will receive no further consideration. It was suspected, for example, that the particle size distribution of the coke might have some effect on the degassing kinetics, but this is not the case. Differences that appear in the degassing data presented for the various graphites should be ascribed mainly to the conditions of let down and subsequent exposure, both of which are poorly defined for most of these graphites.

EXPERIMENTAL

Materials

Mod 2A, Mod 2N and TSX represent commercial nuclear grades of graphite, whereas the other designations refer to experimental lots of graphite. All were subjected to either gas or thermal purification and have ash contents of less than 30 ppm. Mod 2A and Mod 2N were let down in argon and nitrogen, respectively. The atmosphere present during let down of the other graphites is unknown, but an inert atmosphere probably was used in most cases. Texas coke or one of several needle type cokes was used in the production of the various graphites. A regular particle size mix or flour mix of the particular type coke was used as filler. Since neither the type of coke nor the particle size of the coke mix show any significant effect, they are not detailed for the various graphites. All samples have an apparent density between 1.6 and 1.7 g/cm^3.

Procedure

Two systems were used to heat the graphite in vacuo, one utilized a tube furnace for temperatures to 1000°C, the other an induction heater for temperatures to 1800°C. In the latter case, a cylindrical graphite specimen 1-1/4" dia x 1" long mounted on a tungsten wire was contained in a water-cooled quartz tube. A specimen 1-1/2" dia x 2" long contained in a quartz tube was used for the degassing studies with the tube furnace.

The system, with the specimen in place, was evacuated at ~ 30°C to a pressure of 10^{-3} mm Hg or less at the start of a run. The temperature was raised to the desired level and held constant until the rate of release was ~ 2%/hr of the total evolved at this temperature. The desorbate was removed continuously by a Toepler pump and collected in a calibrated manifold equipped with a McLeod gauge and suitable sample bulbs. After collection of the gas was completed at the designated temperature, gas samples were removed and the collection system pumped out prior to raising the temperature to the next desired level. Gas analyses were performed by the Analytical Service Groups using a mass spectrometer and a gas chromatograph.

RESULTS AND DISCUSSION

Loss in Weight of Graphite by Degassing

The loss in weight experienced by the various graphites is 0.01-0.02% when degassed to a maximum temperature of 1800°C. This is in fair agreement with limited data reported by Redmond and Walker [9]. For most specimens, the loss in weight is approximately equal to the original ash content plus the weight of gas removed by heating to 1800°C. A weight loss of approximately 0.005% was observed for the graphites upon degassing to a maximum temperature of 1000°C. The loss in weight noted at 1000°C is greater (in many cases by a factor of 2) than the weight of gas removed. The ash content is not changed significantly by the heat treatment at 1000°C, however, suggesting that part of the weight loss is associated with the initial pumpdown at 30°C.

Volume and Composition of Gas Evolved to 1000°C (Tube Furnace)

The degassing behavior of all the graphites is, in general, quite similar from 30 to 300°C, as seen in Table I. A small volume of gas is evolved

TABLE I

VOLUME AND COMPOSITION OF GAS EVOLVED IN VARIOUS TEMPERATURE INTERVALS UP TO 1000°C

Graphite	Temperature Interval (°C)	Volume (cm^3STP/100cm^3)	Percent of Total to 1000°C	Constituents (Vol.%) H_2	Hydrocarbons	H_2O	CO_2	CO	N_2
Mod.2A	30-300	0.6	11	8	10	38	4	4	36
Mod.2N		0.5	8	10	26	35	6	7	16
AGOT-SP		0.4	6	1	33	32	6	5	21
TSX		0.4	6	2	12	59	5	5	18
SP-GP		0.6	7	8	33	37	7	4	11
SP-TP		0.6	6	8	11	37	4	6	32
SP-21B		0.5	7	3	9	55	5	9	19
SP-22B		0.5	6	6	21	18	11	13	31
SP-23B		0.3	5	1	13	31	8	7	41
SP-26A		0.5	5	4	11	58	6	5	15
SP-28A		0.4	4	4	16	55	5	6	12
SP-29A		0.4	5	6	24	36	7	13	13
Mod.2A	300-600	1.3	25	22	38	15	3	12	10
Mod.2N		1.9	31	13	24	17	13	28	5
AGOT-SP		1.2	19	4	20	19	16	36	4
TSX		1.0	15	20	26	26	7	15	5
SP-GP		2.4	30	19	21	12	13	31	4
SP-TP		2.6	27	16	32	24	7	14	7
SP-21B		1.8	26	24	30	18	7	17	4
SP-22B		2.4	24	25	26	13	10	24	4
SP-23B		1.5	22	16	34	18	9	18	5
SP-26A		2.6	25	20	28	16	10	23	4
SP-28A		1.5	14	18	24	16	13	26	3
SP-29A		2.1	24	20	31	10	11	24	5
Mod.2A	600-1000	3.4	64	83	3	0.6	0.1	12	1
Mod.2N		3.7	61	74	1	0.2	0.5	23	1
AGOT-SP		4.6	74	67	1	3	0.8	21	3
TSX		5.5	80	75	2	2	1	18	2
SP-GP		5.1	63	74	1	0.3	0.2	23	1
SP-TP		6.5	67	75	2	0.3	0.1	21	1
SP-21B		4.6	67	73	3	0.6	0.6	22	1
SP-22B		7.0	71	75	2	0.4	0.2	22	1
SP-23B		4.9	73	75	3	1	0.3	20	1
SP-26A		7.1	69	80	3	0.9	0.8	15	1
SP-28A		8.6	82	82	2	0.5	0.3	15	1
SP-29A		6.2	71	78	1	0.4	0.4	11	9

containing mainly water, nitrogen, and hydrocarbons. Substantial amounts of water are retained at 300°C as evidenced by the composition of the desorbate collected from 300 to 600°C. Very little water is found above 600°C, however. The release of hydrocarbons at the lower temperatures suggests that these compounds are adsorbed on the original graphite, since the reaction rate of hydrogen with carbon is quite low. The small quantity of hydrocarbons found in the desorbate above 600°C is probably due to the cracking of these compounds as they are desorbed from the graphite surface. Methane, as a general rule, comprises about one-half of the total hydrocarbons found. The CO/CO_2 ratio at 600°C is about two, for many of these graphites. A ratio of ~ 0.3 has been reported [10] for several impure graphites that release 8-10 cm^3 of gas/100 cm^3 of graphite between 300 and 600°C. The gas released from 600 to 1000°C consists principally of hydrogen and carbon monoxide with H_2/CO ratios of at least three in all cases. Small quantities of nitrogen appear above 600°C and, as will be seen later, persist to above 1400°C. Although not recorded, small quantities of sulfur compounds (SO_2, H_2S, CS_2) have been found in the gas evolved by a number of the graphites.

Volume-Time Relationships at Temperatures to 1000°C

Data given in Fig. 1 for TSX graphite at 300, 600, and 1000°C are representative of those found for the other graphites at these temperatures. The data were obtained for a single specimen degassed at successively higher temperatures. The degassing of the various high purity graphites at 300°C follows a linear relationship if the volume is plotted against the log of time. Values for the slope A in the expression $V = A \log t + B$ range from 0.07 to 0.13 for the various graphites when V is given as cm^3 STP/100 cm^3 of graphite and t is expressed in minutes. Values for the slope as large as 0.3 have been reported [10] for impure graphites (ash > 400 ppm).

A linear relationship also has been found at 600°C for the various high purity graphites with values for the slope ranging from ~ 0.4 to 0.8. Some of the impure graphites also give a linear relationship [10] but with larger slopes. However, as noted previously, some high calcium graphites yield curves having very large slopes [6-14] during the early stages of degassing but which later decrease rather markedly.

A careful examination of the curve given for 1000°C in Fig. 1 shows that the slope increases with time for about the first 1000 min and then becomes constant. If an average slope is taken for the time interval 100-300 min the value for the slope so obtained is about one-half that found in the linear region beyond 1000 min. Values for the slopes found for the various high purity graphites during the early stages of degassing range from 1.5 to 2.5 compared to 3-5 after prolonged degassing. The impure graphites behave similarly [10], although the slopes during all periods of degassing are larger than those given for the high purity graphites. In many cases, the H_2/CO ratio increases as the degassing proceeds at 1000°C suggesting that the increase in slope is associated with an increased rate of desorption of hydrogen compared to that of carbon monoxide.

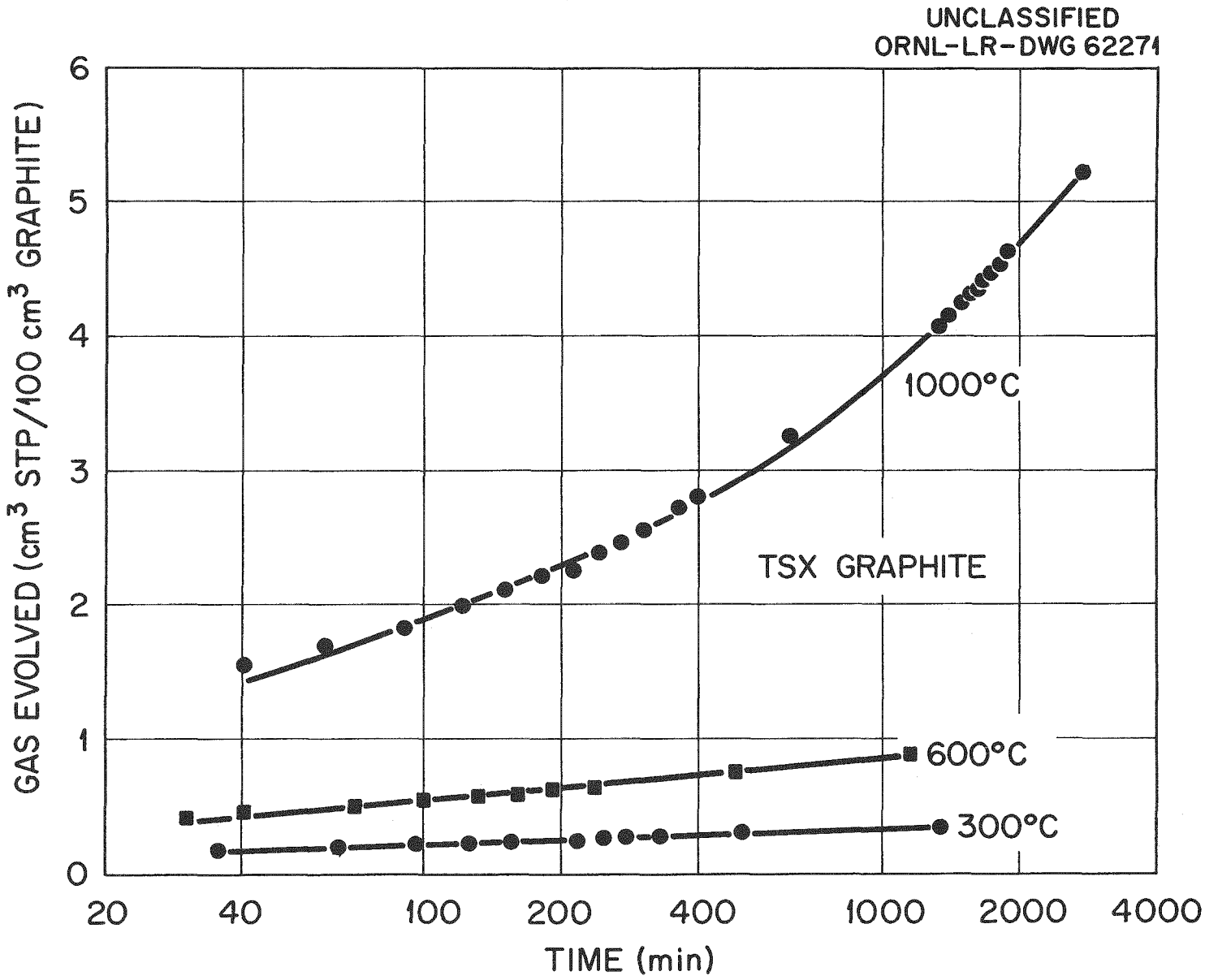

Fig. 1. Volume-Time Relationships for TSX Graphite at 300, 600, and 1000°C

Volume and Composition of Gas Evolved to 1800°C (Induction Heating)

The total volume of gas evolved from 30 to 1800°C and the volume percent of the important constituents of the gas are given in Table II. Carbon dioxide, water and hydrocarbons, which are not included, usually do not exceed one to two percent. A few tenths of a percent of sulfur compounds (H_2S, CS_2) are found occasionally. Volumes ranging from 20 to 68 cm^3 are reported for the various graphites. Wide variations in the H_2/CO ratio also are evident although, in the majority of cases, this ratio is two or greater. It might be noted that the TSX graphite which releases the gas with the smallest ratio has an ash content of ~ 5 ppm. Larger volumes of gas with a H_2/CO ratio of less than one have been reported [10] for several impure graphites (ash > 400 ppm).

The volume and composition of gas evolved by the graphites in several temperature intervals between 30 and 1800°C are given in Tables III and IV. (Carbon dioxide, water, and hydrocarbons are not listed in Table IV, because the volume percent of these constituents is only 0.1 - 0.2 above 1000°C.) The volume of gas evolved by Mod 2A, Mod 2N and AGOT-SP above 1400°C is only some 9 percent of the total evolved to 1800°C. Most of the other graphites evolve approximately one-third of the total in each of the three temperature intervals. The H_2/CO ratio in the evolved gas decreases as the degassing temperature is increased from 1000 to above 1400°C for all the graphites, except Mod 2N. This ratio which is well in excess of unity in the temperature interval 30 - 1000°C for all the graphites is less than one for a number of the graphites in the temperature interval 1400-1800°C. It is interesting to note that Mod 2A and Mod 2N which were let down in argon and nitrogen, respectively, release appreciable amounts of these gases above 1000°C. Argon, which is not chemisorbed, must be trapped in the pore structure during the cooling from high temperature and released when the pores are reopened by high temperature heating. Nitrogen probably behaves similarly, although there is a possibility that part of the nitrogen is chemisorbed. Small amounts of nitrogen are found over the entire temperature range studied in all cases.

These data obtained at temperatures up to 1800°C show some pronounced differences in the degassing behavior of the various graphites. These differences cannot be explained by the minor variations in ash content, the type of coke or the coke particle size of the mix. It is believed that the atmosphere under which the graphites were let down and the exposure between manufacture and degassing are responsible for the variations noted.

REFERENCES

1. P. Lebeau and M. Picon, Action de la Chaleur et du Vide sur le Graphite Artificiel, Compt. rend. 179: 264 (1924).

2. F. J. Norton and A. L. Marshall, The Degassing of Metals, Trans. Am. Inst. Mining Met. Engr. 156: 351 (1944).

3. R. R. Eggleston, R. L. Carter, W. J. Greening, and R. E. Durand, Graphite Outgassing, USAEC Report NAA-SR-1240, North American Aviation, January 21, 1955.

4. R. L. Carter and W. J. Greening, Evolution and Gas from Graphite Moderator Material, Nuclear Engineering and Science Congress, Cleveland, December 12-16, 1955, Print 319.

5. R. L. Carter and R. R. Eggleston, Moderator Graphite for High Temperature Reactors, in Proc. 1st and 2nd Carbon Conference, University of Buffalo, 1956, p. 149.

6. C. A. Odening and J. C. Bowman, Recent Developments in Gas Purification of Graphite, Industrial Carbon and Graphite Conference, London, September 24-26, 1957, p. 537, Society of Chemical Industry, 1958.

7. C. V. Mitchell, National Carbon Company, Parma, Ohio, personal communication.

8. L. G. Overholser and J. P. Blakely, Studies of Gas Evolution by Graphite, US/UK Meeting on the Compatibility Problems of Gas-Cooled Reactors, Oak Ridge National Laboratory, February 24-26, 1960, USAEC Report TID 7597 (Book 2), p. 560, 1961.

9. J. P. Redmond and P. W. Walker, Jr., Gas Content of Graphite, Nature, 186: 72 (1960).

10. L. G. Overholser and J. P. Blakely, Oak Ridge National Laboratory, in Proc. 5th Carbon Conference, Pennsylvania State University, June 19-23, 1961 (In press).

11. G. N. Thomas, Investigations on the Pore Structure and Degassing of Pile Graphite, British Report C/R-176, April 1948.

12. E. J. Burton and P. J. Stokes, The Degassing of Graphite: Progress up to August 1956, British Report IGR-TN/CA-379, August 1956.

13. A. B. McIntosh and W. G. O'Driscoll, Compatibility Problems of Graphite Moderators, Industrial Carbon and Graphite Conference, London, September 24-26, 1957, p. 519, Society of Chemical Industry, 1958.

14. R. C. Asher, The Degassing of Graphite, in US/UK Meeting on the Compatibility Problems of Gas-Cooled Reactors, Oak Ridge National Laboratory, February 24-26, 1960, USAEC Report TID-7597 (Book 2), p. 504, 1961.

15. J. P. Redmond, Hydrogen Sorption on Graphite at Elevated Temperatures, Ph. D. Thesis, Pennsylvania State University (1959).

TABLE II

VOLUME AND COMPOSITION OF GAS EVOLVED TO 1800°C BY VARIOUS GRAPHITES

Graphite	Volume Evolved to 1800°C (cm^3(STP)/ 100cm^3 graphite)	Constituents (Vol. %)		
		H_2	CO	N_2
Mod.2A	20	85	9	3
Mod.2N	24	59	32	6
AGOT-SP	23	75	19	5
TSX	31	53	42	3
SP-GP	48	65	32	2
SP-TP	68	65	30	2
SP-21B	39	65	31	3
SP-22B	26	55	40	3
SP-23B	45	65	28	4
SP-26A	36	60	30	7
SP-28A	41	61	33	2
SP-29A	46	71	26	2

TABLE III

VOLUME AND COMPOSITION OF GAS EVOLVED BY VARIOUS GRAPHITES (30-1000°C, INDUCTION HEATING)

Graphite	Volume (cm^3 STP/100 cm^3)	Percent of Total to 1800°C	Constituents (Vol. %)					
			H_2	Hydrocarbons	H_2O	CO_2	CO	N_2
Mod.2A	12.6	64	93	1	0.2	0.1	6	1
Mod.2N	15.7	65	56	1	1	2	38	3
AGOT-SP	10.6	46	78	3	0.1	0.7	16	1
TSX	11.0	36	68	1	2	1	27	1
SP-GP	18.8	39	78	1	1	1	18	1
SP-TP	25.0	37	70	3	1	2	23	2
SP-21B	16.2	42	73	2	0.6	0.8	24	1
SP-22B	10.1	39	78	1	0.4	0.4	20	1
SP-23B	19.8	44	76	2	0.6	1	19	1
SP-26A	13.4	37	56	1	0.3	0.5	28	14
SP-28A	16.6	41	71	2	1	0.8	25	1
SP-29A	19.7	43	84	1	0.5	0.4	14	1

TABLE IV

VOLUME AND COMPOSITION OF GAS EVOLVED IN THE TEMPERATURE INTERVALS 1000-1400°C and 1400-1800°C (INDUCTION HEATING)

Graphite	Temperature Interval (°C)	Volume (cm^3 STP/100cm^3)	Percent of Total to 1800°C	Constituents (Vol. %) H_2	CO	N_2
Mod.2A*	1000-1400	5.4	27	78	10	5
Mod.2N		6.7	28	66	22	10
AGOT-SP		10.6	45	76	19	3
TSX		10.4	34	57	37	3
SP-GP		14.3	30	65	32	2
SP-TP		22.7	33	65	31	2
SP-21B		15.0	39	67	29	2
SP-22B		7.2	28	66	28	4
SP-23B		12.5	28	59	34	6
SP-26A		13.3	37	75	21	3
SP-28A		13.4	33	65	31	2
SP-29A		12.8	28	70	27	2
				*6% Argon		
Mod.2A**	1400-1800	1.8	9	50	27	7
Mod.2N		1.9	8	62	15	20
AGOT-SP		2.1	9	59	37	4
TSX		9.3	30	31	62	4
SP-GP		15.3	32	47	49	3
SP-TP		20.6	30	59	38	2
SP-21B		7.5	19	43	49	7
SP-22B		8.3	32	17	76	6
SP-23B		12.7	28	56	38	5
SP-26A		9.4	26	45	46	7
SP-28A		10.6	26	39	52	4
SP-29A		13.4	29	54	41	4
				** 16% Argon		

IMPURITIES IN A LIQUID METAL COOLANT AND THEIR EFFECT ON THE FUEL ELEMENT CANNING MATERIALS NIOBIUM AND VANADIUM

By V. M. Sinclair, R. A. H. Pool and A. E. Ross

Dounreay Experimental Reactor Establishment
United Kingdom Atomic Energy Authority
Thurso, Caithness, Scotland

INTRODUCTION

The Dounreay Fast Reactor at the United Kingdom Atomic Energy Establishment near Thurso in Scotland is an unmoderated liquid metal cooled reactor with fuel elements each consisting of annular uranium-1/2 % chromium alloy contained within a niobium outer and a vanadium inner can. Full details of the reactor system have been published elsewhere [1,2].

It is planned to operate the reactor with primary coolant inlet temperatures in the region of 200°C and with power levels up to 60 MW. Operation of the reactor at power levels of 20 and 30 MW entails maximum niobium can temperatures of 330 and 400°C and vanadium can temperatures of 390 and 480°C, respectively. The liquid metal coolant, a 70/30 sodium potassium alloy, is known to contain non-metallic impurities such as hydrogen, oxygen, nitrogen, and carbon which at these temperatures may attack the fuel element cans.

To effect clean-up of the primary coolant, cold and hot traps have been included in the reactor circuit. The cold traps were designed to operate at 120°C and remove oxygen from the coolant, allowing operation of the reactor with fuel element can temperatures up to 350°C without there being corrosion of the fuel cans by oxygen. The hot traps contain zirconium at temperatures of 600-650°C to act as a getter for the removal of oxygen from the coolant down to low levels of less than 4 ppm (the solubility at 120°C), to enable can temperatures of higher than 350°C to be achieved without corrosion by oxygen.

This paper reviews the properties of hydrogen, nitrogen, oxygen, and carbon in the primary coolant and the effects of these non-metallic impurities on the niobium and vanadium fuel can metals under operating conditions of the Dounreay Fast Reactor. The corrosion of niobium and vanadium by oxygen is well known and is referred to only briefly in this paper.

HYDROGEN IN THE PRIMARY COOLANT SYSTEM

Hydrogen may enter the primary coolant in a number of ways: firstly, atmospheric moisture may leak into the blanket gas and form hydride and oxide by reaction with the liquid metal; secondly, unsatisfactory manufacture and

storage of fuel elements could result in moisture entering the sodium thermal bond to form caustic soda which, on charging of the fuel element, would react further with the primary coolant to liberate hydrogen; thirdly, it may enter as oil used to protect the bulk NaK during storage, the oil reacting with the NaK to form hydrogen and carbonaceous material on raising the temperature of the primary coolant. Another possible source of hydrogen is the moisture absorbed on "steam-stripped" components, (steam-stripping is the process used for removing liquid metal from components being withdrawn from the primary circuit), since when they are re-introduced into the primary circuit the moisture would react with the liquid metal.

This section of the paper summarizes the data obtained at the U.K.A.E.A. Establishments at Dounreay and Culcheth and in the United States and elsewhere on the interaction of hydrogen with the primary coolant NaK and with other metals of interest in the D.F.R., viz., niobium, vanadium, and zirconium.

Sodium-Potassium-Hydrogen System

It is well known that sodium and potassium react with hydrogen to form salt-like crystalline compounds containing hydrogen as the anion. Reaction is relatively rapid at temperatures above 250°C but is quite slow below 150°C.

The phase diagram of the NaK-hydrogen system over the temperature range of interest in the D.F.R., i. e., 100°C to 600°C, is of the form shown in Figure 1. The diagram consists of three parts: (i) a two phase hydrogen-rich region of solid hydride and gaseous hydrogen; (ii) a three phase region of hydrogen gas, solid hydride, and liquid metal; and (iii) a metal-rich region consisting of gas and liquid only. Equilibrium in these three regions can be represented thus:

Region (i)

$$(NaK)H \text{ (solid plus dissolved NaK)} \rightleftharpoons NaK \text{ (liquid in solution in hydride)} + 1/2\ H_2\text{(gas)}$$

Region (ii)

$$(NaK)H \text{ (solid, saturated with NaK)} \rightleftharpoons NaK\text{(liquid, saturated with hydride)} + 1/2\ H_2\text{(gas)}$$

Region (iii)

$$(NaK)H \text{ (unsaturated solution in NaK)} \rightleftharpoons NaK\text{(liquid containing dissolved hydride)} + 1/2\ H_2\text{(gas)}$$

In the central three phase region of the NaK-hydrogen phase diagram the hydrogen partial pressure, at any given temperature, is fixed and independent of the composition and is, of course, the dissociation pressure of the metal hydride (See Figure 2). The pressure of hydrogen at various temperatures has been measured by several workers over the temperature range 250°C to about 600°C[3,4]. The most reliable data are probably those of Herold[4] who found the pressure of the hydrogen obeyed the following equation:

$$\log_{10}P = g + h/T \qquad (1)$$

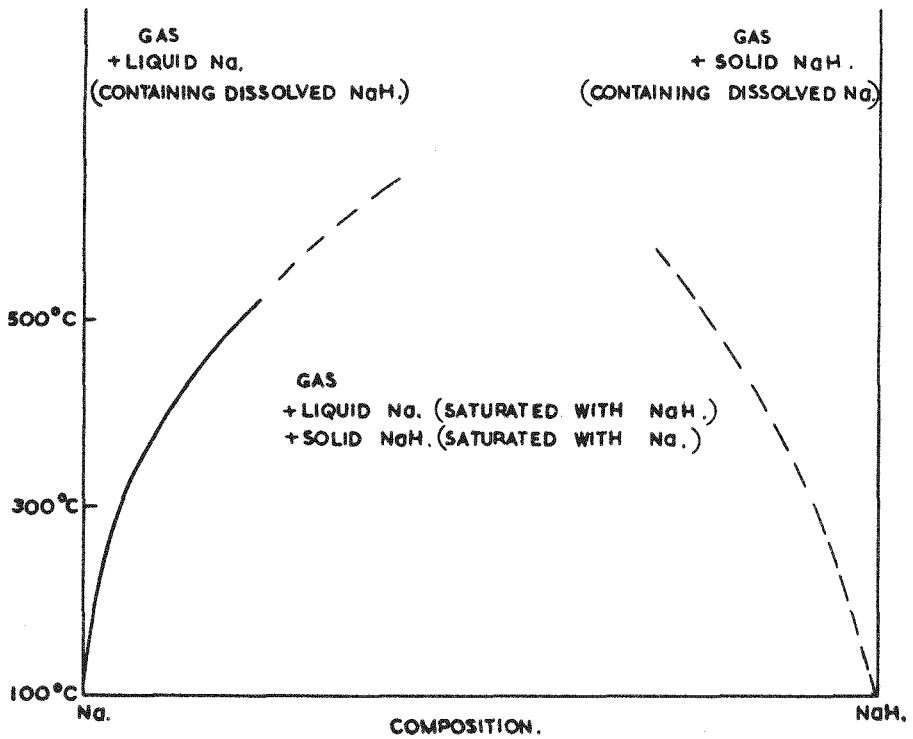

FIG. I. SODIUM-HYDROGEN PHASE DIAGRAM.

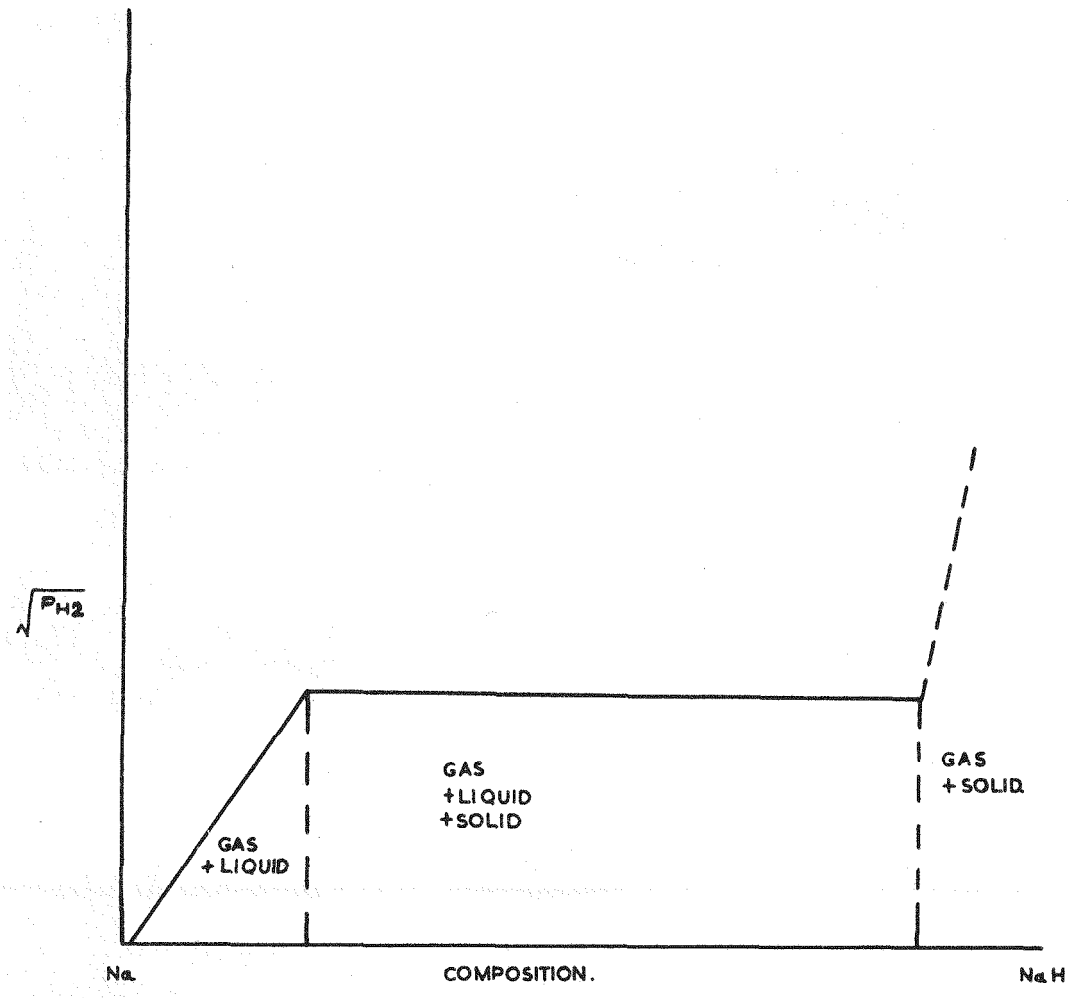

FIG. 2 SODIUM-HYDROGEN COMPOSITION-PRESSURE DIAGRAM
(AT CONSTANT TEMPERATURE)

where P is the pressure of hydrogen (mm Hg) in equilibrium with the hydride, T is the temperature in degrees Kelvin, while for NaH g = 11.66, h = - 6100, and for KH g = 11.69, h = - 6175.

In the sodium-rich two phase region the constant for the equilibrium is given by:

$$K_{a(T)} = a_{NaK} \times a_{H_2}^{\frac{1}{2}} \times a_{(NaK)H}^{-1} \qquad (2)$$

where

$K_{a(T)}$ is the equilibrium constant at temperature T

a_{NaK} is the activity of the NaK

a_{H_2} is the activity of the hydrogen gas

$a_{(NaK)H}$ is the activity of the dissolved hydride.

In solutions containing relatively small quantities of dissolved hydride, i. e., solutions containing up to the terminal solubility at temperatures below 400°C, the activity of the hydrogen gas may be replaced by the pressure of the gas, the activity of the dissolved hydride by its concentration, and the activity of the bulk metal can be assumed to be constant. Hence the equilibrium can be expressed to a satisfactory approximation more conveniently by the expression

$$K_{(T)} = P_{H_2}^{\frac{1}{2}} \times C_{(NaK)H}^{-1} \qquad (3)$$

It follows that in the unsaturated solution at any temperature the concentration of the dissolved hydride in the liquid metal is proportional to the square root of the hydrogen partial pressure.

In a reactor system which is being efficiently cold-trapped the concentration of the hydride in solution will be the terminal solubility of the hydride at the cold trap temperature. However, the hydrogen equilibria in the reactor primary coolant system will be governed by the activity of the hydrogen in the vicinity of the fuel elements, and since temperatures in this region are much higher than that of the cold trap, it is essential that the variation with temperature of the thermodynamic activity of hydrogen in an unsaturated NaK system be known.

Some preliminary measurements of the variation at constant composition (i. e., constant hydride content) of the thermodynamic activity of hydrogen in unsaturated NaK have been made in the following manner.

Specimens of niobium were immersed at various temperatures in NaK which had been cold-trapped over a range of temperatures. After the niobium had come to equilibrium with the system the specimens of niobium were withdrawn and their hydrogen content measured. Niobium was chosen for this work since the hydrogen-niobium system had been studied fairly thoroughly and niobium was one of the metals in the reactor whose performance was of importance. Using published data[5,6] which in some cases had to be extrapolated, the activity of hydrogen in the niobium was calculated (in the context of this

paper this is equivalent to the pressure of the hydrogen in equilibrium with the metals). The relationship between temperature of the system, the cold-trapping temperature, and the hydrogen activities measured in these experiments is shown in Figure 3.

These figures for the variation of hydrogen activity in unsaturated solution with temperature can be used to calculate the variation of solubility of the hydride with temperature as follows.

The dissociation pressure of the hydride can be written as $\log_{10}P_{D\ (T)} = g + h/T$, where $P_{D(T)}$ is the dissociation pressure of the hydride at temperature T, with g and h as constants. Similarly the terminal solubility, $C_{S(T)}$, of the hydride at temperature T can be written as $\log_{10}C_{S(T)} = m + n/T$ where m and n are constants.

From equation (3) at any given temperature T it can be shown that

$$P_{H_2(T)} = P_{D(T)} \times \frac{C^2_{(T)}}{C^2_{S(T)}} \qquad (4)$$

where $P_{H_2}(T)$ is the partial pressure of hydrogen at temperature T, when the concentration of hydride in solution at the same temperature is $C_{(T)}$.

Taking logarithms and substituting for $P_{D(T)}$ and $C_{S(T)}$ gives

$$\log_{10}P_{H_2(T)} = g + h/T + 2\log_{10}C_{(T)} - 2(m + n/T)$$

differentiating with respect to 1/T at constant composition, i. e., constant $C_{(T)}$, it follows that

$$\frac{d\log_{10}P_{H_2}}{d\,\frac{1}{T}} = h - 2n \qquad (5)$$

From Figure 3 the value for $\frac{d\log_{10}P_{H_2}}{d\,\frac{1}{T}}$ is -2128 and must equal h - 2n. Data for the variation of dissociation pressure of the hydride of sodium with temperature are reasonably well founded and a value for h from the data of Herold[4] is -6100. From the work described above it follows that n is equal to -1990. This compares with values of -6820 and -4650 from the desorption plus filtration and the absorption data of Williams, et al [7], respectively.

It can be seen from this work on hydriding of niobium in liquid NaK that the solubility of hydrogen appears to be less influenced by temperature than has heretofore been thought.

Niobium-Hydrogen System

Niobium reacts with hydrogen and is an exothermic hydride former. The system has been found to consist essentially of a single phase solid solution

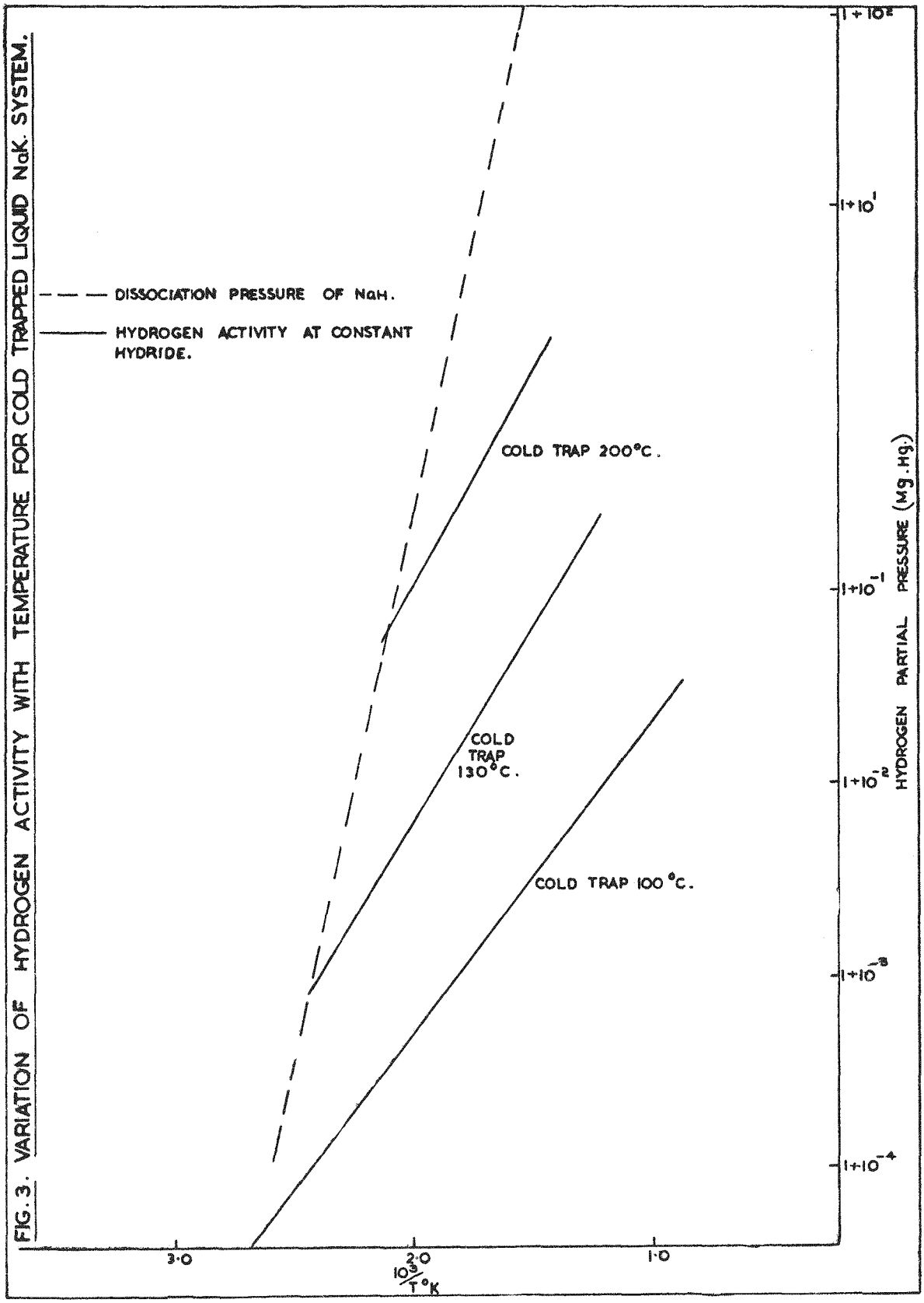
FIG. 3. VARIATION OF HYDROGEN ACTIVITY WITH TEMPERATURE FOR COLD TRAPPED LIQUID NaK. SYSTEM.
DISSOCIATION PRESSURE OF NaH.
HYDROGEN ACTIVITY AT CONSTANT HYDRIDE.
COLD TRAP 200°C.
COLD TRAP 130°C.
COLD TRAP 100°C.
HYDROGEN PARTIAL PRESSURE (Mg.Hg.)
1+10²
1+10¹
1+10⁻¹
1+10⁻²
1+10⁻³
1+10⁻⁴
3·0
2·0
1·0
10³/T°K

of hydrogen in the metal, the body centered cubic structure of the metal expanding as the hydrogen concentration increases. A two phase region, both phases being body centered,has been found at low temperatures and at low hydrogen partial pressures. Representative isopleths taken from the work of Komjathy[5] and of Albrecht et al[6] which are of interest in the study of hydrogen equilibria in the Dounreay Fast Reactor are shown in Figure 4.

Rates of reaction between hydrogen and niobium have been measured by Albrecht et al[6]; however, these have been measured for the gas-solid reaction and cannot be used in calculations involving the uptake of hydrogen from a liquid metal system containing dissolved hydride. It has been found in static tests at Dounreay that the rate of uptake of hydrogen by niobium from NaK is much quicker than the corresponding gas reaction over the temperature range investigated, i. e., below about 400°C. The difference may be due, firstly, to the hydrogen being present in the gas phase as molecules and in the NaK as ions, therefore absorption of hydrogen by niobium from the gas phase and not the liquid metal involves the dissociation of a hydrogen molecule since it is likely that the hydrogen exists as ions in both niobium and sodium; the activation energy for the former absorption process would be larger than for the second. Secondly, the alkali metal may change the surface of the niobium, e. g., by removing a protective surface layer of oxide, and the magnitude of this change may well depend on whether the liquid metal is static or flowing and of low or high oxygen content.

A study has been made of effects of hydrogen on the room temperature mechanical properties of the niobium used for reactor fuel cans (this metal has been found to contain 80 to 620 ppm oxygen, 30 to 100 ppm nitrogen, and 7 to 30 ppm hydrogen on a w/w basis). It was found that up to 60 ppm w/w of hydrogen in the niobium does not affect the mechanical properties of interest in the D.F.R., 70-90 ppm causes a decrease in the ultimate tensile strength of the niobium, while 100-110 ppm causes the metal to show a brittle fracture in a simple bend test and lowers its ultimate tensile strength to about 50% of that observed on the normal material. Further increase in the hydrogen content to 200-300 ppm renders the metal fragile and easily powdered. From these figures it can be seen that the presence of hydrogen in a niobium can is undesirable. The partial pressure of hydrogen in equilibrium with niobium containing 100 ppm hydrogen at various temperatures is given in Table I.

Vanadium-Hydrogen System

Vanadium, like niobium, is an exothermic hydride former. Again it has been found that hydrogen enters into interstitial sites expanding the normal lattice of the metal. It has been suggested[8] that at low concentrations of hydrogen there are two types of hydrogen sites available for the hydrogen, the regular interstitial sites in the normal lattice and sites which occur at disturbed regions of the lattice. The latter sites are thought to be low energy sites, the hydrogen entering these before filling the normal interstitial positions. Representative isopleths from this work which have been used at D.E.R.E. are shown in Figure 5. Experience at D.E.R.E. suggests that the rates of reaction of hydrogen in liquid metals with vanadium are somewhat faster than those with niobium.

A study has been made of the effects of hydrogen on the mechanical properties of the vanadium metal used for fuel element cans (the vanadium

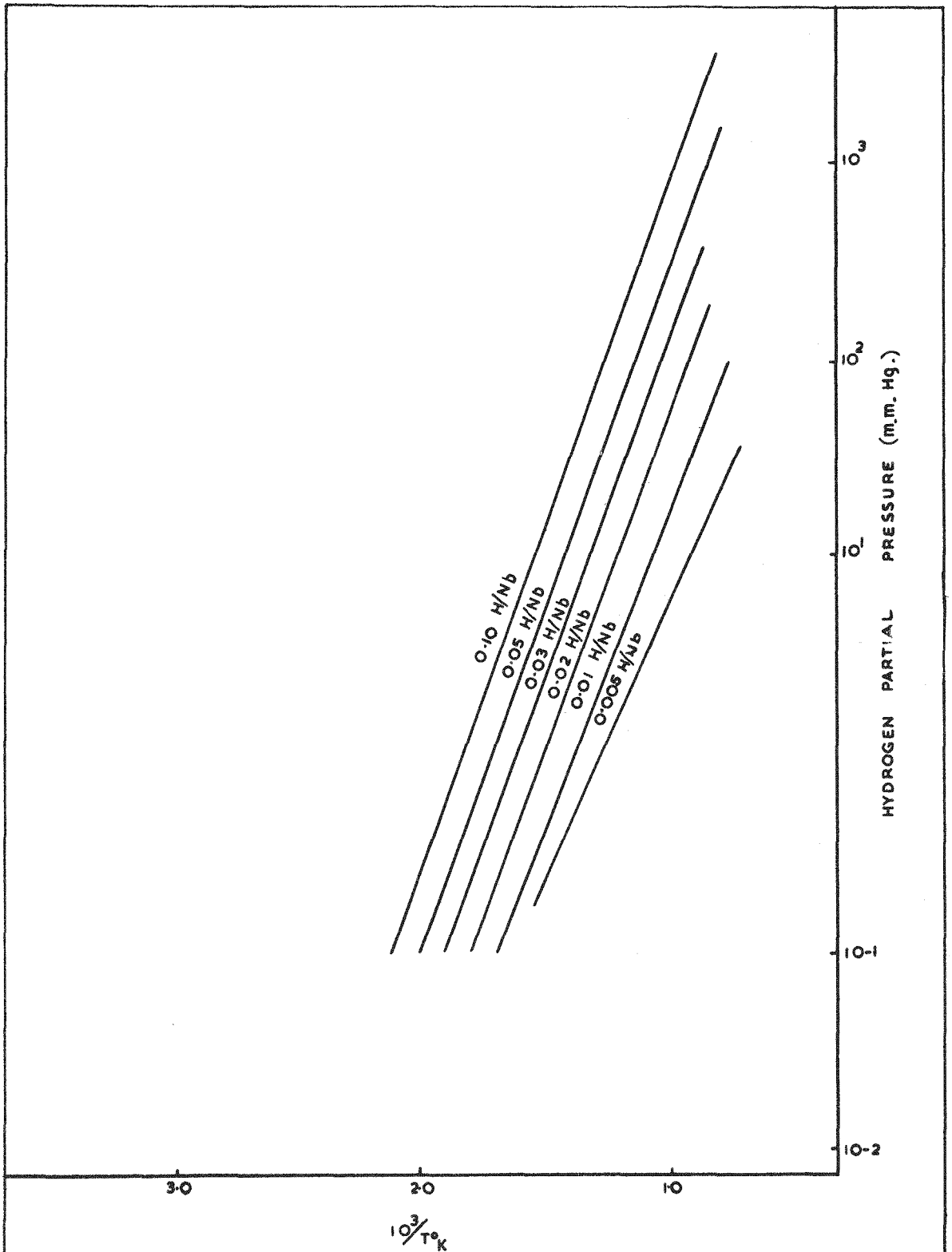

FIG. 4. NIOBIUM ISOPLETHS.

TABLE I

HYDROGEN PARTIAL PRESSURES IN EQUILIBRIUM WITH (a) SODIUM SATURATED WITH SODIUM HYDRIDE AND (b) NIOBIUM CONTAINING 100 PPM HYDROGEN

Temperature	Pressure of Hydrogen in Equilibrium with Sodium Hydride	Pressure of Hydrogen in Equilibrium with Niobium Containing 100 ppm Hydrogen
(°C)	(mm Hg)	(mm Hg)
200	0.03*	0.003*
250	0.7	0.02*
300	8	0.08*
350	60	0.25
400	> 100	0.6
450	> 100	1.2
500	> 100	2.5
600	> 100	8

* Extrapolated data.

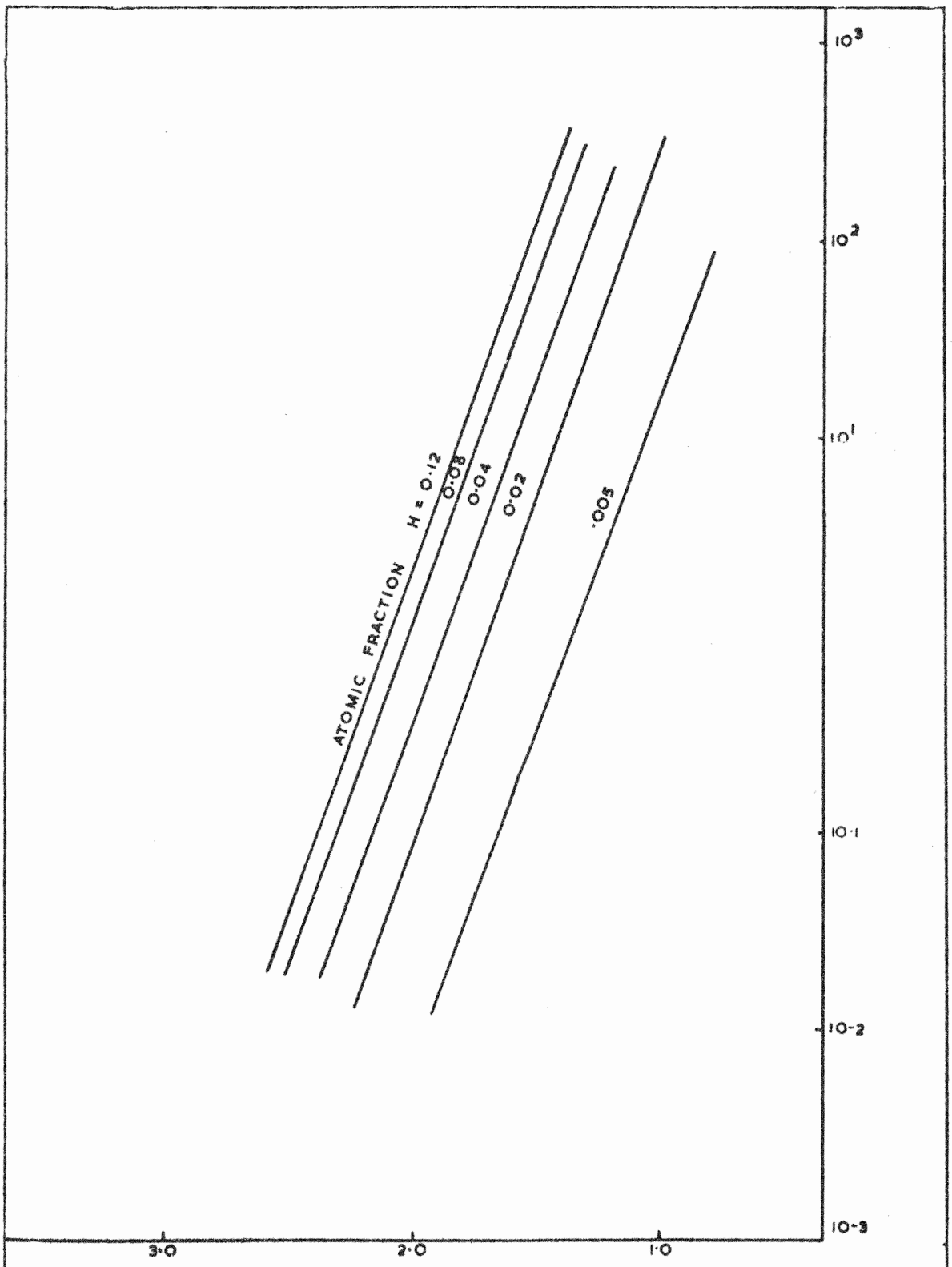

FIG. 5 VANADIUM ISOPLETHS.

usually contains from 10 to 66 ppm hydrogen, 110 to 1700 ppm oxygen, and 20 to 800 ppm nitrogen on a w/w basis). The presence of hydrogen has been found to be deleterious in vanadium; between 60 and 80 ppm w/w hydrogen has been found to lower the room temperature tensile strength of the vanadium markedly and cause it to exhibit a brittle fracture in a simple bend test.

Zirconium-Hydrogen System

Zirconium is used in the hot traps of the Dounreay Fast Reactor as a getter for oxygen. Its role in the hydrogen equilibria in the reactor is however of interest. Zirconium is an exothermic hydride former like niobium and vanadium, though the phase system is much more complicated; this is shown in Figure 6.

The zirconium in the hot traps of the D.F.R. will be approximately 600°C and the phase diagram shows that at this temperature, before any large uptake of hydrogen by the zirconium takes place, the system must be in the Zr β + δ region[9] (Figure 6). This requires hydrogen pressures in excess of those which would embrittle the lower temperature regions of the fuel elements. Zirconium at 450°C would have a large capacity for hydrogen at a satisfactory low partial pressure of hydrogen[10](Figure 7).

HYDROGEN EQUILIBRIA IN THE PRIMARY COOLANT SYSTEM OF A LIQUID METAL COOLED REACTOR

If the activity of the hydrogen in the liquid metal is greater than the activity of hydrogen required to embrittle niobium or vanadium, then hydrogen will pass from the liquid metal into the fuel element metals and embrittle them. Two methods of avoiding embrittlement are apparent: (a) to exclude hydrogen from the system and keep the total amount present below the amount required to embrittle fuel elements; or (b) to keep the thermodynamic activity of the hydrogen in the liquid metal in the vicinity of the fuel elements below that which would cause embrittlement.

With regard to the first method it is not now feasible to achieve complete exclusion of hydrogen in the D.F.R. Analysis of deposits removed from cold parts of the primary coolant system has shown that they contain a large proportion of hydride and the amount of deposit is thought to be sufficient to embrittle a complete fuel element charge. Even if this material was removed there would still be the likelihood that some elements would, because of temperature or position, be more likely to embrittle than others.

With regard to the second condition, involving control of the hydrogen activity in the vicinity of the fuel elements, if niobium or vanadium is immersed in hot NaK which is saturated with hydride then it is known that the niobium or vanadium can metals will be embrittled by hydrogen since the partial pressure of hydrogen in such a system is greater than that required to embrittle these metals(Table I). In the reactor system the concentration of hydride will be controlled by the cold trap, the elements being at a much higher temperature than the cold trap temperature. In these circumstances the temperature of the cold trap must be selected so that the activity of the hydrogen in the NaK is less than that of hydrided niobium or vanadium. Reference to Figure 8 shows that for a fuel element operating at 200°C or above effective cold-trapping of the reactor must be carried out near 100°C if

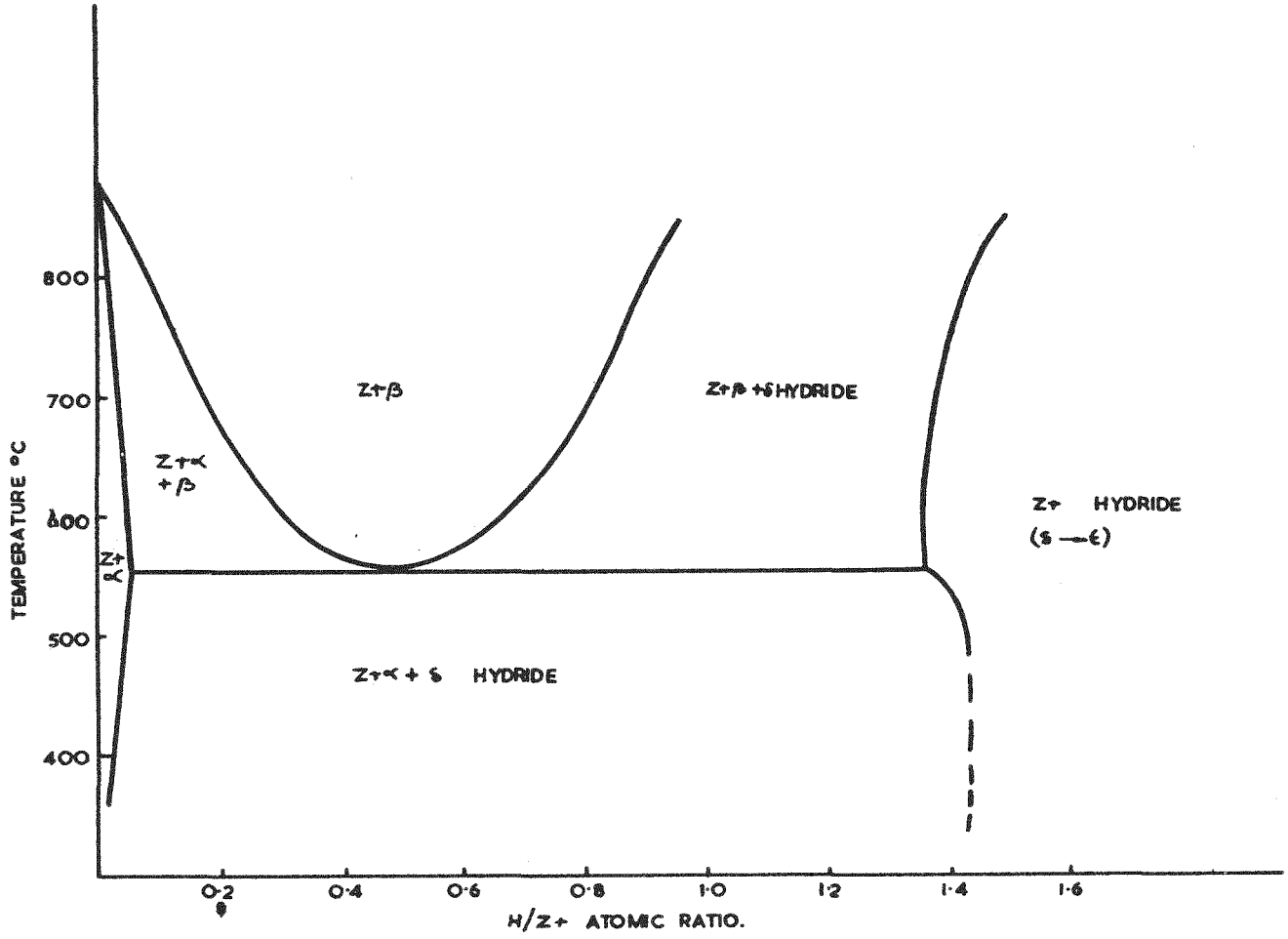

FIG. 6 ZIRCONIUM -HYDROGEN PHASE DIAGRAM.

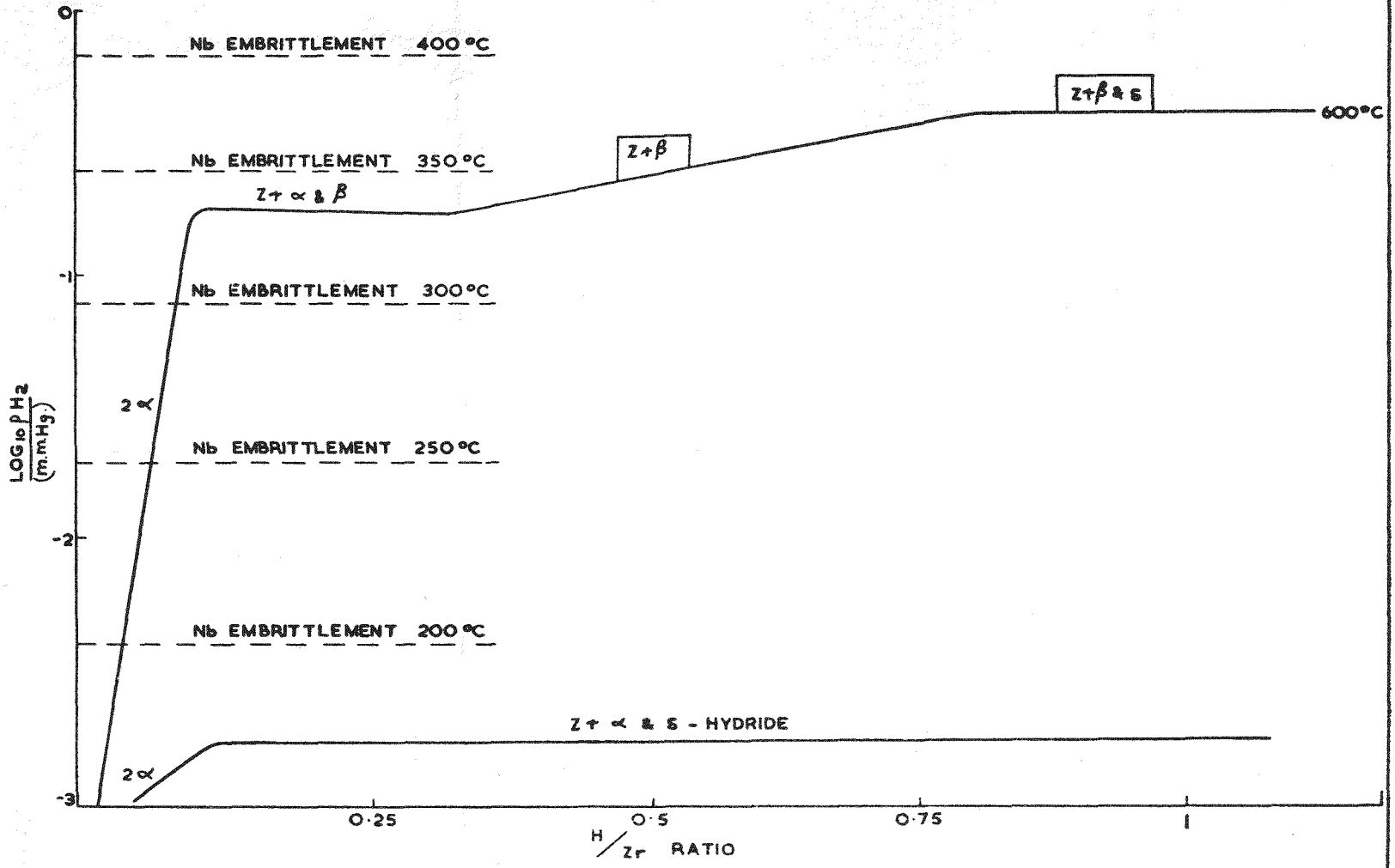

FIG. 7.
PARTIAL PRESSURE OF HYDROGEN IN EQUILIBRIUM WITH ZIRCONIUM AT CONSTANT TEMPERATURE & THE RELATIONSHIP WITH THE HYDRIDING OF NIOBIUM.

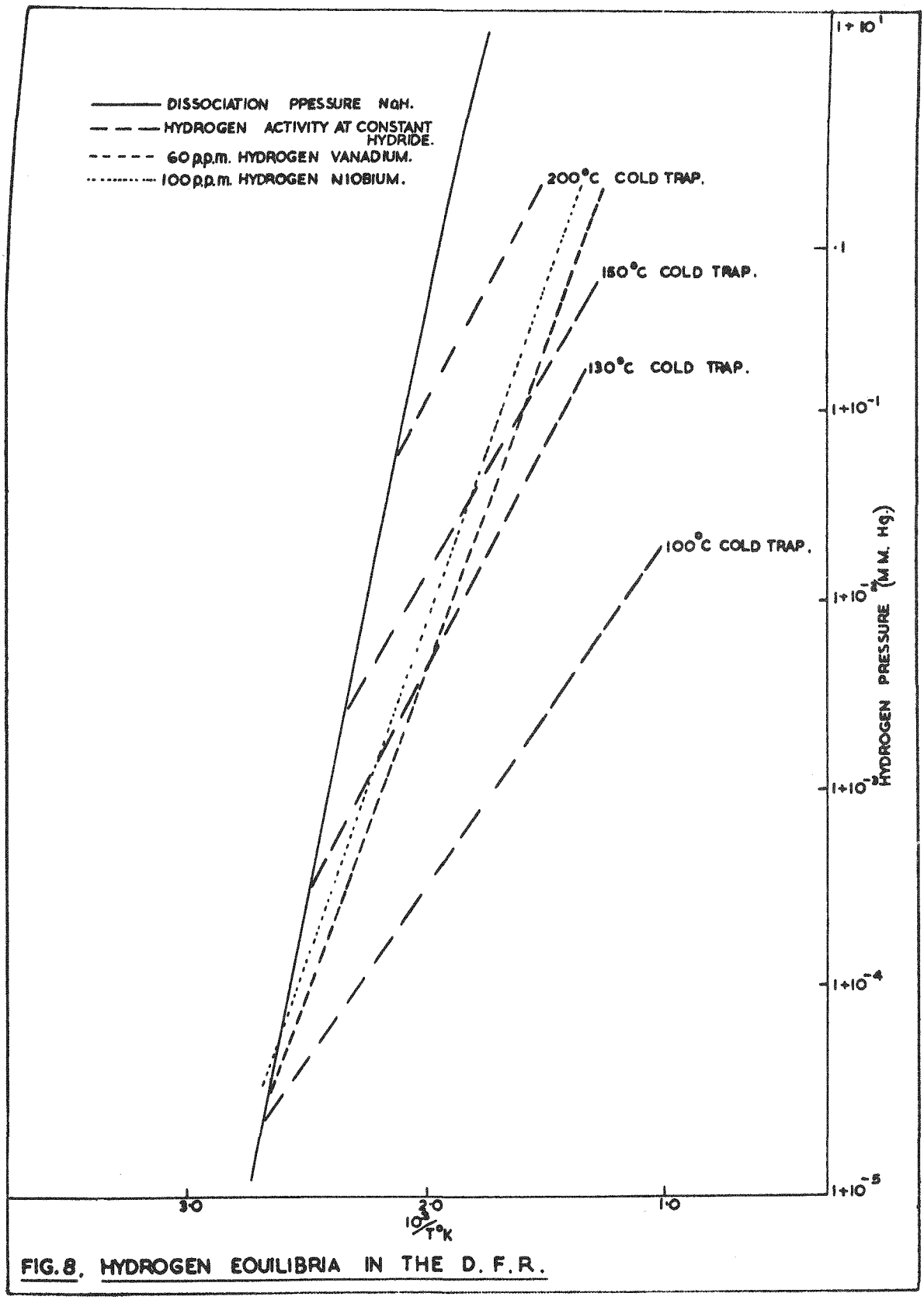

FIG. 8. HYDROGEN EQUILIBRIA IN THE D. F. R.

embrittlement is to be avoided. Some experiments carried out at the Culcheth laboratories of the U.K. Atomic Energy Authority[11] have shown that if a fuel element is operating in the region of 350°C, cold-trapping of the NaK at 200°C is unsatisfactory and embrittlement of the niobium and vanadium takes place; cold-trapping at 150°C is not quite satisfactory as slight embrittlement is still experienced but cold-trapping at 100°C is fully effective in preventing embrittlement. If the reactor is in a shut-down condition then the temperature of the fuel elements may drop to about 150°C and it is possible, on an equilibrium basis, for niobium to become, or be very close to being, embrittled. However, it is unlikely that equilibrium will be reached at these very low temperatures within the lifetime of an element in the reactor since the reaction rates are fairly slow. It is concluded therefore that for all operations including shut-down cold-trapping at 100°C will be adequate for preventing embrittlement.

On present evidence cold-trapping is also an effective means of preventing corrosion of niobium by oxygen for fuel temperatures up to 350°C but above this temperature it is necessary to employ hot traps containing zirconium at 600°C to achieve lower oxygen levels. Study of the zirconium-hydrogen system shows that at 600°C zirconium is not an effective hydrogen getter (Figure 7). The capacity of zirconium for hydrogen at this temperature is small until the partial pressure of the hydrogen is well above that required to embrittle the lower temperature regions of the niobium and vanadium fuel cans. However, from theoretical considerations zirconium at below 450°C should be a better getter for hydrogen. Experimental studies with zirconium below 450°C have shown that inhibition of hydrogen absorption takes place, due possibly to surface films of oxide on the zirconium, but that nickel plating of the zirconium is largely effective in overcoming this inhibition. Of the two alternatives, cold-trapping at 100°C or "hot" trapping at 450°C, for keeping the hydrogen in the liquid metal below levels causing embrittlement of the can metals, cold-trapping is the more attractive, both practically and economically.

The stages in the clean-up of the primary liquid coolant in D.F.R. for fuel temperatures reached at power levels up to 60 MW will therefore be as follows.

1. Operations of cold traps at 100°C for removal of both oxygen and hydrogen from the NaK for fuel can temperatures up to 350°C.

2. Isolation of these cold traps from circuit, introduction of hot traps containing zirconium at 600°C for oxygen control, and clean cold traps to be operated at 100 to 120°C for hydrogen control.

NITROGEN, OXYGEN, AND CARBON IN THE PRIMARY COOLANT

Vanadium and niobium are known to react with nitrogen, oxygen, and carbon at elevated temperatures to form compounds with these elements. This section of the paper summarizes the available data on the effects of the presence of these elements in the primary coolant of the D.F.R. on niobium and vanadium.

Nitrogen and the Fuel Can Metals

At temperatures of 300 to 350°C both niobium and vanadium are known to

react slowly with gaseous nitrogen, but reaction is rapid at temperatures of 500 to 600°C. The presence of nitrogen in these metals is deleterious, leading to embrittlement of the metal; it has been found, for instance, that 1800 ppm of nitrogen causes embrittlement of vanadium at room temperature[12]. The partial pressures of nitrogen in equilibrium with the stoichiometric nitrides of niobium and vanadium are extremely low (NbN, 10^{-34} atmospheres at 300°C and 10^{-20} ats. at 600°C; VN, 10^{-24} and 10^{-12} at the corresponding temperatures). These are to be compared with a partial pressure of $10^{0.5}$ atmospheres when nitrogen is used as blanket gas or $10^{-3.5}$ atmospheres for argon blanket gas containing 100 vpm nitrogen as impurity.

Experiments at D.E.R.E. have shown that at slow liquid metal flow rates niobium or vanadium immersed in NaK under a nitrogen blanket gas are not attacked by nitrogen at temperatures below 350-400°C. Uptake of nitrogen by vanadium appeared to commence at about 400°C and samples showed uptake of 600 ppm in six days; no uptake of nitrogen by niobium was found at this temperature. As the temperature rose the uptake of nitrogen by vanadium increased and niobium also showed signs of uptake of nitrogen when immersed for five days at 550°C. These experiments, conducted in a hot test facility in the reactor when the reactor was being cold-trapped at 100°C, showed a plugging temperature near 120°C and a bulk liquid metal temperature of 160°C.

Experience in America indicates that steels immersed in sodium will nitride at temperatures above 450°C when nitrogen is used as a cover gas[13]. It would be expected that steels would be less susceptible to nitriding than vanadium or niobium since a much higher partial pressure is required in the formation of iron nitride (10^{3} atmospheres at 300°C for Fe_4N compared with 10^{-34} for NbN).

There are three means whereby nitrogen can reach the fuel can surfaces via the liquid metal:

1. By direct entrainment of small gas bubbles into the liquid metal
2. By compound formation with NaK
3. By compound formation with impurities in the NaK.

In the case of entrainment, nitriding of cans could occur if the entrained bubbles reach the surface of the cans and remain there for an appreciable length of time. Compound formation between nitrogen and NaK may occur under the influence of radiation. Compounds of alkali metals such as azides and nitrides have been formed by the reaction of these metals with nitrogen which has been activated by an electric discharge[14], and it may well be that a similar mechanism would be operative if the electrical discharge was replaced by a radiation field. Compounds formed in this manner would readily dissociate at temperatures of 300°C and upwards releasing nitrogen throughout the liquid metal including those surfaces in contact with the fuel cans. Compounds of nitrogen with impurities have been reported as being responsible for the nitriding of steels[15] but the evidence for this is not completely conclusive.

Since the rate determining step in the nitriding of fuel cans is probably the entry of nitrogen into the liquid metal from the blanket gas, the changeover to an argon blanket gas which is being made in the Dounreay Fast Reactor should minimize the problem. The use of commercial argon or helium in America seems to have eliminated the problem of nitriding of steel. The use of zirconium near 600°C in the reactor circuit as a getter for oxygen should be an additional safe-

guard in that zirconium should function as an excellent getter for nitrogen in these temperature regions provided inhibition of absorption by surface films does not occur.

Oxygen and the Reactor Metals

The presence of oxygen in the liquid metals of the primary circuit is known to be deleterious since both niobium and vanadium are oxygen corroded in this medium. Work at Culcheth Laboratories in loop experiments has shown that corrosion of niobium and vanadium at 350°C does not exceed 10^{-4} in. per month in a flowing circuit which is being cold-trapped at 140°C (using the Culcheth data for oxygen solubility [16] (Figure 9), this represents an oxygen content of about 6 ppm). Using a zirconium getter at 600-650°C, niobium and vanadium fuel cans may be operated in a liquid metal up to temperatures of 600°C without encountering oxygen corrosion problems.

If oxygen enters the lattice of the metals niobium and vanadium it can lead to embrittlement of these metals. Loonis[12] showed that 1500 ppm of oxygen can give rise to embrittlement in vanadium at room temperatures while according to workers at Oak Ridge embrittlement of niobium at room temperatures can be caused by 3000 ppm of oxygen. Since the niobium outer can is the structural portion of the element and a decrease in its mechanical ductility could be serious, some experimental work has been done on the possible embrittlement of niobium in liquid NaK.

Experiments were conducted with specimens of niobium immersed in the NaK primary circuit of the Dounreay Fast Reactor, under conditions of a bulk NaK temperature of 160°C and plugging temperatures of 120-130°C. These experiments showed no uptake of oxygen up to a temperature of 600°C (Table II).

CONCLUSIONS

The presence of hydrogen in the primary coolant of the Dounreay Fast Reactor can lead to embrittlement of the niobium and vanadium fuel cans. This hydrogen can be effectively controlled by cold-trapping the primary coolant near 100°C. When the reactor is being hot-trapped by zirconium, to allow fuel elements to operate at temperatures up to 600°C without oxygen corrosion, a cold-trap is still essential for hydrogen control.

The Dounreay Fast Reactor was designed to operate with a nitrogen blanket gas at a pressure of 50 psi. More recent work has indicated that at temperatures above 400°C vanadium can take up nitrogen and above 550°C niobium can take up nitrogen from a liquid metal coolant if a nitrogen blanket gas is used. To minimize a possible nitriding of these metals it has been decided to change to argon as a blanket gas in the D.F.R.

Control of oxygen levels in the primary coolant can be achieved by operation of a cold trap at 120°C for niobium and vanadium can temperatures up to 350°C and by a hot trap containing zirconium at 600 to 650°C for can temperatures above 350°C. No evidence for embrittlement of niobium has been found in experiments conducted at niobium temperatures up to 600°C in a test facility in the D.F.R.

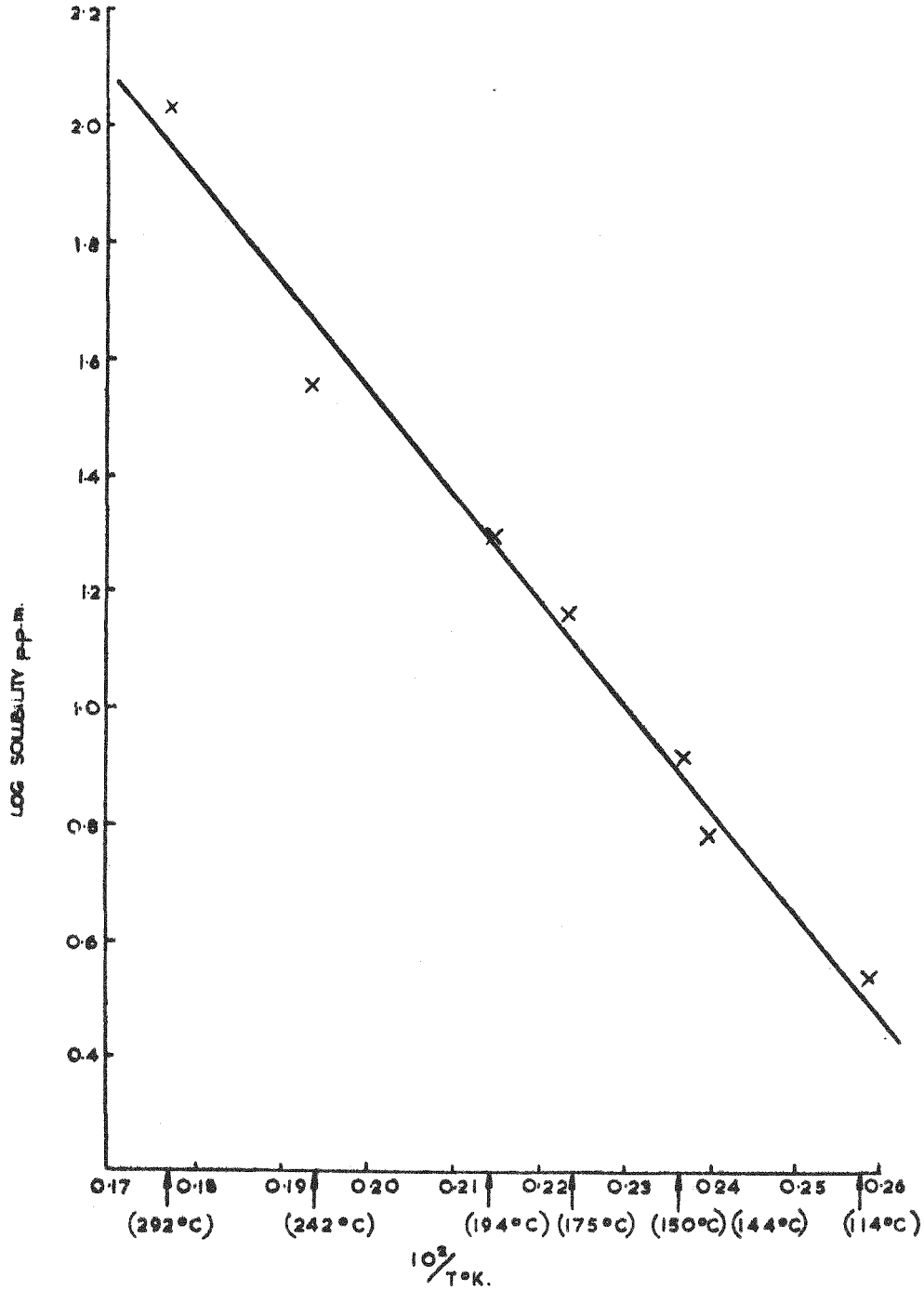

FIG. 9 SOLUBILITY OF OXYGEN IN SODIUM OVER THE TEMPERATURE RANGE 100-300°C.

TABLE II

OXYGEN UPTAKE BY NIOBIUM TEST PIECES

Temperature (°C)	Time (days)	Oxygen Content of Specimens (ppm w/w)
Starting Material		200
		80
		150
		220
		130
		210
275	21	220
300	10	240
350	13	300
400	7	510
450	9	460
550	25	310
600	5	270
650	6	170

Niobium and vanadium are attacked at high temperatures by carbon in a liquid metal circuit, the attack leading to the formation of carbides on the surface of test specimens. This only becomes a problem for reactor power levels approaching the ultimate design figure and control of the carbon content in the primary circuit of the D.F.R. may then be necessary.

REFERENCES

1. C. J. Turner and L. R. Williams, Proc. of Second U.N. Inter. Conf. on the Peaceful Uses of Atomic Energy, Vol. VI, p. 486 (1958); H. Cartwright, J. Tatlock, and R. R. Matthews, Proc. of Second U.N. Inter. Conf. on the Peaceful Uses of Atomic Energy, Vol. IX, p. 316 (1958).

2. Symposium on the Dounreay Fast Reactor, December 1960, Institute of Mechanical Engineers, London.

3. M. D. Banus, The Sodium-Sodium Hydride-Hydrogen System at 500-600°, J. Am. Chem. Soc., 77: 2007 (1955).

4. A. Herold, Tensions de Dissociation de Hydrures Alcaline, Comptes Rendus 228: 686 (1949).

5. K. Komjathy, The Niobium-Hydrogen System, Journal of the Less Common Metals, 2: 466 (1960).

6. W. M. Albrecht, W. D. Goode,and M. W. Mallett, Reactions in the Niobium System, J. Electrochem. Soc., 105: 219 (1958).

7. D. D. Williams, J. A. Grand, and R. R. Miller, J. Phys. Chem., 61: 379 (1957); NRL-Memo-424.

8. Per Kofstad and W. E. Wallace, Vapor Pressure Studies of the Vanadium-Hydrogen System at Thermodynamics of Formation and of the Vanadium-Hydrogen Solid Solutions, J. Am. Chem. Soc., 81: 5019 (1959).

9. C. E. Ells and A. D. McQuillan, A study of the Hydrogen Pressure Relationship in Zirconium-Hydrogen System, J. Inst. Met. 85: 89 (1956).

10. E. A. Gulbransen and K. F. Andrew, Solubility and Decomposition Pressures of Hydrogen in Alpha-Zirconium, J. of Met., 7: 136 (1955).

11. C. Tyzack, Culcheth Laboratories, U.K.A.E.A., personal communication.

12. B. Loonis, Brittle-Ductile Transition in Vanadium, Report ISC-1037, Iowa State College, March, 1958.

13. E. G. Brush, USAEC Report KAPL-M-EGD-21, 1955.

14. N. V. Sidgwick, The Chemical Elements and Their Compounds, Oxford University Press, p. 85, 1959.

15. R. L. Ashley, et al., SRE Fuel Element Damage Interim Report, USAEC Report NAA-SR-4488, November 30, 1959.

16. A. Thorley, Culcheth Laboratories, U.K.A.E.A., personal communication.

PREPARATION OF CERAMIC-COATED NUCLEAR-FUEL PARTICLES[a]

By J. M. Blocher, Jr., M. F. Browning,
A. C. Secrest, V. M. Secrest, and J. H. Oxley

Battelle Memorial Institute, Columbus, Ohio

INTRODUCTION

As operating temperature levels are raised, metals lose their utility as fission-product retentive-cladding materials for nuclear fuels. Thus, if we are ever to have high-temperature power reactors for more efficient indirect conversion of fission heat to electrical energy, we must find an adequate substitute for the metal claddings which have served so well at lower temperatures. The alternative is to "jump from the frying pan into the fire" and settle for a "dirty" coolant system.

This dilemma logically leads to the consideration of ceramics as cladding materials. However, two general characteristics of ceramic materials militate against their use. These are permeability and lack of ductility. It immediately becomes evident that ceramic cans cannot simply be substituted for metal cans.

General Atomic[1] plans to come close to this by employing a purge gas stream through an annulus between the graphite-canned fuel slug and the wall of the main coolant gas channel. In this way, the leaking fission products can be removed in a small-volume system and prevented from reaching the main coolant stream. However, this is a substitute for effective fission-product retention at the source.

In 1957 it was recognized, apparently by several groups independently, that coated particulate fuels might be the answer to this problem. As the size of the fuel element is decreased, and as its shape more nearly approaches spherical, the stresses developed for any reason in the coating decrease for a given coating thickness. The problem then becomes one of how to mass produce these miniature fuel elements with integral, impermeable, and stable coatings.

Fortunately, such a means is available in the form of chemical vapor-deposition reactions in a gas-fluidized or otherwise agitated bed of the fuel particles. It appears that almost any desired ceramic material may be applied

[a]This work was carried out under AEC Contract No. W-7405-eng-92.

in this way and, more important, a product may be obtained which is more dense than that obtained by normal ceramic techniques.

Although not directly related to the subject of this paper, a large variety of metal coatings may be applied similarly, and they are very useful as reaction barriers and for fission-product retention (See Paper No. 7). In fact, our own work with coated nuclear-fuel particles was initiated with metal coatings[2,3] and a large effort in that area has continued.

Any chemical vapor-deposition or "vapor-plating" reaction should be adaptable for fuel-particle coating, although the use of barrier coatings may be necessary in some cases to prevent reaction of the fuel material with reactants or products of the chosen coating reaction. Powell[4] in his book "Vapor Plating" reviews the reactions which were known up to 1955.

Interest in ceramic-coated nuclear-fuel particles increased sharply in early 1960 when their significant fission-product retention during irradiation was demonstrated. Since then, several Government laboratories and a large number of industrial firms have become active in the development of these materials. It is the purpose of this paper to review the progress of work at Battelle on coatings of alumina, beryllia, magnesia, and pyrolytic carbon.

METHOD OF PARTICLE COATING

For a reaction to be useful in chemical vapor deposition, all of the reactants and products but one must be gaseous at the deposition temperature, and the kinetics of the reaction must be reasonably favorable. The following have been used for the ceramic coating of nuclear-fuel particles.

$$Al_2Cl_6(g) + 3H_2O(g) = Al_2O_3(s) + 6HCl(g)$$

$$Al_2Cl_6(g) + 3CO_2(g) + 3H_2(g) = Al_2O_3(s) + 6HCl(g) + 3CO(g)$$

$$BeCl_2(g) + H_2O(g) = BeO(s) + 2HCl(g)$$

$$BeCl_2(g) + CO_2(g) + H_2(g) = BeO(s) + 2HCl(g) + CO(g)$$

$$MgI_2(g) + H_2O(g) = MgO(s) + 2HI(g)$$

$$ZrCl_4(g) + 2H_2O(g) = ZrO_2(s) + 4HCl(g)$$

$$2YCl_3(g) + 3H_2O(g) = Y_2O_3(s) + 6CHl(g)$$

$$2CrOCl_2(g) + H_2O(g) + H_2(g) = Cr_2O_3(s) + 4HCl(g)$$

$$CH_4(g) = C(s) + 2H_2(g)$$

$$C_2H_2(g) = 2C(s) + H_2(g)$$

Figure 1 is a schematic diagram of one piece of fluidized-bed apparatus used at Battelle for the alumina-coating of 100-gram experimental lots of UO_2-powder particles. The quantity of material handled in this type of equipment has been limited to about 100 grams, since this is a convenient quantity for preparation and evaluation.

Hydrogen, partially saturated with $Al_2Cl_6(g)$, is led into the bottom of the Vycor reactor through a preheater section. Water vapor in a carrier gas, or a mixture of hydrogen and CO_2, is introduced through an axial tube terminating in the fluidized bed where mixing of the reactants is permitted to occur. The bed of particles to be coated is supported on a conical bottom terminating in a pig-tail-shaped capillary to prevent drainage of the bed into the preheater. The walls of the reactor above the fluidized bed are held at bed temperature to minimize the deposition of Al_2O_3 "soot" and prevent condensation of unreacted aluminum chloride. Particles impinging on the wall in this area can adhere. This can lead to two problems: (1) removal of the particle from the reaction, and/or (2) pick-up of porous alumina before the particle falls back into the bed.

A 16-μ coating on a 120-μ particle requires a two-fold increase in bed volume. As the result of this expansion, particles hung up on the walls in the early stages can later be abraded off and returned to the bed. This results in non-uniform distribution of particle coating thickness.

Downstream of the fluidized bed are expanded sections and traps to permit disentrainment of soot which would otherwise plug exit lines. Finally, the reactant gas is passed through water to absorb the HCl by-product. Periodic titration of the resulting solution is used to monitor progress of the reaction.

In earlier alumina-coating work, a straight tube without a preheater section was used. This has the real disadvantages of (1) early plugging of the reactor by the 25 to 50 percent of alumina that is formed as soot, and (2) greater incidence of soot particles in the coating. A potential disadvantage is the fact that in a non-isothermal bed, temperature cycling of the particles can lead to internal strains in the coating. This appears to be a significant effect in the case of MgO coatings on UO_2 where a greater thermal expansion differential exists between the base and coating.

Coatings of BeO, ZrO_2, Y_2O_2, and Cr_2O_3 have been prepared in apparatus similar to that used for the Al_2O_3 work, with the halides fed into the bottom of the reactor and the hydrolyzing agent fed in at the top. However, for the preparation of MgO coatings, the problem of the low volatility of the halides prompted the use of the fluidized bed itself as a flash vaporizer for the halides fed as a solid. In this case, wet hydrogen was fed into the bottom of the reactor while solid MgI_2 particles about 1 mm in diameter were fed from a vibrating hopper into the bed. At a bed temperature of 1000°C, the MgI_2 (m.p.= 634°C, b.p. = 1020°C) required about 0.5 second to vaporize, as indicated by the behavior of those particles which hit the wall, well down into the lower third of the bed.

Pyrolytic-carbon coatings are prepared by the thermal decomposition of hydrocarbons, usually methane or acetylene. One of the reactors used in the carbon-coating work is shown in Figure 2. This unit, consisting of an induction-heated graphite tube, can be used at least up to 2000°C. A mullite tube reactor in a Globar furnace is used up to 1450°C.

An induction-heated rotating-barrel coater was investigated for the application of pyrolytic-carbon coatings above 1500°C. However, its use was abandoned because of the particle-to-particle non-uniformity of coating thickness. The fluidized bed is believed to be superior in averaging the

contacting of particles with the reactant vapors.

In the one-inch-diameter experimental fluidized-bed units described here, the rate of fluidizing gas flow used will vary from 2 liters(S.T.P.) per hour for CO_2 particles 50μ (0.002-in.) in diameter to 100 liters per hour for those 1500μ (0.06-in.) in diameter. The same conical bed-support geometry has been successfully used in a 3-inch-diameter reactor and with some modification in a 5-inch-diameter reactor. In applying niobium coatings to 2.5 Kg lots of 125-μ UO_2 in a 3-inch diameter reactor, a flow of 3000 liters (STP) per hour of hydrogen is used.

Al_2O_3 COATINGS

Figure 3 is a macro view of alumina-coated particles under oblique lighting which reveals the transparency of the coating.

The temperature of deposition is the most effective variable in determining coating properties. However, the rate of deposition and the presence of impurities are very significant. Figure 4 contrasts the structure and properties of alumina coatings prepared by the steam hydrolysis of Al_2Cl_6 vapor under a variety of conditions.

Coatings deposited at temperatures from 500°C to about 900°C are amorphous or may contain γ and K Al_2O_3. They are porous and have 50 to 80 percent of the density of sapphire. Above 900°C the coatings become translucent, more dense, and begin to show α-alumina crystallites in X-ray diffraction. In the range of about 900°C to 1000°C, these crystallites range in size from 0.05 to 1μ. In many samples prepared in this range, the α-crystallites appear to be embedded in a glassy matrix.

At deposition temperatures above about 1100°C, the deposits are more coarsely crystalline and grain boundaries can be seen to extend radially through the coating. Petrographic examination of thin sections has indicated preferred orientation in the crystalline coatings, with the c axis lying perpendicular to the radius. Confirmation by X-ray diffraction is pending. Additional preferred orientation is noted in the "spikes" or surface protrusions which are formed under some conditions. However, this has not been fully characterized.

Particular attention should be given to the material represented by the particle in the middle of the upper row of Figure 4. About 500,000 particles from this lot were incorporated into a graphite sphere of the type developed by Sanderson and Porter for the Pebble Bed Reactor. This sphere was irradiated in the Battelle Research Reactor to a burnup of 6 percent of the U^{235} over a period of 160 days at an average temperature of 700°C. The ratio of fission gas released to that generated was initially very low and rose slowly during the experiment, e. g., from 10^{-7} to 10^{-2} for Xe^{133} which had the greatest release rate[5].

Figure 5 shows what is believed to be the principal reason for fission-gas release, that is, cracking of about 3.5 percent of the coatings. This points up the importance of coating strength, and the determination of the mechanisms of stress development in the coatings. In this connection, it is interesting to note the behavior of a composite coating consisting of a dense 1000°C coating over a layer of the amorphous 700° variety. Crystallization of the amorphous

coatings at elevated temperatures (48 hours at 1100°C) invariably results in rupture of the dense outer coating. This fact is disappointing in that it was hoped that porous Al_2O_3 could be used as a fission-product sump or as a stress-relieving barrier. On the other hand, the observation is encouraging in that the behavior of the particles in the irradiation test described above may have been markedly better had it not been for the accidental inclusion of a layer of "porous" material in the preparation of the coatings. Many more cracks were observed in the outer layer of dense alumina than in the less dense inner layer. This suggests radiation-induced or thermally induced changes in the porous layer as a possible major source of damage.

Irradiation tests of fully dense coatings now getting under way should shed light on this question.

It should be noted here that the "porosity" shown in the amorphous layers of alumina coating is exaggerated by normal polishing techniques which remove portions of the softer material from the surface. Actually, the porosity is on a submicron scale, as indicated in Figure 6, which contrasts the large-grained UO_2 with adjacent layers of dense and porous Al_2O_3.

Recent effort has been concentrated on the evaluation of coatings prepared at higher temperatures (1100 to 1400°C) which presumably would be more stable than those prepared at 1000°C. Unfortunately, these coatings have been contaminated with 0.1 percent of 1.5% silicon, apparently by corrosion of the quartz and mullite reactors used thus far. Like contaminated coatings prepared at 1000°C, they have been free of spines or surface protrusions. The strength of the high-temperature coatings, as indicated by crushing tests on individual particles, has been lower than that of the 1000°C coatings, although both coatings are as hard as sapphire. The explanation of the lower strength may lie in the weakness of the bond between the radial grains. The significance of this factor is being studied.

BeO COATINGS

Like those of crystalline alumina, only the contaminated coatings of BeO have been free of surface protrusions. Of probably greater significance is the fact that only the contaminated coatings (0.1 to 2 percent silicon or aluminum, or 2 percent carbon) have been dense and transparent as well as being relatively smooth.

Coatings prepared by hydrolysis of $BeCl_2$(g) at temperatures of from 700 to 1100°C (uncontaminated by transfer of materials from the $BeCl_2$ feed or from the reactor) have been porous, having densities as low as 40 percent of theoretical and with a spiny surface in thicknesses above 20μ (See Figure 7). An answer as to whether uncontaminated coatings prepared at higher temperatures will be dense awaits the redesign of equipment to prevent transfer of corrosion products.

Coatings prepared by thermal decomposition of beryllium basic acetate at temperatures of from 500 to 900°C have been contaminated with carbon (2 to 8%) despite their smoothness and apparent high density. Coatings prepared either from the chloride or from the basic acetate at lower temperatures, e. g., 500°C, in the presence of water vapor contain hydroxy residues which are removed as water vapor on heating to higher temperatures under vacuum.

On the basis of recent observations regarding possible growth mechanisms of porous coatings, additional modifications of the process will be studied. It is hoped that these will lead to the preparation of BeO coatings equivalent to those of Al_2O_3 in density, without having to introduce the complication of adding contaminants as another variable.

MgO COATINGS

The addition of MgI_2 granules of a bed of UO_2 particles fluidized by moist hydrogen at 1000°C was found to be quite effective as a method of coating the UO_2. About 70 percent of the MgI_2 was converted to oxide on the particles. The coatings were translucent and of uniform thickness. However, the coating developed visible cracks, apparently the result of differential shrinkage, on cooling to room temperature. Coatings were applied to particles which were subjected to oxidation with and without intermediate cooling to room temperature. Exfoliation of the failed particles was a clear indication of oxidation. These tests indicated that differential contraction was indeed a problem, and that uncracked MgO coatings offered significant protection against oxidation of the UO_2. It is believed that this problem can be circumvented and that suitable specimens can be prepared for evaluation in radiation.

PYROLYTIC-CARBON COATINGS

Shortly after the encouraging fission-product retention results were obtained for the alumina-coated particles, pyrolytic-carbon coatings were investigated for General Atomic's Peach Bottom Reactor[1] and Sanderson and Porter's Pebble Bed Reactor [5]. The fission-gas retentivity of pyrolytic-carbon coatings was similar to that of alumina coatings, as evidenced by fission gas release on post-irradiation heating. Figure 8 gives typical results.

Figures 9 and 10 show two types of pyrolytic-carbon coatings obtainable.

As would be expected, the properties of pyrolytic-carbon coatings vary with the conditions of preparation. Higher temperature and lower rates of deposition favor the more dense columnar structure. Whether the most dense structure is most desirable remains to be seen. Other factors such as the "fit" at the grain boundaries must be considered. Large-grained vapor-deposited coatings have been deficient on this score in many cases. Another factor is the relative ability of the structures to propagate strains induced by radiation damage.

SUMMARY

The foregoing discussion indicates the promise of coated nuclear-fuel particles and the practicability of their fabrication. Their future in nuclear reactor technology will depend on how effectively we approach the problem of evaluating the multitude of variables introduced by their use.

Although functional coatings may evolve rapidly from the present effort, it is believed that years of development will precede their optimization.

ACKNOWLEDGEMENTS

I should like to acknowledge the work of Dale Vaughan in the areas of X-ray diffraction and electron microscopy, and the petrographic work of Jack

Lennon. Richard Burian is credited with the post-irradiation examination of the alumina particles in the SP-5 experiment. Harvey Rosenberg and Russel Barnes are responsible for the fission-gas release data on post-irradiation heating. The advice and interest of Dr. R. W. Dayton is also gratefully acknowledged.

REFERENCES

1. General Atomic Division, General Dynamics Corporation, 40 MW (E) Prototype High-Temperature Gas-Cooled Reactor Research and Development Program, USAEC Report GA-1640, April 1960.

2. J. H. Oxley, J. F. Hannah, J. M. Blocher, Jr., and I. E. Campbell, Coating of Uranium Dioxide Powders with Metallic Tungsten Films, USAEC Report BMI-1297, October 8, 1958; Ind. Eng. Chem., 51: 1391 (1959).

3. J. M. Blocher, Jr., N. D. Veigel, J. H. Oxley, V. M. Secrest, and E. R. Rose, Fluidized-Bed Coating of UO_2 Powder with Niobium and Other Elements, USAEC Report BMI-1440, May 25, 1960.

4. C. F. Powell, I. E. Campbell, and B. W. Gonser, Vapor Plating, John Wiley and Sons, Inc., New York, 1955.

5. Sanderson and Porter Company, Fuel Element Development Program for the Pebble Bed Reactor Final Report, USAEC Report NYO-9064, April 30, 1961.

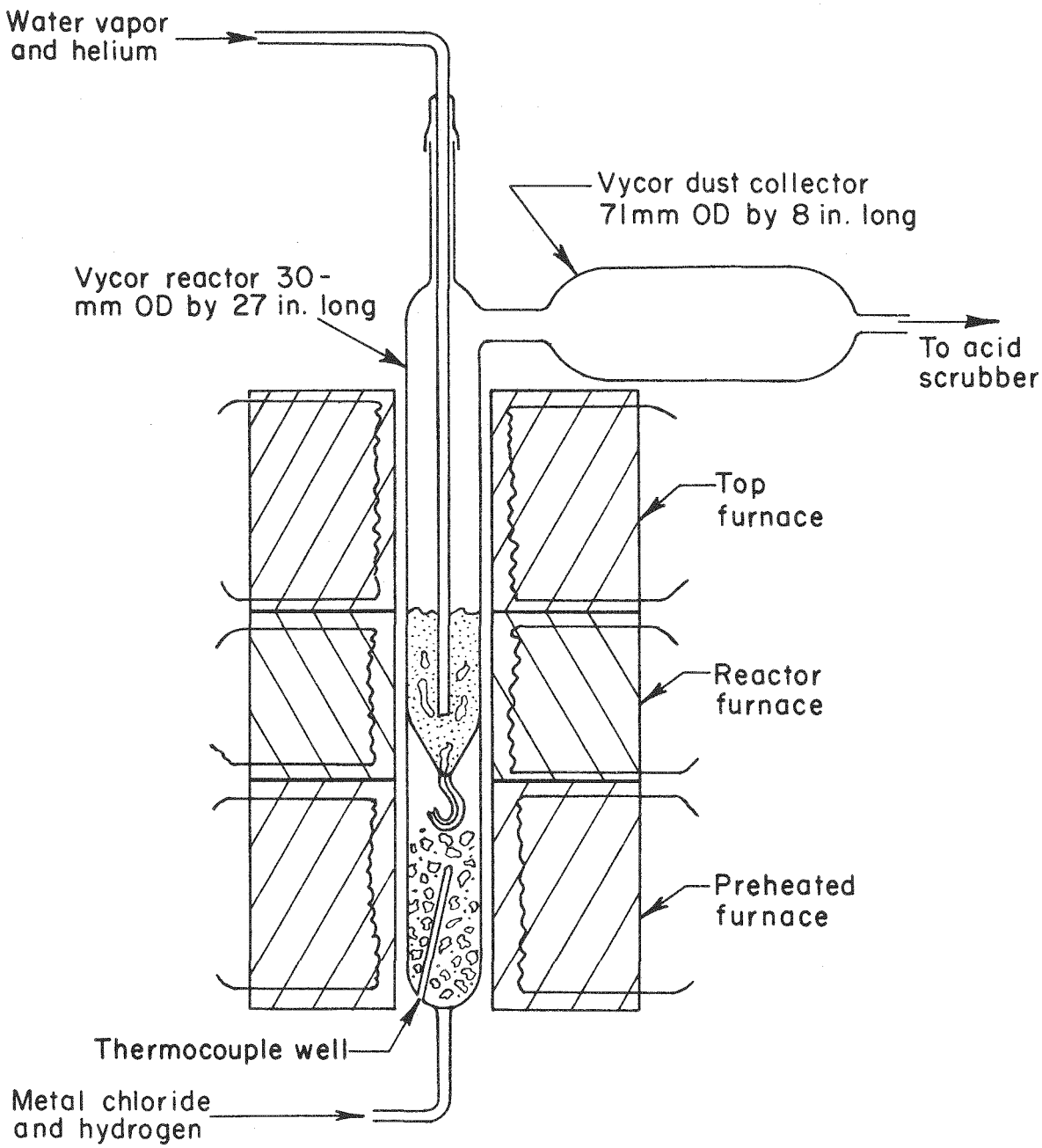

Figure 1. Fluidized-Bed Unit for Alumina Coating of Fuel Particles. (N-82686)

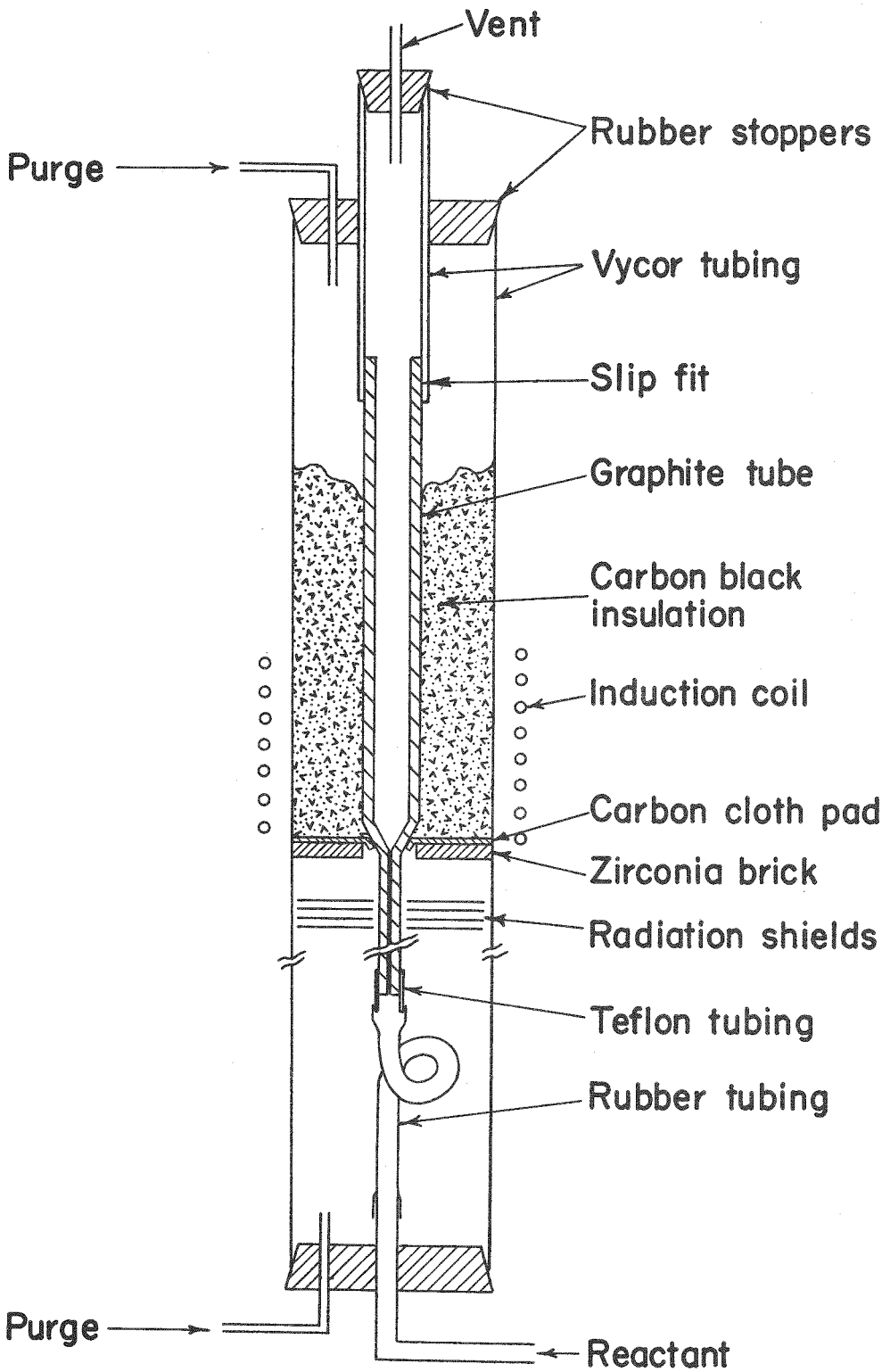

Figure 2. Induction-Heated Fluidized-Bed Unit for Prolytic-Carbon Coating. (N-82982)

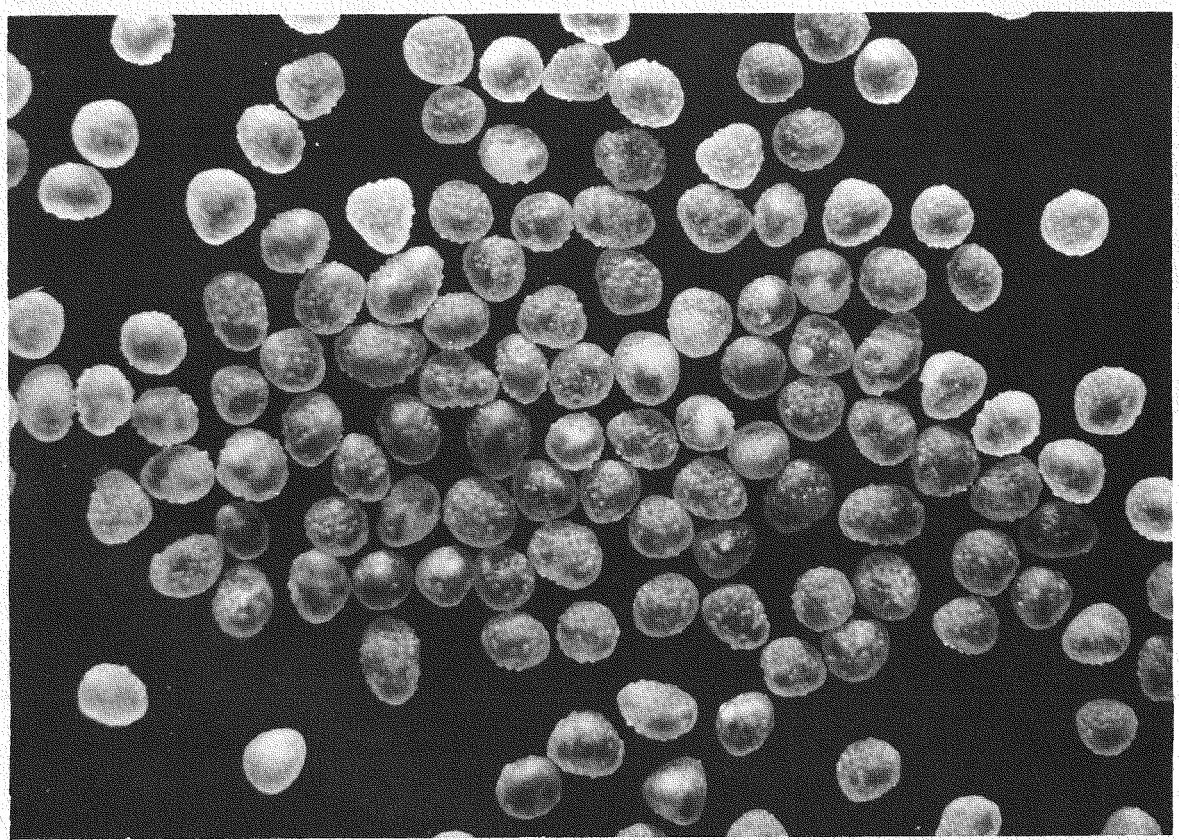

Figure 3. 125- UO_2 Particles Coated with 35 of Al_2O_3 at 1000°C. (N-76006)

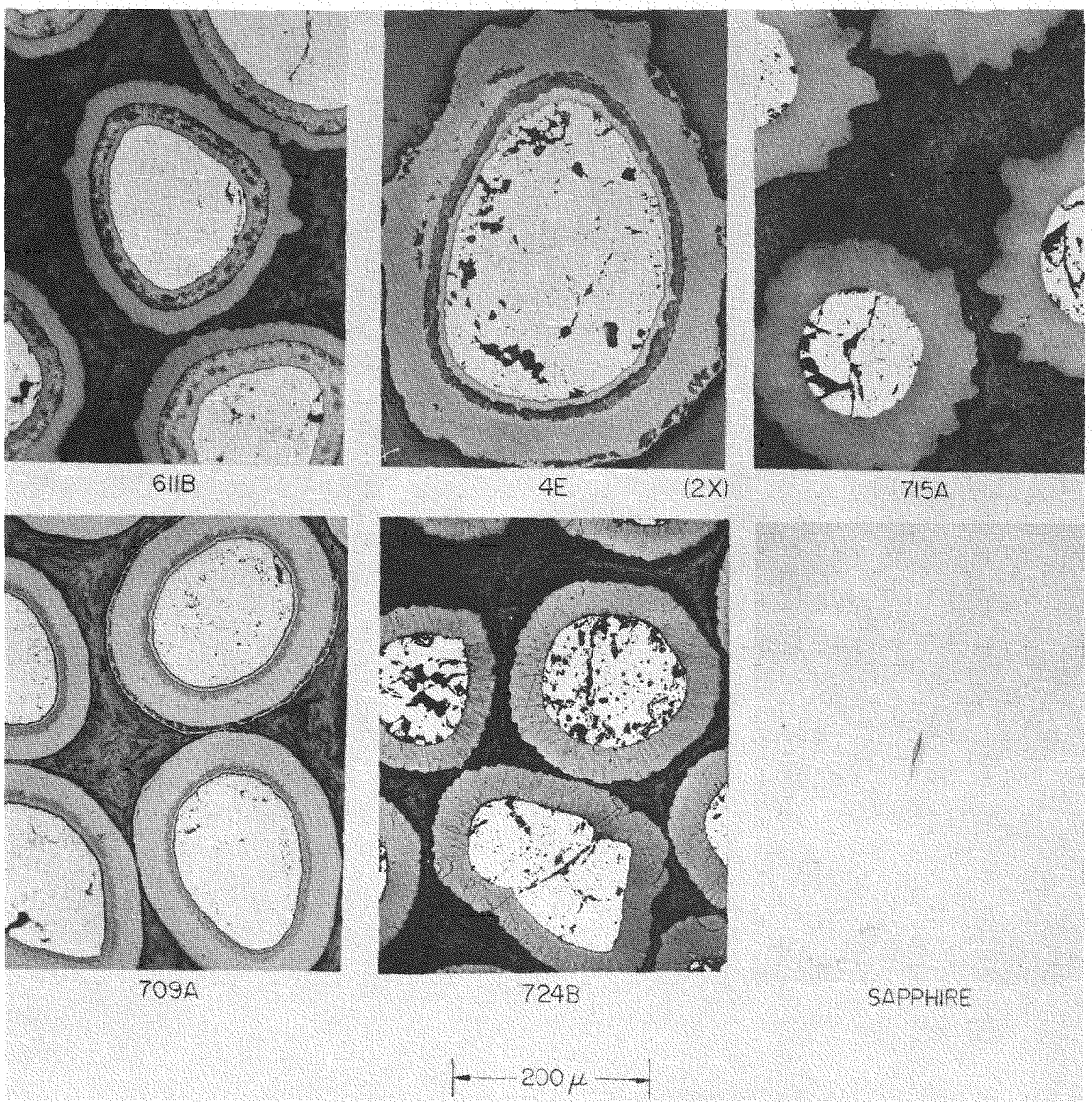

Figure 4. Al_2O_3-Coated UO_2

Lot 611B	Porous 700°C. coating between layers of dense 1000°C. coating.
Lot 4E	Six-step, nominal 1000°C. coating. (Material for SP-5 capsule experiment)
Lot 715A	Two-step, 1000°C. coating.
Lot 709A	Contaminated 1000°C. coating (6000-ppm. Si, 2000-ppm. Mg)
Lot 724B	Three-step 1400°C. coating.

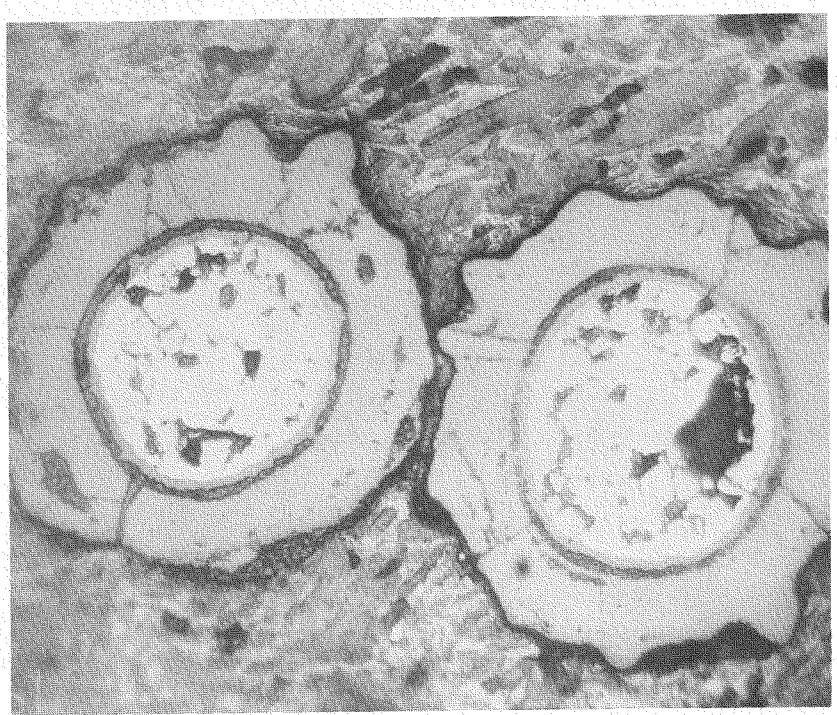

Figure 5. Typical Failed Particles from Lot 4E After Irradiation to 6 per cent Burn-Up of U^{235} in 160 Days at 700°C.

Figure 6. Electron micrograph of Al_2O_3-Coated UO_2 (Lot 4E). (N-79982)

Bottom, UO_2
Middle, dense Al_2O_3
Top, porous Al_2O_3

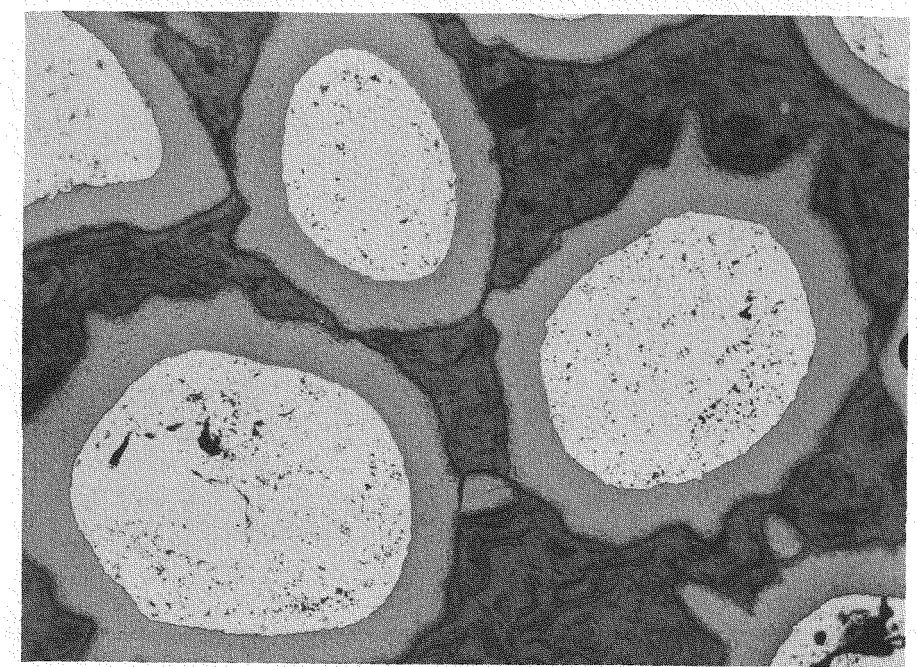

Figure 7. BeO-Coated UO_2.

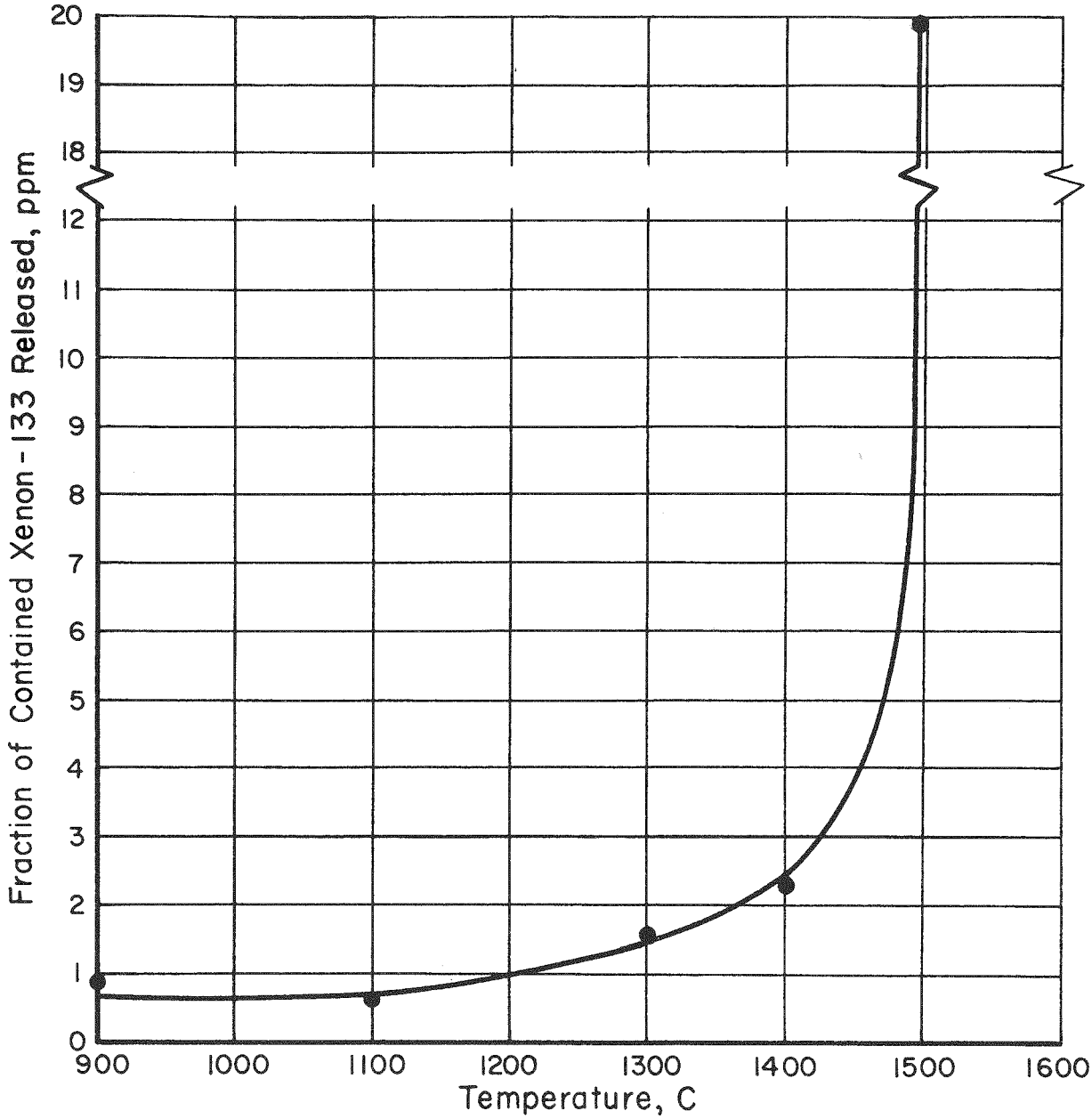

Figure 8. Xenon^{-133} Release Characteristics of Carbon-Coated UO_2 Particles after Neutron Activation. (N-82690)

38 μ of carbon on 127 μ diameter UO_2.

Particles held approximately 2 hours at each temperature level.

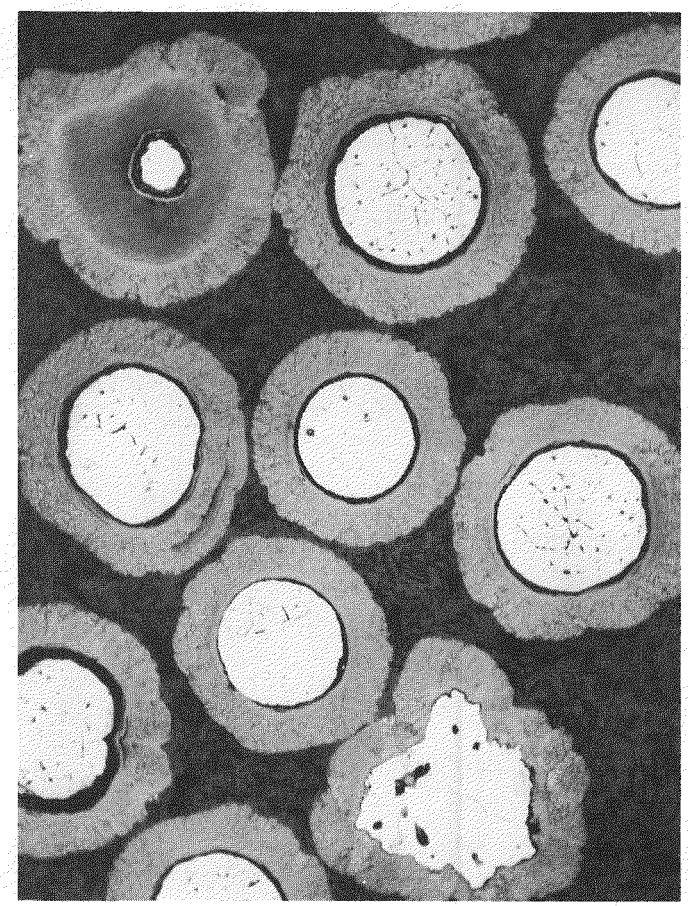

Normal Illumination. (N-78859)

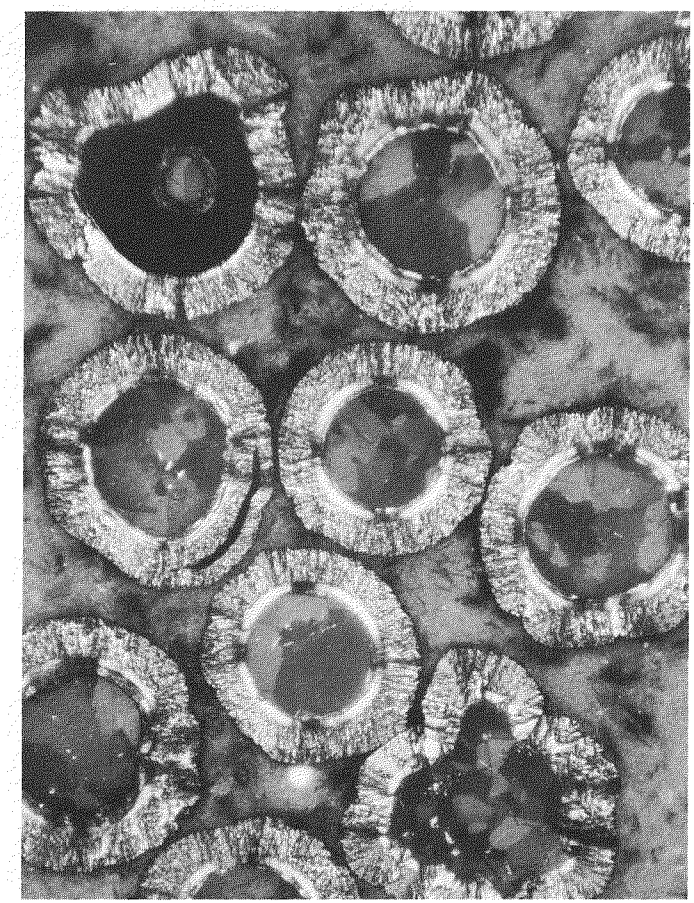

Polarized Light. (N-78860)

Figure 9. Pyrolytic Carbon-Coated UC_2, Columnar Coating.

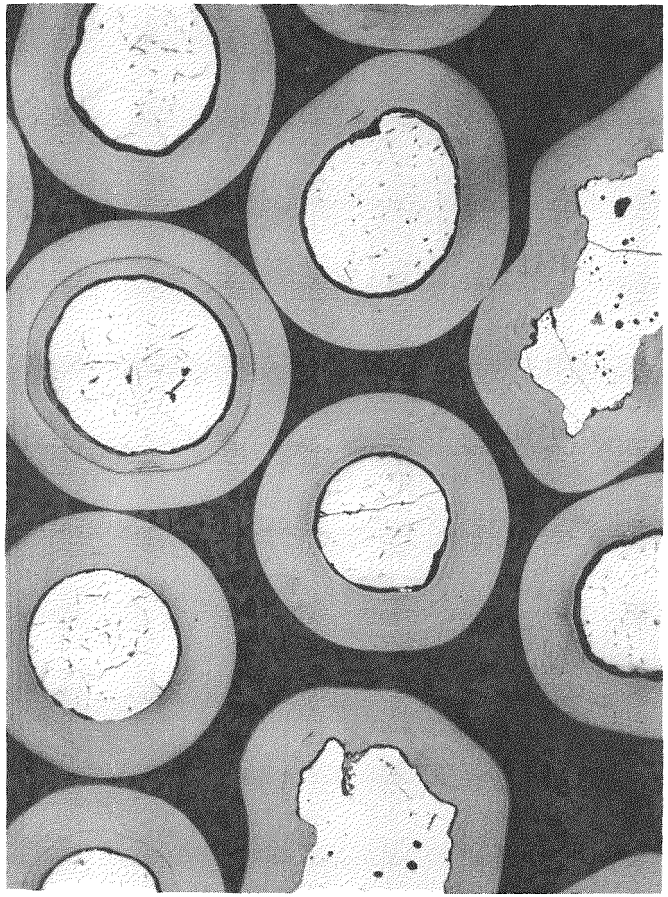

Normal Illumination. (N-78861)

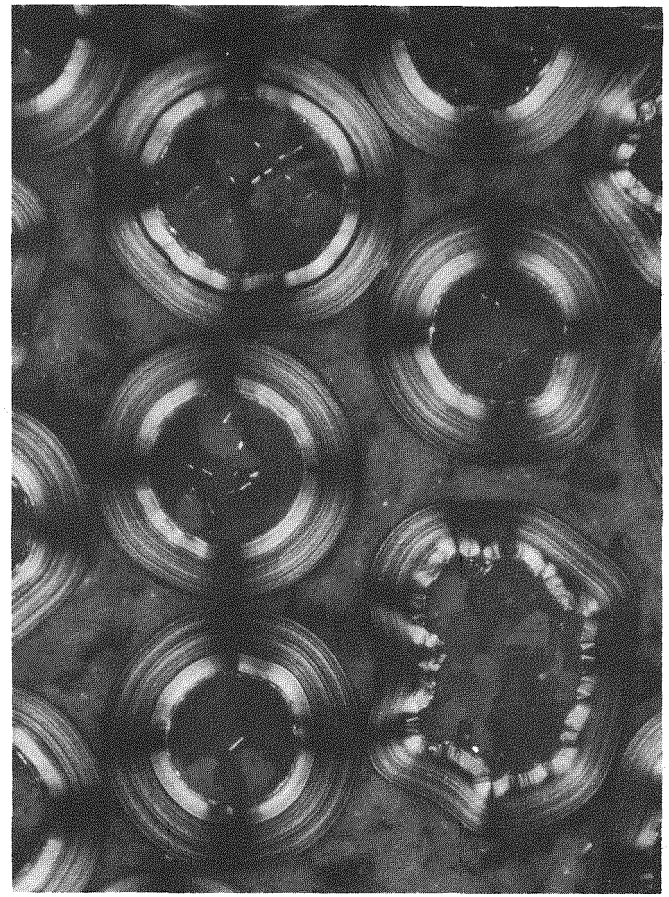

Polarized Light. (N-78862)

Figure 10. Pyrolytic Carbon-Coated UC_2, Laminar Coating.

INVESTIGATIONS OF NUCLEAR FUEL-BEARING GLASSES[a]

By Paul A. Lockwood

Physics Research Laboratory
Owens-Corning FIBERGLAS Corporation
Technical Center, Granville, Ohio

In 1956, Owens-Corning Fiberglas Corporation produced samples of fibrous glass containing small amounts of uranium oxide for Rensselaer Polytechnic Institute to use in chemo-nuclear process experiments. The development of glass compositions containing varying amounts of urania and having different physical and chemical properties was initiated to supply further samples as the chemo-nuclear process experiments became more sophisticated. From the knowledge of the properties of these glasses, additional use concepts were considered and the program was expanded to cover glass compositions containing oxides of uranium, thorium, plutonium, and combinations of these fuel materials.

During the past three years, the development of nuclear fuel-bearing glasses has continued with two objectives. The first objective is to determine the maximum amount of fuel materials that can be contained in glasses and to produce glass compositions which have varying physical and chemical properties. This requires a system of screening the various glass compositions to find those most suitable for forming into fibers. Glasses with forming characteristics suitable for fiberizing can usually be formed readily into massive objects. The best glasses are then formed into fibers for study of the chemical and physical properties. The usual properties investigated are the liquidus and softening point temperatures of the glasses, density, tensile strength, and chemical durability of the fibrous glass. The second objective of the investigations is to supply samples of radioactive fuel-bearing glasses to interested AEC contractors.

It is obvious that the development of new glass compositions can involve the investigation of an infinite number of slightly varying compositions. It is therefore important that a selection method be used which will rapidly screen out the unsatisfactory compositions. The method for doing this accepted in the fibrous glass industry involves producing about ten grams of each glass. Batch materials used in commercial glass making are utilized with the exception that

---

a. This work was performed by Owens-Corning Fiberglas Corporation under Rensselaer Polytechnic Institute Subcontract 441.37-1 and AEC Prime Contract AT-(30-1)-2489.

all are -200 mesh which favors rapid melting and earlier achievement of homogeneity. After the fuel material has been thoroughly mixed with the rest of the batch material, it is placed in a small platinum crucible and melted at 2650°F for 45 minutes in a gas-fired furnace. After the first melting operation, the crucible is quenched in water, the glass is pulverized, mixed, and remelted. If the first melting is incomplete, the remelt is usually at 2850°F instead of 2650°F but otherwise the cycle is simply repeated. Where the fuel material is near the limit of solubility, a third remelting is added to try for complete solution of the fuel material.

Assessment of the glass for fiberization capability comprises several techniques of which the simplest is to visually observe the glass for excessive crystalline material. For fuel-bearing glasses this is somewhat more complicated than usual. Such glasses quite often are exceedingly dark in a massive form and crystalline material cannot always be determined by visual observation even with a binocular microscope. The next selection technique comprises a fiberizing test consisting of melting a pea-size piece of cullet on a heated platinum alloy strip. A platinum probe is used to attempt to draw a fiber from the melt. By means of this test a trained technician can determine the melting temperature of the glass, the approximate fiberizing temperature of the glass if the fibers can be formed, the devitrification tendency of the glass, and lastly an approximation of the surface tension of the glass. This test proved to be the most important sorting technique although glasses which passed this test but were marginal were tested for viscosity range versus temperature and rate of devitrification.

Using this method we have investigated many compositions in the following three ternary systems: U_3O_8-SiO_2-Na_2O; ThO_2-SiO_2-Na_2O; and U_3O_8-SiO_2-Al_2O_3. The ternary system of U_3O_8-SiO_2-Na_2O (Figure 1) was studied because it appeared to have the most promise for producing glasses. The silica-soda binary compositions are well known and glasses usually can be produced when modified by addition of small to moderate amounts of other materials. A second reason for studying urania-bearing glasses is that depleted urania can be used for a long series of laboratory experiments and irradiation samples can be made by a direct substitution of enriched urania for depleted urania.

In Figure 1 there are two general areas: one represents glasses directly formable into usable fibers and the second area represents fiberizable glasses which can be leached. The first area was examined for compositions with maximum urania content and to determine which compositions would be most suitable for fiber forming. A glass with the composition of 50 weight percent U_3O_8, 10 weight percent soda, and 40 weight percent silica produced one of the better fiber forming glasses and had the highest urania solubility. Attempts to produce glasses containing more than 50 weight percent U_3O_8 in this ternary system were not too successful. There is also a glass down in the area of 35 weight percent U_3O_8, 10 percent soda, 55 percent silica which was a fairly good glass but not quite what was desired. For this reason the composition was modified by replacing 5 percent silica with 5 percent calcium oxide. This composition is designated as RX-78 glass which has been used quite extensively for experimentation throughout the program. Other compositions were melted in which all or part of the soda was replaced by lead oxide, barium oxide, zinc oxide, or potassium oxide. In some instances calcium oxide, magnesium oxide, aluminum oxide, or zirconium oxide was substituted for part of the silica. The last materials loosen up the silica network to produce glasses of widely varying properties. All the oxides used have low thermal neutron macroscopic absorption cross sections. Large amounts of boron oxide, which is one of the favorite modifying

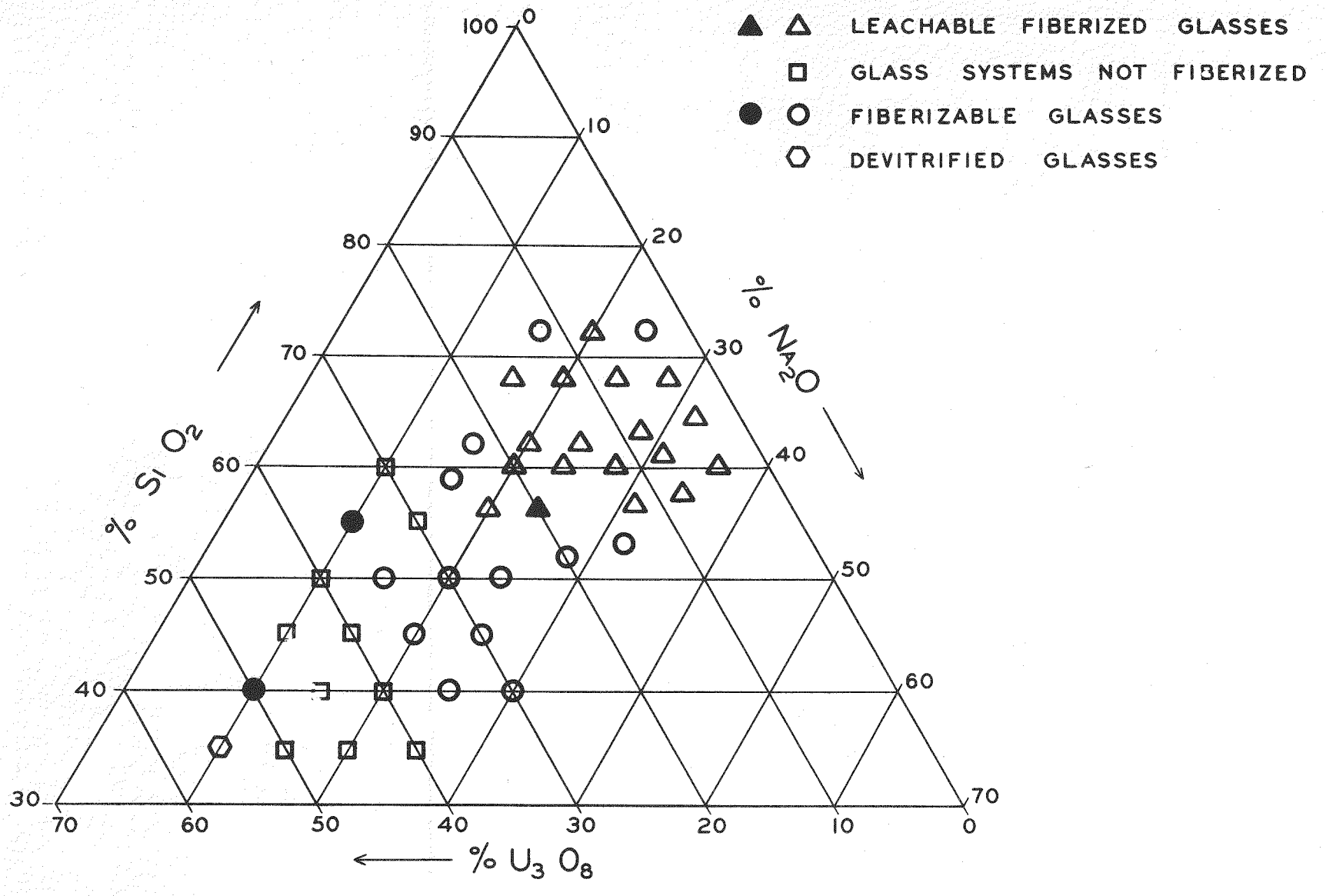

FIG. 1 URANIA - SILICA - SODA TERNARY

39482

agents for glasses, were not used obviously because of their high thermal neutron macroscopic absorption cross section which was true of many other oxides with large cross sections. A few glasses were made containing small amounts of boron oxide for experiments with a burnable "poison."

The leaching of urania glasses shown in Figure 1 was undertaken in order to produce glass fibers more refractory than was possible by formation from molten glass. These more refractory glass fibers were produced in the following manner. Fibers containing a large amount of soda and a moderate amount of urania were first fiberized and then leached with various acids to remove most of the soda. It is a well-known fact that the silica-soda glasses can be leached to remove the soda and the resulting porous network of silica can be fired at moderate temperatures to compact the almost pure silica into a solid body which could not be formed readily in a more direct manner. In the case of some multi-component glasses, various constituents can be leached out more or less selectively. In other words, the rate of leaching varies for the different constituents.

This selective leachability was utilized in the soda-urania-silica glasses, whose compositions are indicated by triangles in Figure 1, to produce fibers which have a refractoriness far above that achievable with conventional fiber-forming equipment. This is done by leaching out the soda and then stopping the leaching operation before the urania begins to leach. Like most chemical processes, this is actually a rate condition and a small amount of the urania is leached while a small amount of the soda is left in the glass. These amounts are only about one percent of the original constituents. An example of this is RX-137 glass which initially contained 25 percent soda and 20 percent urania, but after leaching this glass consisted of approximately 67 percent silica and 33 percent urania. After firing, these fibers have a softening point above 2300°F.

The thoria-silica-soda ternary (Figure 2) was also studied. We found that the thorium oxide had a much more limited solubility in that only approximately 30 percent thorium oxide could be incorporated in glasses studied in this ternary and that a glass with only 20 percent thorium oxide had the best fiber-forming characteristics. Glasses in this ternary were not as amenable to leaching treatments and results were far less successful than the urania glasses. A study of the quaternary using thorium oxide, uranium oxide, with silica and soda was made and a composition with 20 percent thorium oxide plus 20 percent uranium oxide had excellent fiber-forming properties.

The urania-silica-alumina ternary (Figure 3) was studied in an effort to produce more refractory fibers by direct forming. To study glasses in this ternary it was necessary to utilize a new high temperature forming system developed by Owens-Corning Fiberglas through its corporate research. The melting points of glasses studied in this system were above 3000°F, with some above 4100°F. Fibers have been formed with tensile strengths of 100,000 psi at 1600°F and softening points in the 2000-2400°F range. We hope to develop a glass in this system--or a modification of a glass in this system--which will have tensile strengths of 100,000 psi above 2000°F.

In addition to glass compositions in the three ternary systems mentioned above it was desirable to develop glasses containing plutonium oxide. The study of plutonium oxide-containing glasses could not be done at the Owens-Corning Fiberglas laboratories due to a lack of suitable facilities. In a cooperative program with Rensselaer Polytechnic Institute and the Mound Laboratory, we sent standard fiber-forming equipment to Mound Laboratory and gave advice concerning

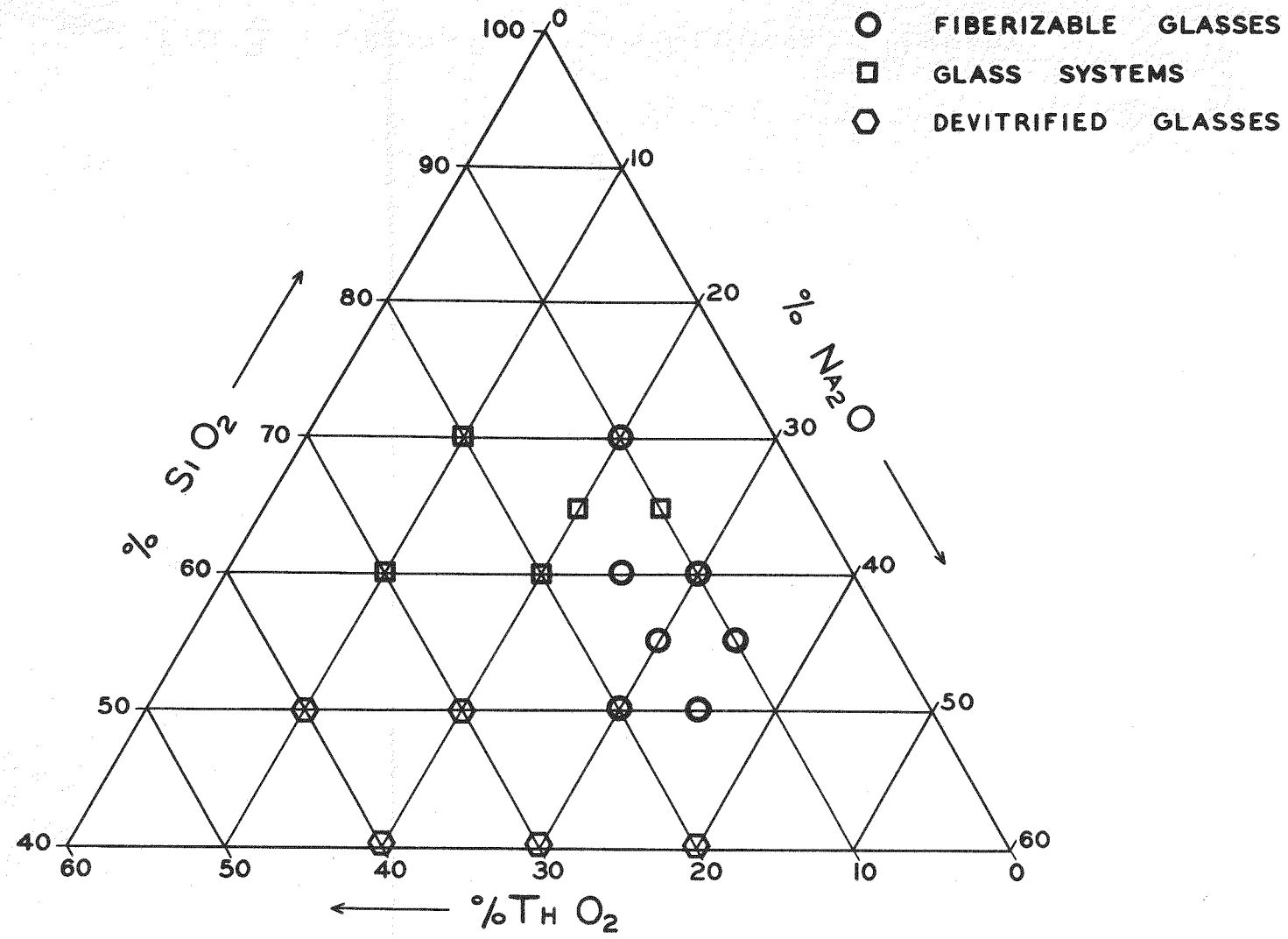

FIG. 2 THORIA - SILICA - SODA TERNARY

39483

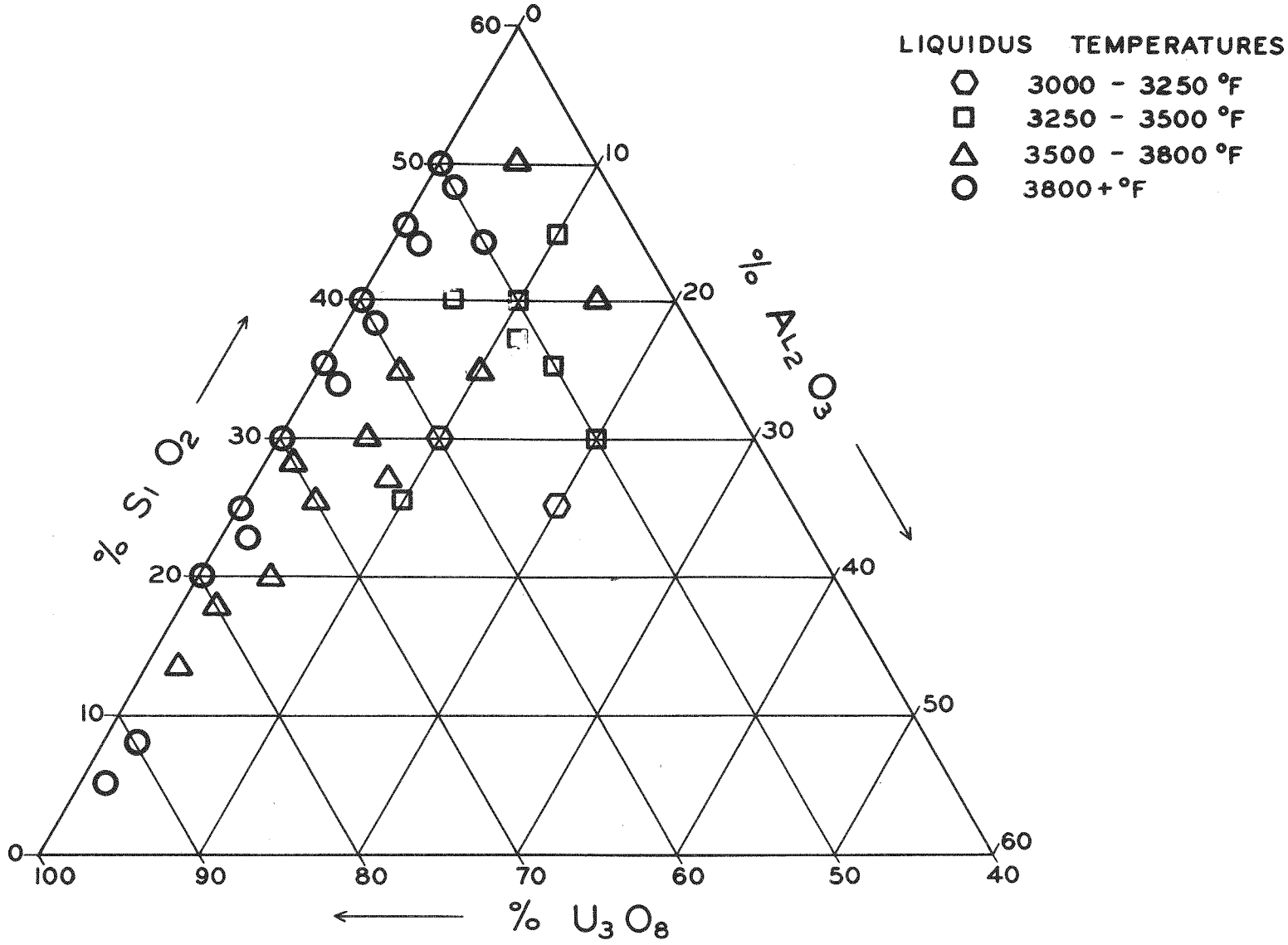

39480 FIG. 3 URANIA - SILICA - ALUMINA TERNARY

the design of equipment for melting and fiberizing glasses containing plutonium oxide in glove boxes. A paper on the Mound Laboratory work follows.

The glass composition studies just described indicated that certain glasses warranted further development in terms of actual production of fibers utilizing a laboratory single orifice fiber-forming position. Figure 4 shows a schematic diagram of the fiber-forming equipment. The glass is melted in an electrically heated precious metal pot and flows through a small orifice at the bottom. When the glass reaches the right viscosity, a drop forms at the orifice and can be attenuated by winding on the winder shown at the bottom of the diagram. The fiber diameter is determined by the glass composition, its temperature, the diameter of the orifice, and the winding speed.

The diameter of the glass fibers can be varied and for these experiments we have utilized fibers from 2 to 175 microns in diameter. The exceptionally fine fibers have been produced as single continuous fibers and mats whereas the coarse fibers have been produced only as single continuous fibers. Consideration has been given to several different types of mat configurations as well as to the possibility of weaving these fibers into open mesh cloth.

During fiber-forming operations it is often desirable to coat the fibers with various materials to protect them or facilitate their later use. These coatings may consist of inorganic materials which can be dispersed or dissolved in water, organic materials which are fluid from room temperature to several hundred degrees Fahrenheit, or metals which melt below 1300°F. Aluminum is the most important of the low-melting metals. Glass fibers can also be coated with another glass. As is well known, fibrous glass reinforced plastics produce a composite material with greatly improved physical and mechanical properties as compared to the same plastic without the fibrous glass reinforcement. An extension of this work is the placing of glass fibers in metal matrices of which, for fuel fabrication, aluminum is the most promising. The fuel composite has improved properties as compared to aluminum alone, especially at higher temperatures, and the Clevite Corporation is producing some MTR fuel plates for test purposes.

The next phase of the program involves the determination of the physical properties of glass fibers which had been drawn from the laboratory forming position. Table I gives a comparison of two fuel-bearing glasses, RX-70 containing 50 percent urania and RX-78 containing 35 percent urania, with a commercial fibrous glass composition. The density of the two fuel-bearing materials is higher in proportion to the urania content as would be expected and fiber tensile strengths, while lower, are comparable. The liquidus temperature of both fuel-bearing glasses is higher than that of the commercial glass which leads to some problems in forming fibers of these glasses. Although the liquidus temperatures are higher, the softening points are close to that of the commercial glass. The softening point is normally 200 to 400°F above what is considered the maximum usable working temperature.

Table II gives a list of tensile strengths at elevated temperatures of fuel-bearing glasses including the RX-70 and RX-78 and four high temperature glasses. The tensile strengths of the commercial glass and RX-70 and RX-78 are too low to be useful at temperatures above 1000°F whereas the other four glasses shown have tensile strengths in the usable range at 1600°F and 1800°F.

At the present time fuel-bearing glass fibers appear to have the most promise for use in chemo-nuclear process reactors which are being studied.

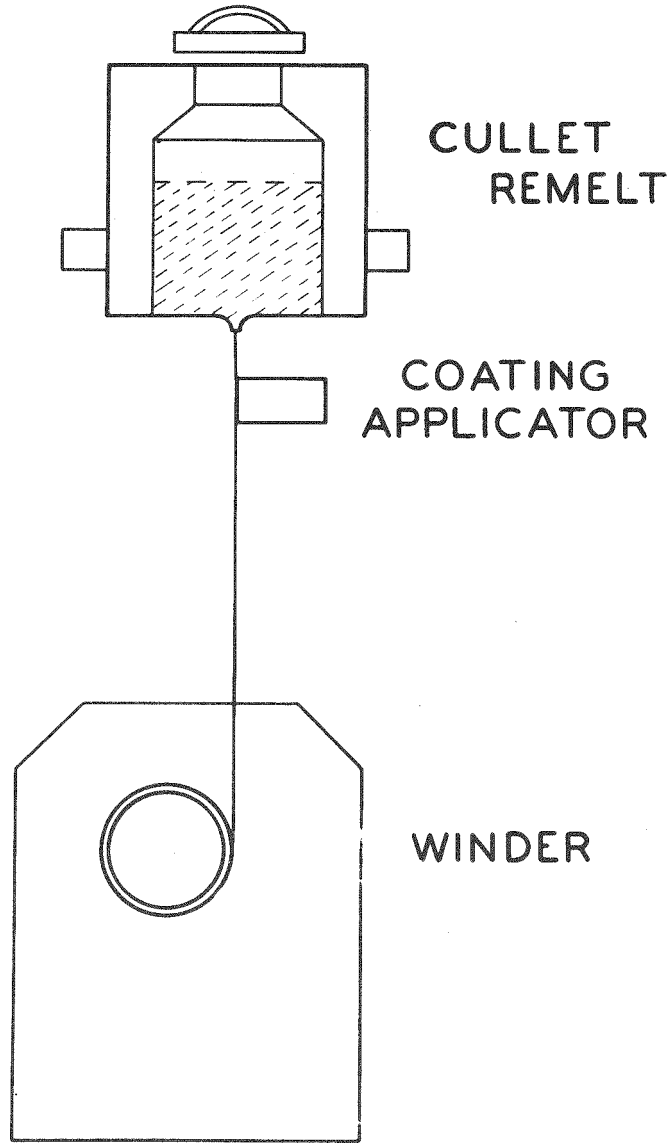

39485

FIG. 4 SCHEMATIC DIAGRAM OF EXPERIMENTAL GLASS FIBER FORMING SYSTEM

PHYSICAL PROPERTIES
FUEL-BEARING GLASSES VS A COMMERCIAL GLASS

TYPE OF GLASS		RX-70	RX-78	"E"
WEIGHT, U_3O_8	%	50	35	0
TENSILE STRENGTH	KSI	352	420	500
SPECIFIC GRAVITY		3.66	3.22	2.55
LIQUIDUS POINT	°F	2370	2360	2035
SOFTENING POINT	°F	1540	1435	1555

39482

ULTIMATE TENSILE STRENGTH
(ELEVATED TEMPERATURES)

GLASS	URANIUM OXIDE WEIGHT, %	ROOM TEMP. KSI	1000°F KSI	1600°F KSI	1800°F KSI
"E"	0	500	240		
RX-78	35	420	145		
RX-70	50	352	166		
RX-255	50	156		98	
RX-267	55	209		50	
RX-308	60	141		118	69
RX-335	65	123		80	67

The exceptionally fine fiber diameter is useful in allowing the fission fragments to escape into the process fluid for utilization of the fission fragment energy to promote the chemical reactions involved. Glass fibers could also be considered for organic moderated reactors where organic coatings could be placed on the fibers, or glass fiber reinforced plastic configurations developed. Glass-clad fuel fibers could also be utilized where the outer glass cladding would prevent the escape of the fission fragments into the organic coolant and moderator. Composites of aluminum and glass fibers might be utilized in test reactors which use aluminum fuel elements in order to increase their operating temperature without major redesign considerations. Glass-clad glass fibers could possibly be utilized as fuel elements in gas-cooled reactors to take advantage of the exceptionally large surface area for good heat transfer. While most of the work under the present contract has dealt with fibrous glass, there is no reason why massive glass could not be utilized for atomic energy purposes, primarily in power reactors. The massive glass could be utilized as a solid material or possibly as a partially crystallized glass such as Pyroceram or as a very viscous liquid. More irradiation studies must be made on glass systems to provide valid estimations of glass as a potential reactor fuel material.

In conclusion, the accomplishments of this research on nuclear fuel-bearing glasses can be summarized as follows:

1. About 400 glass compositions containing oxides of uranium, thorium, and plutonium or combinations of these oxides have been investigated.

2. Urania glasses containing 50 percent by weight U_3O_8 have been produced in standard forming equipment and urania glasses with as high as 65 percent by weight U_3O_8 have been formed in special high temperature equipment.

3. Thoria glasses containing 20 percent by weight ThO_2 and 20 percent by weight ThO_2 and U_3O_8 have been developed and successfully fiberized.

4. Several urania glasses have been produced with properties similar to commercial fibrous glass for utilization in a wide variety of forms and conditions and special high temperature glasses are available for studies at 1600°F and above.

5. Samples of nuclear fuel-bearing glasses have been utilized in experiments concerning chemo-nuclear reactors and aluminum fuel elements for test reactors. Preliminary tests are also being made in several other reactor systems.

REFERENCES

1. R. H. Baskey, Fabrication of Core Materials From Aluminum-Coated Fuel-Bearing Fiberglas, Paper presented at a Meeting of the American Nuclear Society, Chicago, Illinois, November 1961.

2. P. Harteck and Seymour Dondes, Producing Chemicals with Reactor Radiations, Nucleonics, 14, [7] (1956).

3. P. Harteck, Seymour Dondes, and J. W. Michener, Glass Fibers in Nuclear Reactor Technology, Proceedings of the Second UN International Conference on the Peaceful Uses of Atomic Energy, Vol. 7, p. 544, September 1958.

4. G. Lellouce and Meyer Steinberg, Industrial Chemical Production by Chemo-Nuclear Processes with Special Reference to the Production of Fixed Nitrogen, USAEC Report BNL-574, Brookhaven National Laboratory, March 1960.

5. C. D. Wirkus and D. R. Wilder, Uranium Glasses: I. Fundamental Considerations. II. Uranium Silicate Glasses, Reports IS-107 and IS-158, Iowa State University, February and June 1960.

DEVELOPMENT OF PLUTONIUM BEARING GLASS FOR A REACTOR FUEL

By P. A. Tucker, L. V. Jones, and L. J. Wittenberg

Mound Laboratory
Monsanto Research Corporation

Mound Laboratory is currently engaged in a study to incorporate plutonium oxide in glass for the development of a new fuel material for nuclear reactors. Fuel-bearing glass systems are particularly attractive as potential reactor fuels for three basic reasons: (1) they are simple and inexpensive to manufacture and reprocess, (2) they can be formed by conventional techniques into a variety of structural forms, and (3) they possess chemical and thermal stability which permit operation at temperatures as high as 1000°C. The application of uranium-bearing glass fibers has been described previously by Harteck and Dondes[1] . Studies of uranium and thorium bearing glasses are reported in this document by Lockwood (See Paper No. 5).

The Mound investigation was initially concerned with the extent of the solubility of plutonium oxide in the glass and the degree to which the glassy structure minimizes the toxicity and radiological hazard associated with handling plutonium. The ability to form fibers, the chemical durability, the physical properties and the radiation stability of the glass were also of interest.

A plutonium-bearing glass in the appropriate structural form may be applicable as fuel for power and materials testing reactors. As very fine fibers, a plutonium-bearing glass is particularly attractive as a potential fuel for chemonuclear reactors.[2] These high strength fibers offer a large surface area for heat transfer, and the small diameter of the fibers permits the fission products to escape efficiently from the glass matrix. These products would be continuously removed in the coolant. The recoil energy of the fission fragments can be effectively utilized in radiation-chemical processes such as nitrogen fixation and synthesis of chemicals from hydrocarbons.

Preparation of Glasses

The silicate glass mixtures, which were supplied through the cooperation of Owens-Corning Fiberglas Corporation Technical Center, were ground until the material passed through a 200-mesh screen. The plutonium oxide, which was prepared by decomposition of plutonium peroxide, was weighed inside an alpha

glovebox and placed with weighed portions of the silicate glass powder in a tightly covered bottle. The bottle was agitated for blending of the components. The mixture, which weighed from 5 to 10 grams, was carefully transferred from the bottle into a platinum-rhodium crucible which was covered with a tight-fitting rubber sleeve to prevent contamination of the outside of the crucible.

The crucible containing the mixture was passed from the glove box into an open front fume-hood where the rubber sleeve was removed. The crucible was placed on a specially designed support stand and heated by induction to 1600-1700°C (Figure 1). The upper temperature range was limited by the melting point of the crucible material. As the temperature increased, the undissolved plutonium oxide tended to separate by gravity segregation. To minimize this effect and to increase the rate of dissolution of the plutonium oxide, the mix was intermittently agitated. A support flange around the center of the crucible (See Figure 2) allowed heating of the crucible in either an upright or inverted position. As the viscous liquid flowed to the open end of the crucible when it was in an inverted position, the heating was interrupted to prevent the liquid from flowing out of the crucible. When the crucible was returned to the upright position and heated, the liquid flowed down the walls to the bottom of the crucible. This procedure was repeated several times during the homogenization cycle. At the completion of the homogenization cycle, which required up to four hours, the molten glass was allowed to drop as beads (Figure 2) into a cool receiver. The dark green color and clarity of the glass, especially in the tear-drop end, indicated that the plutonium was a soluble constituent of the glass.

To draw fibers of the plutonium-bearing glass by the continuous-filament process, the glass beads were placed in a platinum-rhodium bushing which was located in a standard alpha glove box. The bushing holding the glass served as an electrical resistance element in a low voltage circuit. When the bushing was heated to about 1300°C, a glass fiber could be pulled from the lower tip of the bushing (See Figure 3).

The fiber was coiled at constant speed on a mandrel driven by a variable speed motor (Figure 4). Figure 5 shows a coil formed from a continuous filament of glass fibers removed from the mandrel. Fibers of less than 10 to over 30 microns in diameter were obtained. The fiber diameter was governed by the speed of the mandrel, the temperature of the bushing, and the external cooling of the fiber as it was drawn from the bushing.

Results

Plutonium oxide dissolved readily in the silicate glasses. Up to 20 weight percent plutonium oxide was dissolved in a simple sodium silicate glass. Since this glass was hygroscopic, aluminum oxide, calcium oxide and potassium oxide were added as modifiers; however, as these constituents were added, the solubility of plutonium oxide decreased. Fifteen weight percent plutonium oxide could be dissolved in these complex silicate glasses at about 1600°C. Table I gives the compositions of the original parent glass system and three of the more durable formulations along with maximum concentrations of plutonium oxide which could be dissolved in each. Zirconium oxide and zinc oxide were also incorporated as constituents of experimental compositions to improve the chemical durability of the glass, but each oxide restricted the solubility of plutonium oxide to such an extent that its use was impractical.

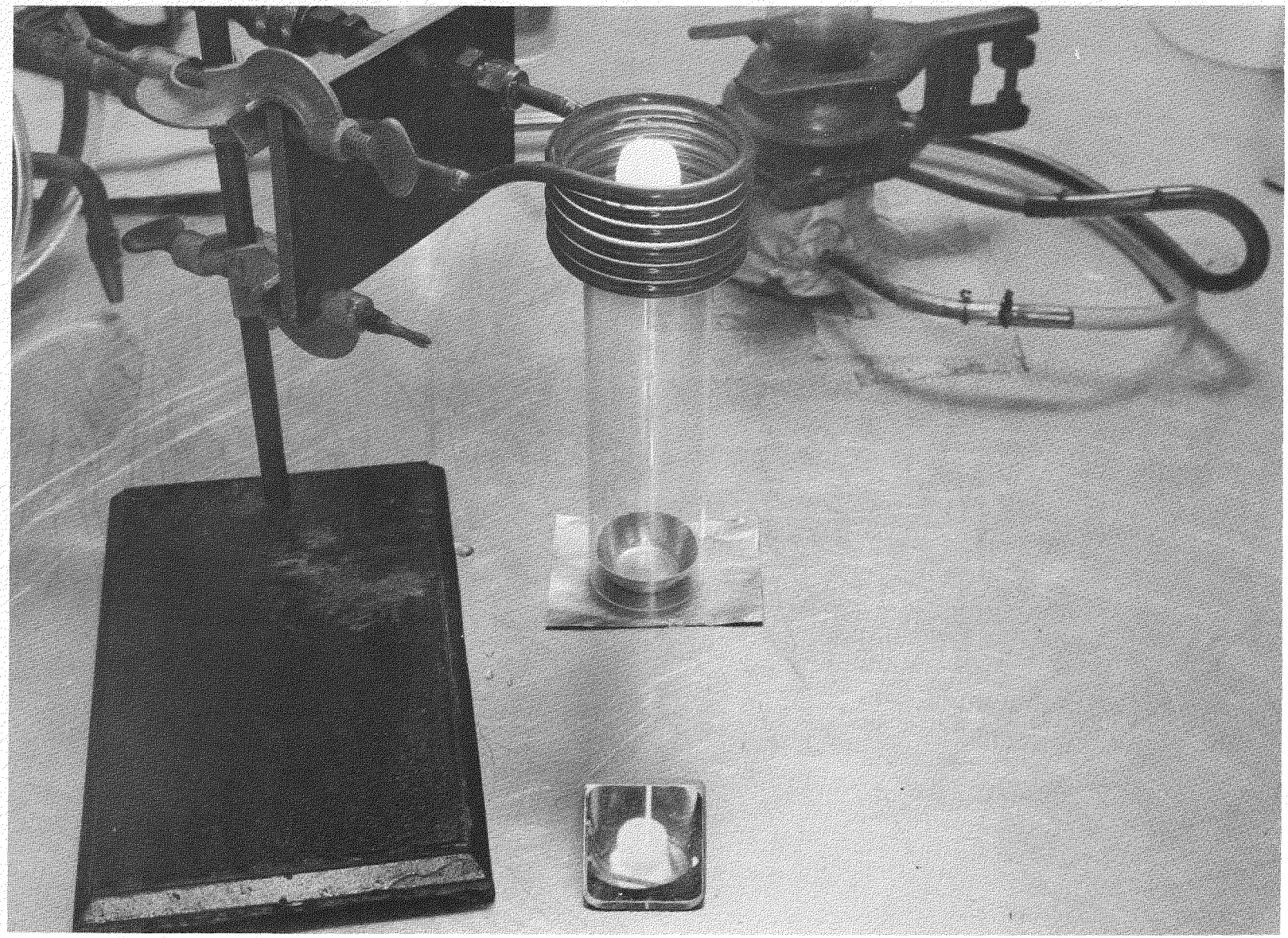

FIGURE 1

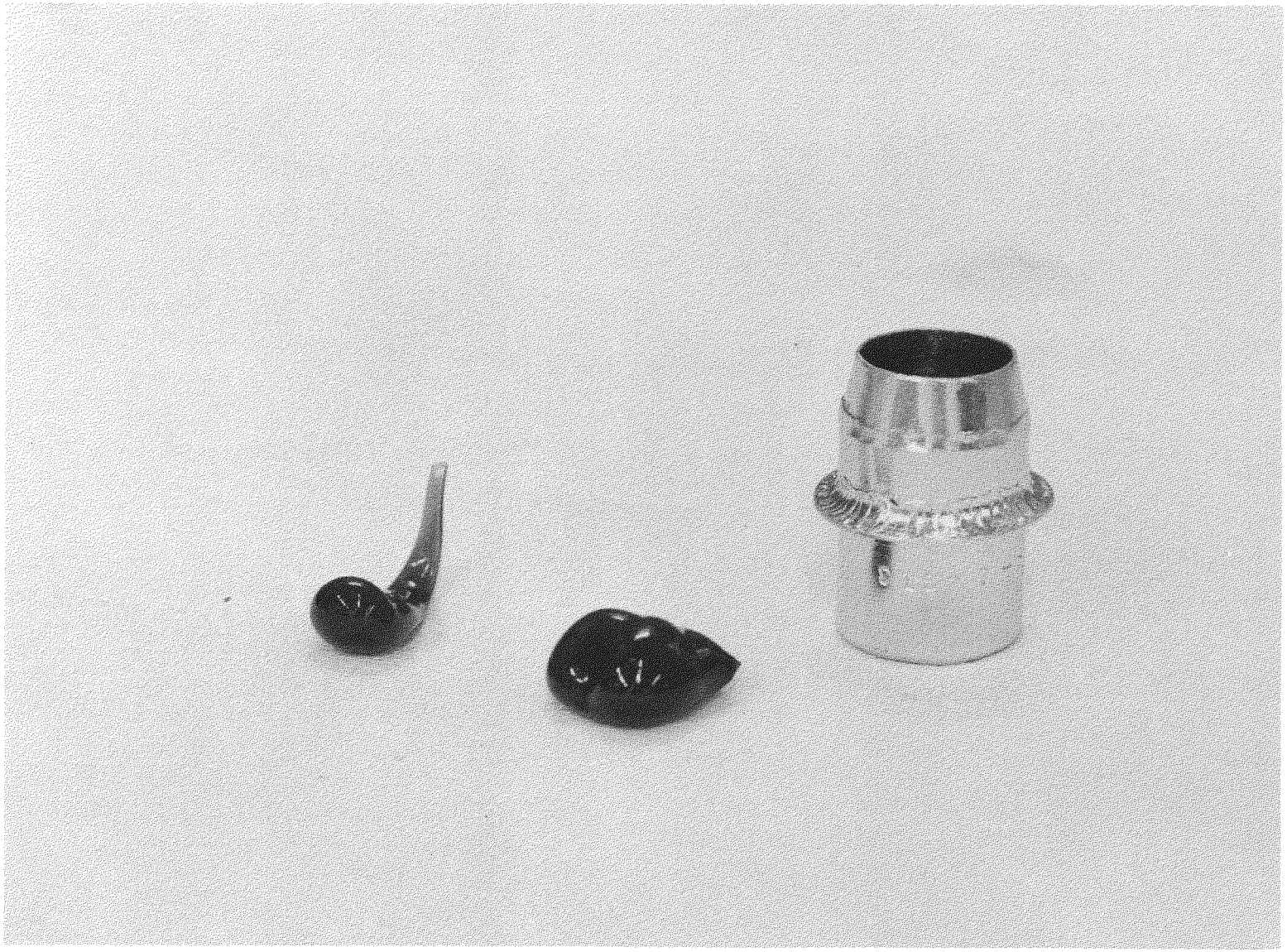

FIGURE 2

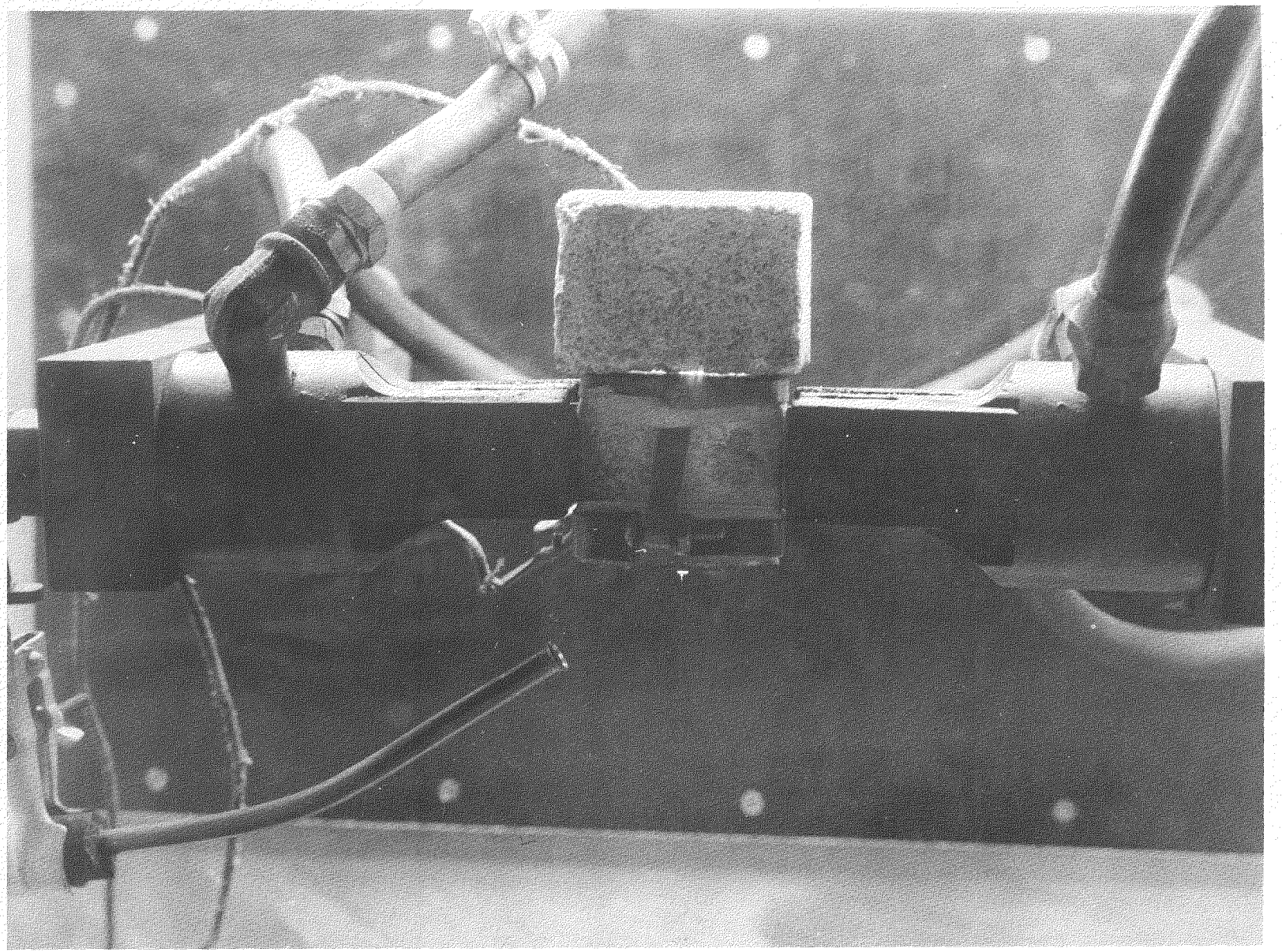

FIGURE 3

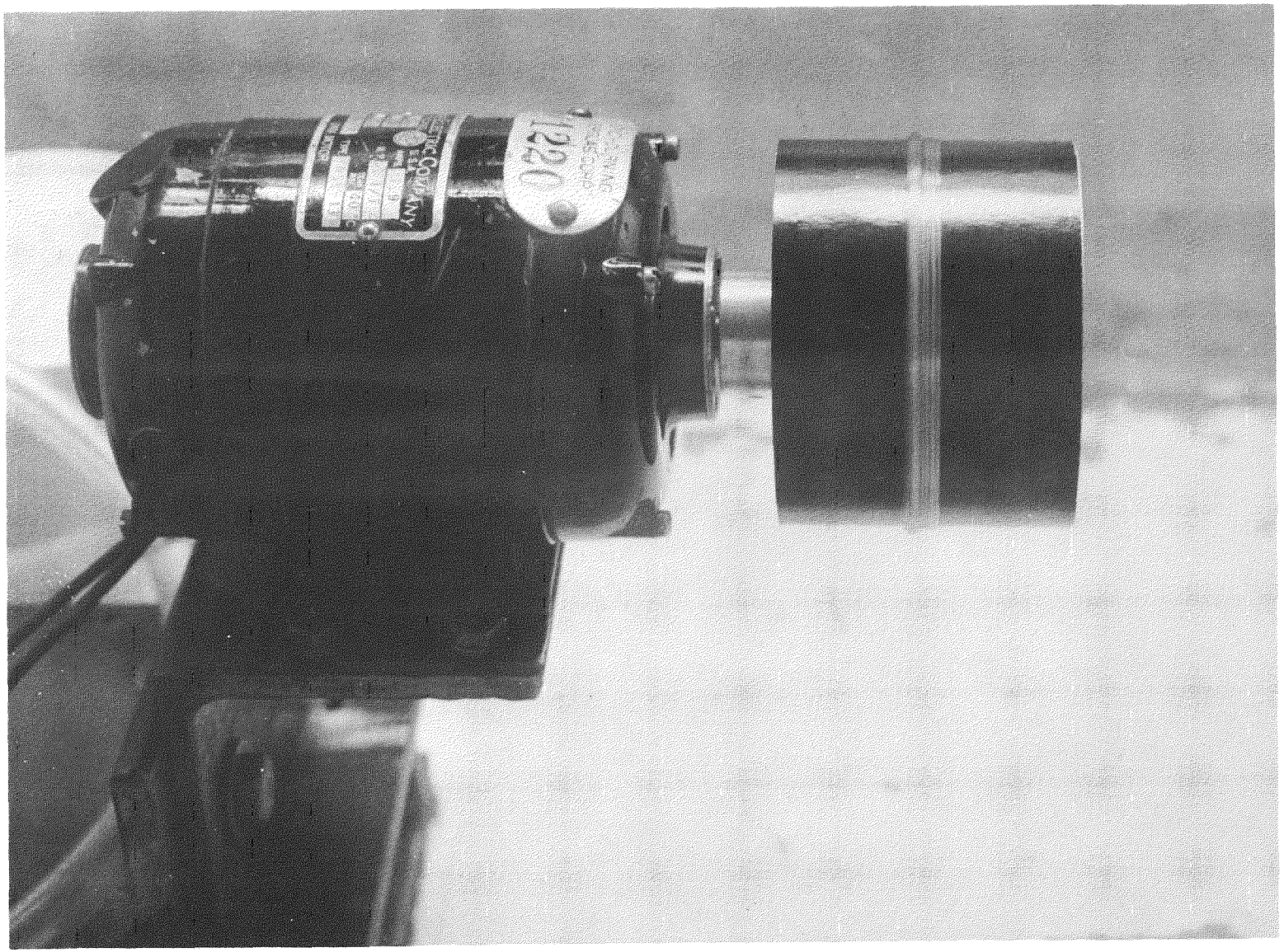

FIGURE 4

FIGURE 5

More plutonium oxide could be dissolved than the maximum concentrations listed in Table I if the dissolution process were carried out at higher temperatures; however, the homogeneous liquids could not be cooled to the solid state in massive form without some devitrification. A composition containing 30 weight percent plutonium oxide was liquefied at high temperature and appeared to be homogeneous; but on cooling, equilibrium crystallization of plutonium oxide, the apparent primary phase for the composition, immediately occurred in the liquid. Since the fibers are rapidly air-quenched, as they are formed, a bushing capable of operating at a higher temperature would probably allow fibers of greater than 20 weight percent plutonium oxide to be drawn without devitrification.

All of the silicate glass compositions containing completely dissolved plutonium oxide were successfully fabricated into fibers by the continuous-filament process.

Testing Program

Plutonium-bearing glass beads and fibers were subjected to physical, chemical, and irradiation tests to evaluate the quality of the glass. The glass beads were monitored for loose surface contamination by wiping with a soft filter paper. The paper was assayed by standard alpha counting techniques. No plutonium contamination could be wiped from the surface of any freshly prepared beads. Beads composed of glasses which were known to be hygroscopic yielded plutonium from the surface after exposure to laboratory air for several days. No loose plutonium could be wiped from the surface of the more durable glasses after nearly one year of exposure.

Sections of the glass fibers were microscopically examined for homogeneity and their diameters were measured. The fiber diameters varied from approximately 10 to 30 microns. Microscopic examination of the homogeneous plutonium-bearing glass in polarized light did not reveal any anisotropism. Only vitreous material was observed. In cases where the plutonium solubility limit had been exceeded at the temperature of the fiber-drawing operation, crystals of plutonium oxide were seen in the glass fibers. These crystals were perfectly shaped cubic structures encased in the glass fiber. Single crystal X-ray analysis of these crystals is planned.

The ultimate tensile strength of the glass fibers was determined by the use of a tensile tester which consisted essentially of a sensitive, pre-calibrated, Jolly balance spring. A single fiber was attached with Duco cement to the ends of a fiber mount cut from stiff paper. The paper was attached to the extension arms of the tensile testing machine and carefully severed by cutting at the center. A slight tension was applied to align the fiber in the load axis. The fiber was then re-cemented to the paper in this aligned position. After the cement was thoroughly dry, the load was increased until the fiber failed.

Since the fibers for the tensile test were unwound from a coil of fibers, the surfaces of the fibers were sometimes scratched, which significantly decreased the tensile strength in comparison to a fiber which had not rubbed against other fibers. The tensile strengths of some of the plutonium-bearing glass fibers are shown in Table II. The tensile strengths of the parent glass fibers without the plutonium oxide were about 10 percent higher.

The effect upon the tensile strength of continuous alpha bombardment from the decay of the plutonium was measured. For fibers which had an initial tensile strength of 129,000 psi, no decrease was observed after five weeks. In addition, fibers which were over one year old retained their initial appearance. These tests indicated that the alpha particles escaped from the fibers without causing appreciable damage to the glass structure.

The chemical durability of the glass was determined when glass fibers, which had a large surface area, were leached in various liquids. Weighed quantities of the fibers, such as the coil of fibers in Figure 5, were placed in jars and covered with a known volume of liquid. The jars were stored at room temperature without agitation. At various intervals small aliquots of the liquid were removed and placed on a stainless steel slide. The liquid was evaporated and the plutonium content on the slide was determined by standard alpha counting techniques.

The amount of total plutonium oxide leached by room temperature water was very small for the three glasses, B, C, and D, shown in Table II. The good chemical durability of Glass D was further shown by additional leach tests which resulted in the removal of 0.32 percent of the total plutonium oxide after a 120-day leach in 0.1 normal hydrochloric acid and the removal of 0.88 percent of the plutonium oxide after an 86-day leach in 0.5 normal nitric acid.

Initial irradiation tests are in progress on glass fibers which contain 10 weight percent plutonium oxide. The fibers are being irradiated in the Brookhaven National Laboratory reactor at a flux of about 10^{13}/neutrons/sec/cm^2 at 70°C. After irradiation for one day, equivalent to 0.08 percent of plutonium burnup, the fibers were intact and retained their original green color. They were, however, very brittle and were easily broken when gripped with tweezers. The ends of the individual fibers appeared to be frayed. This initial test indicated that the low-temperature irradiation of the fibers was very destructive. This irradiation damage may possibly be removed by a self-annealing process when the fibers are irradiated at a higher temperature.

Other Applications

The incorporation of an alpha-emitting isotope into a silicate parent glass to form a stable glass system free of loose contamination suggested that these glasses might be used as neutron sources or as alpha sources. Both sources have application as instrument standards.

Since beryllium is one of the best target materials for producing neutrons by the alpha-neutron reaction, beryllium oxide was incorporated with plutonium oxide into a parent glass to form glass neutron sources. A 5.9-gram bead containing 11 weight percent plutonium oxide and sufficient beryllium to obtain a beryllium to plutonium atom ratio of 6.5 to one gave a yield of 3000 neutrons per second. For the alpha-neutron reaction, this was only 5.3 percent efficient due to the dilution of the alpha emitter and the target material by the inert constituents in the glass.

Commercial fluoride glasses, based on beryllium fluoride, contain large quantities of two efficient target materials for neutron production, beryllium and fluorine. To produce a glass neutron source with a more efficient yield than that obtained with the silicate glass, plutonium tetrafluoride was

dissolved in fluoride glasses containing beryllium fluoride, aluminum fluoride, calcium fluoride, magnesium fluoride, barium fluoride, silicon tetrafluoride, cerium tetrafluoride and thorium tetrafluoride. Hydrolysis of the fluorides during homogenization was prevented by adding ammonium acid fluoride to the starting mixtures. The plutonium tetrafluoride dissolved rapidly at about 900°C. A 2.85-gram bead containing four weight percent plutonium tetrafluoride had a beryllium to plutonium atom ratio of 27 to 1. It gave a yield of 2411 neutrons per second, representing an efficiency of 27 percent based on the alpha-neutron reaction for beryllium.

Individual fibers of a glass containing ten weight percent plutonium oxide were evaluated as alpha sources. Fibers were chosen whose diameters were less than 30 microns, the approximate range of the alpha particle in the glass. The fibers were counted while held in a special fiber mount in such a manner that they were completely surrounded by the counting chamber. Thus, the counts were absolute measurements of the alpha emission from the fibers. A fiber 18 microns in diameter and one-inch long gave a total emission of 158,200 counts per minute. This was 80 percent of the total theoretical disintegrations per minute in the fiber based on its known content of plutonium-239. Self-absorption of the fiber and the inability of the instrument to count low-energy alpha particles accounted for the remaining 20 percent of the total disintegrations. Since the escape of the alpha particles is efficient and the durability of the glass is very good, the glass fibers are an effective alpha source.

Since an alpha source in the form of a glass fiber would not be suitable for many applications, the experimental plutonium-bearing glasses were fabricated into a different shape. A parent glass without plutonium was placed in the shallow sample well of a stainless steel container and fused. A short length of glass fiber or a very small bead of the plutonium-bearing glass was placed atop the glass in the center of the sample well and heated to fuse the fiber or bead into the glass surface. The addition of plutonium-bearing fibers or beads of different sizes to each of four sample containers produced alpha sources in each of the ranges of 10^4, 10^5, 10^6, and 10^7 counts per minute. Glass alpha sources with a higher range of counts could presumably be made by increasing the concentration of plutonium oxide and the surface area of the source.

Summary

Plutonium oxide can be dissolved in silicate glasses to form a homogeneous material which greatly reduces the toxicity problem associated with handling plutonium. The fibers drawn from these glasses have high tensile strengths and good chemical durability. The value of these fibers as a reactor fuel material has yet to be demonstrated.

The immediate plans for the work will be concerned with the development of higher plutonium concentration in the glass and higher softening-temperature glass. In addition, the feasibility of a massive glass reactor fuel element which can be operated at a temperature such that the glass is a semi-fluid will be investigated. The utilization of such a plutonium-bearing glass fuel element will be directed toward the fast breeder reactor concept.

TABLE I

COMPOSITIONS AND MAXIMUM PuO_2 SOLUBILITIES OF GLASS SYSTEMS

Experimental Glass No.	Parent Glass Wt. Percent						Maximum Solubility Wt. Percent PuO_2
	SiO_2	Al_2O_3	CaO	MgO	Na_2O	K_2O	
A	70.0	-	-	-	30.0	-	20
B	69.4	2.6	5.6	-	16.8	5.6	$15 < X < 20$
C	66.6	5.6	4.0	1.6	20.2	2.0	15
D	66.6	5.6	5.6	-	16.6	5.6	15

TABLE II

TENSILE STRENGTH OF Pu-BEARING GLASS FIBERS

Experimental Glass No.	Wt. Percent PuO_2	Tensile Strength, psi
A	15	101,500
B	10	136,000
C	10	132,600
D	10	125,000

TABLE III

PERCENT OF TOTAL PuO_2 LEACHED FROM PLUTONIUM BEARING GLASS FIBERS IN ROOM TEMPERATURE WATER

Experimental Glass No.	Leach Time (Months)			
	1	2	3	10
A	0.34	-	-	-
B	0.18	0.25	0.31	-
C	0.17	0.21	0.26	-
D	0.07	0.11	0.15	0.37

Acknowledgements

The authors gratefully acknowledge the helpful discussions with Mr. Paul Lockwood and Mr. Ralph Tiede of Owens-Corning Fiberglas Technical Center and the assistance of Mr. Kenneth Phipps of Mound Laboratory who performed many of the laboratory experiments.

References

1. P. Harteck and S. Dondes, Glass Fibers - A New Form of Reactor Fuels, Nucleonics, 15: 8, 94 (1957).

2. Chemonuclear Reactors - Where Do They Stand?, Nucleonics, 19: 2, 47 (1961).

Figure Captions

1. Apparatus for Homogenizing Glass.

2. Homogenization Crucible and Plutonium-Bearing Glass.

3. Fabrication of a Plutonium Glass Fiber.

4. Plutonium Glass Fibers on Mandrel.

5. Plutonium-Bearing Glass Fibers.

DEVELOPMENT OF PROTECTIVE METAL COATINGS FOR UO_2 AND U PARTICLES[a]

by L. P. Pepkowitz, B. L. Vondra, and F. Shipko

Nuclear Materials and Equipment Corporation
Apollo, Pennsylvania

The preparation of some interesting new fuel materials at the Nuclear Materials and Equipment Corporation is accomplished by a novel method of coating individual fuel particles. A strong, uniform, corrosion resistant, impervious metallic coating is applied to individual spherical particles of uranium dioxide or uranium metal. Some phases of this work have been reported by Cain, et al.[1] In the case of UO_2 spheres, the coatings can act as barriers against the interaction of the oxide with reactive matrices such as zirconium in the case of dispersion elements and conversely they can also suppress the deterioration of the matrix by preventing or at least inhibiting the diffusion of fission products into the matrix. The coatings will also suppress the release of fission products to the coolant. In addition, the metallic coating has the important advantage of improving the overall thermal conductivity of a properly consolidated mass of ceramic particles by providing a continuous metallic, heat-conducting network to the surface of the element.

The coating of pure uranium metal particles, or uranium particles containing small amounts of alloying metals such as zirconium, niobium, and molybdenum, can be of great significance to the reactor industry since it may provide the key to the preparation of corrosion and radiation damage resistant fuel for use at high temperature and high burnup in reactors utilizing natural or very low enrichment, high specific uranium density, fuel. Heavy water and graphite-moderated reactors fall into this category. In these cases, the use of uranium carbide or uranium oxide may be impractical or borderline, and what is required is metallic uranium. By coating particles of pure uranium metal or alloys containing only a minimum of inert materials, and consolidating these by extrusion, rolling, or by any other of the common techniques, one should obtain an element of superior corrosion resistance as well as radiation damage resistance. This is a consequence of the fact that the particles of uranium metal would be individual islands surrounded by a matrix of corrosion-resistant material. Thus, even if one of the barriers were penetrated by corrosion or abrasion, little damage would result to the element as a whole, since multiple barriers would have to be penetrated for appreciable damage. Moreover, since the coatings would apply very significant mechanical constraint to the particles, the

a. Work performed under U. S. Atomic Energy Commission Contract AT(30-1)-2264.

radiation damage resistance should improve very significantly. In addition, the creep resistance and other high temperature mechanical properties would be improved.

In all cases, these desirable effects would be obtained with the addition of a minimum of inert material, thus allowing maximum uranium density, since the coating technique allows for optimum placement of the metal as contrasted with ordinary powder metallurgical techniques, whereby particles are merely mixed together prior to compaction. A more detailed discussion of the advantages of the use of coated particles together with a description of possible compaction and consolidation methods is given in a previous report[2] and need not be elaborated upon here.

HORIZONTAL-TYPE REACTOR FOR VAPOR PHASE COATING

From the outset of the program the horizontal-type reactor has been advocated and utilized by the authors' company. Among the salient advantages that can be listed for this concept are the following:

1. Scale up to larger quantities can be more easily achieved since there is no dependence on gas flow for fluidization; the agitation is produced mechanically. Conversely, a highly dependent parameter is eliminated since the regulation of the gas flow is only related to the rate of chemical reaction and not the mechanical agitation of the spheres.

2. The apparatus can be simply fabricated from metal such as stainless steel and is, therefore, rugged and shock proof.

3. The use of much higher temperatures can be investigated than with vertical, fluidized glass apparatus.

4. There is an over-all element of safety in using metal equipment in that vigorous exothermic reactions, hydrogen blow back, etc., do not result in rupturing or shattering the equipment with the associated dangers of losing uranium and contaminating the work area. This point is especially important when highly enriched uranium is involved.

Apparatus in which the reactor is supported at each end in a yoke arrangement and agitated by a vibrator is described in detail in a previous report.[3] This apparatus is capable of coating approximately 500 grams of UO_2 spheres, 100-140 mesh, at a time. For example, 8 to 10 microns of niobium can be deposited in 14 to 16 hours of operation.

TYPES OF COATINGS

Coating procedures were developed for a large number of materials such as Nb, Cr, Mo, V, Ni, Cu, Si, Be, Nb-5V as well as duplex coatings such as Nb over Mo, Cr over Nb, etc. In addition, methods have been developed for coating with various oxides such as Al_2O_3, BeO, ZrO_2, pyrolytic carbon, carbides, etc.[a] Particle sizes have ranged from 200 mesh to 1/4 inch spheres. The methods developed by this company can be applied to many other substrates such as metals, alloys, other oxides, carbides, and silicides, providing they are stable under

[a] Development of oxide, carbide, and pyrolytic carbon coatings was not supported by an AEC contract. This work was financed entirely by company funds.

the coating conditions.

COATING METHODS

A variety of procedures has been used in depositing suitable coatings. These include vapor phase reduction of halides, thermal decomposition of metal-organic compounds (Cr), metal vaporization, electrolytic reduction and chemical displacement methods. For convenience, Table I presents in a tabular form the techniques developed under the contract. The reader is referred to a previous report[3] for details. Figures 1, 2, 3, 4, and 5 illustrate some of the coatings that have been obtained.

PROBLEMS IN COATING URANIUM METAL

There are many problems that arise in coating uranium metal which are not apparent when coating UO_2. Among these are surface treatment, chemical attack, diffusion of uranium, compatibility of barrier layers and desired coating, etc. A detailed consideration of these problems has been reported[3] but the following paragraphs will indicate the types of problems encountered.

Surface Treatment

It was immediately obvious that one of the major controlling conditions for adherent bonded coatings was the cleanliness of the metal surface. All oil, grease, oxide, and other surface contaminants must be rigorously removed before adherent coatings can be laid down. The interference of the oil and grease is obvious but the presence of traces of oxide results in the formation of an unbonded metal envelope instead of an adherent coating.

Chloride Attack

The direct deposition of metal coatings, such as niobium, by the vapor phase reduction of the chloride is not feasible because of the severe attack on uranium by HCl and Cl_2 produced during the reduction reaction. As in the case of the coating of UO_2 using $CrCl_3$, a resistant undercoat is required. Niobium coatings laid down without a protective undercoat are nonadherent, powdery, and contain inclusions of uranium chloride.

Penetration of the Protective Undercoat by Uranium

The first undercoat applied to eliminate the chloride attack was nickel which was most conveniently applied electrolytically. The bath used was the Watt type - SO_4 bath previously[2] described. A bright adherent coating was deposited but after the subsequent niobium coating step as described in the section on COATING METHODS, the duplex coating was blistered and was easily peeled away from the U-Mo substrate. Metallographic examination showed that the failure was caused by uranium penetrating the nickel undercoat at niobium deposition temperatures. The blistering was caused by the chloride reaction with the uranium which completely penetrated the one mil nickel coat.

In retrospect, this phenomenon was to be expected since nickel and uranium form a eutectic at 740°C, approximately the temperature at which the niobium coating was applied.

TABLE I

SUMMARY OF COATING PROCEDURES

Coating Material	Substrate	Starting Compound	Method	Temp. (°C)	Approx. Rate (microns/hr)
Nb	UO_2	$NbCl_5$	Vapor phase reduction	800	0.75
	U	$NbCl_5$	Vapor phase reduction over barrier layers	800	0.75
Cr	UO_2	$CrCl_3$[a]	Pyrolysis plus Vapor phase reduction	550 ~750	1
		$CrCl_2$[b]	Vapor phase reduction	770	1
		Cr dicumene	Pyrolysis	425	0.25
		Cr metal	Vacuum evaporation	-	5
Mo	UO_2	$MoCl_5$	Vapor phase reduction	770	2
V	UO_2	VCl_4	Vapor phase reduction	1000	1.5
Nb-5V	UO_2	$NbCl_5$ VCl_4	Vapor phase reduction	1050	2
Si	UO_2	$SiCl_4$	Vapor phase reduction	900	2
Be	UO_2	Be metal	Vacuum evaporation	1500	?
Ni	U	$NiSO_4$	Electrolytic	25	15
Cu	U	$CuSO_4$	Chemical Displacement	25	-

[a] Requires Ni barrier layer.

[b] Over a Nb undercoat.

This phenomenon, however, has a significant advantage since the bond between the uranium and the nickel is very strong. Adherent coatings of niobium could be applied if the nickel layer was thick enough. At least two mils were required to prevent the uranium from penetrating to the nickel-niobium interface during the time interval required for depositing the niobium but an undercoat of this thickness is undesirable.

Copper was next investigated as a barrier layer to prevent the penetration of uranium. The copper was deposited by displacement from an acid $CuSO_4$ bath. No diffusion of uranium through the copper layer could be detected. However, it was very difficult to prevent the formation of an oxide layer at the Cu-U interface.

The formation of the oxide layer despite the careful cleaning of the uranium surface is undoubtedly a result of the method of depositing the copper. In the displacement reaction, uranium is the reductant and accordingly is oxidized as the copper metal is precipitated from solution. It is possible that the oxide layer could be eliminated by some other method of depositing the copper such as vaporization or electrolysis.

Deposition of Niobium Over the Barrier Layer

The deposition and adherence of niobium to either a copper or nickel layer presents no problems but the excess thickness of nickel required to prevent the chloride attack on uranium or the oxide layer at the copper-uranium interface makes either system unusable. However, a 3-layer coating proved to be an excellent solution to the problem. A thin nickel-base coating provided a tightly bonded layer on which a thin film of copper could be deposited as a diffusion barrier. Finally, the niobium could be deposited by the usual vapor phase reduction of the pentachloride without any deleterious effect on the uranium substrate.

EXTRUSION STUDIES

One of the major developments in this program has been the demonstration that coated particles are particularly satisfactory in the fabrication of dispersion-type elements by extrusion, hot pressing, etc. The particles retain their integrity and show no signs of breaking up, stringering, or rupturing of the coating. This phase of the application of coated particles is still in its infancy and should be investigated in much more detail.

One area of great significance is the study of the interactions of the coating with the UO_2 and matrix during extrusion, compacting, etc. It had previously been observed that the severe pressures and relatively high temperatures necessary for co-extruding coated UO_2 spheres in a Zircaloy-2 matrix provided good conditions for evaluating the crushing resistance of the coatings and spheres. In addition, the possible reactions occurring at extrusion temperatures and pressures between coating and matrix and coatings and UO_2 can be ascertained.

Microscopic examination of polished sections of each of the extruded elements indicated the presence of an excellent metallurgical bond between the coating and the Zircaloy-2 matrix. In addition, there was no evidence of fracturing of the UO_2 spheres or rupturing of the coating thus indicating the effectiveness of the coated particle concept for such applications.

Metallographic examination of polished sections also indicated various types of interactions which occurred during the extrusion process. No apparent evidence of interaction was observed between the Zircaloy-2 matrix and Cr, W, or pyrolytic carbon coatings. There was also no indication of interaction between the UO_2 spheres and Mo or W coatings. However, reaction zones were observed between the Zircaloy-2 matrix and Nb and Mo coatings and between the UO_2 and the carbon and Nb coatings.

Based on previous metallurgical experience, it was most unlikely that the 25 minute heat treatment at 1360°F could cause the observed diffusion zone reaction. Accordingly, a number of experiments were performed to establish whether the heat treatment alone or compacting with and without heat treatment could cause the interaction. Small lots of each of the six different metal coated spheres were vacuum heat treated for 1 hour at 1360°F. In addition, small compacts of the spheres were prepared and examined after 1 hour at 1360°F. There were no discernable effects as a result of these treatments and no indication of the interactions produced during the extrusion process.

PREPARATION OF Nb-UO_2 COMPACTS

It was previously reported[2] that agglomerated platelets of UO_2-Nb could be formed in situ. The UO_2 spheres were coated with Nb and the interstices between the spheres filled with niobium metal. It was pointed out that it should be possible to arrange the geometry of the process to prepare other shapes besides the original platelets. This has been done. In fact, cylinders, discs, and plates have been formed by this technique.

Following the preparation of the original platelets, a number of schemes were tried to produce various shapes. One of these was to pack the spheres in a copper retained ring and deposit the niobium by the hydrogen reduction of the halide. The results were quite promising but the diffusion of niobium down through the compact was limited so that the interstices in the top portion were filled while the lower part of the compact still had unfilled areas.

This difficulty was eliminated by using stainless steel wire mesh as the mold. The temperature for the deposition was ~800°C while the other conditions were those previously described for the $NbCl_5$-H_2 reaction. Under these conditions, very good impregnation by Nb occurred. A visual estimate from the cross sections indicated that more than 80% of the voids were filled with metal.

The success in forming these various types of compacts now makes possible the application of coining, hot pressing, or other techniques in densifying the body. A 0.3 inch diameter niobium compact was cold pressed at 31,000 psi to determine whether the compact was ductile enough to be pressed to higher densities. The result is shown in Figure 6. Although in this trial there is some evidence that some of the UO_2 spheres fractured, the fragments were contained in the volume of the original sphere. A microscopic examination indicated that the density is close to theoretical with practically no voids in the interstices. The Knoop hardness of the matrix was 158.6 before cold pressing and 160 after pressing, indicating the high purity and ductility of the niobium was not altered by the cold working.

Consolidated bodies prepared by this method were corrosion tested for three days in 500°F water at 750 psi. Weight gains did not exceed 25 mg/dm^2 as compared to 23.5 mg/dm^2 for electron beam melted Nb samples included in the same tests. Visual and microscopic examination of the corrosion tested samples

revealed no exposed fuel and a very thin light grey corrosion film on the Nb.

To put this process in the right perspective in regard to economical preparation of fuel elements, the filling in of the voids requires only 1/10 the time required for the original coating of the UO_2 spheres. This can be directly ascribed to the rapidly decreasing specific surface area. This phenomenon was also observed when coatings were applied to large spheres of 1/4" diameter. In this case, 100 microns of niobium were deposited on the spheres in a much shorter time than is required to deposit 10 microns on 100 micron diameter spheres. Because of this very significant increase in deposition rate and the associated economics which will be realized, serious consideration should be given to utilizing this approach for various fuel element programs. Furthermore, this attractive technique should be applicable to other metals which can be deposited from the vapor phase such as Mo, V, etc. This procedure holds great promise for the economical preparation of dispersion-type elements and should be investigated in greater detail.

CHEMICAL AND METALLURGICAL EVALUATION

The chemical purity and hardness of various coatings were evaluated together with the various properties of the coatings enumerated above. Details are given in another report.[3]

REFERENCES

1. F. Cain, B. Vondra, and F. Forscher, Coated Particles, International Atomic Energy Symposium, Vienna, Austria, May 13, 1960.

2. Final Report (on Coating Fuel Elements), Period November 15, 1958 through November 14, 1959, USAEC Report NUMEC-NYO-2801, 1960.

3. Final Report, Period November 15, 1959 through November 14, 1960, Corrosion and Radiation Damage Resistant Fuel Materials (Coating of Uranium and UO_2 Fuel Particles), USAEC Report NUMEC-NYO-9187, Sept. 1960.

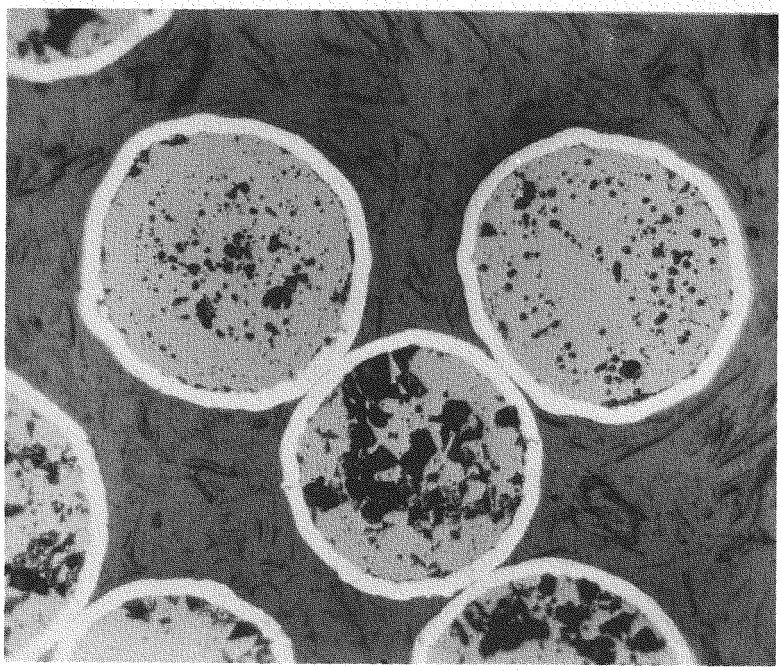

Figure 1. Niobium Deposit (8-10 microns) on UO_2. 250X.

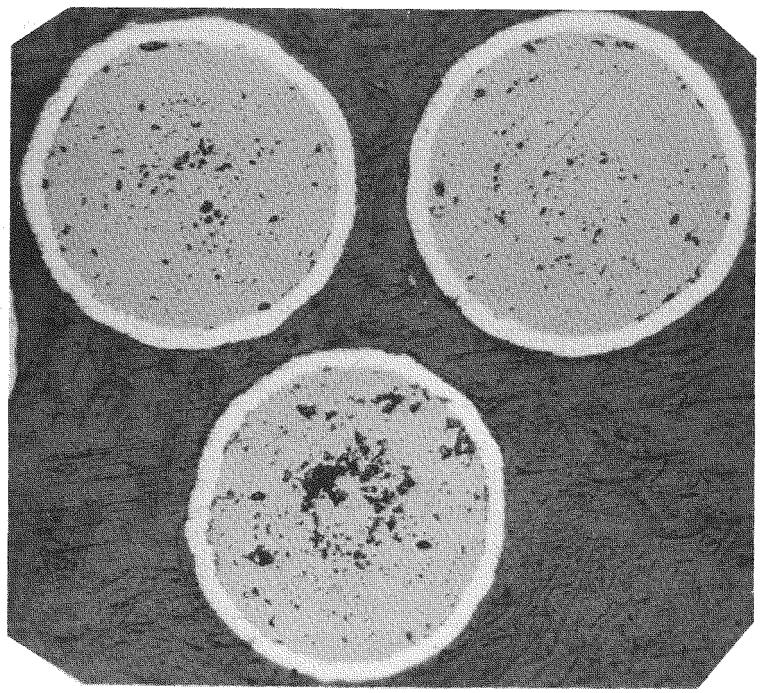

Figure 2. Chromium Deposit (8 microns) Thin Niobium Undercoat. 250X.

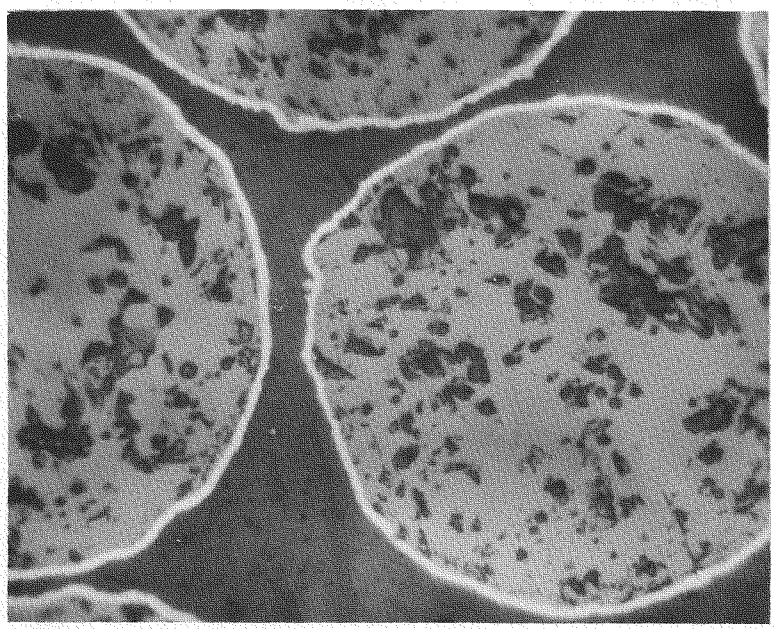

Figure 3. Chromium Coating (2 microns) of UO_2 Spheres by Pyrolysis of Chromium Dicumene. 250X.

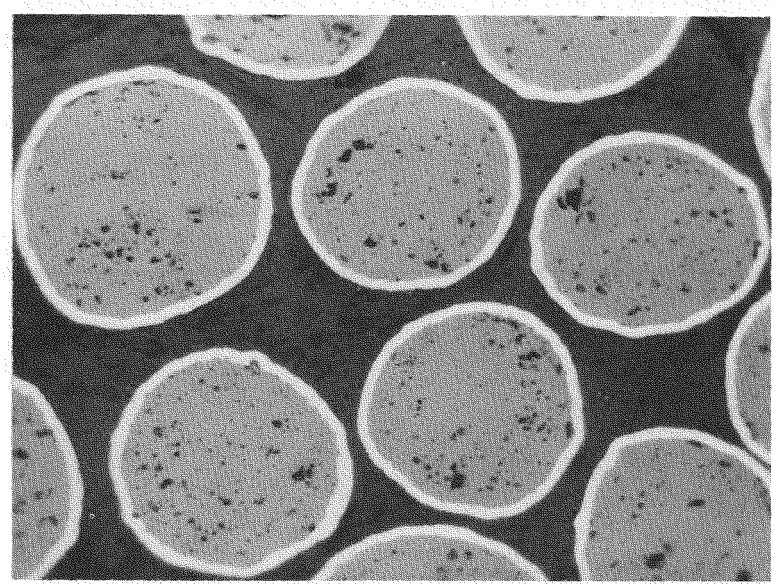

Figure 4. Molybdenum Coating on UO_2 Spheres, 4-5 Microns. 250X.

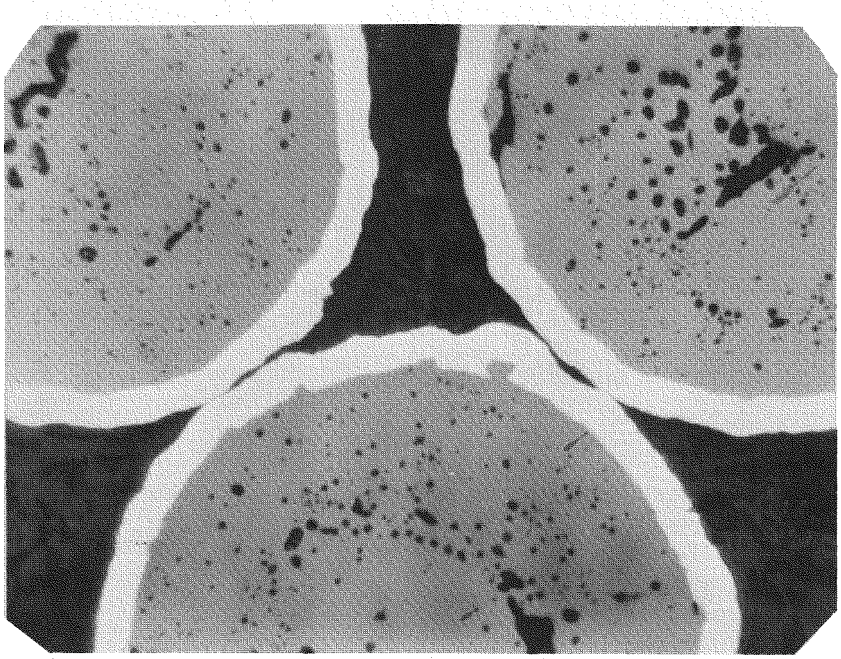

Figure 5. Niobium - 5 Vanadium Coating on UO_2 Spheres. 500X.

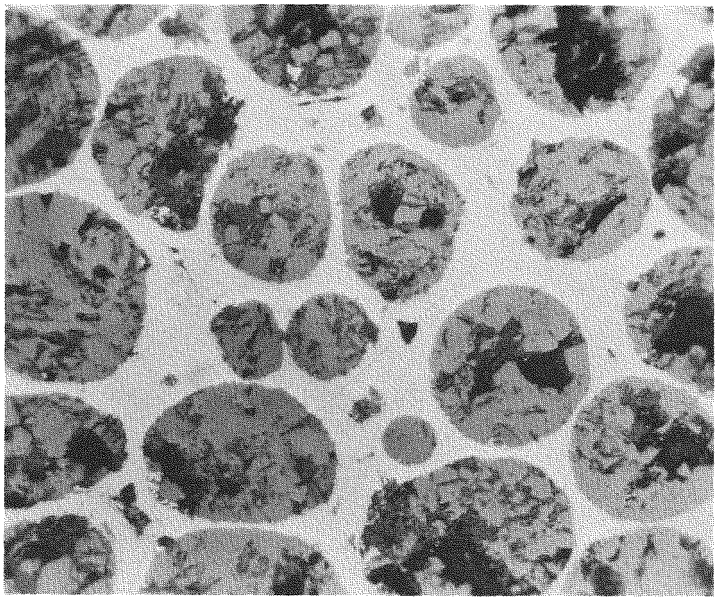

Figure 6. Fuel Body Containing UO_2 Spheres in HB Matric made by Walide Reduction and Subsequent Cold pressing at 31,000 psi. 250X.

SPECTROPHOTOMETRY OF AQUEOUS HOMOGENEOUS REACTOR FUEL COMPONENTS AT ELEVATED TEMPERATURES AND PRESSURES[a]

W. C. Waggener, A. J. Weinberger, and R. W. Stoughton

Oak Ridge National Laboratory,[b] Oak Ridge, Tennessee

ABSTRACT

Aqueous homogeneous reactor fuel solution components have been examined spectrophotometrically in the wavelength range 0.34 to 1.2μ as a function of time, temperature, and overpressure of H_2 and/or O_2. In measurements made on degassed solutions in a titanium and sapphire optical cell, the 0.42μ band of U(VI) and the 0.82μ band of Cu(II) showed a monotonic absorptivity increase with temperature from 4 to 280°C by factors of 2.3 and 2.0, respectively. By use of a prototype cell designed for liquid-gas equilibration, the course of reactions (reduction, hydrolysis, precipitation, oxidation, and re-solution) of the uranium and copper in the presence of either or both H_2 and O_2 was followed concomitantly. Cu(II) and U(VI) were found to be reduced successively to Cu(I) or (0) species (insoluble) and U(IV) species (essentially soluble at 25°C but insoluble above 150 to 200°C). The changing spectrum of the system generally was uncomplicated by turbidity; reduction of Cu(II) as well as aggregation of U(IV) hydrolytic species occurred preferentially at the titanium cell wall. Hydrolysis of U(IV) was slowly reversible with temperature. Reoxidation of reduced species with O_2 was comparatively rapid, and additional absorbing species (possibly Cu and/or U intermediates or Ti corrosion products) were sometimes observed.

---

[a] To be submitted for publication in Nuclear Science and Engineering.

[b] Operated by Union Carbide Corporation for the U.S. Atomic Energy Commission.

PREPARATION AND PROPERTIES OF FLUOROCARBONS OF INTEREST IN REACTOR TECHNOLOGY

by F. W. Bloch, D. R. MacKenzie and R. H. Wiswall, Jr.

Brookhaven National Laboratory
Upton, New York

INTRODUCTION

A survey of the known properties of fluorocarbons shows how valuable they could be in the reactor field if their radiation stability should prove good; and such a survey also provides reason to expect good stability. Chemically they are, of course, extremely stable, for reasons which are partly thermodynamic and partly kinetic. For all fluorocarbons which have been measured, the enthalpies, and no doubt also the free energies, of formation are negative. For CF_4, for example, the heat of formation is -218 kcal; and even the acetylenic fluorocarbons are expected to be stable relative to decomposition into their elements.[1] Furthermore, there is experimental reason to believe that the carbon-fluorine bond is considerably stronger than the carbon-hydrogen bond. Values of 118 to > 154 for $D(CF_3\text{-}F)$ and of 145 for $D(C_6F_5\text{-}F)$ have been published.[2,3,4] For comparison[3] $D(CH_3\text{-}H) = 102$ and $D(C_6H_5\text{-}H) = 104$.

The favorable kinetic factor is illustrated by the fact that such strongly exothermic reactions as

$$C_nF_{2n+2} + (n + 1)Fe \rightarrow nC + (n + 1)FeF_2$$

or

$$CF_4 + 2\ H_2O \rightarrow CO_2 + 4HF$$

take place only at high temperatures. The failure of fluorocarbons to corrode metals and oxides is of course of great practical importance.

The nuclear properties of these compounds are also interesting. The thermal neutron absorption cross sections of carbon and fluorine are 0.009 and 0.0032 barns, so that neutron loss in a fluorocarbon medium is all but negligible. They have, through their carbon content, some moderating ability. For example, 1 cc of $C_{12}F_{10}$ contains about 0.07 gram atoms of carbon, which may be compared with the corresponding quantity for graphite, 0.15.

Considering all their properties, it would be surprising if there should not prove to be some nuclear applications for fluorocarbons, in such services as coolants, slurry vehicles, working fluids for heat engines, hydraulic fluids, lubricants, etc., provided only radiation stability is achieved.

In the past three years, several papers on the radiation chemistry of liquid fluorocarbons have appeared.[5,6,7,8] The results were most interesting and valuable, but the picture they provided was by no means complete and a much larger scale and more systematic research program seemed to be called for in this field. In particular it would be desirable to obtain data which would permit comparison of aliphatic, alicyclic and aromatic fluorocarbons with each other and with the corresponding hydrocarbons, and to elucidate the mechanisms of radiolysis. As a first step toward this rather large objective, we have chosen to investigate the fluorocarbon analogs of those aromatic hydrocarbons which have proved to be among the most stable of all organic compounds, the polyphenyls and naphthalene.

SYNTHETIC METHODS

The fluorocarbon analogs of benzene, naphthalene and biphenyl, and also the corresponding saturated compounds, can be obtained from Imperial Smelting, Ltd., of Avonmouth, England. This has been a useful source, although the materials as received have required further purification, as described below. For such higher molecular-weight compounds as the perfluoroterphenyls no commercial source exists. The most promising synthesis is the defluorination of a more saturated fluorocarbon of the proper cyclic structure by passing its vapor over hot nickel or iron, as described by J. C. Tatlow et al.[9] Thus to make C_6F_6 the reaction, starting with perfluorocyclohexane, is

$$C_6F_{12} + 3\ Fe \xrightarrow{500^\circ C} C_6F_6 + 3\ FeF_2 \qquad (1)$$

Since Tatlow has successfully applied such reactions to the synthesis of perfluoronaphthalene and perfluorobiphenyl (this method is probably the one used by our English suppliers of these compounds) it is worth trying for perfluoroterphenyl.

Saturated starting materials can be made in various ways, the best-known probably being the fluorination of the corresponding hydrocarbon or its aromatic analog with CoF_3. The organic vapor is passed over the solid fluorinating agent, which is usually stirred by some mechanical device. In the present work a modification was tried: the use of a fluidized bed of CoF_3. This technique allows temperature control in the extremely exothermic reaction. The reactor consisted of a vertically mounted $1\frac{1}{2}$" i.d. nickel tube, which was charged with $1\frac{1}{2}$ lbs. of commercial CoF_3. The powder could be fluidized by flowing helium or argon up through it at a rate of 5 to 10 l/min. In a fluorination run, the bed temperature was raised to 200° to 300°C by external resistance heating. The fluidizing gas, or part of it, was then caused to bubble through a container of the liquid to be fluorinated, which was thus carried into the reactor as a dilute vapor. With this apparatus, several fluorination runs were carried out on benzene, under various conditions of temperature, rate of feed, etc. The results were disappointing in that a very large number of products were formed, and almost none of the completely saturated C_6F_{12}. Formation of fines was also a problem.

In the hope of getting more complete fluorination of the hydrocarbon, and of avoiding the necessity of regenerating the CoF_3 from CoF_2 by fluorination, recourse was had to direct fluorination by hydrocarbon in a fluidized bed. This work was carried out as a joint effort of the authors with L. P. Hatch and

J. J. Reilly, Jr., also of Brookhaven. They had made the observation that a fluidized bed of aluminum oxide is a good medium for fluorination, the oxide particles remaining unattacked and undergoing negligible attrition up to 600°C. With such a bed, the procedure was to introduce dilute fluorine and dilute organic vapor through separate nozzles near the bottom of the column. The reaction products were removed from the gas leaving the column by cold traps, as before. The most important variables were temperature, organic feed rate, and ratio of fluorine to organic. The method has not been completely evaluated, but preliminary results have shown that fewer and more fully fluorinated products were formed from benzene than in the CoF_3 bed, and reasonable yields of C_6F_{12} were obtained. Runs have also been carried out on terphenyl, with the aim of making perfluoroterecyclohexyl. The product consisted of an ether-soluble fraction, of low volatility. The latter has proved difficult to separate into individual compounds. Due to the short residence time of the reactants in the bed (two to six seconds, in the equipment used), it appears that there is appreciable degradation when attempting to completely fluorinate large molecules such as terphenyl. New reactors are now being built, to run in a series of perhaps three, with only a fraction of the total fluorine requirement being added in each bed.

Another route to saturated fluorocarbons, which avoids the use of either CoF_3 or F_2, is the electrochemical method of J. H. Simons.[10] When a current is passed through a solution of an organic compound in liquid anhydrous HF, highly fluorinated products are formed. In the case of benzene, for example, one first prepares a derivative which is soluble in HF, benzoyl fluoride. On the passage of current, a number of products are formed, including C_6F_{12}, but by far the most abundant product is $C_6F_{11}COF$. This compound can be hydrolyzed to the carboxylic acid, which can be thermally decomposed:

$$C_6F_{11}COOH \xrightarrow[\text{in graphite}]{\text{pyrolysis}} C_6F_{10} + CO_2 + HF$$

The perfluorocyclohexene formed is an even better starting material for the Tatlow reduction step (reaction 1) than the wholly saturated fluorocarbon. Much interesting work has been done on this and similar series of reactions at the Monsanto Research Corporation's Everett (Massachusetts) laboratories, on behalf of the Air Force;[11] but it has not yet been applied to the compounds of most concern to us.

A possible synthesis of the heavier fluorocarbons on a very small scale is one that exploits the polymerization that often results from irradiation. Just as biphenyl under irradiation forms quaterphenyl and hydrogen, so the corresponding fluorocarbon might condense in a similar way; and if an equimolar mixture of perfluorobenzene and perfluorobiphenyl were irradiated, one might hope to find perfluoroterphenyl among the products. Accordingly, such a mixture was in fact made up and irradiated in the Brookhaven reactor. The assay of the radiolysis products is still in progress.

PURIFICATION OF MATERIALS

None of the fluorocarbons wanted for radiolysis and thermal decomposition studies could be obtained in pure form. In the case of the aromatic compounds, although total impurities were of the order of 2-5%, the hydrogen content was not known. In the case of the aliphatic fluorocarbons, hydrogen content was believed to be very low, but the materials were mixtures of isomers. In all cases, the most efficient, if not the only, way to purify the desired compounds

was by preparative scale gas-liquid chromatography (GLC).

The GLC behavior of the different classes of fluorocarbons is illustrated in Figure 1. The aromatic C_6F_6 has quite good retention times on both diisodecyl sebacate and polypropyleneglycol columns, while the alicyclic C_6F_{12} (perfluorocyclohexane) and C_8F_{16} (perfluoroethylcyclohexane) come through very rapidly, even at room temperature. In order to obtain reasonable resolution of alicyclic and aliphatic fluorocarbons with standard length columns, it is necessary to use a fluorocarbon or "Kel-F" type oil such as the "Halocarbon" oil used for the two bottom chromatograms. With this stationary phase at -20°C, mixtures of fluorocarbon gases are easily resolved, except for the CF_4-C_2F_6 pair.

The chromatograms in Figure 1 were all obtained with analytical columns using a Perkin-Elmer 154-C and a Model 500 F & M. The F & M Model 500 was also used for gram-scale purification. Preparative scale columns were the standard F & M 8-foot columns of 5/8-inch internal diameter. "Chromasorb W" was used as the support, and three different stationary phases, Ucon LB-550-X (polypropylene glycol), silicone oil #710, and "Halocarbon" oil 14-25 (chlorotrifluoroethylene polymer). Column operating conditions for the various separations are given in Table I.

TABLE I

PREPARATIVE SCALE GLC COLUMN OPERATING CONDITIONS

Compound purified	Stationary phase	Column length, ft.	Column temperature, °C	He flow rate, cc/min.	Sample Size ml.
C_6F_6	Silicone oil 710	8	65	240	1.0
	Ucon LB-550-X	8	65	240	0.8
$C_{12}F_{10}$	Ucon LB-550-X	8	150	360	0.25
$C_{10}F_{18}$	Halocarbon 14-25	16	100	500	0.5

In the case of two commercial starting materials, perfluorobiphenyl and perfluorodecalin, one stationary phase was sufficient to remove the impurities present. With the commercial hexafluorobenzene, however, two were required. As shown in Figure 2, the majority of the impurities were removed by the silicone 710 column. Those remaining all had retention times longer than C_6F_6 using the Ucon stationary phase, and were removed from it by passing through the Ucon preparative scale column.

Figure 3 shows an analytical scale chromatogram of perfluorodecalin using a Halocarbon stationary phase. The cis and trans isomer peaks were partly resolved as was the impurity peak on the leading edge of the main peaks. In order to remove this impurity and achieve a reasonable yield of the main components on a preparative scale, two 8-foot columns were used in series.

Preparation of Samples for Irradiation

After GLC purification the only remaining contaminant of any significance is water formed by condensation during trapping of the product. The treatment used to remove water was to shake the liquid fluorocarbon overnight with P_2O_5 in an evacuated container with a break seal. The sample was then transferred by vacuum distillation into a bulb where it was given several melt-freeze cycles with pumping before transfer under vacuum into the weighed nickel cells.

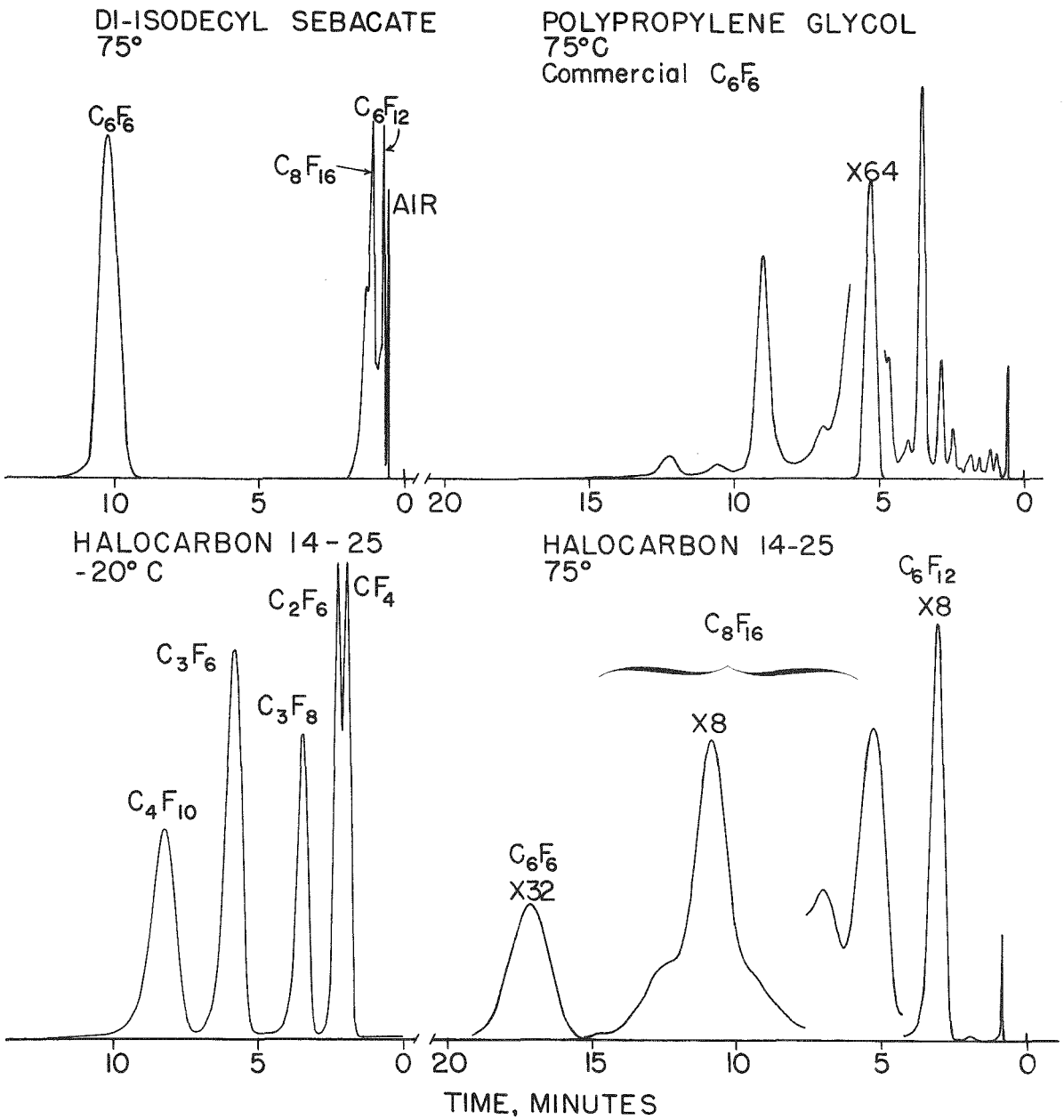

Figure 1. Chromatograms of Fluorocarbons on Different Stationary Phases.

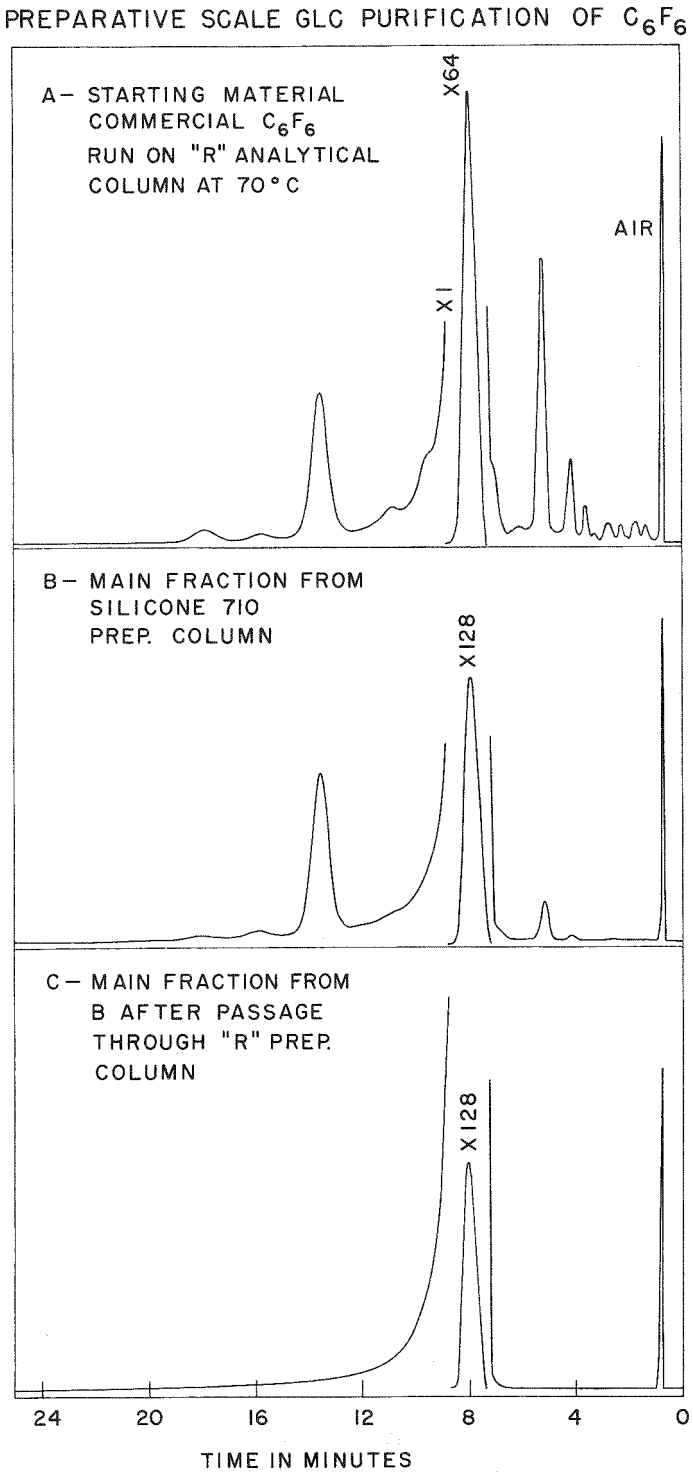

Figure 2. Chromatographic Purification of C_6F_6.

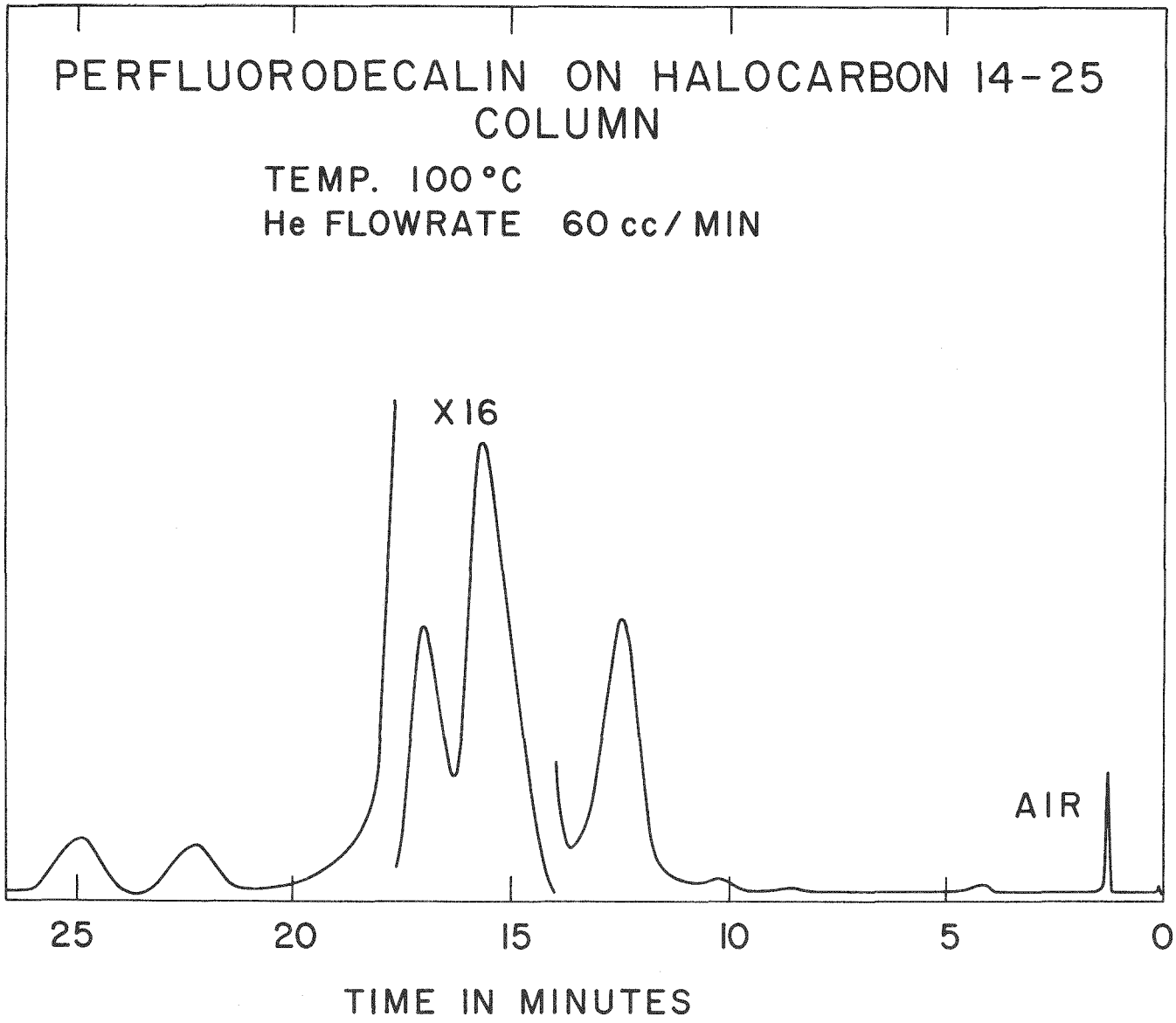

Figure 3. Chromatogram of Perfluorodecalin.

The cells were connected to the nickel inlet tubing. After filling the cells, the valves were closed off and the assembly removed from the vacuum system for reweighing.

IRRADIATIONS

Electron, γ-ray, and reactor irradiations were carried out on several of the unpurified commercial materials using both glass and nickel cells. The irradiations with impure materials were of use as familiarization runs and for comparison with the work of others such as Wall[7] with relatively pure C_6F_6. Comparison of glass and metal cells showed the desirability of the latter, since considerable reaction with the glass occurred during irradiation. Other workers[5,6,7] have reported negligible reaction with aluminum during fluorocarbon irradiations, and we have observed only slight, if any, reaction with nickel at room temperature. Since we hope eventually to perform irradiations at temperatures of the order of 400-500°C, we shall continue to use nickel cells in the work with purified materials.

Although gas phase irradiations of purified C_6F_6 have been carried out with Kr^{85} (internal source) and Co^{60} γ-rays (external source), the discussion in this paper will be limited to liquid phase irradiations with Van de Graaff electrons. The compounds irradiated were those whose purification was discussed in the previous section--perfluorobenzene, perfluorobiphenyl and perfluorodecalin.

Approximately 4 ml samples of liquid were irradiated in cylindrical cells 1.8 cm long and 1.6 cm inside diameter with 0.005 in. thick windows. The windows degraded the incident 1.5 Mev electrons in the Van de Graaff beam to an average of 1.3 Mev. Doses given were a little under 10^9 rads at dose rates of 2×10^5 rads/sec. The C_6F_6 and $C_{10}F_{18}$ irradiations were done at room temperature, while the $C_{12}F_{10}$ (MP 68°C) was irradiated at 100°C. In the $C_{12}F_{10}$ irradiations the valve and connecting tubing between valve and cell were heated to prevent $C_{12}F_{10}$ which distilled out of the cell from solidifying outside the cell and thus being removed from the reaction zone.

Processing of Products

a. Gases

After irradiation the cells were attached to a vacuum system of the type shown in Figure 4. With the cell contents just frozen, the valve was opened and any condensible gases were frozen over with liquid nitrogen into the Ward still, W, for a short time such as 1/2 minute. With the valve closed cell contents were then melted, refrozen, and the cell again opened to the Ward still for about 1/2 minute.

The Ward low-temperature still was constructed and operated essentially as described by LeRoy.[12] Gases from CF_4 up to C_6 fluorocarbons could be roughly separated into fractions of different carbon number. These fractions were measured in the calibrated gas burette B, and could then be removed for analysis by mass spectrometer or GLC at the point shown in the diagram.

b. Liquids and Solids

In the case of the perfluorobenzene and perfluorodecalin, unchanged starting material and irradiation products liquid at room temperature were removed from the cell by vacuum distillation. In the case of perfluorobiphenyl,

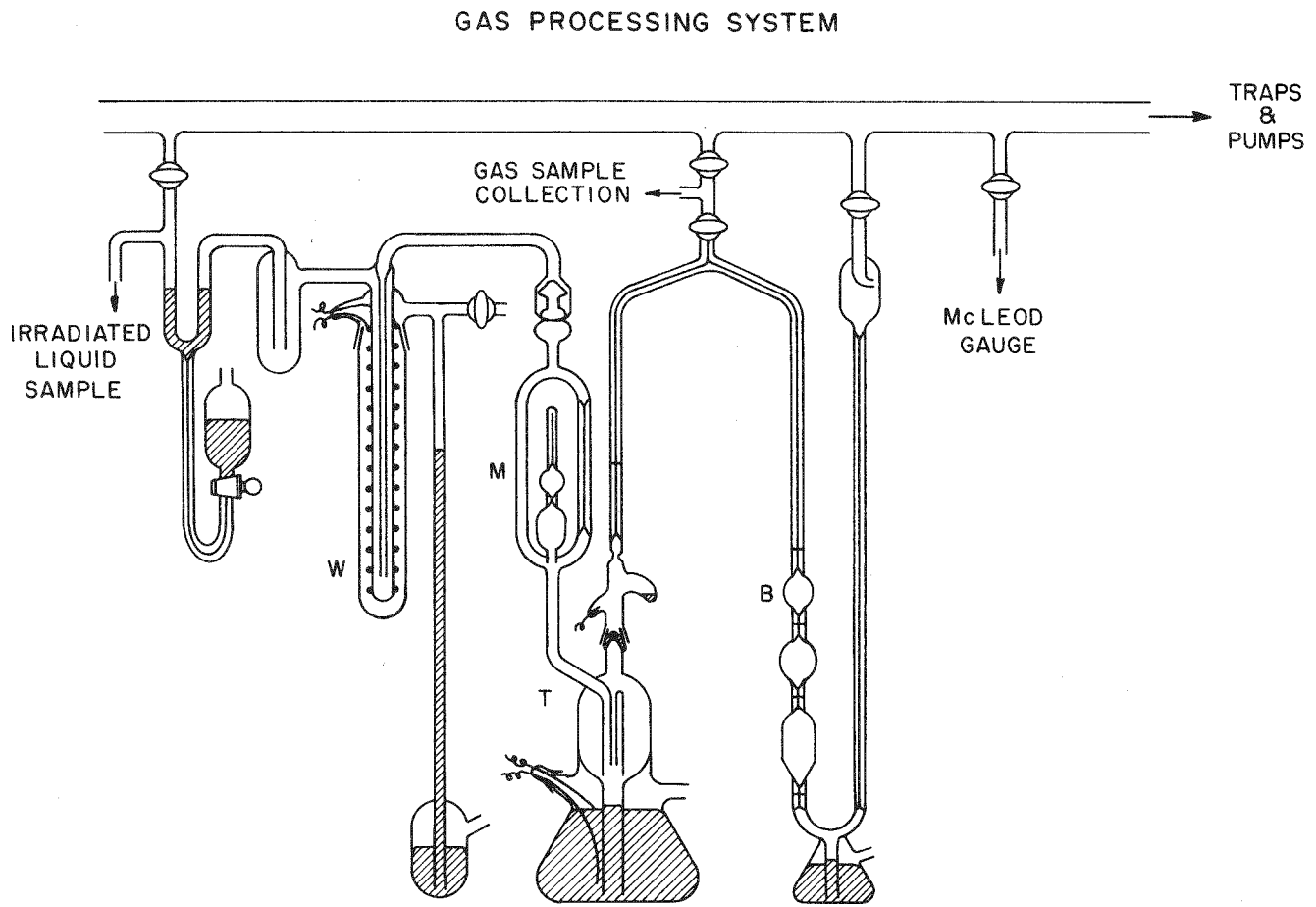

Figure 4. Apparatus for Analysis of Gaseous Radiolysis Products.

the cell was heated to liquefy the contents[a] and the volatile components were removed by vacuum distillation through heated tubing into a cold trap. The trap was then warmed to just liquefy the distillate, and a fraction lighter than $C_{12}F_{10}$ was collected in a second cold trap, most of the $C_{12}F_{10}$ remaining behind on the walls of the warm trap.

The solid residues in the cells were treated with solvents to obtain rough fractionation. It was found, for example, that all the lower boiling residues were fairly soluble in ether, and the ether insoluble residues were labelled "high boilers." These latter fractions were quite soluble, but not completely so, in fluorocarbons such as C_6F_6 and perfluoroethylcyclohexane, in which they could be conveniently introduced into a chromatograph.

The liquid and solid fractions were processed on analytical GLC columns, the liquid fractions isothermally, the solid both isothermally and with linear temperature programming to temperatures of 400°C or higher. The latter has proved useful for examining the high-boiler components, though standards will be needed before these can be identified any further than simply as C_{18}'s, C_{24}'s, etc. In fact even for identification of many liquid products, standards would be most helpful. Some single component collections have been made using analytical columns and components were examined by IR spectrophotometry and molecular weight determination. Now that considerable operating experience has been gained using preparative scale columns, it is planned to use them for processing irradiation products and to obtain enough material for both elemental analysis and molecular weight determination wherever possible. A mass spectrometer able to handle liquid and solid fluorocarbons is not yet available to us, but would be invaluable.

RESULTS

As yet only a few products other than gases have been identified and measured. However, G-values have been determined for total gas yield and polymer formation. Polymer is defined as material of higher molecular weight than the starting compound, since this fits in conveniently with the processing methods employed. Because the exact nature of the polymeric material was not determined, G-values for polymer formation are expressed in terms of disappearance of monomer.

Results of our irradiations are summarized in Table II. Wall's results with C_6F_6 are given for comparison, as are results of other workers for the hydrocarbons benzene and biphenyl.

Our G-values for C_6F_6 radiolysis agree very well with those of Wall obtained under comparable experimental conditions. Our gas yield in the γ-irradiation using a nickel cell is similar to Wall's, although an order of magnitude higher than that obtained in our electron irradiation in nickel. We have found that γ-irradiations always give somewhat higher gas yields than electron irradiations. Polymer yields were definitely influenced by degree of purity of the C_6F_6, and our lower G-value for purified material is in good agreement with Wall's. The perfluorobiphenyl radiolysis gave extremely low gas yields and a polymer yield somewhat over half that of C_6F_6.

---

[a] It is assumed the temperature required for liquefaction is no higher than the melting point of $C_{12}F_{10}$; in fact, it is almost certainly lower.

TABLE II

AROMATICS

Laboratory	Compound	Purity	Type of Irradiation	Container	G_{gas}	$G_{polymer}$
BNL	C_6F_6	commercial	electron	pyrex	0.036	2.8
BNL	C_6F_6	commercial	$Co^{60}\gamma$	nickel	0.017	2.6
BNL	C_6F_6	purified	electron	nickel	0.001	2.15
NBS[7]	C_6F_6		γ	nickel	0.01	2.01
ANL[13]	C_6H_6		γ	pyrex	0.051	0.93
BNL	$C_{12}F_{10}$	purified	electron	nickel	0.0001[a] (approx)	1.4[a]
California Research Corp.[14]	$C_{12}H_{10}$		$Co^{60}\gamma$	pyrex	0.007[b]	0.25[b]

ALICYCLICS

BNL	C_8F_{16}	commercial	$Co^{60}\gamma$	nickel	0.75	2.2
BNL	$C_{10}F_{18}$	purified	electron	nickel	0.15	1.2

[a] Irradiation temperature 100°C
[b] Irradiation temperature 80°C

Comparing the two aromatic fluorocarbons studied with their hydrocarbon analogues shows that the overall stabilities of the fluorocarbons are lower than those of the hydrocarbons. Although the fluorocarbons undergo more reaction to form high molecular weight compounds than do the hydrocarbons, they are more stable to fragmentation leading to gaseous products than are the hydrocarbons.

Of considerable interest is the relatively high stability of the alicyclic fluorocarbons studied. Gas yields were much higher than for the aromatics but polymer yields were of the same order, if not even lower. This state of affairs is in direct contrast to that observed with hydrocarbons where the alicyclics are much less stable to irradiation than are the aromatics.

SUMMARY

Fluorocarbons always have much greater thermodynamic stability than the corresponding hydrocarbons (for example, ΔF_f of CH_4 is -12 kcal/mole; for CF_4, ΔF_f is -152 kcal/mole) and it is reasonable to hope that their radiation stability may also exceed that of hydrocarbons. Should this be the case, one would have available a group of compounds of which some members, at least, should have applications in nuclear technology.

A systematic survey of the radiation chemistry of fluorocarbons has been undertaken, in which carefully purified compounds are being tested under reproducible conditions. The goal is to obtain quantitative information on the effects of radiation and high temperature, both separately and combined, on representatives of various classes of fluorocarbons such as the aliphatics, aromatics and alicyclics (to use hydrocarbon terminology), and to compare their behavior with that of the corresponding hydrocarbons.

A great deal of effort has had to be put into development of chromatographic and other analytical methods, and into preparative scale GLC. This is largely because of the lack of standards or even information concerning fluorocarbons. In fact, most of the higher molecular weight compounds desired as starting materials are unavailable commercially. As a result, work on the synthesis of these compounds has been undertaken using fluidized bed techniques.

Several one- and two-ring fluorocarbon compounds obtained commercially have been purified and subsequently irradiated using 1.5 Mev Van de Graaff electrons. Gaseous products have been analyzed by means of a low temperature LeRoy still and gas chromatography. G values which were obtained for formation of gas and of polymer indicate that the overall stability of the aromatic fluorocarbons tested is of the same order as that of the corresponding hydrocarbons.

REFERENCES

1. R. M. Potocki and D. E. Mann, Thermal Properties of Fluorine Compounds, NBS Report No. 1439, 1952.

2. J. R. Dacey and J. W. Hodgins, Canadian J. Res. 28, 173 (1950).

3. V. Dibeler, R. Reese, and F. Mohler, J. Chem. Phys. 26, 304 (1957).

4. J. Reed and B. S. Rabinovitch, J. Phys. Chem. 61, 598 (1957).

5. J. H. Simons and E. H. Taylor, J. Phys. Chem. 63, 636 (1959).

6. R. R. Burford et al, paper presented at ACS Meeting, Atlantic City, September 1959.

7. L. A. Wall, R. E. Florin and D. W. Brown, Report NBS 6126, September 1958 and J. Res. NBS 64A, 269 (1960).

8. R. F. Heine, paper presented at ACS Meeting, New York, September 1960.

9. J. C. Tatlow et al., Nature 183, 586, 588 (1959).

10. J. H. Simons (Ed.), Fluorine Chemistry, p. 414, Academic Press, New York, 1950.

11. J. W. Dale et al., Report NP-8781.

12. D. J. LeRoy, Can. J. Research, B, 28, 492 (1950).

13. S. Gordon, A. R. Van Dyken, and T. F. Doumani, J. Phys. Chem. 62, 20 (1958).

14. K. L. Hall, private communication.

THE STANDARD FREE ENERGY OF FORMATION OF ThC_2 FROM ELECTROMOTIVE FORCE MEASUREMENTS[a]

By J. J. Egan and J. Bracker

Brookhaven National Laboratory, Upton, New York

ABSTRACT

EMF measurements on the cell Th, ThF_4(s)/CaF_2(s) ThF_4, ThC_2, C(s) between 700 and 1000°C yielded the free energy of formation of ThC_2. At 800°C, ΔF^o = -29.6 ± 0.1 kcal. Estimates of the entropy and the heat of formation from the temperature coefficient gave values of ΔS^o = -7.2 cal $mole^{-1}deg^{-1}$ and ΔH^o = -37.4 kcal/mole.

All components of the cell were solid at the temperatures used. Since CaF_2 is a pure anionic conductor, no possibility of interference from junction potentials arose. The cells were operated over a period of three to four days, and the reproducibility with time and temperature cycling was ± 3 mv. Details are given on the experimental arrangement of the cell and the preparation and handling of the components. Other cells using liquid electrolytes, which were not entirely satisfactory, are discussed.

---

[a]The information in this paper has been submitted for publication in the Journal of Physical Chemistry.

Be U

PREPARATION OF HIGH PURITY BERYLLIUM OXIDE

by R. E. Moore, J. H. Shaffer, and H. F. McDuffie

Oak Ridge National Laboratory[a]
Oak Ridge, Tennessee

INTRODUCTION

The intrinsic requirements of a moderator material for high temperature nuclear reactors have stimulated interest in the properties of beryllium oxide. The availability of very nearly pure beryllium oxide is highly desirable for evaluating the effects of impurities and specific additives on the sintering characteristics and irradiation behavior. As a result of a comprehensive survey of beryllium purification processes,[1] it was concluded that solvent extraction processes offered the possibility of achieving very high purity. An extraction process, previously reported to be useful in analytical separations and decontamination procedures,[2,3,4] was selected for development as a preparative method. The process consists of extracting a solution of beryllium acetylacetonate, $Be(CH_3COCHCOCH_3)_2$, in carbon tetrachloride with an aqueous solution containing ethylenediaminetetraacetic acid (EDTA). Beryllium is largely retained in the organic phase while most metallic impurities are complexed with EDTA in the aqueous phase. The beryllium is subsequently back-extracted into nitric acid and precipitated as hydroxide with ammonium hydroxide. Beryllium oxide is prepared by calcining the pure hydroxide at 600-1000°C.

THE EXTRACTION SYSTEM

Distribution Ratios

A preliminary study of distribution ratios (aqueous/organic) of beryllium and many other metal ions was made at room temperature (25 ± 2°C) using equal volumes of solutions with the following original concentrations: aqueous phase, 0.1 m metal nitrate, 0.12 m EDTA; organic phase, 0.78 m acetylacetone in CCl_4. Solids crystallized from many of the aqueous metal nitrate-EDTA solutions; they were removed before equilibration with the organic phases. Consequently, the initial metal concentrations of these solutions were somewhat less than 0.1 m. While these determinations may not be identical to those applicable to an optimized purification process in which the reagent concentrations may be vastly different, they are of interest as a guide in the

a. Operated by Union Carbide Corporation for the U. S. Atomic Energy Commission.

3

development of such a process.

The distribution ratio for beryllium was found to vary from 0.015 to 34.5 over the pH range 5.1 to 1.1. In a purification process the extraction curve for beryllium in the absence of EDTA would be more relevant because only enough EDTA would be present to ensure the complexing of impurities. Under these conditions the distribution ratio varies from 0.01 to 11.0 over the pH range 7 to 1.1. Values for aluminum, the impurity most difficult to remove, vary from 0.42 to 48.5 over the pH range 6.0 to 1.5 with the most efficient separation occurring at pH ~ 4.5. Distribution ratios for many elements are so high (>100) that their removal from beryllium should present no difficulty. Included among these are Na^{+}, K^{+}, Ca^{+2}, Ba^{+2}, Sr^{+2}, Zn^{+2}, Cu^{+2}, Ni^{+2}, Ce^{+3}, and the anionic impurities such as B, P, Si, etc.

For convenience, most batch extractions were carried out with saturated EDTA solutions containing excess EDTA. After equilibrations with organic phases, the pH values of the aqueous phases were in the range 3.3 to 4.2. At pH 3.3 the distribution ratios for Be^{+2}, Be^{+2} (no EDTA), Al^{+3}, and Fe^{+3} were approximately 0.045, 0.035, 2.0, and 35 respectively. The distribution ratio for Mg^{+2} was about 1.7 over the entire pH range 1.4 - 6.7, but in the absence of EDTA, the values were well over 100. If the starting material in a purification process contains a large amount of magnesium, a preliminary aqueous extraction without EDTA is desirable.

The Organic Phase

The phase diagram of the organic system CCl_4-$CH_3COCH_2COCH_3$-$Be(CH_3COCHCOCH_3)_2$ at 27°C is shown in Fig. 1. This diagram is based on the solubilities of beryllium acetylacetonate in acetylacetone, carbon tetrachloride and one solution of acetyl acetone in carbon tetrachloride. The liquid area permits a wide choice of compositions which may be used in contact with an aqueous EDTA phase. Compositions containing only a small amount of acetylacetone are preferred in order to minimize the loss of this reagent to the aqueous phase.

THE PURIFICATION PROCESS

The procedure outlined below was used successfully for the preparation of a number of 50 gram batches of high-purity beryllium oxide.

(1) Preparation of the Organic Solution: Beryllium hydroxide is dissolved in a solution of acetylacetone and carbon tetrachloride. The reaction

$$Be(OH)_2 + 2CH_3COCH_2COCH_3 \rightarrow Be(CH_3COCHCOCH_3)_2 + 2H_2O$$

produces water which floats on the denser organic solution and is removed.

(2) Extraction with Water: This step is desirable if the starting material contains a large amount of magnesium. Alkali metals, chloride, fluoride, etc., should also be removed.

(3) Extraction with EDTA Solution: This step removes all metallic impurities which form stable EDTA complexes. The use of a saturated solution containing excess EDTA is convenient because pH adjustments are unnecessary. The EDTA extraction may be repeated as many times as necessary to achieve the desired degree of purity.

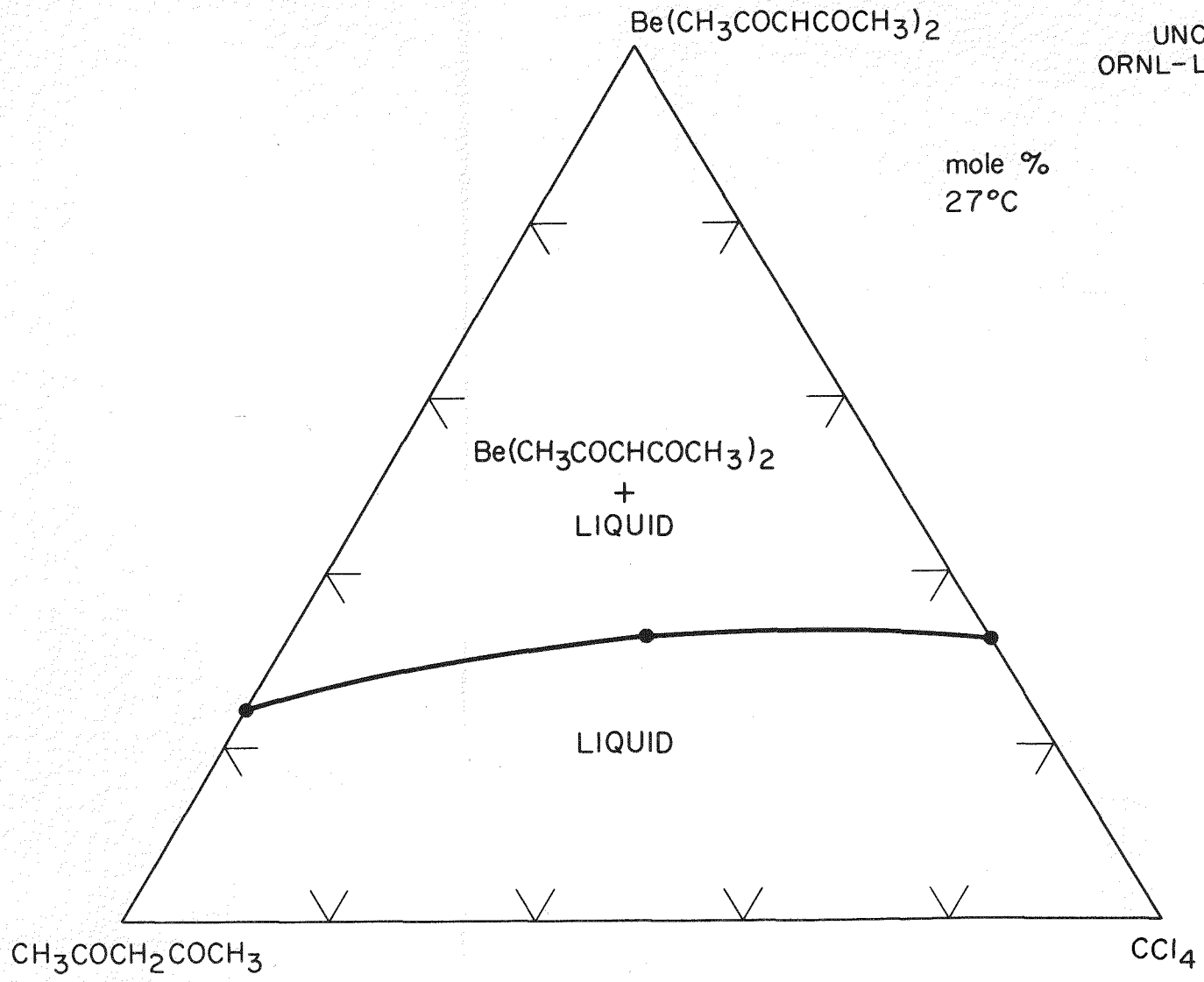

Phase Diagram of Organic System.

Figure 1. Phase Diagram of Organic System.

(4) Back-Extraction of Beryllium: Most of the beryllium is extracted into nitric acid solution if the final pH is less than 1. If a concentrated organic solution is used, a considerable amount of acetylacetone is lost to the aqueous phase since the reaction

$$Be(CH_3COCHCOCH_3)_2 + 2H^+ \rightleftharpoons Be^{+2} + 2CH_3COCH_2COCH_3$$

produces two moles of acetylacetone per mole of beryllium ion. Dilution of the organic phase with carbon tetrachloride before the back-extraction minimizes this loss.

(5) Precipitation of Beryllium Hydroxide: Beryllium hydroxide is precipitated upon addition of pure ammonium hydroxide solution to the aqueous nitric acid solution. If a concentrated organic solution is used in the process and not diluted with carbon tetrachloride before the back-extraction, beryllium acetylacetonate will precipitate with the hydroxide. One way to minimize this difficulty is by precipitating the acetylacetonate at pH 2.5 - 3.0 and washing it from the aqueous solution with carbon tetrachloride. The addition of excess ammonium hydroxide will then precipitate beryllium hydroxide almost exclusively.

(6) Calcining to Oxide: The hydroxide samples were calcined in covered porcelain dishes at 600-1000°C to ensure the complete volatilization or decomposition of any beryllium acetylacetonate present. In some preparations, however, some of the material decomposed to leave a carbon residue in the product.

ANALYSIS OF PURIFIED BERYLLIUM OXIDE

The results of spectrographic analysis (J. A. Norris and Z. Combs, ORNL) of one of the purest 50 gram beryllium oxide preparations are as follows:

Impurity	ppm
B	< 1
Co, Cu, Li, Mn, Na, Pb, Sn	< 5
Al, Ca, Cr, Fe, K, Mg, Mo, Ni, Rb, Si, Sr, Ti, V	< 10
Ba, Zn	< 20
P, F	not detected

All metallic impurities were thus found to be below the present spectrographic limits of detection. The results of this analysis were confirmed by the Oak Ridge Y-12 Plant Spectrographic Laboratory and National Spectrographic Laboratories, Inc., Cleveland, Ohio. Other 50 gram batches have been prepared in which the analyses were similar except that traces of sodium and magnesium, less than 5 and 10 ppm respectively, were found. The analysis of the beryllium hydroxide used as starting material indicated the following impurities in terms of ppm in BeO: Mg, 500; Si, 200; Cr, 60; Al, 50; Ca, 50; Fe, 50; Na, 50; Mn, 20; B, 0.5; P and F, present.

Spectrographic analysis is not a good method for anionic elements such as fluorine or phosphorus, but these elements should have been removed completely. The presence of small amounts of carbon resulting from the thermal decomposition

of some of the residual beryllium acetylacetonate during calcining of the hydroxide can not be detected by the spectrographic method.

MATERIALS AND TECHNIQUES

Reagents

Eastman Kodak acetylacetone (2, 4-pentanedione, EK1088), Merck reagent grade ethylenediaminetetraacetic acid, Mallinckrodt analytical reagent carbon tetrachloride, and B and A reagent grade nitric acid were used without further purification. Deionized water was prepared by passing distilled water through an Illco-way research model deionizer obtained from Illinois Water Treatment Company, Rockford, Illinois. Ammonium hydroxide solution was made by passing ammonia gas into deionized water in a polyethylene container. Deionized water and ammonium hydroxide were stored in polyethylene bottles before use.

Beryllium hydroxide was Berylco Grade I obtained from The Beryllium Corporation, Reading, Pa. The spectrographic analysis is given in the preceding section. Excess water content (25%) was determined by calcining a weighed quantity to the oxide.

Avoidance of Contamination

All liquid phase equilibrations were carried out in polyethylene bottles, and separations of phases were accomplished with polyethylene siphons. The equipment was cleaned with nitric acid before use. Additions of reagents and solution transfers were accomplished with a minimum of exposure to laboratory air.

Equilibration of Phases

With liquid volumes as large as 1-2 gallons, the mechanical shaker used provided only surface agitation. Nevertheless, 1/2 to 1 hour seemed to be sufficient time for attainment of equilibrium. Rate studies with 25 ml of each phase showed that the extraction of beryllium in both directions is so rapid that equilibrium is attained in a few seconds under violent agitation. Several hours were required to dissolve beryllium hydroxide in the organic phase.

A Typical Purification Experiment

The following were added to a clean two gallon polyethylene bottle: 400.3 g $Be(OH)_2$, 1900 ml acetylacetone, 2235 ml CCl_4, and one gallon deionized water. After five hours agitation with a mechanical shaker, the $Be(OH)_2$ had dissolved. The aqueous phase above the organic solution was removed by applying vacuum through a clean polyethylene tube. One gallon of deionized water was added, the bottle was shaken for 1/2 hour, and the aqueous phase was removed. One gallon of deionized water and 20 g EDTA were added, the bottle was shaken for 1/2 hour, and the aqueous EDTA solution was removed. The EDTA extraction was then repeated twice. Approximately 1 gallon of an aqueous solution containing 600 ml concentrated nitric acid was added, and the bottle was shaken for 1-1/2 hours. Then the organic phase was removed from the bottom of the bottle by applying vacuum to a polyethylene tube. The aqueous phase was poured into another clean polyethylene bottle, and ammonium hydroxide solution was added to adjust the pH to 2.5, at which point beryllium acetylacetonate had precipitated throughout the solution. One gallon CCl_4 was added, the bottle was then added to the clean aqueous solution to precipitate $Be(OH)_2$. The hydroxide

was filtered onto Whatman No. 42 filter paper (24.0 cms) in a polyethylene buchner funnel, and washed with CCl_4 and then with acetone (the acetone wash was omitted in other experiments). After partially drying the $Be(OH)_2$ in the funnel below 100°C, the wet $Be(OH)_2$ cake was transferred to a porcelain dish. The covered dish was heated step-wise in a muffle furnace to 700°C and held at this temperature for one hour. The BeO product weighed 49 g. Since the $Be(OH)_2$ contained 25% excess water, the percentage recovery of BeO is approximately 28%. By varying the relative quantities of reagents, the percentage recovery can be increased; in most experiments between 30 and 50% was recovered.

CONCLUSION

A solvent extraction process for obtaining high-purity beryllium oxide has been demonstrated. Initial laboratory-scale quantities have been prepared for such purposes as improved spectrographic standards, sintering studies and irradiation experiments. Current studies of the extraction system are aimed at the determination of optimum conditions for large-scale production.

ACKNOWLEDGEMENTS

The authors are especially grateful to W. R. Grimes for encouragement and helpful discussions in connection with this work. It is a pleasure to acknowledge the assistance of D. B. Wagoner, W. M. Johnson, and B. F. Hitch who performed much of the detailed laboratory work. J. A. Norris and co-workers were responsible for spectrographic analyses of oxide samples. W. F. Vaughan and co-workers performed chemical analyses of solutions used for determination of distribution coefficients.

REFERENCES

1. R. E. Moore, Purification of Beryllium Compounds: A Literature Survey, USAEC Report ORNL-2938, Oak Ridge National Laboratory, June 1960.

2. J. A. Adam, E. Booth, and J. D. H. Strickland, Anal. Chim. Acta. 6, 462 (1952).

3. I. P. Alimarin and I. M. Gibalo, J. Anal. Chem. U.S.S.R. (Engl.) 11, 405 (1956).

4. J. D. Buchanan, J. Inorg. Nucl. Chem. 7, 140 (1958).

SURFACE TENSION OF FUSED SALTS: AN EMPIRICAL CORRELATION[a]

by Richard B. Ellis and William S. Wilcox

Southern Research Institute
Birmingham, Alabama

Numerous attempts have been made to derive theoretical or semitheoretical equations for the surface tension of fused salts. Several attempts to relate surface tension to heat of vaporization[1,2,3] have been moderately successful for covalent liquids but not for the highly ionic liquid salts. Other approaches based on heat of fusion,[4,5] which have had some success with liquid elements, have likewise failed when applied to fused salts.

Recently, statistical mechanical approaches, developed for single-species liquids composed of uncharged rigid spheres, have been adapted to fused salts. Reiss and Mayer[6] obtained an equation based only on the density of the salt and the hard-core diameters of the ions:

$$\gamma = \frac{kT}{4\pi a^2}\left[\frac{12y}{1-y} + \frac{18y^2}{(1-y)^2}\right] \qquad (1)$$

$$y = \frac{\pi a^3 \rho}{6}$$

where γ is surface tension, k is Boltzman's constant, T is temperature, a is the average hard-core diameter of the ions, and ρ is the number density of ions. These authors used the distance of closest approach in gaseous molecules as the average hard-core diameter of the cation and anion. This equation gives values of the right order of magnitude for the surface tensions of alkali metal halides, alkaline earth metal halides, and the chlorides of zinc and cadmium. However, the surface tensions calculated by this equation increase with increasing temperature, contrary to experimental observation. Therefore, close agreement between calculated and experimental values depends on choice of temperature.

Stillinger[7] has adapted Fowler's[8] surface tension equation for use with uni-univalent fused salts:

$$\gamma = \frac{c(ze)^2}{16D} - \frac{\pi kT\, c^2 a^4}{2}\, g_m(a) \qquad (2)$$

[a] This work was performed under the sponsorship of the U. S. Atomic Energy Commission, Contract No. AT-(40-1)-2073.

in which c is the number density of ion-pairs (1/2 ρ defined above), z is the number of charges per ion, e is the charge on the electron, D is the dielectric constant of the fused salt, k, T, and a have same significance as above, and $g_m(a)$ is the mean pair correlation function at contact distance a. The mean pair correlation function may be evaluated according to the Reiss-Frisch-Lebowitz theory[9] by

$$g_m(a) = \frac{4 - 2y + y^2}{4(1 - y)^3} \qquad (3)$$

in which y is the same as defined above. Stillinger prefers to use the collision diameter calculated from compressibility data for the hard-core diameter, a, instead of the gas-molecule distance chosen by Reiss and Mayer; however, differences between the two diameters are small. Choice of a value for the dielectric constant is troublesome, since there are no direct experimental data. Van Artsdalen suggested the value 3, while Stillinger recommends the use of values based on optical properties, which range from 2 to 4. As a result of the relative magnitudes of the two terms in Equation (2), an uncertainty of 50 percent in D gives an uncertainty of about 30 percent in γ. The temperature variation of the surface tension calculated by Equation (2) is in the right direction but is not of the right magnitude.

Before these theoretical equations were published, we had begun a search for an empirical correlation in order to:

a. check existing data for gross errors,
b. estimate values where no experimental data exist,
c. serve as a proving ground for suggested models of the structure of the liquid surface.

Since fused salts are composed of ions, it is apparent that the structure of the liquid surface will be largely governed by a balance of coulombic forces. Also, x-ray and neutron diffraction data on fused salts indicate a short-range order similar to that in the crystalline solid, modified by a long-range disorder. The crystal lattice energy may be taken as a first approximation to the short-range forces acting between the ions of the liquid. Since the ions in the surface are not surrounded symmetrically by other ions, they will be subjected to polarization by the field of the underlying ions. The energy involved in this polarization will reduce the surface energy. For purposes of correlation with surface tension, we have chosen a function consisting of the lattice energy and the polarization energy, $\chi = E_L - E_\alpha$. In order to put these factors into terms of energy per unit area, a model structure of the surface is needed.

A reasonable model for the surface of salts of the symmetrical valence type, MX, is that of the (100) plane of the NaCl crystal, that is, alternate positive and negative ions in the surface, each with an ion of opposite charge immediately below. In the crystal, the surface area per ion-pair is $2(r_c + r_a)^2$, where r_c and r_a are the crystal radii of the cation and the anion respectively. The fact that the ions must be farther apart in the liquid than in the solid may be taken into account by assuming that the expansion in surface area is proportional to the expansion in volume;

$$\frac{A_l}{A_s} = (V_l/V_s)^{2/3}$$

where A is the surface area, V is the molar volume, and the subscripts refer to

the liquid and solid states.

The choice of a model for salts of unsymmetric valence type, such as MX_2, is complicated by the fact that they do not all have the same crystal structure. Also, the structures for some MX_2 salts are not known. However, they may be considered to lie between the extremes of the predominantly ionic type with the fluorite structure and the predominantly covalent type with the CdI_2 structure. In both of these structures, it is reasonable to consider the surface layer to consist entirely of anions, with one anion per "molecule" in the surface. For the fluorite structure, the anions are in cubic packing, while for the CdI_2 structure the packing is hexagonal. The area per molecule for the cubic packing is $4r_a^2$ and that for the hexagonal packing is $4r_a^2 \sin 60^\circ$, or $2\sqrt{3}\, r_a^2$. The difference between these two areas is not large enough to be significant for the present purpose, and so only the cubic packing is used here.

The energy of polarization of a surface ion by the field, F, of an immediately underlying ion of opposite charge is

$$\frac{\alpha F^2}{2} = \frac{\alpha}{2}\left(\frac{ze}{a^2}\right)^2 = \frac{z^2e^2\alpha}{2a^4}$$

where α is the polarizability of the surface ion, z is the number of charges on the underlying ion, e is the electron charge, and a is the interatomic distance, or the sum of the ionic radii. The correlation functions for MX and MX_2 salts, put into units of ergs per cm^2, are:

$$\chi_{MX} = \left[\frac{4.185 \times 10^{10} U}{N} - \frac{(\alpha_c + \alpha_a)z^2e^2}{2(r_c + r_a)^4}\right] \frac{1}{2(r_c + r_a)(V_l/V_s)^{2/3}}$$

$$\chi_{MX_2} = \left[\frac{4.185 \times 10^{10} U}{N} - \frac{\alpha_a z^2e^2}{2(r_c + r_a)^4}\right] \frac{1}{4r_a^2(V_l/V_s)^{2/3}}$$

In these equations, U is the crystal lattice energy in kilocalories per mole, N is Avogadro's number, and the other symbols have already been identified. When the MX salts are univalent, as in the alkali metal halides, z = 1, while for MX_2 salts z = 2.

For purposes of correlatation, values of the surface tensions are taken at a "corresponding temperature" that is 20 percent higher than the melting point on the absolute scale, $\Theta = 1.2\ T_m$. In calculating the correlation functions, the molar volumes of the liquid, V_l, are taken at this temperature. The values of V_s are taken at room temperature because the lattice energies and the ionic radii are evaluated at room temperature.

A number of investigators suggest that the total surface energy should be used instead of surface tension. Bloom uses the term surface heat content per unit area, $H_{s/a} = \gamma - (d\gamma/dT)T$, which is independent of temperature. Although our correlation function is dependent on temperature, there is some interest in comparing $H_{s/a}$ with χ taken at a particular corresponding temperature.

Table I contains values of our correlation function χ_{MX}, of experimental surface tension data at $\Theta = 1.2\ T_m$, and of surface heat content for the alkali metal halides. Table II contains χ_{MX_2}, γ_Θ, and $H_{s/a}$ for the alkaline earth

Table I. Monovalent Halides

Salt	χ_{MX} ergs/cm^2 x 10^{-3}	γ_θ ergs/cm^2	$H_{s/a}$ ergs/cm^2	Source
LiF	16.48	227.3	389.2	10
		213.8	346.5	20
LiCl	8.82	125.0	200.4	10
		119.5	180.7	12
		118.4	180.4	20
NaF	10.37	174.3	335.6	10
		141.1	272.2	20
NaCl	6.16	98.7	190.4	10
		96.4	216.2	11
		100.7	196.1	12
NaBr	5.34	92.6	178.2	10
		87.2	161.8	11
NaI	4.36	78.7	135.6	10
		71.4	171.9	11
		76.1	158.6	20
KF	7.20	125.0	240.2	10
KCl	4.55	82.9	173.2	10
		83.7	175.1	11
		85.1	181.4	12
		85.1	180.2	13
		83.3	172.2	14
KBr	4.01	74.1	159.3	10
		74.8	161.9	11
		76.4	157.8	20
KI	3.34	66.0	135.3	10
		62.5	162.5	11
RbF	6.51	109.3	202.3	10
RbCl	4.07	81.1	183.7	10
RbBr	3.65	77.1	156.1	10
RbI	3.08	68.1	146.0	10
CsF	5.26	92.7	181.9	10
CsCl	3.26	77.2	162.7	10
		76.4	140.7	13
CsBr	2.84	71.5	137.5	10
CsI	2.42	63.4	126.0	10

Table II. Divalent Halides

Salt	χ_{MX_2} ergs/cm² x 10^{-3}	γ_θ ergs/cm²	$H_{s/a}$ ergs/cm²	Source
$MgCl_2$	22.6	65.	77.	17
$CaCl_2$	22.3	141.	188.	15
		138.	196.	16
		144.0	180.1	13
$CaBr_2$	20.2	110.4	165.6	19
CaI_2	14.6	81.4	103.5	19
$SrCl_2$	23.9	156.4	232.4	19
$SrBr_2$	20.5	141.7	190.0	19
SrI_2	14.7	108.2	145.3	19
$BaCl_2$	20.4	146.3	263.1	14
$BaBr_2$	17.2	139.1	222.0	19
BaI_2	13.1	127.4	177.3	20
$CdCl_2$	25.9	80.1	101.3	18
		80.8	109.0	20
$SnCl_2$	24.0	94.	155.	20
$PbCl_2$	23.3	120.3	222.1	11
		118.7	233.7	12
		120.7	214.2	18

metal halides and for the chlorides of cadmium, lead, and tin. In Figures 1 and 2 the surface tensions and the surface heat contents of the MX salts are plotted against χ_{MX}. The lines were obtained by the method of least squares, excluding the data for the fluorides and LiCl, which seemed to have excessively large deviations. Surface tension measurements were then made in our laboratory on NaF, LiF, and LiCl. In the case of NaF our values for γ_Θ and $H_{s/a}$ were in very close agreement with those predicted by the correlation. For LiF, our value of γ_Θ was closer to the correlation line than Jaeger's value but it was still not in agreement, while our value of $H_{s/a}$ was in even poorer agreement. For LiCl, our data agreed with those of Duke, which were in good agreement with the correlation for γ_Θ but not for $H_{s/a}$.

In Figures 3 and 4, γ_Θ and $H_{s/a}$ for MX_2 salts are plotted against χ_{MX_2}. In Figure 3, the line is drawn arbitrarily through the points for $SrCl_2$ and SrI_2. The more covalent salts, $MgCl_2$, and $CdCl_2$, and $SnCl_2$ are scattered in the lower right corner of the graph. When $H_{s/a}$ is plotted against χ_{MX_2}, Figure 4 , there is a strong tendency for the data to fall into families according to the cations. It is interesting that a line drawn through the points for $MgCl_2$ and $CdCl_2$ is parallel to the lines for the alkaline earth families. There is a tendency for the compounds with more covalent character to have lower values of χ_{MX_2}, although $PbCl_2$ does not conform to this generality.

CONCLUSIONS

It is apparent that the correlation function χ_{MX} works fairly well with the alkali halides on an empirical basis. Therefore it may be inferred that the model structure assumed here is reasonable, although the existence of some other reasonable model is not necessarily precluded. The value of the correlation in disclosing gross errors is demonstrated in the case of sodium fluoride.

The limited success with the divalent halides indicates that, while there is some validity in our basic assumptions, there must be some other significant factors involved. There is a suggestion that the degree of covalent character may be important.

REFERENCES

1. J. H. Hildebrand, Solubility, 3rd ed., Chemical Catalog Company, New York, 1950.

2. J. F. Joliet, Comp. rend. 230, 2006 (1950).

3. P. K. Chatterjee, J. Technol. Bengal Eng. Coll. 2, No. 1, 49 (1957).

4. N. R. Mukerjee, J. Chem. Phys. 19, 502 (1951).

5. R. L. Choate and L. H. Lund, J. Chem. Phys. 19, 1062 (1951).

6. H. Reiss and S. W. Mayer, J. Chem. Phys. 34, 2001 (1961).

7. F. H. Stillinger, to be published.

8. R. H. Fowler, Physica 5, 39 (1938).

9. H. Reiss, H. L. Frisch, and J. L. Lebowitz, J. Chem. Phys. 31, 369 (1959).

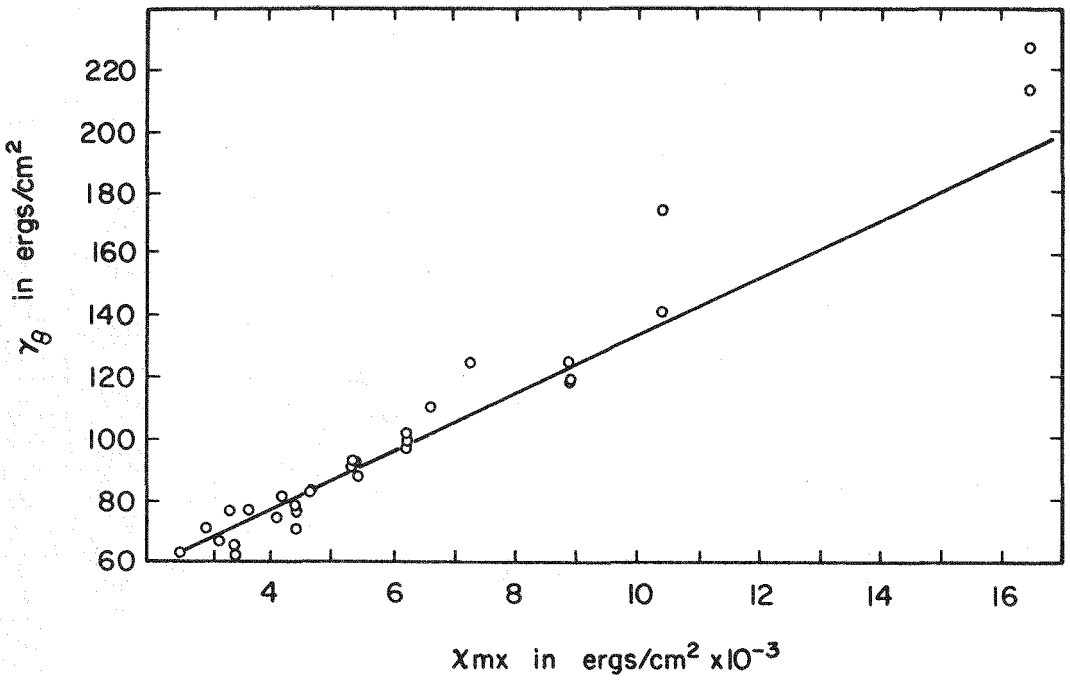

Fig. 1. Monovalent Halides

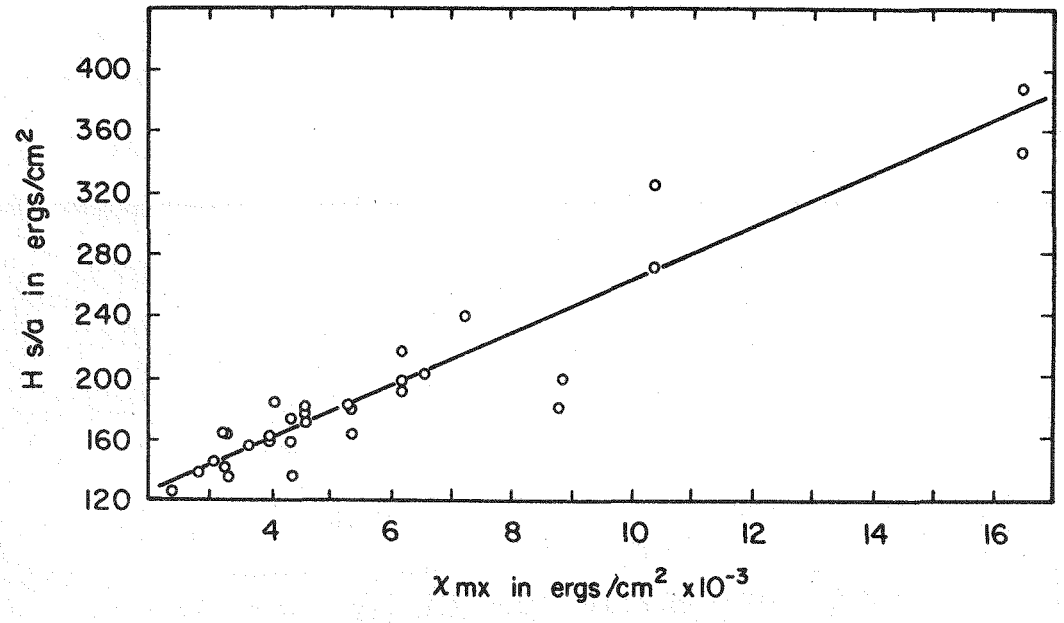

Fig. 2. Monovalent Halides

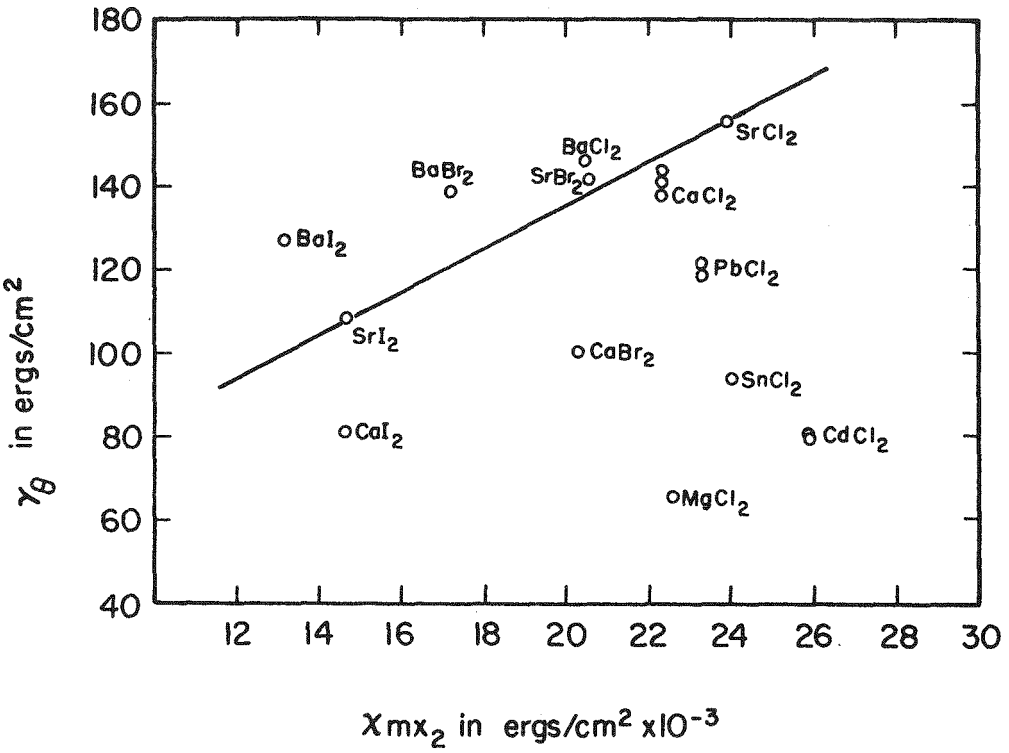

Fig.3. Divalent Halides

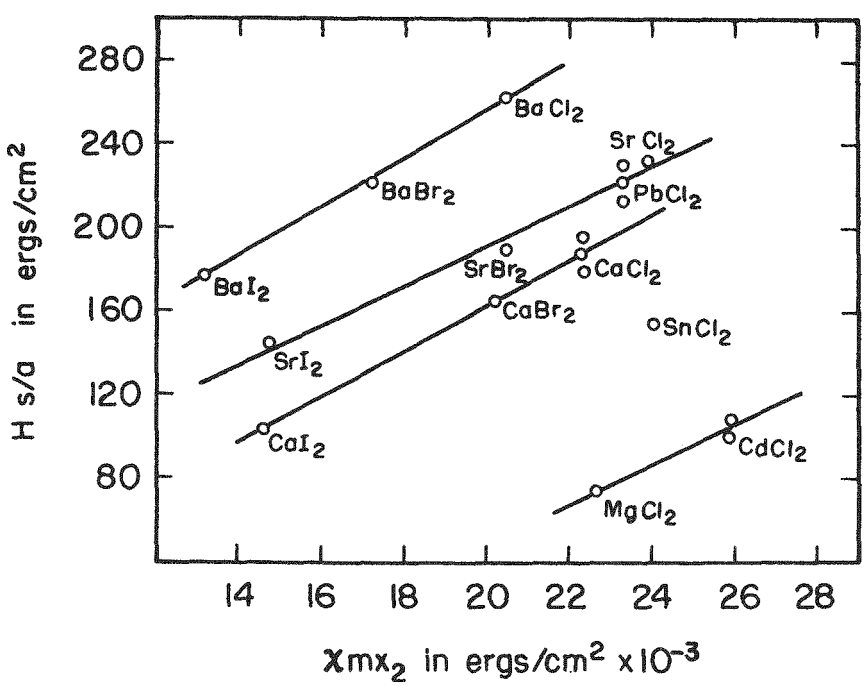

Fig.4. Divalent Halides

10. F. M. Hager, Z. anorg. allgem. Chem. 101, 1 (1917).

11. H. Bloom, F. G. Davis, and D. W. James, Trans. Faraday Soc. 56, 1179 (1960).

12. J. L. Dahl and F. R. Duke, J. Phys. Chem. 62, 1498 (1958).

13. R. L. Seifert, U.S.A.E.C. Report TID-6289.

14. J. S. Peake and M. R. Bothwell, J. Am. Chem. Soc. 76, 2656 (1954).

15. V. P. Barzakowski, Bull. Acad. Sci. USSR, No. 5, 825 (1940).

16. K. L. Strelets and O. G. Desyatnikov, J. Appl. Chem. 28, 35(1955)(Eng. trans.).

17. O. G. Desyatnikov, Zh. Priklad. Khim. 29, 793 (1956).

18. N. K. Boardman, A. R. Palmer, and E. Heymann, Trans. Faraday Soc. 51, 277 (1955).

19. R. B. Ellis, J. E. Smith, and E. B. Baker, J. Phys. Chem. 62, 766 (1958).

20. R. B. Ellis and A. C. Freeman, unpublisned data.

RECENT DEVELOPMENTS IN THE CHEMISTRY OF THE MOLTEN-SALT REACTOR EXPERIMENT

By F. F. Blankenship and W. R. Grimes

Oak Ridge National Laboratory[a]
Oak Ridge, Tennessee

ABSTRACT

The Molten-Salt Reactor Experiment, which will operate at 10 Mw (thermal) is scheduled to go critical early in 1964. This machine, which is intended to demonstrate the feasibility of long-term operation and maintenance of a circulating fuel reactor, will operate at 1200 to 1250°F. A molten fluoride mixture containing both uranium and thorium fluorides will serve as the fuel; heat will be transferred from the fuel to a coolant mixture of LiF and BeF_2. The reactor assembly will be constructed of INOR-8, with graphite in direct contact with the molten fuel serving as moderator. An operating lifetime in excess of two years is planned.

A mixture of LiF and BeF_2 serves as the solvent for the UF_4 and ThF_4. Possible difficulties with precipitation of UO_2 on inadvertent contamination of the system are avoided by incorporation of ZrF_4 in the melt. Oxide-fluoride behavior and phase relationships in this complex system which lead to choice of the final fuel composition ($LiF-BeF_2-ZrF_4-ThF_4-UF_4$, 70-23-5-1~1 mole %) will be described. Purification processes, based on treatment of the molten mixtures with anhydrous HF and H_2, have been applied to minimize the oxide ion concentration of the fuel as well as corrosivity due to presence of oxidizing cations.

The presence of graphite in contact with the molten fuel poses some problems. A variety of experiments has shown that graphite is neither attacked nor wetted by the fuel mixture. Penetration of the graphite by the nonwetting fluid (of relatively high surface tension) under modest pressures, as in the reactor, will be appreciable but quite tolerable. In-pile experiments to demonstrate that the situation is similar to the fissioning fuel mixture will be discussed.

Permeation of the graphite by fission product Kr and Xe will, of course, occur with consequent deposition of the daughter products of these materials within the graphite. This accumulation of appreciable nuclear poison within the

---

[a] Operated by Union Carbide Corporation for the U.S. Atomic Energy Commission.

moderator can be reduced by apparatus for stripping the Kr and Xe from the circulating salt stream; more effective control of this problem, however, depends on development of less permeable graphites.

URANIUM OXIDE PRESSURE-TEMPERATURE-COMPOSITION RELATIONSHIPS FROM 1000 TO 2000°K[a]

By Carl A. Alexander

Battelle Memorial Institute, Columbus, Ohio

and

Thomas S. Shevlin[b]
The Ohio State University, Columbus, Ohio

INTRODUCTION

The numerous investigators who have conducted equilibrium and X-ray diffraction studies of the uranium oxide-oxygen system have seen fit to represent their results in a conventional temperature-composition diagram. While such a diagram is useful in depicting the possible phases at a specific temperature, it can give no information concerning the oxygen pressure necessary to maintain the various phases at equilibrium.

In most experimental studies temperature and oxygen pressure are more easily controlled variables than is composition, hence a pressure-temperature diagram may be more meaningful than the existing diagram.

LITERATURE CITED

Data for construction of a pressure-temperature-composition phase diagram to temperatures of approximately 1400°K already exist in the literature. Specific references utilized in this compilation are: Gronvald's high temperature X-ray diffraction[1], Biltz and Muller's tensimetric dissociation pressure study[2], Ackermann and Thorn's dissociation pressure study[3], Blackburn's gravimetric effusion study[4], and Aronson and Belle's emf equilibrium investigation[5].

All the above investigations are in general agreement, at least at temperatures above 1000°K. A brief description of the system is as follows: a fluorite phase exists from an O/U ratio of 2.00 to 2.20, with this phase region extending to higher O/U ratios with increasing temperature. The

---

[a]Work supported under AEC Contract W-7405-eng-92.

[b]Present address: University of Washington, Seattle, Washington.

limiting value is about 2.24 at 1400°K but there is indication based on the yet unpublished work of Roberts and Walter[6] that this may shift slightly to higher O/U ratios with increasing temperature. At O/U ratios from about 2.20 to 2.25, and at temperatures below 1400°K, the U_4O_9 phase exists. There is some question concerning existence of this phase above an O/U ratio of 2.25. An O/U ratio of 2.25 is regarded herein as the upper composition limit for this U_4O_9 phase. There is some disagreement between the diffraction results and equilibrium investigations concerning the lower O/U limit of the orthorhombic phase. Both Biltz and Muller, and Blackburn find about 2.60 for this boundary and find it to be independent of temperature. Diffraction studies have shown that the boundary shifts to lower O/U ratios with increasing temperature. The Blackburn values are accepted in this paper on the basis of his close examination of the orthorhombic portion of the system. The temperature-composition diagram based upon the above considerations is shown in Figure 1.

CONSTRUCTION OF A PRESSURE-COMPOSITION ISOTHERM

Construction of an isotherm consisted of plotting a series of partial molal free energies, $\overline{G}$, as a function of composition. $\overline{G}$ is the energy change in dissolving a mole of oxygen in sufficient quantity of oxide such that the composition of the oxide is unchanged. It is related to the dissociation pressure by the relation: $\overline{G} = RT \ln P_{O_2}$. The manner in which this construction was accomplished was by first establishing the free energies for the two phase regions from dissociation pressure data. By use of the temperature-composition diagram the composition limits for the phase regions were obtained.

Aronson and Belle have shown[5] that the change of free energy with composition is not linear. An assessment of their data indicates, however, that no gross errors would occur if the fluorite phase region were treated linearly. Figure 2 illustrates this in that the smooth curve is that based on thermodynamic values with the data of Aronson and Belle superimposed upon it.

It was concluded that a similar procedure could be used at other temperatures. From dissociation pressure determinations over the fluorite-orthorhombic two-phase region, a value for the partial molal free energy could be obtained. From thermodynamic data for UO_2 and $UO_{2.24}$ and assuming a linear variation of free energy with composition, it would be possible to establish the free energy variation over the monophasic region providing sufficiently reliable data were available. By use of vapor pressure data it is possible to establish the dissociation pressure for the two-phase region and the free energy of formation of the condensed phases to temperatures of the order of 2000°K.

USE OF VAPOR PRESSURE DATA IN FREE ENERGY CALCULATIONS

Vapor pressure determinations carried out by the authors in the orthorhombic phase region and in the two-phase, orthorhombic-fluorite region may be employed to determine the dissociation pressures. The general reaction leading to a volatile oxide for uranium oxides in a higher oxidation state than 2.00 is

$$UO_{2+x} + \frac{1-x}{2} O_2 \longrightarrow UO_3(g).$$

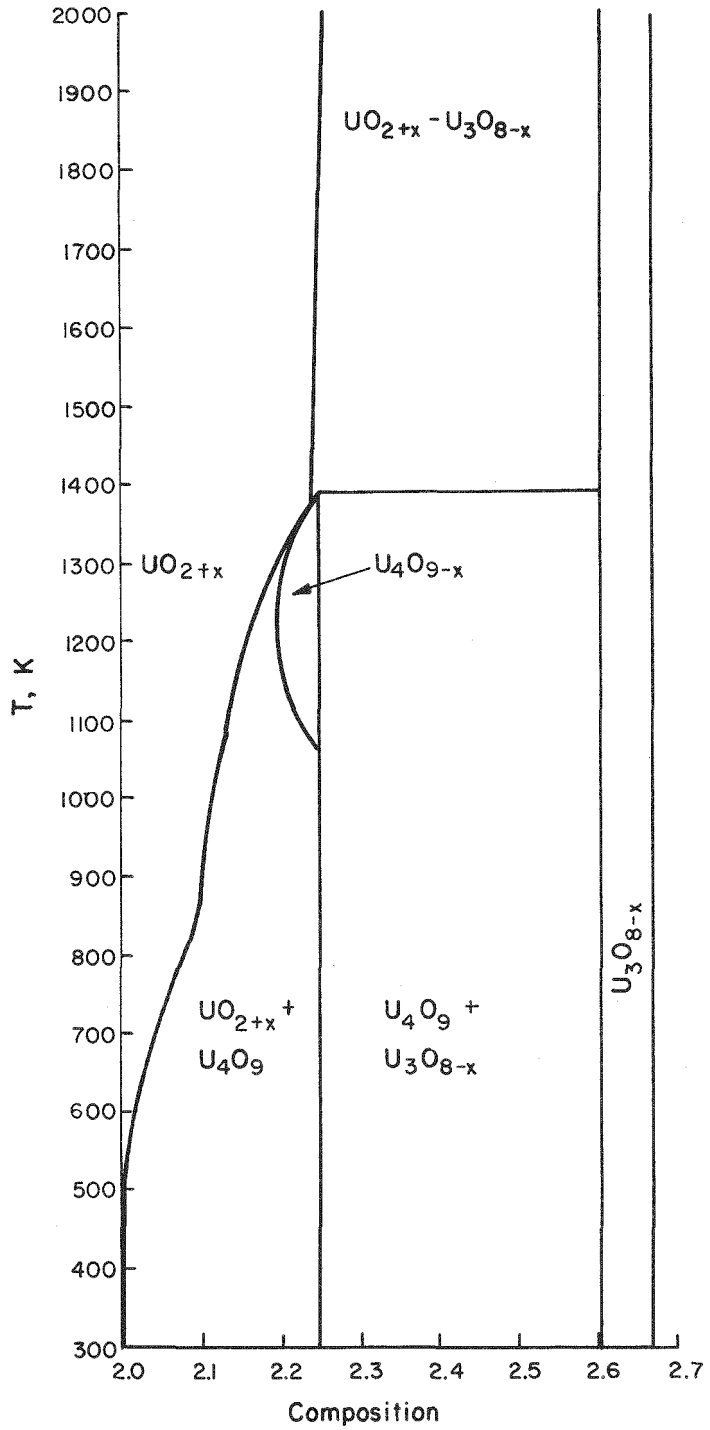

FIGURE I. TEMPERATURE-COMPOSITION DIAGRAM FOR URANIUM OXIDE

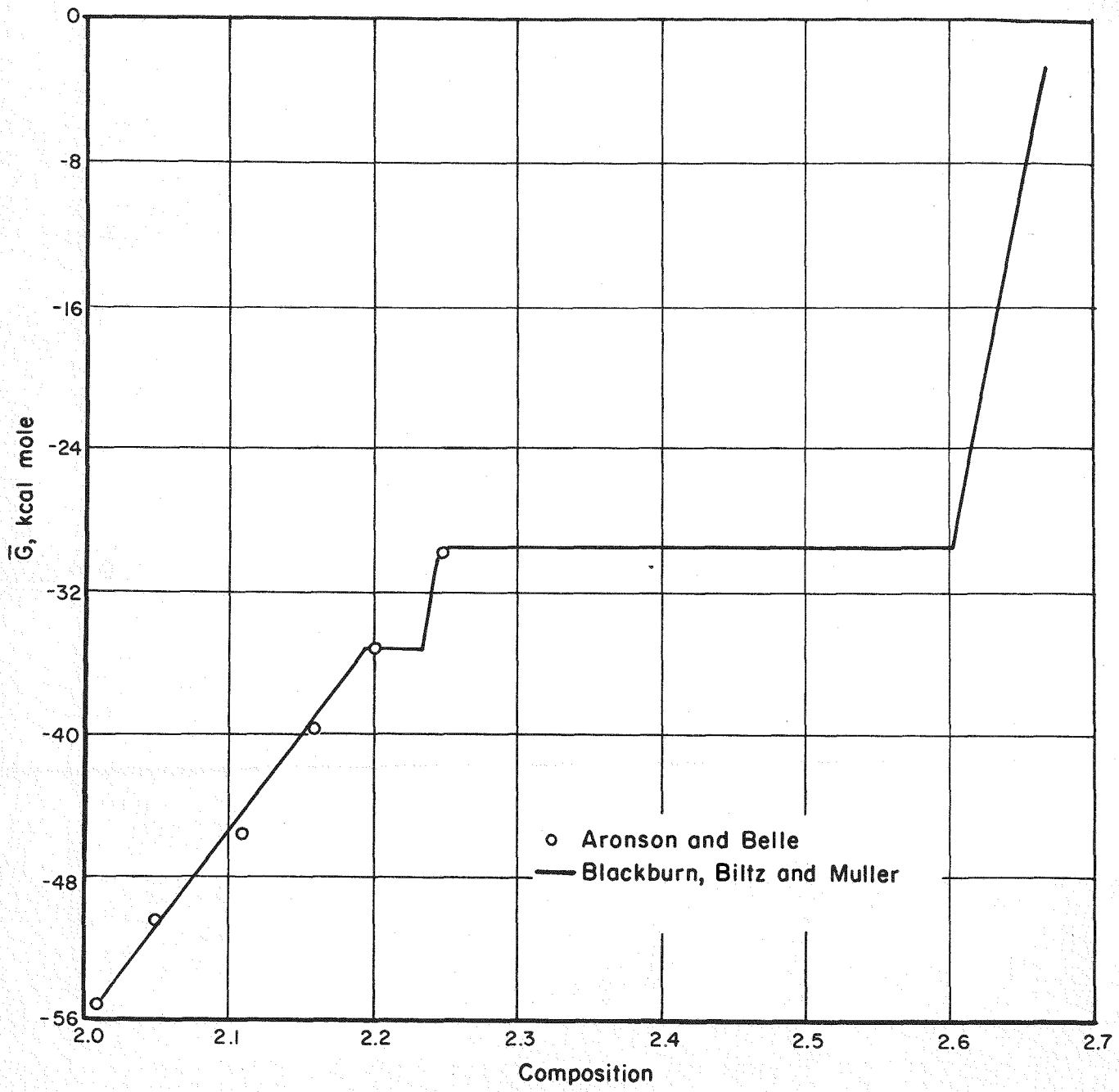

FIGURE 2. PARTIAL MOLAL-FREE ENERGY VS COMPOSITION AT 1250 K

The above reaction was investigated in the orthorhombic phase region at four oxygen pressures; i. e., 1 atm, 0.21 atm., 0.03 atm, and 0.009 atm, the last three being in a diluent of argon or nitrogen to make a total pressure of one atmosphere. In a phase region consisting of one condensed phase of two components, in equilibrium with a gas phase, there are two degrees of freedom. By using a constant oxygen pressure the composition is fixed, and at any specific temperature the system becomes invariant. Increasing the temperature with the fixed oxygen pressure will result in a change of composition to a lower O/U ratio.

In the two-phase orthorhombic-fluorite region there is one degree of freedom, and merely fixing the temperature defines the system. By decomposing U_3O_8 to the two-phase composition and then making vapor pressure determinations, vapor pressure values for this two-phase region have been obtained. (This phase of the investigation will be reported more fully in a later publication.) The vapor pressure in the two-phase region then may be considered that of $UO_{2.60}$. Since the composition of the condensed phase in the investigations carried out with fixed oxygen pressures is becoming less rich in oxygen with increasing temperature, it would be expected that at some temperature this O/U ratio would be 2.60. This temperature would be the temperature at which the vapor-pressure curve determined at a constant oxygen pressure intersected the curve representing the two-phase region. The four values for the dissociation pressure determined in this manner are shown with an extrapolation of oxygen equilibrium pressures in Figure 3. Establishment of these values was based on data obtained at this laboratory, although vapor pressure at 1 atm oxygen and in 0.21 atm have previously been reported[7] based on work at three laboratories. Since two-phase data were not obtained in that investigation, only data obtained at this laboratory were used for the sake of consistency.

The dissociation pressure may then be combined with the vapor pressure data and the free energy of formation of $UO_3(g)$ to determine the free energy of formation of the condensed phase. With the boundary at $UO_{2.24}$, the ΔG was calculated to be $-264{,}900 + 41.06T$; allowing the boundary to change to $UO_{2.26}$ would change ΔG to $-266{,}000 + 41.35T$. Combining these with the free energy of formation of UO_2, and assuming a linear relationship between partial molal free energy and composition, it becomes possible to construct isotherms at various temperature intervals. The 1600°K isotherm is shown in Figure 4, along with an extrapolation based on Aronson and Belle's investigation. For this case, it was considered that the fluorite phase existed to an O/U ratio of 2.25. In a similar manner additional isotherms were constructed to cover the temperature range to 2000°K. From these isotherms the pressure-temperature diagram shown in Figure 5 was derived.

The 0.21 atm O_2 isobar, corresponding to air is shown in Figure 6, along with results of thermogravimetric investigations by Lynch, et al.,[8] Budnikov, et al.,[9] and our own investigation. Budnikov's work would indicate that the transition to the fluorite phase may occur 20 degrees lower than has been indicated. Budnikov's X-ray diffraction of his quenched samples, which indicated the U_4O_9 phase, has been verified in our work. A UO_2 pellet as well as a powdered charge was loaded in argon and heated to 1850°K. At this temperature air was passed over the uranium oxide and a vapor pressure determination made. The value for the vapor pressure was lower than that found for the two-phase region as is predicted. At the end of the vapor pressure run, the system was purged with argon and rapidly cooled. The pellet was intact

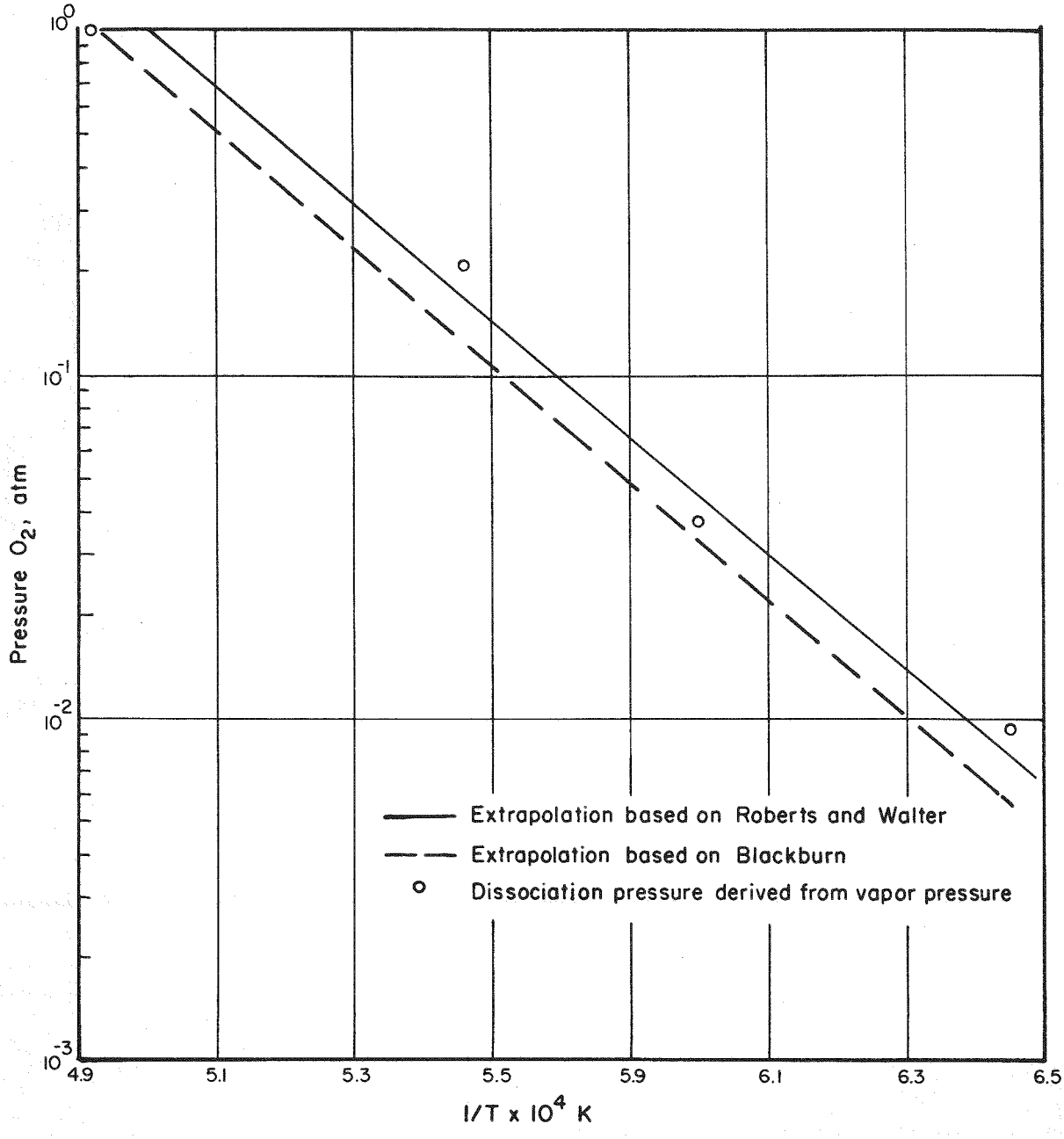

FIGURE 3. DISSOCIATION PRESSURE FOR THE ORTHORHOMBIC-FLUORITE TWO-PHASE REGION

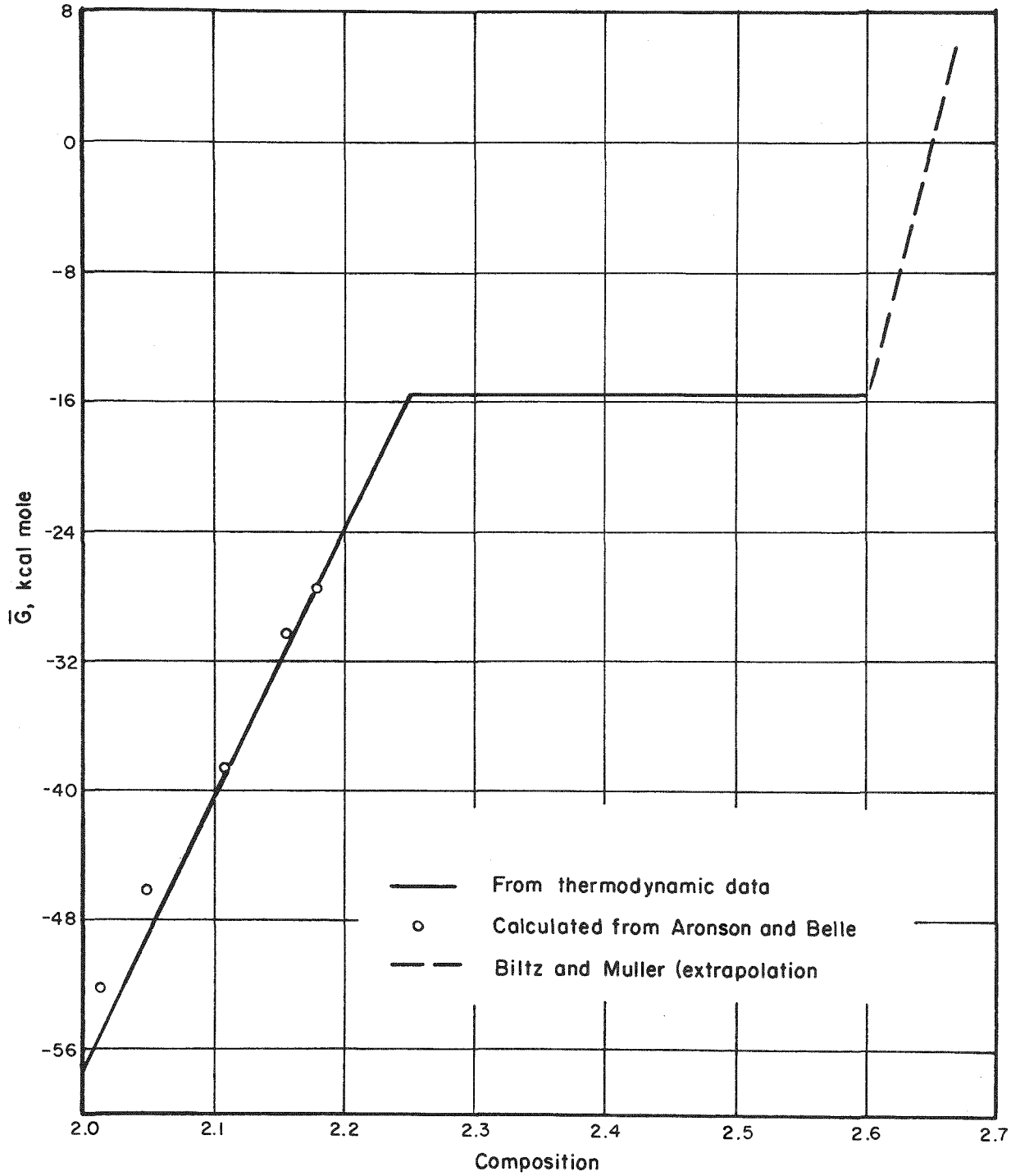

FIGURE 4. PARTIAL MOLAL-FREE ENERGY VS COMPOSITION AT 1600 K

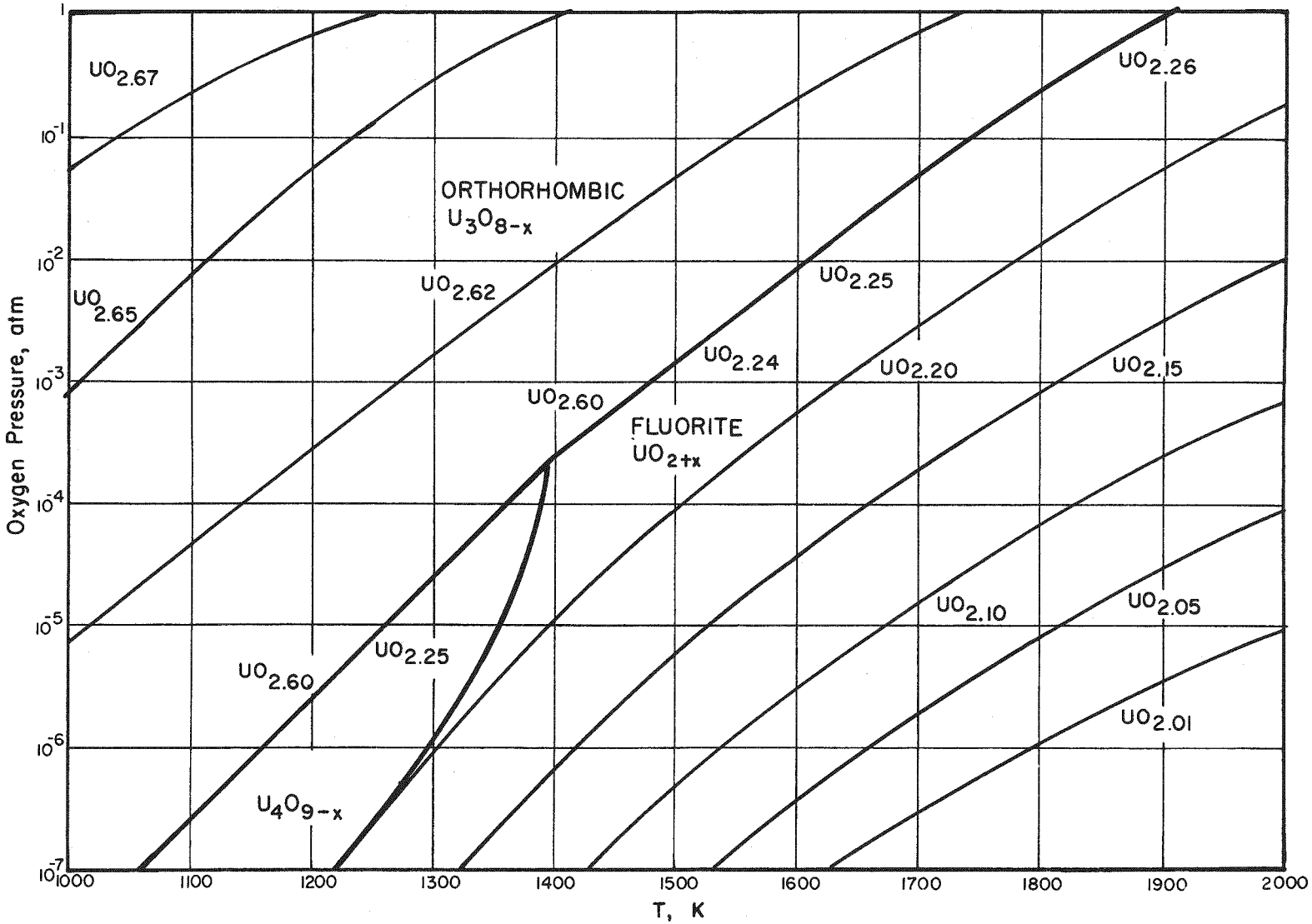

FIGURE 5. PRESSURE–TEMPERATURE-COMPOSITION OF URANIUM OXIDE

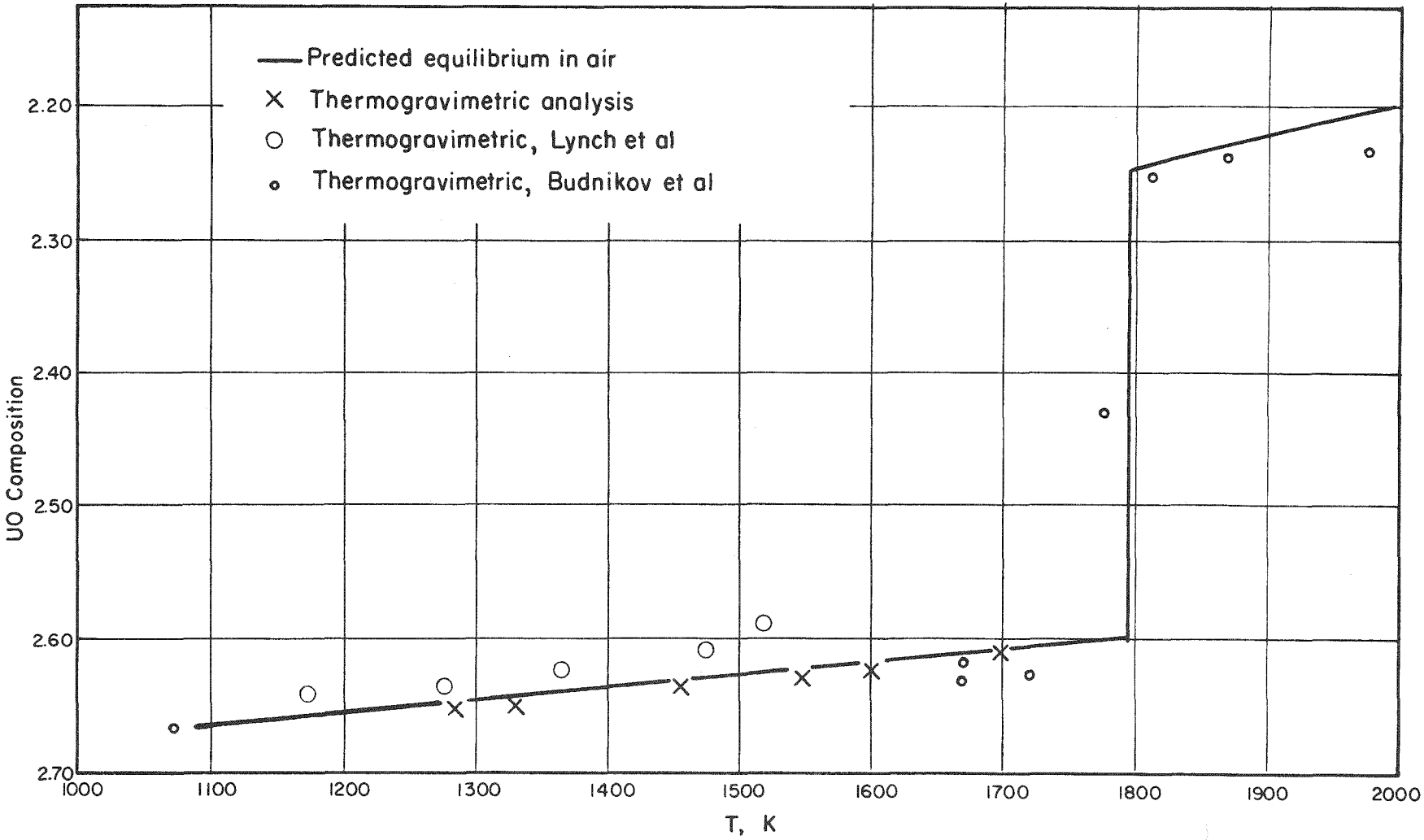

FIGURE 6. PREDICTED EQUILIBRIUM IN AIR COMPARED WITH EXPERIMENTAL VALUES

indicating that it was not oxidized sufficiently to transform to the orthorhombic phase where a non-isotropic volume expansion of over 30 percent would occur. An X-ray powder pattern indicated the pellet was U_4O_9. It is considered, however, that at temperature the charge was in the fluorite phase, and transformed upon cooling, since it would appear that the U_4O_9 phase cannot exist at temperatures above 1400°K.

CONCLUSIONS

In conclusion, a phase diagram has been constructed to be consistent with the data of as many investigators who have studied the uranium oxide-oxygen system at temperature, as is possible. Also, consistency with the fundamental thermodynamic data was a requirement in its construction. In some cases rather arbitrary choices had to be made. It does not appear possible to predict how accurate this diagram may be at the high temperature - low O/U ratio region. It is considered, however, that the diagram is at least semi-quantitatively accurate, and should offer a basis for future investigators to compare their experimental values.

REFERENCES

1. P. Gronvold, J. Inorg. Nucl. Chem., 1: 357 (1955).
2. W. Biltz and H. Muller, Z. Anorg. Allg. Chem., 163: 257 (1927).
3. R. J. Ackermann and R. J. Thorn, 133rd American Chemical Society Meeting, San Francisco, April, 1960.
4. P. E. Blackburn, J. Phys. Chem., 62: 897 (1958).
5. S. Aronson and J. Belle, J. Chem. Phys., 29:151 (1958).
6. J. Belle, Uranium Dioxide: Properties and Nuclear Applications, (To be published in J. Inorg. Nucl. Chem.).
7. R. J. Ackermann, R. J. Thorn, C. Alexander, and M. Tetenbaum, J. Phys. Chem., 64: 350 (1960).
8. E. D. Lynch, J. H. Handwerk, and C. L. Hoenig, J. Am. Ceram. Soc., 43: 520 (1960).
9. P. P. Budnikov, S. G. Tresvelski, and V. I. Kuchakovski, D.A.N., 128: 85 (1959); (AEC-TR-4035).

RELEASE OF FISSION PRODUCTS FROM REACTOR-GRADE UO_2 BY DIFFUSION, OXIDATION, AND MELTING

By G. W. Parker, G. E. Creek, and W. J. Martin

Oak Ridge National Laboratory[a]
Oak Ridge, Tennessee

INTRODUCTION

An important aspect of nuclear reactor safety hinges on a knowledge of the diffusion and dispersal of fission products from various types of nuclear accidents. The experimental demonstration of fission product release from overheated reactor-type UO_2 has been the subject of an extensive program[1] intended to serve as a guide in hazards evaluations according to the maximum-credible-accident analysis of a particular reactor.

A comprehensive review of the status of fission product release from UO_2 by Cottrell and others[2] points out the need for experimental data on the diffusion of fission products other than the rare gases, but has very little data concerning the effect of oxidation of UO_2 on diffusion. A study of fission product release by the oxidation of UO_2 in air was therefore one of the primary objectives of the present investigation. Since most clad UO_2 fuel elements are designed to be filled with helium for heat removal, diffusion of fission products out of elements heated in this medium is also pertinent to the hazards evaluation. Both air and CO_2 may be present in the atmosphere to which melted fuel elements are exposed. Accordingly, results obtained on melting UO_2 in impure helium, in air, and in CO_2 are reported.

In part, the present report summarizes a comparison of the release rates observed as a function of burnup or fission density in the fuel, a variable which has not been previously investigated in experiments of this type. This investigation represents the initial phase of an extensive series of parametric studies which is expected to include the effect of specimen size, pressure at meltdown, irradiation temperature, and chemical changes resulting from exposure to other environments such as steam.

---

[a] Operated by the Union Carbide Corporation for the U.S. Atomic Energy Commission.

OXIDATION OF UO_2 TO U_3O_8 IN AIR

Previous studies[3,4,5] of the oxidation rate of UO_2 at various temperatures, indicate that there is an induction period for temperatures up to 600°C, which has been suggested[3] to be due to nucleation followed by growth of U_3O_8. An alternate explanation is that the initial surface area is increased by the peeling off of the first layer of U_3O_8. The unoxidized UO_2 surface is undoubtedly much rougher than at the beginning and results presented below indicate that the oxidation rate is quite dependent on surface area. The rate after the initial induction period is probably controlled by diffusion through a thin layer of U_3O_8 which cracks upon accumulation of sufficient stress from the large difference in density between UO_2 and U_3O_8. At higher temperatures, the accumulated oxidized layer is probably more plastic so that there is less cracking of the oxide film and a slowly decreasing oxidation rate to 900°C is observed. Between 1000 and 1450°C, oxidation is more rapidly completed but a non-stoichiometric oxide having the U_3O_8 structure is produced.

Considerable controversy exists over the exact rate of UO_2 oxidation at a given temperature. A few recent experiments have shown this to be largely an effect of variations in density, method of manufacture, and specific surface area. Figure 1 illustrates this last effect, showing a comparison with similar data of Peakall and Antill.[3]

Fission product release resulting from this complex oxidation process is reflected in the summary of release data shown in Figure 2. The results show surprising differences in release behavior among the various fission products at different temperatures, with ruthenium exhibiting the highest volatility above 1000°C and with the release of both iodine and the rare gases significantly lower at the higher temperatures. These results may only apply to trace concentrations of fission products and possibly are not typical of rates at high fission density.

RELEASE OF FISSION PRODUCTS BY HIGH-TEMPERATURE DIFFUSION INTO PURE HELIUM

In a previous report,[1] the enhancement of fission product release by oxidation in impure helium was clearly demonstrated. In order to relate the diffusion parameter to the results obtained by others,[6,7] traces of oxygen were removed from the helium by passing it over hot zirconium. Diffusion constants obtained in flowing purified helium correlate well with results obtained by other experimenters using the high-vacuum annealing method. The significant results of the helium diffusion experiments are shown in Figures 3 and 4. In Figure 3 the fraction of the volatile fission products released by diffusion in 5.5 hours is shown as a function of temperature in the range 900 to 2200°C. These curves are applicable only to trace fission product concentrations. It is of interest that both iodine and tellurium exceed the rare-gas diffusion rate by a factor of 3 to 5. A plot of the apparent diffusion coefficient D' for the fission gases shown in Figure 4 indicates the existence of two processes having distinctly different energies of activation. The slope observed at temperatures above 1800°C is apparently indicative of UO_2 sublimation as well as grain growth.

In order to illustrate the effect of the burnup parameter on diffusion in helium, a series of studies is compared in Table I. At all temperatures above 1400°C, a decided increase in release accompanies a higher irradiation. However, at 1400°C, the opposite seems to be true, at least in the case of iodine and tellurium. At higher burnup levels this reversal in release behavior may not be observed. A significant difference in the rate-of-release curves for

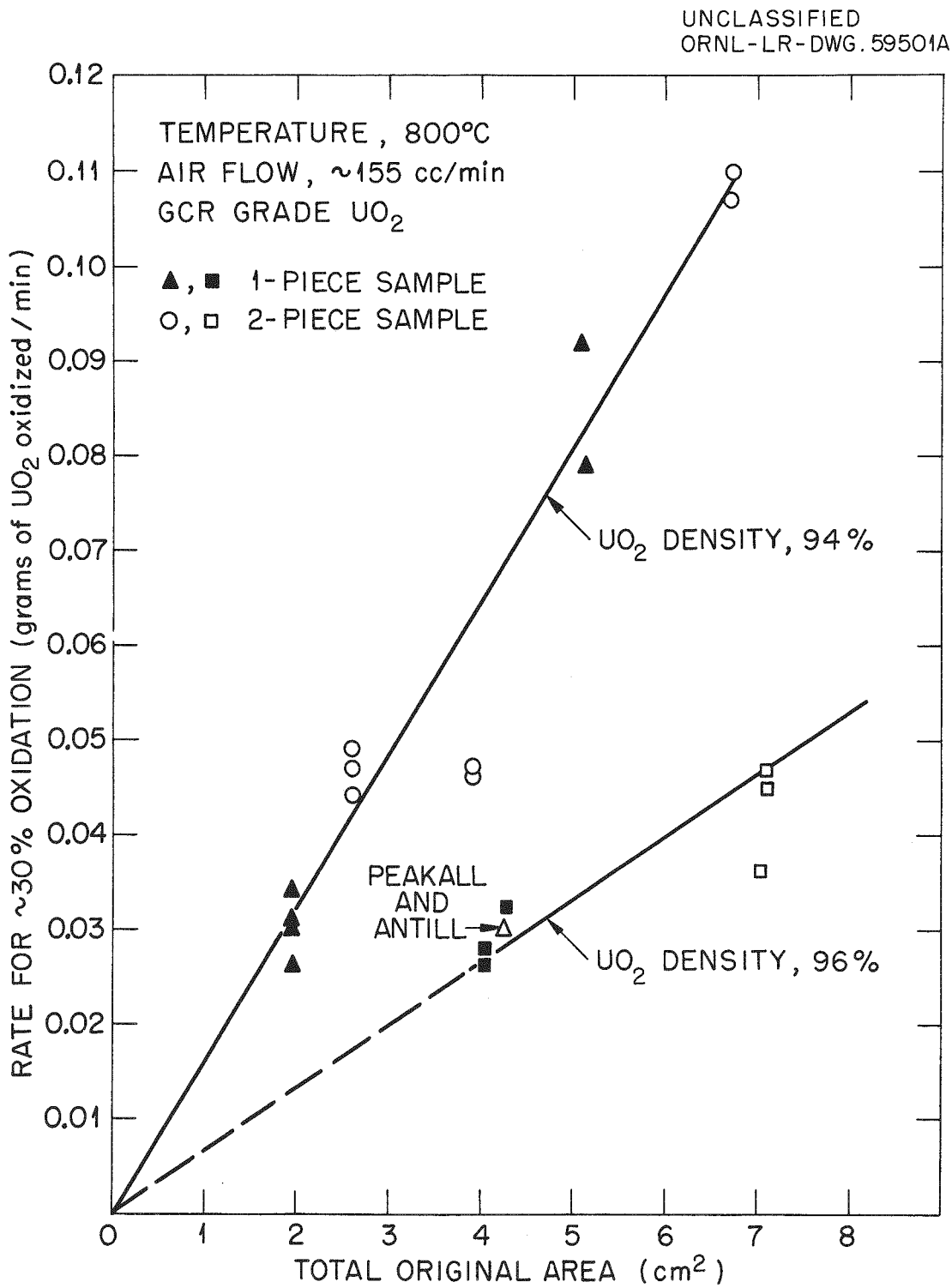

Figure 1. Initial Rate of Oxidation of UO_2 in Air as a Function of Surface Area and Density.

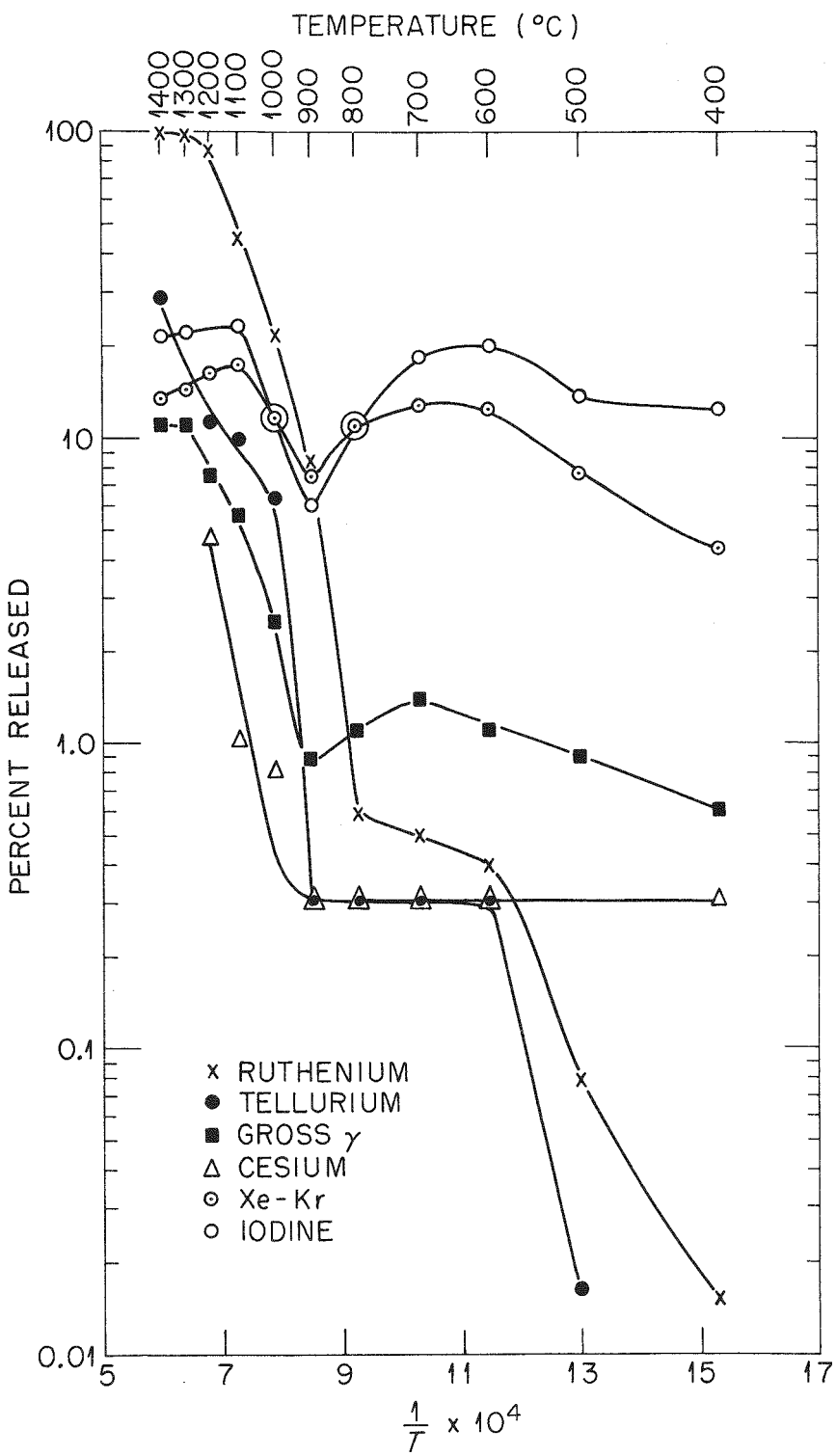

Figure 2. Fission Product Release by the Oxidation of UO_2 to U_3O_8 in Air, Showing Discontinuity Between 600° and 900°C.

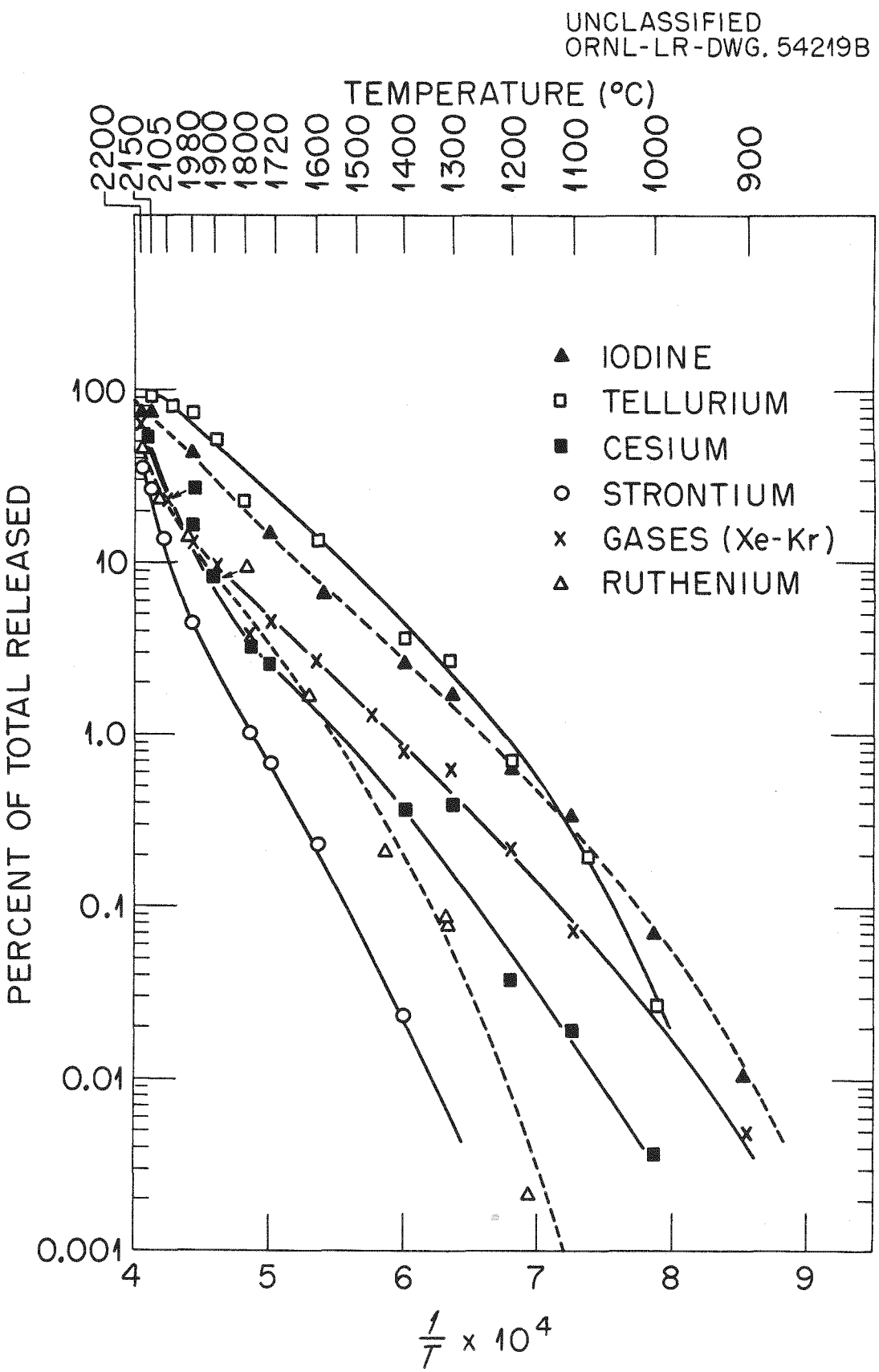

Figure 3. Fission Product Release from PWR UO_2 by Diffusion into Pure He (5.5 Hr Heating).

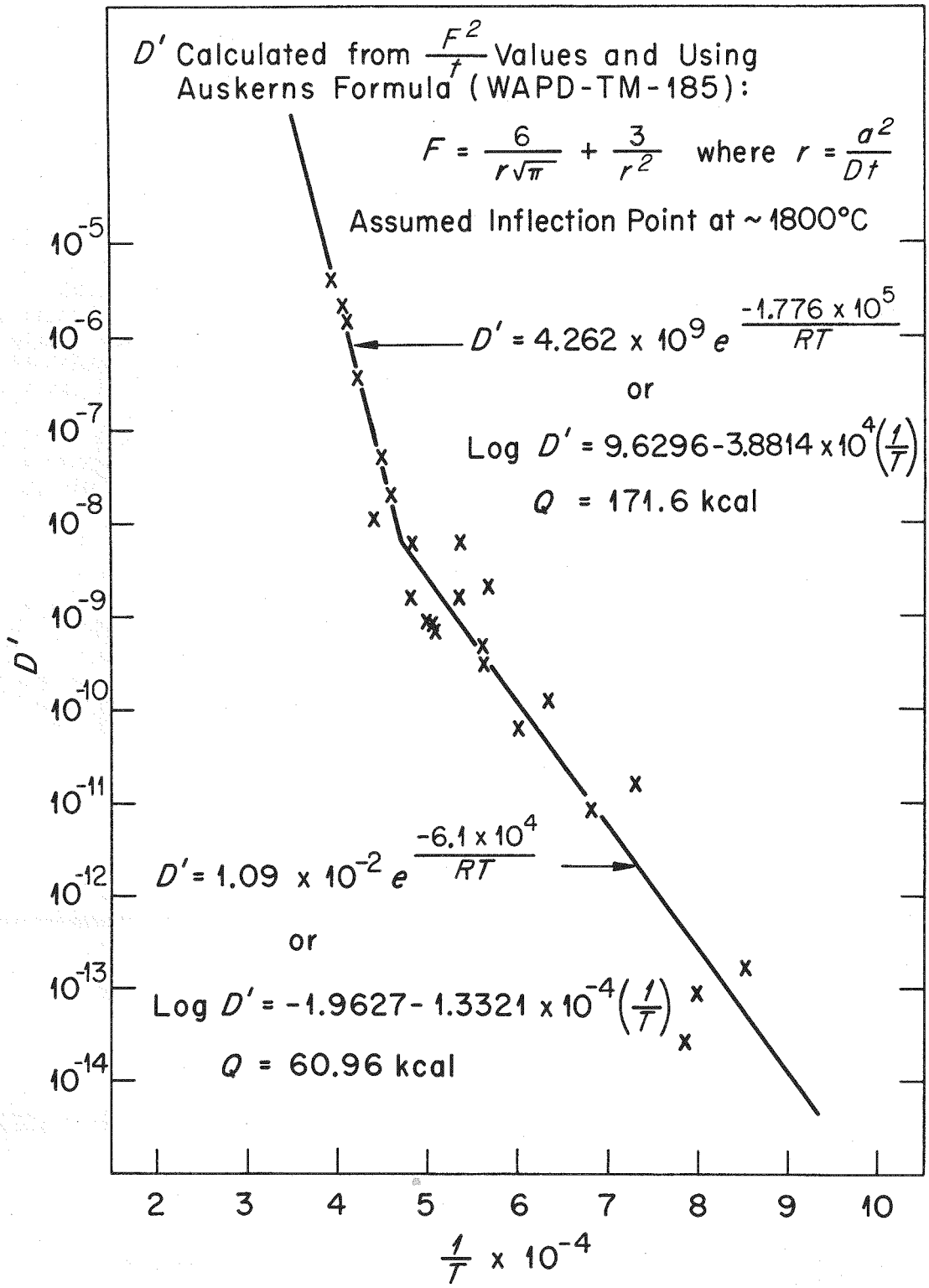

Figure 4. Rare Gas Diffusion from PWR UO_2 in Helium.

trace-irradiated UO_2 and for a 1000-Mwd specimen is illustrated in Figure 5. The initial "burst" effect is characteristic of all diffusion curves; however, the enhanced cooling peak obtained with the more highly irradiated material suggests the possibility of a trapping process, such as closed pores that developed by plastic deformation during irradiation. The gas contained in some of these pores may be released by fracture on cooling.

RELEASE OF FISSION PRODUCTS ON MELTING UO_2 IN IMPURE HELIUM, IN AIR, AND IN CO_2

Uranium dioxide meltdown may be postulated to occur as a result of a serious loss-of-coolant accident in large, non-gas-cooled reactors. In a series of experiments involving the melting of small UO_2 specimens in a carbon-arc-image furnace, high release rates were experienced for most of the so-called "volatile" fission products: rare gases, iodine, tellurium, cesium, and ruthenium. Sample size had an effect on the extent of release, apparently indicating incomplete melting of all but the smallest samples. On the other hand, atmospheric environment (helium, air, or CO_2) did not have a serious effect on volatility. Table II shows slightly lower release rates at trace-level irradiation for a CO_2 atmosphere as compared to rates obtained with higher burnup material; however, at higher irradiation levels, only ruthenium remains below the release rate in helium and air.

SIZE OF PARTICLES RELEASED FROM UO_2 MELTED IN AIR AND HELIUM

The range of sizes of particles collected on Millipore filters, as well as their identification as U_3O_8 (from the melting done in air) and as UO_2 (from the melting done in helium), was established by means of electron microscope techniques.[8] The average diameter of the crystalline U_3O_8 was 0.1 μ while the spherical particles from helium melts averaged about 0.02 μ. The released fission products were all adsorbed on the vaporized uranium oxides (U_3O_8 or UO_2), with some variations, according to the distance that the particle traveled before plating out occurred. Particle size studies are discussed in more detail in another report.[9]

REFERENCES

1. G. W. Parker, G. E. Creek, and W. J. Martin, Fission Product Release from UO_2 by High Temperature Diffusion and Melting in Helium and Air, USAEC Report ORNL CF 60-12-14, Oak Ridge National Laboratory, February 1961.

2. W. B. Cottrell et al., Fission Product Release from UO_2, USAEC Report ORNL-2935, Oak Ridge National Laboratory, September 1960.

3. K. A. Peakall and J. E. Antill, J. Nuclear Materials, 2 (2), 194 (1960).

4. D. T. Livey and P. Murray, The Technology of Urania and Thoria, in Metallurgy and Fuels, Progress in Nuclear Energy, Series V, Vol. 1, Pergamon Press, New York, 1956.

5. S. Aronson et al., J. Chem. Phys., 27, 137 (1957).

6. H. H. Booth and G. T. Rymer, Determination of the Diffusion Constant of Fission Xenon in UO_2 Crystals and Sintered Compacts, Atomic Energy of Canada Limited, Chalk River report CRDC-720, August 1958.

TABLE I

A COMPARISON OF THE RELEASE OF FISSION PRODUCTS FROM UO_2 BY DIFFUSION IN PURE HELIUM AFTER IRRADIATION AT TRACE LEVEL AND AT 1000 MWD/TON

Temperature (°C)	Irradiation Level	Percentage of Individual Fission Products Released						
		Xe-Kr	I	Te	Cs	Ru	Sr	Ba
1400	Trace	0.8	4.0	3.9	0.02	0.02	0.001	
	1000 MWD/T	0.8	0.9	0.8	2.6	0.001	0.1	
1610	Trace	2.7	6.5	12.1	1.7	1.5	0.1	
	1000 MWD/T	2.6	3.7	12.0	12.0		2.0	17.0
1780	Trace	3.7	11.7	21.0	3.2	6.9	1.0	
	1000 MWD/T	12.0	24.0	67.0	27.0	11.0	9.0	39.0
1980	Trace	12.3	41.0	75.0	15.0	13.4	4.2	8.7
	1000 MWD/T	29.0	53.0	74.0	84.0		15.0	57.0

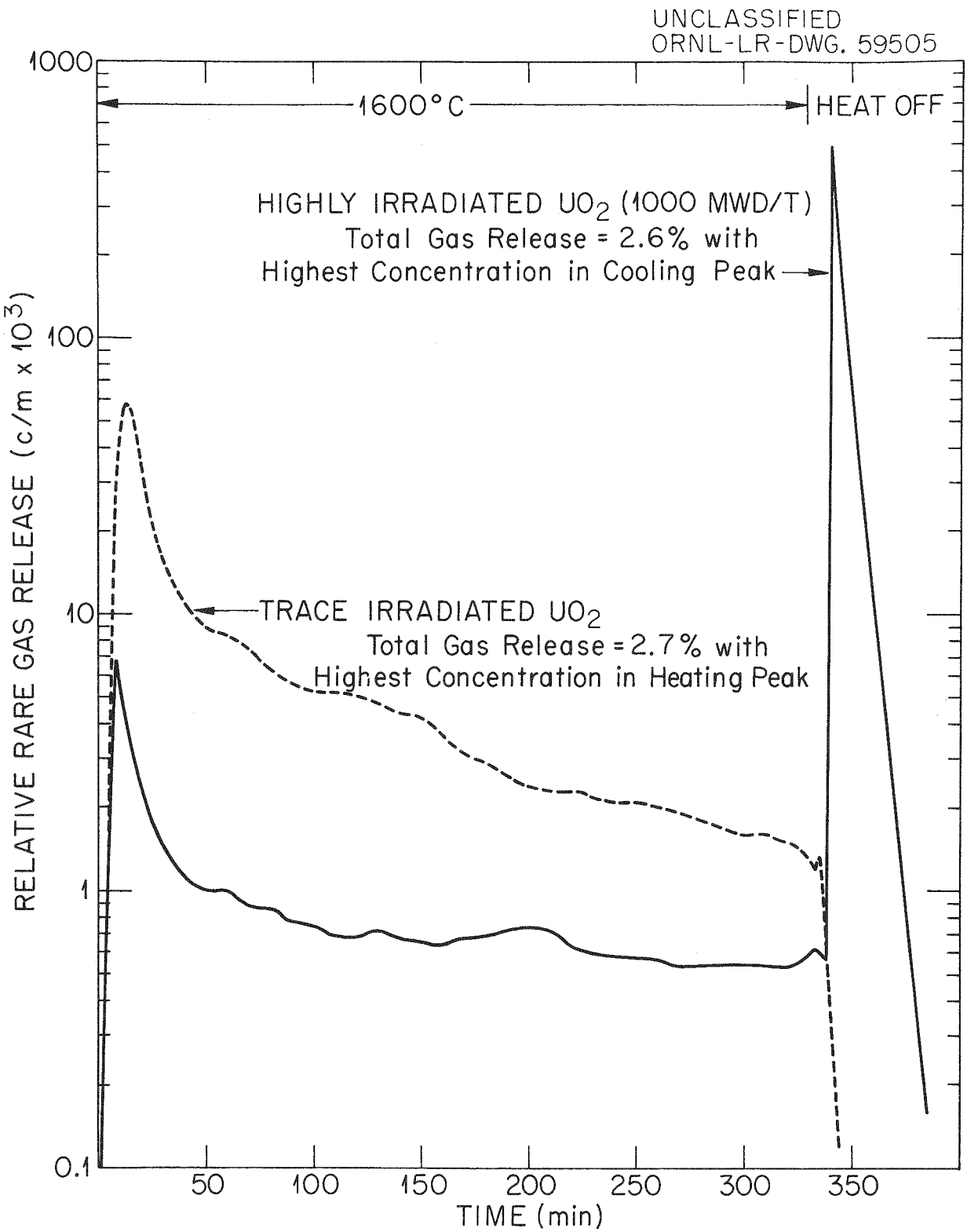

Figure 5. Rate of Rare Gas Diffusion from UO_2 into Pure He as a Function of Time.

TABLE II

A COMPARISON OF THE RELEASE OF FISSION PRODUCTS ON MELTING GCR UO_2
(O/U RATIO 2.04, 95% THEORETICAL DENSITY) IN IMPURE HELIUM,
IN AIR, AND IN CO_2 AFTER IRRADIATION AT VARIOUS LEVELS

Atmosphere	Irradiation Level	Wt. of Sample (g)	No. Results Averaged	Percentage of Individual Fission Products Released								
				Xe-Kr	I	Te	Cs	Ru	Sr	Ba	Rare Earths	UO_2 Vaporized
Helium (Impure)	Trace	0.22	2	99.5	89.7	92.0	91.3	61.0	2.1	4.6	2.2	
	2800 MWD/T	0.03	3	99.9	92.2	98.2	98.5	90.4	2.1	6.6	5.1	21.2
Air	Trace	0.2	2	98.4	94.9	79.1	37.7	67.7	0.2	0.5	0.5	
	2800 MWD/T	0.04	3	100.0	99.7	93.6	92.5	95.0	0.4	1.8	3.0	
CO_2	Trace	0.2	3	80.6	76.8	71.2	60.9	44.9	0.3	1.1	0.85	14.1
	2800 MWD/T	0.02	3	99.9	98.7	98.6	90.2	74.3	0.5	2.5	2.8	
	11000 MWD/T	0.05	3	99.9	99.9	99.0	96.6	79.1	0.6	2.9	2.3	

7. J. L. Scott, Determination of the Diffusion Constant of Fission Xenon in UO_2 Crystals and Sintered Compacts, USAEC Report ORNL CF-60-8-15, Oak Ridge National Laboratory, September 1960.

8. T. E. Willmarth and T. G. Harmon, Oak Ridge National Laboratory, personal communication.

9. G. W. Parker, G. E. Creek, and W. J. Martin, Fuel Element Decomposition Products, Seventh Air Cleaning Conference, Brookhaven National Laboratory, October 10-12, 1961, USAEC Report ORNL-TM-21, October 1961.

A THEORY FOR CALCULATING THE RELEASE OF FISSION GASES FROM DEFECTIVE SHEATHED CERAMIC FUEL ELEMENTS[a]

By H. S. Dreyer, Aerojet-General Nucleonics,
San Ramon, California

INTRODUCTION

One of the important parameters in any reactor system is the release of fission products from a defective fuel element to the environment. Methods of calculating the release of the fission gases to obtain agreement with experiments have been the concern of many researchers. The results obtained by different organizations and applied to the release of fission products from an ML-1 fuel element is plotted in Figure 1. This figure demonstrates the difficulty of predicting the release of fission gas from a newly-designed fuel element based on a diffusion model without experimental data from the specific design under consideration. A survey of fission product release from UO_2 up to the end of 1959 is given by Cottrell, et al[1]. This document concludes that diffusion of fission gases out of the fuel is the only mechanism that accounts for the experimental observations to that date.

Two fission gas release experiments have been reported in the literature since this report; one by R. F. S. Robertson[2] on defective fuel in the Experimental Boiling Water Reactor (EBWR); and the other, by F. V. Brutschy and R. W. Osborne, on defective fuel in the Vallecito Boiling Water Reactor (VBWR)[3]. Using the data presented by Robertson for a 48-in. sheathed element in the EBWR, the total number of Xe^{133} atoms per second produced by recoil[4] was compared to the total number of Xe^{133} atoms per second escaping from the defect. The result gave a mean resident time in the sheathing of 8.3 days for a Xe^{133} atom. Since more atoms are available from recoil than escape from the defect, diffusion of the atoms down the annulus between the fuel and the sheath must play a significant role in the escape of fission products.

This paper proposes a method of calculating the release of fission gases from defective sheathed ceramic fuel elements at steady state based on the release of the gases by recoil followed by subsequent diffusion of the molecules down the annulus to the defect.

---

[a]This paper is based on work performed as part of the Army Gas-Cooled Reactor Systems Program under AEC Contract No. AT(10-1)-880 by Aerojet-General Nucleonics, San Ramon, California.

OPERATING TIME 3000 HOURS

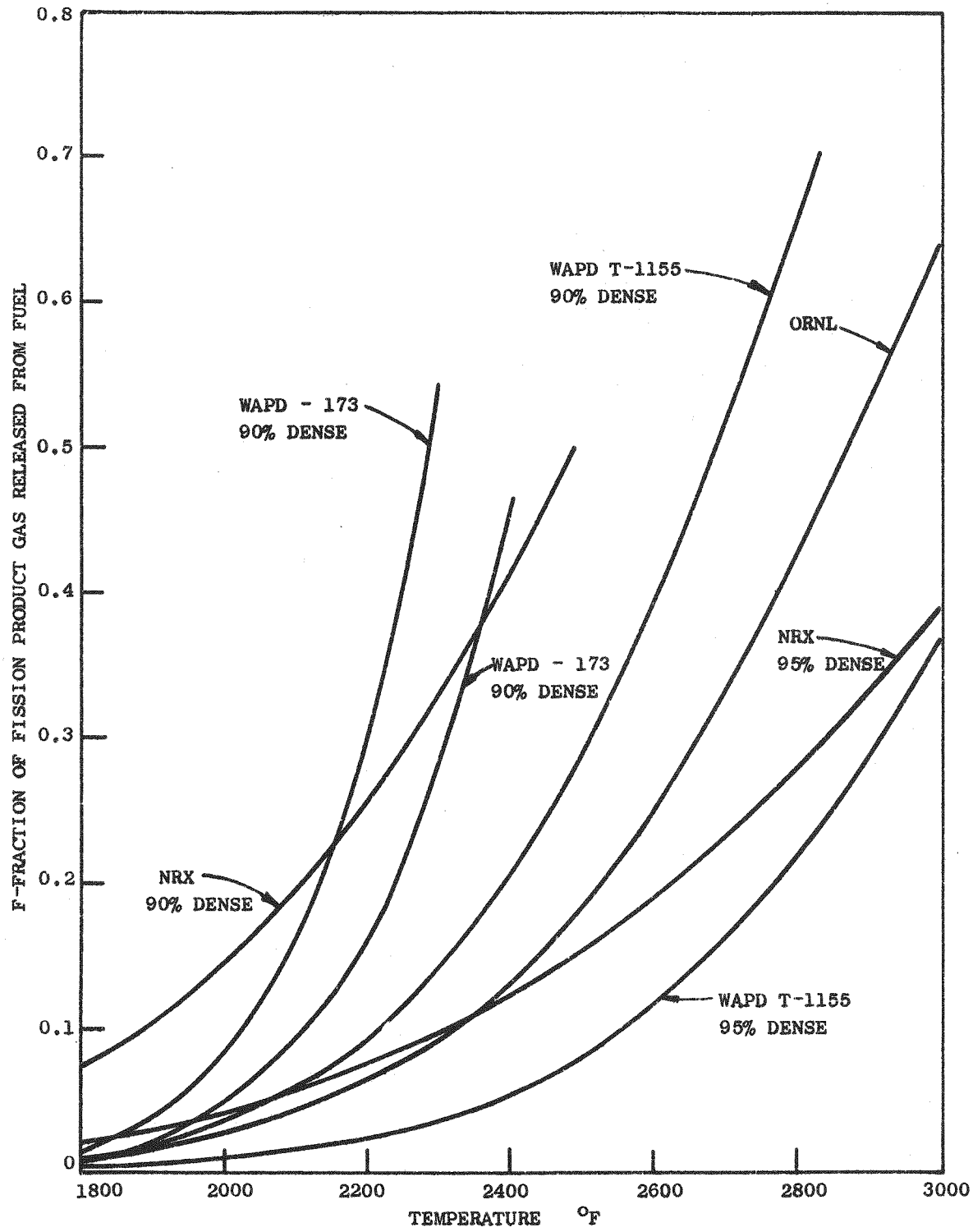

RELEASE OF FISSION PRODUCTS FROM A DEFECTIVE ML-1 FUEL ELEMENT

FIGURE 1

NOMENCLATURE

A - area of annulus, cm^2

a_1 - inner radius of sheath, cm

a_2 - radius of fuel, cm

C - total conductance

C_o - conductance of defect in sheathing

C_a - conductance of annulus

c - kinetic velocity of atoms, cm/sec

F_a - atoms recoiling off fuel per cm^2, atoms/cm^2-sec

F_o - atoms recoiling off fuel per cm^2 per cm length, atoms/cm^2-sec

F_e - atoms per second of F_o that are escaping from defect

H - circumference of ID sheath, cm

K_i - constant ith isotopes

L - length of fuel, cm

l - mean free path, cm

M - molecular weight

N_o - number of atoms produced per unit time

N_i - atoms of N_o after $t = 0$

N_e - atoms per second escaping from defect

P - pressure, mm of mercury

R - average velocity of flow in x-direction along annulus, cm/sec

T - temperature at fuel surface, ^oK

t - time, sec

V_a - average velocity of molecules, cm/sec

Z - atomic number

δ_1 - diameter of molecule of interest

δ_2 - diameter of molecules of coolant

δ_{12} - average molecular diameter

λ_i - decay constant of isotope i, sec^{-1}

SUMMARY

The equations developed for calculating release of fission products from a defectively-sheathed ceramic fuel element are the following:

The equation for molecular-velocity, V_a, is:

$$V_a = \frac{K_i (T^{0.75}) \ (P^{0.5}) \ (M^{0.25})}{\delta_{12} \times 10^{10}}$$

Substituting the molecular weights of the various isotopes results in the following values:

K^{133} =	4.395	K^{85m} =	5.082
K^{135} =	4.677	K^{87} =	5.285
K^{138} =	5.276	K^{88} =	5.140

The flow velocity, R, is found by

$$R = \frac{2}{3} V_a \left[a_1 - \frac{a_2^2}{a_1} \right]$$

The equation for the number of atoms escaping, N_e, for defect above or below the fuel, is:

$$N_e = R \frac{F_o}{\lambda_i} \left[1 - (e)^{-\frac{L\lambda_i}{R}} \right] + \pi a_2^2 F_a$$

When the defect is on the side of the fuel:

$$N_e = 2R \frac{F_o}{\lambda_i} \left[1 - (e)^{-\frac{L\lambda_i}{R}} \right]$$

DISCUSSION

Basic Assumptions

The underlying concepts used in developing the equations for these calculations are;

1. There are no large driving forces causing the fission products to leave the defective pin.

2. The average velocity of the fission products can be obtained from random walk concepts.

3. The flow of fission products in the annulus can be described by Knudsen flow.

4. The conductance of the paths for flow is additive[5] as follows;

$$\frac{1}{C} = \frac{1}{C_o} + \frac{1}{C_a} \qquad \text{(Eq. 1)}$$

5. The xenon and krypton found in the annulus includes only the atoms that escape from the fuel by recoil.

Examination and development of these concepts follows:

1. Driving Force
   a. Pressure - Under steady state conditions, the pressures inside the pins and in the coolant come to equilibrium; therefore, pressure cannot be considered a driving force.

   b. Concentration - The effect of concentration on the diffusion of gases has been found to be only of moderate magnitude[6]. In actual experiments to measure this effect, the maximum change of the diffusion coefficient found was 8%. In the systems under consideration, the change in concentration can be expressed as follows;

      $\Delta c/\Delta t$ = (Production - Decay - Transport)

      Since the only driving force would arise from the transport, this was examined in greater detail. The data from Robertson[2] was again used and the equilibrium value per unit volume based on recoil calculated. The number of atoms per cc of Xe^{133} to be found at equilibrium is 5.85×10^{13}. The number of atoms transported from the element is 0.00091×10^{13} per second, a number too small to have any appreciable effect on the system.

   c. Temperature - Temperature will have some effect, since the neutron flux is not evenly distributed axially. Further, the heat variation does not appear to be a first order effect and, therefore, has not been used as a driving force in this theory except for its effect on the velocity of the particles.

2. Average Velocity

   To obtain the average velocity of the molecules at equilibrium it is necessary to first find the random walk velocity[7] of the particles; multiply each value of the velocity, V_i, by the number of molecules having this value, N_i; add these products and then divide by the total number of molecules. Thus,

$$V_a = \frac{\Sigma N_i V_i}{\Sigma N_i} \qquad \text{(Eq. 2)}$$

   In the systems of concern,

$$N_i = N_o e^{-\lambda t} \qquad \text{(Eq. 3)}$$

   To obtain the random velocity[7]:

$$V_i = 0.798 \sqrt{\frac{lc}{t}} \qquad \text{(Eq. 4)}$$

$$\text{Let } \alpha = 0.798 \sqrt{lc} \qquad \text{(Eq. 5)}$$

This is constant for any given system. From Dushman[5] the mean free path, l, is:

$$l = \frac{2.33 \times 10^{-20} T}{P(\delta_{12})^2} \qquad \text{(Eq. 6)}$$

Also, from Dushman[5],

$$c = 1.46 \times 10^{4} \sqrt{T/M} \qquad \text{(Eq. 7)}$$

The average molecular diameter, δ_{12}, is:

$$\delta_{12} = \frac{\delta_1 + \delta_2}{2} \qquad \text{(Eq. 8)}$$

Substituting for l and c in Eq. 5:

$$\alpha = 1.47 \times 10^{-8} \, T^{3/4} P^{-1/2} M^{-1/4} \delta_{12}^{-1} \qquad \text{(Eq. 9)}$$

Using these expressions and the decay constants of interest, V_a can be evaluated:

$$V_a = K_i T^{3/4} P^{-1/2} \delta_{12}^{-1} \times 10^{-10} \qquad \text{(Eq. 10)}$$

Where the constant K_i assumes the following values for the isotopes of interest:

K^{133} =	4.395	K^{85m} =	5.082
K^{135} =	4.677	K^{87} =	5.285
K^{138} =	5.276	K^{88} =	5.140

3. Flow

Assuming molecular flow[5]:

$$R = 4/3 \left[\frac{V_a}{\int_0^L H/A \, dl} \right] \qquad \text{(Eq. 11)}$$

This equation holds for a tube being fed from one end. In this case, the generation is uniform down the annulus and therefore must be considered on a unit basis. This means that L = 1, and Eq. (11) becomes:

$$R = \frac{2}{3} \left[a_1 - \frac{a_2^2}{a_1} \right] V_a \qquad \text{(Eq. 12)}$$

4. Resistance to Flow

In experiments at EBWR and VBWR[2,3] the calculated conductance of the defect was found to be able to handle much greater quantities of gas than was escaping. Therefore, the defect has not been the determining resistance to flow in the cases under study (See Appendix). In the following discussion, the conductance of the defect has been ignored.

5. Activity Concentration

Since the initial equilibrium calculations show that the number of atoms available from recoil is greater than the number escaping, no further mechanism was considered. This assumption gave good results, without modification. However, if the temperature was raised high enough to affect the equilibrium concentration, no problem would be encountered in incorporating the change in the final equation.

Escape Equation

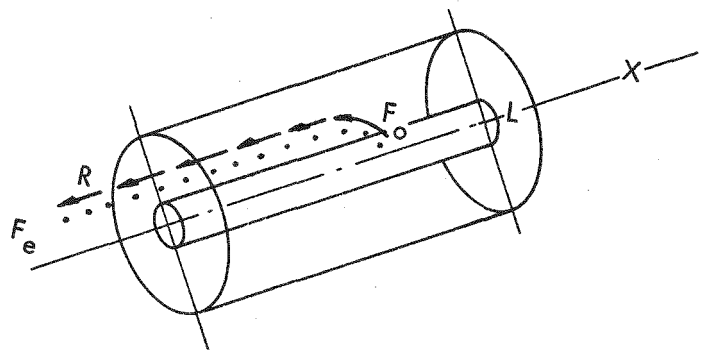

Figure 2

$$N_e = \int_0^L F_e \, dx \qquad \text{(Eq. 13)}$$

$$F_e = F_o (e)^{-\lambda t} \qquad \text{(Eq. 14)}$$

$$R = \frac{x}{t} \qquad \text{(Eq. 15)}$$

$$F_e = F_o \, (e)^{-\frac{x\lambda_i}{R}} \qquad \text{(Eq. 16)}$$

$$N_e = F_o \int_0^L (e^{-\frac{x\lambda_i}{R}}) \, dx \qquad \text{(Eq. 17)}$$

$$N_e = \frac{RF_o}{\lambda_i} \left[1 - (e)^{-\frac{L\lambda_i}{R}} \right]$$

Two cases are to be considered: the defect at the end of the fuel, and the defect on the side of the fuel.

CASE I. DEFECT AT THE END OF THE FUEL

A term must be added when the defect is at the end of the fuel to compensate for the amount being supplied by the end of the fuel. The ap ropriate equation, therefore, looks like this:

$$N_e = \frac{RF_o}{\lambda_i}\left(1 - e^{-\frac{L\lambda_i}{R}}\right) + \pi a_2^2 F_a \qquad \text{(Eq. 18)}$$

If the pellet on the top is covered, the term $\pi a_2^2 F_a = 0$.

CASE II. DEFECT ON SIDE OF FUEL

In this case, the defect is at the side of the fuel and the ends do not contribute to the escape rate, but there are now two paths. The equation is now:

$$N_e = \frac{2RF_o}{\lambda_i}\left(1 - e^{-\frac{L\lambda_i}{R}}\right) \qquad \text{(Eq. 19)}$$

RESULTS

These equations were applied to experiments in the EBWR[2], VBWR[3], and an in-pile AGN experiment in the GETR[8] with the following results:

	(EBWR)[2]			
	Test No. 1	Test No. 2	VBWR[3]	AGN[8]
Fuel	ThO_2-UO_2	ThO_2-UO_2	UO_2	UO_2
Fuel length, in.	3	48	26	22
Fuel diameter, in.	0.300	0.312	0.493	0.177
Coolant	Water	Water	Water	Nitrogen

	Atoms/sec x 10^{-7}		Atoms/sec x 10^{-9}		Microcuries per sec		Millicuries in loop	
Isotope	Meas.	Calc.	Meas.	Calc.	Meas.	Calc.	Meas.	Calc.
Xe^{133}	-	-	9.1	22.6	3.16	1.43	3.32	1.81
Xe^{135}	-	-	1.97	4.89	11.4	6.67	15.54	13.72
Xe^{138}	0.119	0.202	0.126	0.188	38.4[a]	9.75	-	-
Kr^{85m}	-	-	1.64	0.804	2.27	2.38	4.28	3.54
Kr^{87}	-	-	-	-	6.12	4.72	1.82	3.26
Kr^{88}	0.235[b]	1.17	2.35	1.26	5.02	6.04	6.00	7.12

[a] Personal communication with F. Brutschy of GE indicated that this value is high for the average release.

[b] In Robertson[2] on page 19, ". . . the results are low - probably by as much as a factor of two."

CONCLUSIONS

The method presented shows promise for the calculation of the release of fission products from sheathed fuel elements. Certain corrections can be added to the theory; i. e., the clearance between the sheath and the pellets at temperature as well as the correction for non-uniform temperature and non-uniform annulus. Since the results of the calculations obtained are in good agreement with the measured quantities, it was felt that these corrections would not greatly affect the results.

ACKNOWLEDGEMENTS

R. E. Quilici and T. P. Wilcox, both of AGN, have rendered valuable assistance in the support and discussions that helped clarify the above concepts.

APPENDIX A - SAMPLE CALCULATIONS

	Test No. 1[2]	Test No. 2
Wt, U^{235}, gm	2.73	43.5
Pellet diameter, in.	0.300 ± 0.001	0.312 ±
Fuel length, in.	3.1	48
Fuel sheath clearance		
Diameter (cold), in.	0.004	0.010
Axial, in.	0.125	0.125
Sheath material	SS	SS
Sheath defect		
Location	Center of fuel	Top of fuel
Diameter, in.	0.010	0.020

Reactor Operations (20 MW)

		Max.	Ave.
Thermal neutron flux n/cm^2-sec	8×10^{12}	8×10^{12}	4.6×10^{12}
Fissions/sec	3.25×10^{13}	4.83×10^{14}	2.81×10^{14}
Temperature fuel surface, °C	650	1000	800

ANL-Test No. 2

$\delta H_2O = 2.76 \times 10^{-8}$ cm

δ Kr = 3.69×10^{-8} cm

δ Xe = 4.02×10^{-8} cm

T = 1073°K

δ = 9.1

M = 264.12

Z = 106

P = 3.10×10^{4} mm

Average Molecular Kinetic Velocity

$$\bar{V}_{133} = 4.395 \times 10^{-10}\ T^{3/4} P^{-1/2}\ \delta_{12}^{-1}$$

$$\bar{V}_{133} = 1.38 \times 10^{-2}\ \text{cm/sec}$$

Recoil range[4]

$$R_{Kr} = \frac{0.512M}{\rho \sqrt{Z}}$$

M = Molecular weight

Z = atomic number

$$R_{Xe} = \frac{0.414M}{\rho \sqrt{Z}} = 11.67\mu$$

Recoil Contributions

Surface area fuel	303 cm^2
Recoil volume of Xe	0.3536 cc
Total volume of fuel	60.00 cc
Total $f/s_{(ave)}$	2.81×10^{14}
cm^2/cm fuel	2.49

$$F_a = 2.81 \times 10^{14} \times \frac{0.3536}{60.00} \times \frac{1}{303} \times \frac{1}{4} \times 6.5 \times 10^{-2} = 8.88 \times 10^{7}\ \text{atom/cm}^2\text{-sec}$$

$$F_o = 2.49 \times 8.88 \times 10^{7} = 2.21 \times 10^{8}$$

Flow Velocity

$$R_i = \frac{2}{3}\left(a_1 - \frac{a_2^2}{a_1}\right) V_{133} = 4.56 \times 10^{-4}\ \text{cm/sec}$$

Atoms escaping

$$N_e = \frac{R_i F_o}{\lambda_i}\left(1 - e^{-\frac{L\lambda_i}{R}}\right) + \pi a^2 F_a = 4.56 \times 10^{-4}\ 2.21 \times 10^{8}/1.52 \times 10^{-6}$$

$$\left(1 - e^{-\frac{122 \times 1.52 \times 10^{-6}}{4.5 \times 10^{-4}}}\right) + 0.4940 \times 8.88 \times 10^{7}$$

$$N = 2.25 \times 10^{10} + 4.38 \times 10^{7}$$

$$2.25 \times 10^{10}\ \text{atoms/sec}$$

APPENDIX B - EFFUSION

$F = 3638 \sqrt{T/M}$[a]

F = flow rate cm^3 per $sec\text{-}cm^2$

T = temperature, ^oK

M = mass of isotope of interest

[a]Vacuum Symposium Transactions, 1954, p. 139.

For Xe^{133} at 1073^oK:

$F = 3638\sqrt{1073/133} = 1.03 \times 10^4$ $cm^3/sec\text{-}cm^2$

For a 20 mil defect = 21 cm^3/sec

This is equivalent to 5.64×10^{20} atoms/sec at Standard Temperature and Pressure. Since only 9.1×10^9 atoms/sec are escaping from the ANL Test No. 2 and the defect can handle 10^{20}, the defect is not a barrier to the escaping atoms.

REFERENCES

1. W. B. Cottrell, et al., Fission Product Release from UO_2, USAEC Report ORNL-2935, Oak Ridge National Laboratory, September 1960.

2. R. F. S. Robertson, Tests of Defected Thoria-Urania Fuel Specimens in EBWR, USAEC Report ANL-6022, Argonne National Laboratory, May 1960.

3. F. V. Brutschy and R. W. Osborne, Release of Fission Products from UO_2 Fuel, Trans. Am. Nucl. Soc., 2,: 2 (1959).

4. E. R. Smith and P. W. Frank, Recoil Range of Fission Fragments in Zirconium, Report WAPD-TM-198, Westinghouse Electric Corporation, November 1959.

5. S. Dushman, Scientific Foundations of Vacuum Techniques, John Wiley and Sons, Inc., New York, 1949.

6. W. Jost, Diffusion in Solids, Liquids, Gases, p. 422, Academic Press, Inc., New York, 1960.

7. J. Jeans, Kinetic Theory of Gases, p. 222, Cambridge University Press, 1952.

8. Army Gas-Cooled Reactor Systems Program Monthly Progress Report for May 1961, Report IDO-28572, p. 40, Aerojet-General Nucleonics, June 1961.

USE OF THE KING FURNACE IN FISSION PRODUCT RETENTION STUDIES OF GRAPHITE REACTOR FUELS[a]

E. E. Anderson, P. E. Gethard, and L. R. Zumwalt

General Atomic Division of General Dynamics
San Diego, California

INTRODUCTION

Out-of-pile fission product retention studies of thorium, uranium carbide-graphite matrix reactor fuels have been carried out at General Atomic for some time.[1] Since April 1960, fission product release at high temperatures (1000 to 3000°C) has been explored principally by the use of graphite tube resistance furnaces. These are basically adaptations of the type of electric furnace first developed by King[2] for spectroscopic investigations. Three versions of the furnace have been developed and utilized to satisfy specific requirements as discussed below.

GENERAL FEATURES OF THE FURNACE

The King furnace is most suitable for the study of carbide-graphite fuel bodies, such as those designed for the HTGR.[3] This is due to the fact that the graphite tube heater element in which samples are placed and the helium atmosphere employed closely simulate the physical and chemical environment of the actual reactor. The furnace requires little insulation (using only graphite and tantalum radiation shields), so outgassing is minimized and the furnace may be brought to a given temperature very quickly. Thus, with preliminary outgassing under vacuum (order of 30 minutes at 1000°C), the furnace can be brought to operating temperatures of 2000°C in 1 minute and 3000°C in 3 minutes, respectively. Furthermore, the King furnace is readily adapted so the graphite tube serves as a conduit for helium gas to sweep past the sample and carry volatile fission products to a cold finger within the furnace and Xe and Kr to activated charcoal cold traps and associated radiation detection equipment located at a considerable distance from the furnace.

Important features common to all of the King furnaces employed are:

1. A saturable reactance transformer of rating 50 to 75 Kw and a maximum secondary emf of 34 volts for a power supply.

[a]Work performed under U. S. Atomic Energy Commission Contrast No. AT(04-3)-314.

2. Separate water cooling circuits to the dome, the base plate, and the graphite tube electrodes mounted on the base plate. These are each interlocked to the main power supply so the furnace is turned off with loss of coolant flow in any circuit.

3. Viewing ports for temperature measurement and a port with vacuum-tight O-ring seals whereby a stainless steel tube threaded into the exit end of the graphite heater tube conducts the sweep gas out of the furnace. The gas then passes through a flowmeter and thence to the absorber traps.

4. An automatic gas pressure regulating system whereby the helium gas is maintained at a slight positive pressure (1.0-1.5 psig) in the furnace.

Heretofore, temperatures have been controlled manually with temperatures being measured by an optical pyrometer which directly views the sample through the viewing port opposite the gas exit port. An automatic temperature control using lead sulfide infra-red sensitive transducer elements is being employed on one furnace. This may prove desirable for all three furnaces since long runs (of several days duration) which can be only occasionally attended are often required.

DETAILED DESCRIPTION OF THE FURNACES

The first furnace, King I, (See Figure 1 for view of the furnace with the dome on) was designed primarily for the laboratory studies of Xe^{133} release from lightly irradiated fuel bodies at constant temperatures up to about 2000°C. It has the capability of heating samples for a few minutes up to 2600°C, but not for longer due to heat dissipation limitations.

1. Heating Element

The heating element for this furnace is a tube machined from AGOT graphite. A spare element is displayed on the plate above the instrument panel of furnace in Figure 1. The 17-inch heating length (1 5/8" I.D., 1 7/8" O.D.) with an 1/8" wall has a resistance of 0.01 ohm at room temperature. When heated, the temperature is substantially uniform across about 8 inches of the center of this tube.

2. Supporting Electrodes and Baseplate

The heavy ends of the heating element fit into upright copper electrodes and are tightened down by means of graphite collets. Figure 2 shows the graphite tube element and electrode arrangement. These large, water-cooled electrodes protrude through a 1/2" thick stainless steel baseplate and are supported by means of thick insulating discs of cast high-temperature epoxy resin. Cooling of this 27" baseplate is provided by a coil of 1/4" copper tubing underneath, packed with Thermon (graphite-loaded, heat transfer compound). The relatively poor heat conductivity of stainless steel has proved to be a slight drawback with this furnace allowing the neoprene O-ring seals to exceed their temperature limits (about 150°C) if run at higher than 2200°C for extended periods. Stainless steel was originally chosen for strength when operating under vacuum.

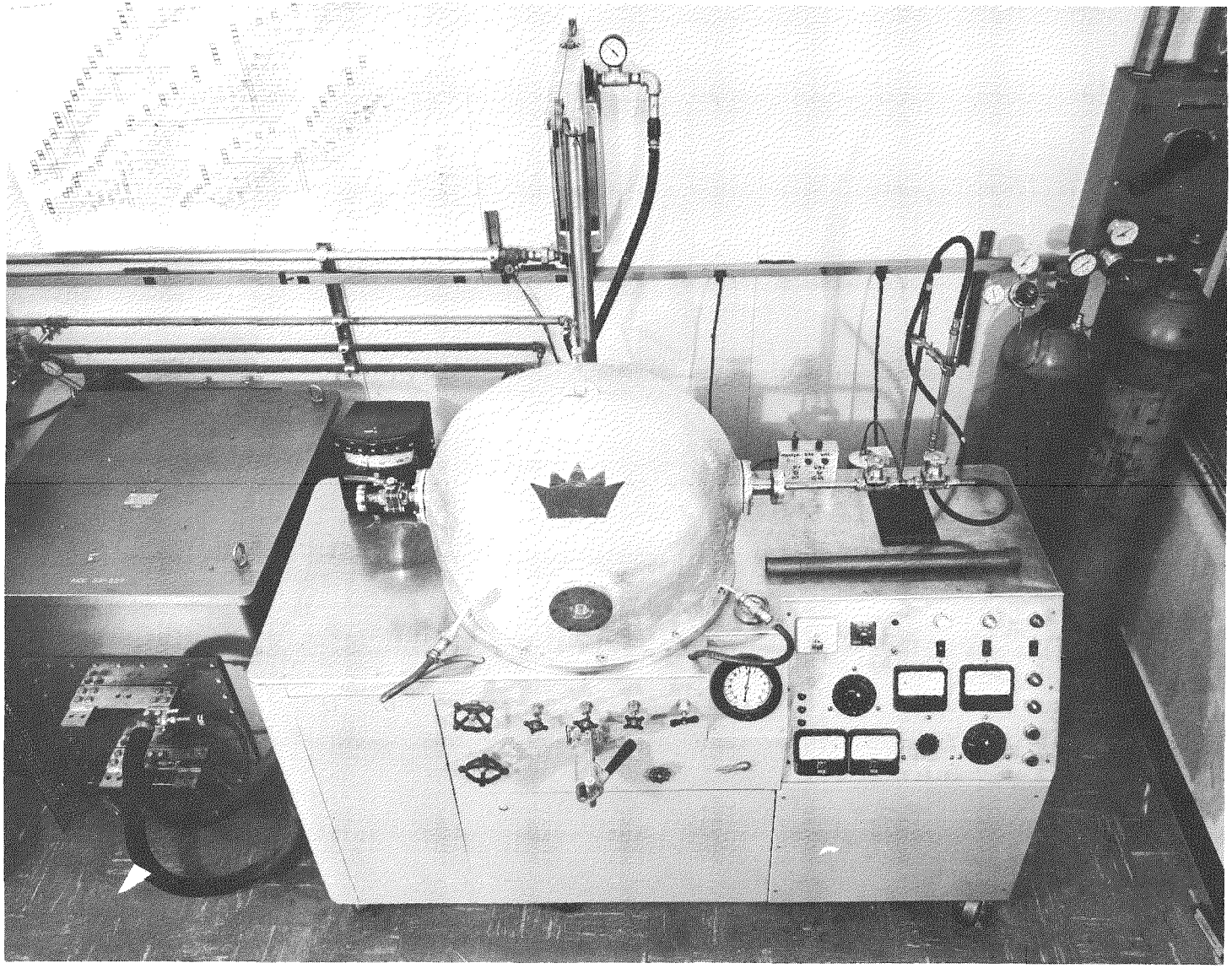

Figure 1 -- King Furnace I. For Fission Product Release Studies up to 2000°C.

Figure 2 -- King Furnace I with Dome Raised, Showing the Graphite Heating Element (Radiation Shielding Removed).

3. Radiation Shielding

The furnace uses a tantalum (0.005" thick) radiation shield around the graphite heating element (Figure 3). This 12" long shield consists of 5 concentric cylinders of metal, three smooth layers separated by two corrugated layers to minimize physical contact between them. The innermost layer is about 1" from the element. This shield yields a 50% efficiency improvement in utilization of power (See Figure 4 for power requirements with and without tantalum shield) and is a necessity in this furnace for runs longer than a few hours at temperatures of 1700°C and above because of the poor heat transfer properties of the stainless steel baseplate. At 1700°C the tantalum shield will hold up well for a long period of time, but if used with temperatures above 2000°C for any length of time it rapidly carburizes and crumbles. The tantalum shield is supported by the innermost of three graphite radiation shields, each with an 1/8" wall and spaces about 1/2" apart. The O.D. of the outermost radiation shield is 8 inches.

4. Power Supply

Power for this furnace is supplied by a saturable reactor transformer rated at 75 KVA with a maximum secondary emf output of 34 volts. Until this transformer achieves its steady state operating temperature (8 hours), a drift in output of about 15% is observed. One means of compensating for this has been by the use of a Chromel-Alumel thermocouple in contact with the outer graphite radiation shield. It takes about an hour for the actual furnace components to achieve their steady state condition. The thermocouple is wired to a Wheelco temperature controller. As the temperature of the outer radiation shield drops due to the downward drift of the transformer, the controller turns on the transformer fine control (which has been set at full scale) just long enough to bring the temperature back. Thus after one hour of operation the furnace can be left unattended overnight without more than a 1% drop in temperature observable the next day. Power is delivered from the transformer to the furnace electrodes by means of large, flexible, water-cooled, copper leads. They connect to the heating element supporting electrodes where the latter extend down beneath the baseplate.

5. Containment

The furnace is contained in an aluminum dome which is suspended from above with a counterbalance arrangement and can be easily raised and swung aside for ready access to the furnace. When in position it is bolted to the baseplate and sealed around its outer edge by means of a large O ring. One end of the heater tube is open to the inside of the dome,while the other end is threaded and accessible from outside the dome by means of a stainless steel tube which passes through a port in the dome wall (utilizing a sliding O-ring seal) and screws into the heater tube. Thus, helium can be drawn from the dome, swept past an irradiated fuel compact and out the dome to a remote trap such as charcoal cooled by liquid nitrogen where xenon and krypton can be collected and monitored. Directly opposite the outlet port is a viewing port (quartz window) providing a view down the length of the heating tube through which samples can be observed while the furnace is in operation. Cooling coils around a single walled hemispherical dome have proven adequate for the design temperature range 1000°C to 2000°C. For steady-state temperatures higher than this insufficient heat is removed to protect the rubber O-ring seals.

Figure 3 -- King Furnace I with Radiation Shielding in Place.

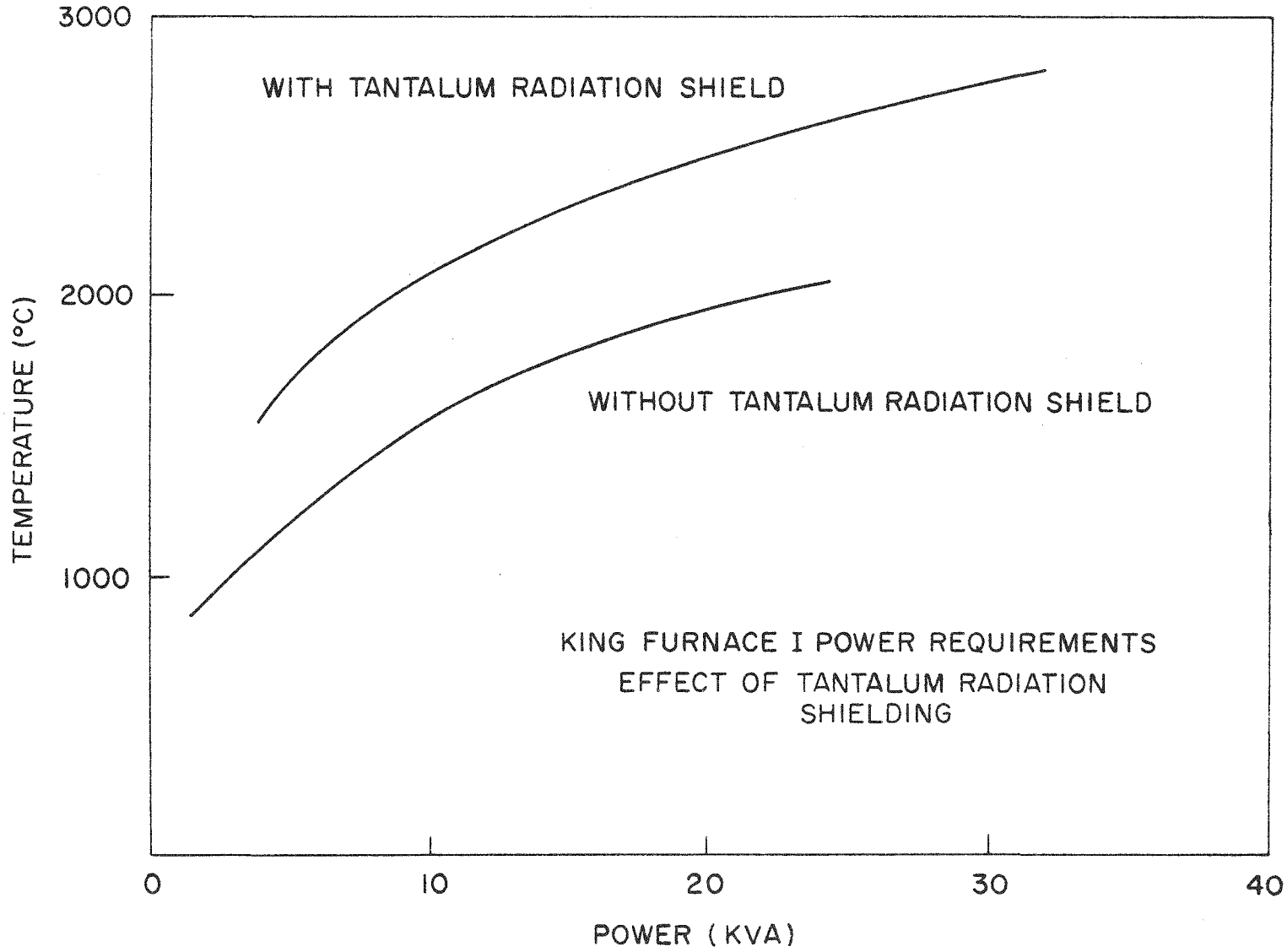

Figure 4 -- King Furnace I Power Requirements. Effect of Tantalum Radiation Shielding.

6. Gas Pressure System

Most of the experiments performed in this equipment have been in an atmosphere of helium (1.0-1.5 psig). The gas pressure in the dome is maintained by a pair of Meletron pressure control switches rated for helium service, one setting the upper, the other setting the lower pressure limit. These control switches operate a pair of solenoid valves, one solenoid admitting helium when the pressure falls below 1.0 psig, and the other dumping helium from the dome to the atmosphere if the pressure exceeds 1.5 psig (as it does while the furnace is heating up). A valve is provided for isolation of these when the furnace is operating under vacuum. They are further protected from inadvertent pumping by means of a valve that automatically opens and admits air when the pressure in the dome falls to 2 lb/sq. in. below atmospheric pressure. A simple needle valve at the exit of the purge gas controls the flow of helium.

7. Vacuum System

Evacuation of the apparatus is accomplished by means of a Cenco Hyvac 14 mechanical pump and a 4" diffusion pump (MCF, 300 Consolidated Electrodynamics Corp.) utilizing Dow Corning 703 silicone fluid. These pumps are connected to a 1.5" diameter manifold which leads to a 4" diameter opening in the baseplate. Through a series of valves the roughing pump can operate directly on the system with the diffusion pump isolated, or it can operate as the back-up pump for the diffusion pump. Throughout the furnace housing system connections are sealed by means of neoprene O-rings. Silicon O-rings are used in contact with the baseplate because of their higher temperature tolerance. Pressure is measured by means of an ionization (Phillips) gauge.

8. Cooling System

The three main water coolant circuits control the temperature of the dome (4 gal/min), baseplate (1 gal/min), and the supporting electrodes (1.5 gal/min). If the furnace were to operate with any one of these items uncooled, the result would be disasterous for the equipment. Since the furnace is tied directly into a closed system soft water loop, flow control switches on the outlet ends of the components are used to protect the furnace. Should the flow of water to the outlet fall below a predetermined limit for any of the three components, a circuit breaker is tripped shutting down the furnace. The circuit breaker must then be reset manually before the furnace can operate again.

The second furnace, King II, (See Figure 5) was originally designed for remote control operation in the General Atomic LINAC (linear electron accelerator) and Hot Cell facilities with steady operating temperatures not to exceed 2000°C. The design features for this furnace are essentially the same as for furnace I with the following exceptions:

1. The furnace baseplate was mounted on a vertically adjustable frame for operating at various heights above the floor. The height of the horizontal graphite tube heating element thus was adjustable from as low as 40" above ground level to 65". This maximum height was necessary for proper height adjustment when the furnace was used as the heat source for LINAC irradiation experiments. The minimum height was required for use in the hot cell operations where a minimum shielding height would be desired.

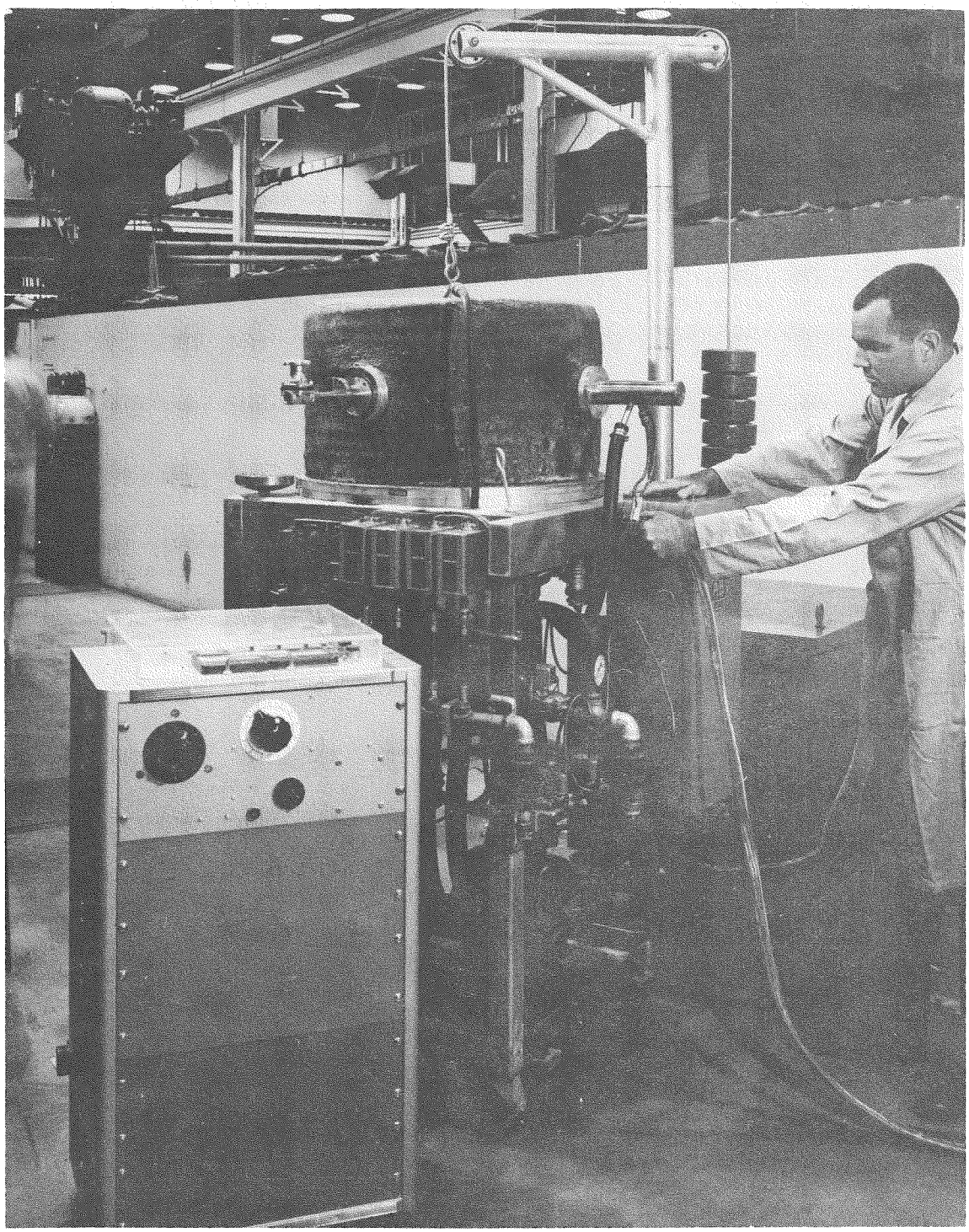

Figure 5 -- King Furnace II. For Fission Product Release Studies with a Linear Accelerator. (The Beam Tube can be seen Protruding from the Dome above the Operator's Hands.)

2. Four screw jacks at the four corners of the bottom frame supports provided rigid location as well as leveling adjustment.

3. In order to provide a beam path when used in the linear accelerator facility, a 2" diameter water-cooled stainless steel tube was designed to penetrate the water-cooled dome perpendicular to and on the same level as the furnace heater element. A centerline along the length of the beam tube bisects the center of the furnace tube. The outside end of the beam tube was welded shut with a 10-mil stainless steel window, while the inside end was closed with a 3/8" thick fansteel target containing 80% tungsten converter target. The beam tube was evacuated with the furnace roughing pump to 10^{-3} mm. The fansteel converter target penetrated into the dome to within 4 inches of the heater tube which contains the fuel specimen.

4. The furnace element was provided with radiation shields made up to a 3" diameter graphite tube and five layers of 0.005" thick tantalum foil nested between this tube and the furnace element.

5. This furnace was designed to operate at temperatures no higher than 2000°C steady state. For this reason an all aluminum baseplate was chosen instead of the stainless steel used on the original furnace. The dome was converted from a hemisphere top to a flat top and was cooled with concentric coils of 3/8" copper tubing held on to the dome with "Thermon", a graphite-filled cement with good heat transfer qualities.

6. A 50 KVA saturable reactor power supply was chosen to power this furnace since maximum temperature requirements were not so high.

7. In the design of this furnace it was necessary to provide remote electrical control when operating in an inaccessible area such as a linear accelerator or hot cell. The following is a list of controls that were remotely operated from a distance of about 150 feet.

a. Power supply (Variac control, with voltmeter and ammeter as secondary).

b. Roughing pump.

c. Diffusion pump.

d. Phillips gauge.

e. Water coolant.

f. Inert gas supply.

The third furnace, King III, (See Figures 6 and 7) was designed primarily to operate at steady-state temperatures up to 3000°C in connection with studies of fission product release such as might occur in the event of a reactor accident. The overall design of this furnace is much the same as I and II with the following exceptions.

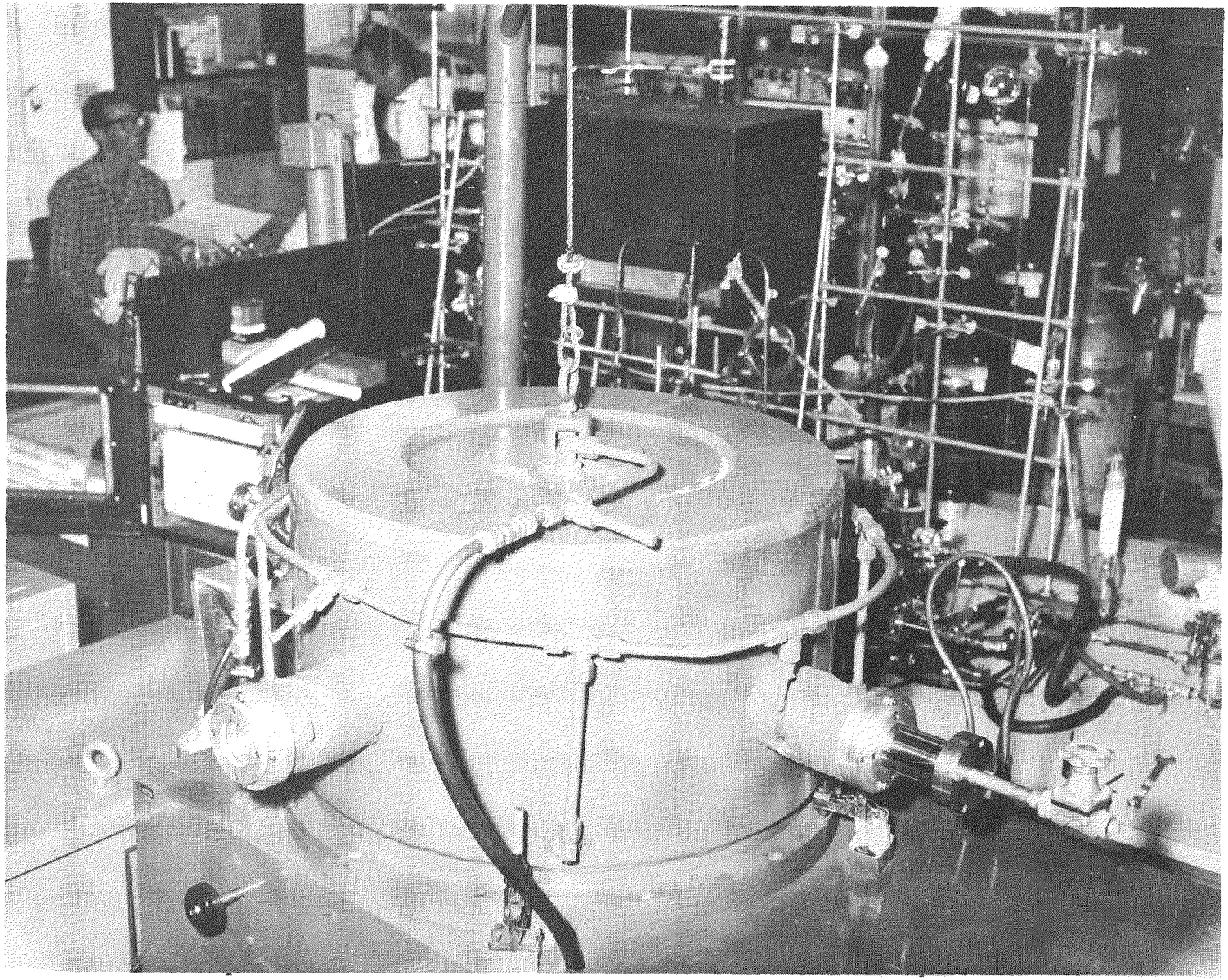

Figure 6 -- King Furnace III. (The Double-Walled Dome Provides the Necessary Cooling for Steady-State Runs up to 3000°C.)

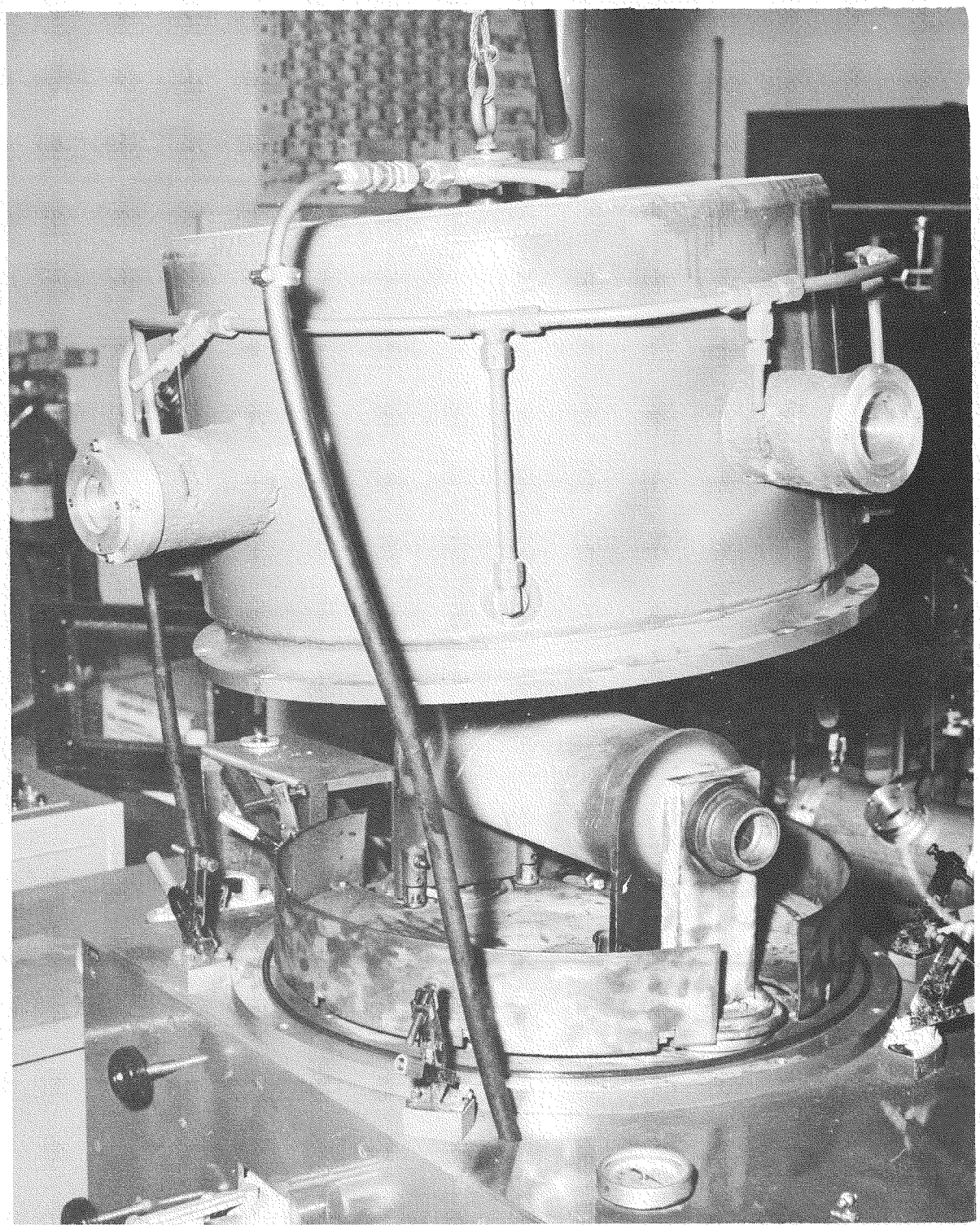

Figure 7 -- King Furnace III. (The Dome has been Raised to Show the Water-cooled Copper Heat Sink Supported over the Baseplate.)

1. Containment Vessel

To improve the efficiency of the water coolant for heat removal, a double-walled vessel was designed with a flat top instead of the hemisphere dome. The flat top was reinforced with 1" thick aluminum for pressure requirements.

The water coolant enters the bottom through four inlets at the base of the vessel 90 degrees apart. A diverting nozzle causes the water to swirl, exiting at the center of the top plate.

The view ports were extended to 6" to protect the O-ring seals.

2. Baseplate Heat Sink

The baseplate for this furnace is 7/8" thick aluminum without exterior water coolant as was designed into the first furnace. Heat removal for the baseplate is accomplished by means of a water-cooled copper heat sink located on top of the baseplate inside the containment vessel. The sink is a 3/16" copper plate covering the entire baseplate and held off the baseplate with 1/2" spacers. The outer rim has a 3" high vertical copper collar welded on to protect the main 24" O-ring, and 3/8" copper tubing is silver-soldered beneath the sink for cooling the sink. The copper tubing exits through the baseplate by standard pipe fitting.

3. Radiation Shielding

The only significant difference in radiation shielding is primarily the use of only graphite. At temperatures of 3000°C, tantalum radiation shielding would of course melt and carburize badly.

The graphite shielding in this furnace is constructed of five 14" long 3/32" thick concentric graphite cylinders nested inside each other with the smallest being 3" diameter and the largest 8" diameter. They are held in place by two graphite end plates grooved for concentricity. The end plates bolt to the water-cooled heat sink.

The shielding is free standing allowing the graphite heating element to be removed without removal of the shielding.

Powered with a 75 KVA saturable reactor, this furnace will operate at a steady state and controllably from 800 to 3200°C without producing external temperatures over 65°C. The water coolant necessary to maintain these conditions is approximately 6-7 gallons/minute.

TYPES OF EXPERIMENTS

The types of experiments carried out may be classified as: (1) annealing experiments with the temperature being held constant for many hours, (2) annealing experiments with the temperature being varied to simulate a reactor excursion, and (3) steady-state release experiments where the fraction F of various shorter-lived volatile activities (particularly those of Kr and Xe) released into a helium purge gas stream are determined for a fuel sample undergoing fission at a constant rate. In the first two types of experiments,

reactor fuel materials comprising uncoated and pyro-C-(pyrolytic-carbon) coated thorium, uranium carbide particles, both alone and incorporated in a graphite matrix, were studied. The fuel bodies tested were mostly those made at General Atomic in connection with metallurgical development work.[4]

The bulk of the annealing experiments involved the determination of the fraction ϕ_{Xe} of Xe^{133} retained as a function of time from fuel materials lightly irradiated in the TRIGA (10^{13} to 10^{14} fissions per sample). More recently, the release of Ba^{140}, I^{131}, and Te^{132} has been determined at the termination of a run by measuring collected activities using a multichannel gamma-ray spectrometer. The barium activity is collected on a nest of four 1/16" thick concentric graphite sleeves placed around the sample, while the iodine and tellurium activities are collected on the copper-plated end of a stainless steel, water-cooled cold finger located centrally in the graphite heater tube about 2 inches downstream of the sample. However, one high-burnup experiment has been carried out (and others are projected) on a small quantity of pyrolytic carbon-coated Th, U^{235} (2.25:1) dicarbide particles, centrally disposed in a graphite matrix 1" diameter by 1". These were irradiated to a fission-to-metal ratio equivalent to full burnup in the HTGR. In this case, the fraction of activity released, ϕ, was determined for both Xe^{133} and Kr^{85} as a function of time.

In the annealing experiments, the activity (Xe^{133} and Kr^{85}, when present) collected on a liquid nitrogen-cooled trap is continuously monitored by a calibrated scintillation crystal detector, single-channel analyzer, gamma spectrometer system. The fractional release in the case of a Xe^{133} run may be determined by driving off all the Xe^{133} at the end of the run by heating the sample to 2400°C or higher for a sufficiently long period (several hours may be required). More generally, the number of fissions occurring in the sample is estimated from a flux monitor and the U^{235} content, or by determining the La^{140} activity in the sample prior to annealing. The other activities, Ba^{140}, I^{131}, and Te^{132}, are determined by counting collected activities using a multichannel gamma-ray spectrometer. Only one point is obtained per experiment for the ϕ vs time curves of these activities. Radiochemical analysis of residual activities in the fuel bodies such as Sr^{90}, Ba^{140}, Cs^{137}, and Sm^{153} may also be carried out at the end of the run to obtain ϕ values.

In the experiments on the steady-state release of shorter-lived Kr and Xe activities from uncoated particle fuel bodies, the General Atomic LINAC was used to generate photofission at a constant rate in samples heated in a King furnace. The furnace used, King II, was especially designed for remote operation, as mentioned above, and was provided with a tungsten target mounted in a re-entrant tube that fit into front viewing port. With this arrangement, the electron beam was brought with little scattering loss to the target located only 4 inches from the graphite heater tube. A cone of gamma rays (energy $\leq$ 20 Mev) passed through the tube and sample contained therein causing photo-fission of the thorium and uranium in the fuel sample. The details of this experiment will be reported elsewhere. However, in brief, the release of Xe^{139}, Xe^{138}, Kr^{89}, Kr^{88}, and Kr^{85m} was determined by a direct comparison technique where a thorium, uranium stearate target (having Th and U in the same ratio as in the fuel material) was placed in the furnace tube operated at room temperature. It thereby served as a fission product release standard where F is known to be unity. This is due to the high emanation power which the thorium and uranium stearate displays for noble gas fission products. Wahl[5] estimates

a > 99% escape from barium stearate (uranium and other stearates behave similarly) in the case of Kr and Xe isotopes with half-lives $\geq$ 4 sec.

EXPERIMENTAL RESULTS

It is beyond the scope of this paper to give a detailed report on the fission product retention behavior of the various thorium, uranium carbide-graphite reactor fuel materials studied to date. However, results from some of the experiments discussed above are presented. Figure 8 gives ϕ (fraction retained) vs t (time) curves for the release of Xe^{133} at several temperatures from uncoated thorium, uranium carbide-graphite fuel body samples. These were prepared by compacting 100 to 200μ (Th, U)O_2 particles with graphite flour and a small amount of pitch, warm (hot) pressing, and heating to about 2000°C to convert the thorium-uranium solid-solution dioxide to the corresponding dicarbide in accordance with procedures developed by Goeddel et al[4]. Figure 9 gives the fission retention curves for Xe^{133} and Kr^{85} release at 1700° from the high burnup compact, containing a relatively small number of pyrolytic-carbon-coated fuel particles, as mentioned above. The Xe^{133} release from a control sample is also given. The latter was only lightly irradiated in the TRIGA reactor. Figure 10 gives a Xe^{133} release curve for a fuel body made with pyro-C-coated particles under a simulated reactor excursion of up to 3000°C. The temperature of the sample as well as the fraction of Xe^{133} remaining is given as a function of time. Figure 11 gives steady-state release fractions, F, determined for Xe^{139} and Xe^{138} at several temperatures using the LINAC in conjunction with the King furnace. The curves given were calculated from characteristic diffusion times obtained, as discussed below, from annealing experimental data on Xe^{133} release (Figure 8).

TREATMENT OF DATA

An examination of fission product retention data as obtained in King furnace experiments indicates that release behavior is not readily explained as a simple diffusion process. As discussed by Lewis[6], in the case of UO_2 fuels fission product release can become very complicated with not only diffusion and recoil processes being involved, but also at high radiation levels knock-on and knock-out processes. Not enough work has been done on fission product release from pyro-C-coated particles to fully understand their behavior. However, it is expected that in-pile, purge capsule steady-state release studies now underway will, along with King furnace annealing studies, help close the gap in our information. On the other hand, in the case of fuel compacts containing uncoated carbide particles quite a bit of data has accumulated. Here there is evidence, on the basis of the approximate independence of release on fuel compact size, that in-pore diffusion in the graphite matrix is not the rate controlling process. Certainly some of the fission products recoil into graphite grains and they then have to diffuse out of these grains (the rate controlling step in this case). However, with 150 to 200 micron particles only a few percent of the fission products recoil out of the particles - the rest of the fission products are deposited in carbide crystallites or grains and have to diffuse through the grains to grain boundaries and then outside of the carbide particles before they reach the relatively porous structure of the graphite matrix.

It has been tentatively postulated that for volatile species, and particularly Kr and Xe, the diffusion of fission products out of the carbide

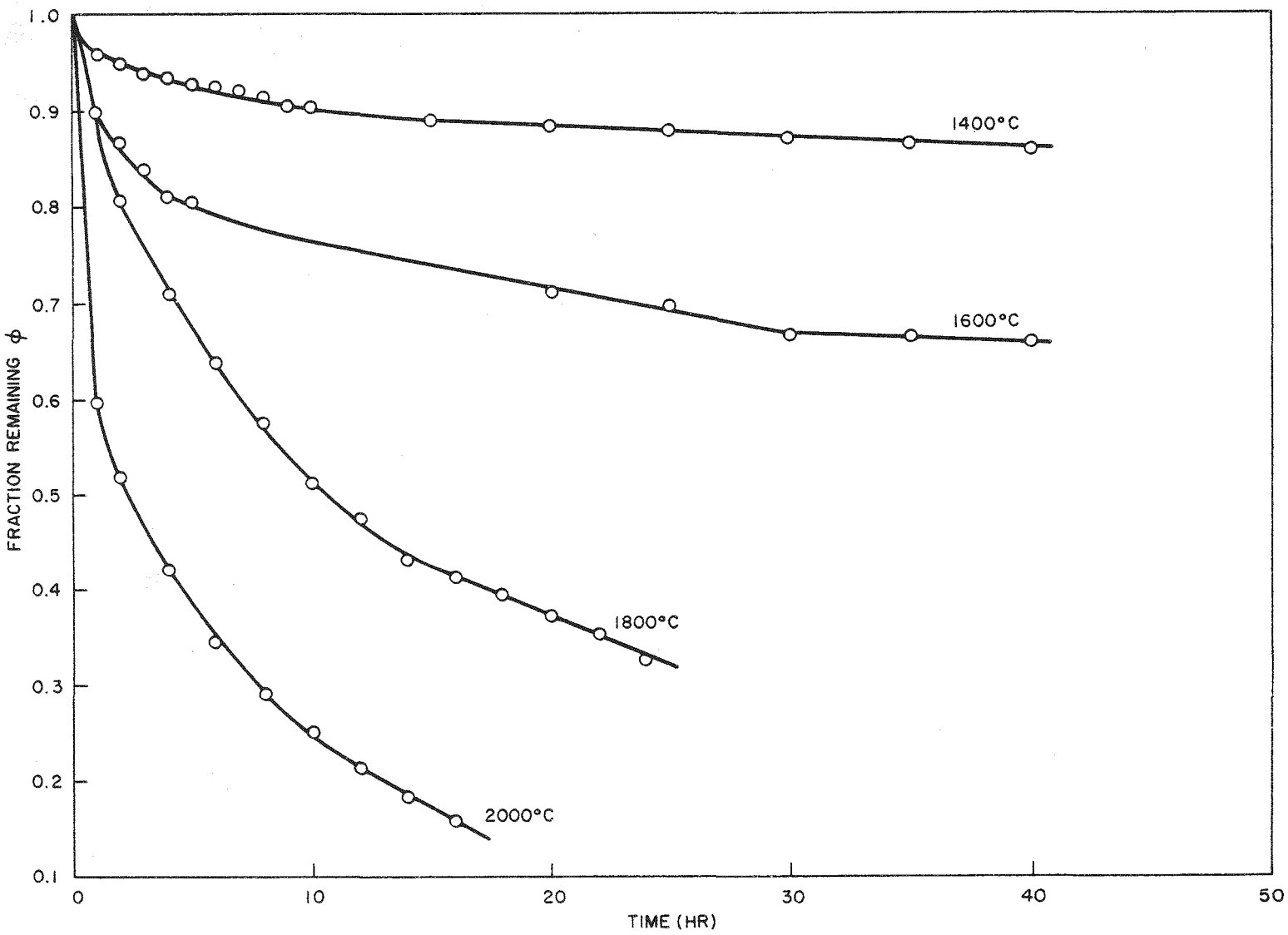

Figure 8 -- Xe^{133} Release from Uncoated-Particle Compacts (Th:U ratio 2.9:1.0).

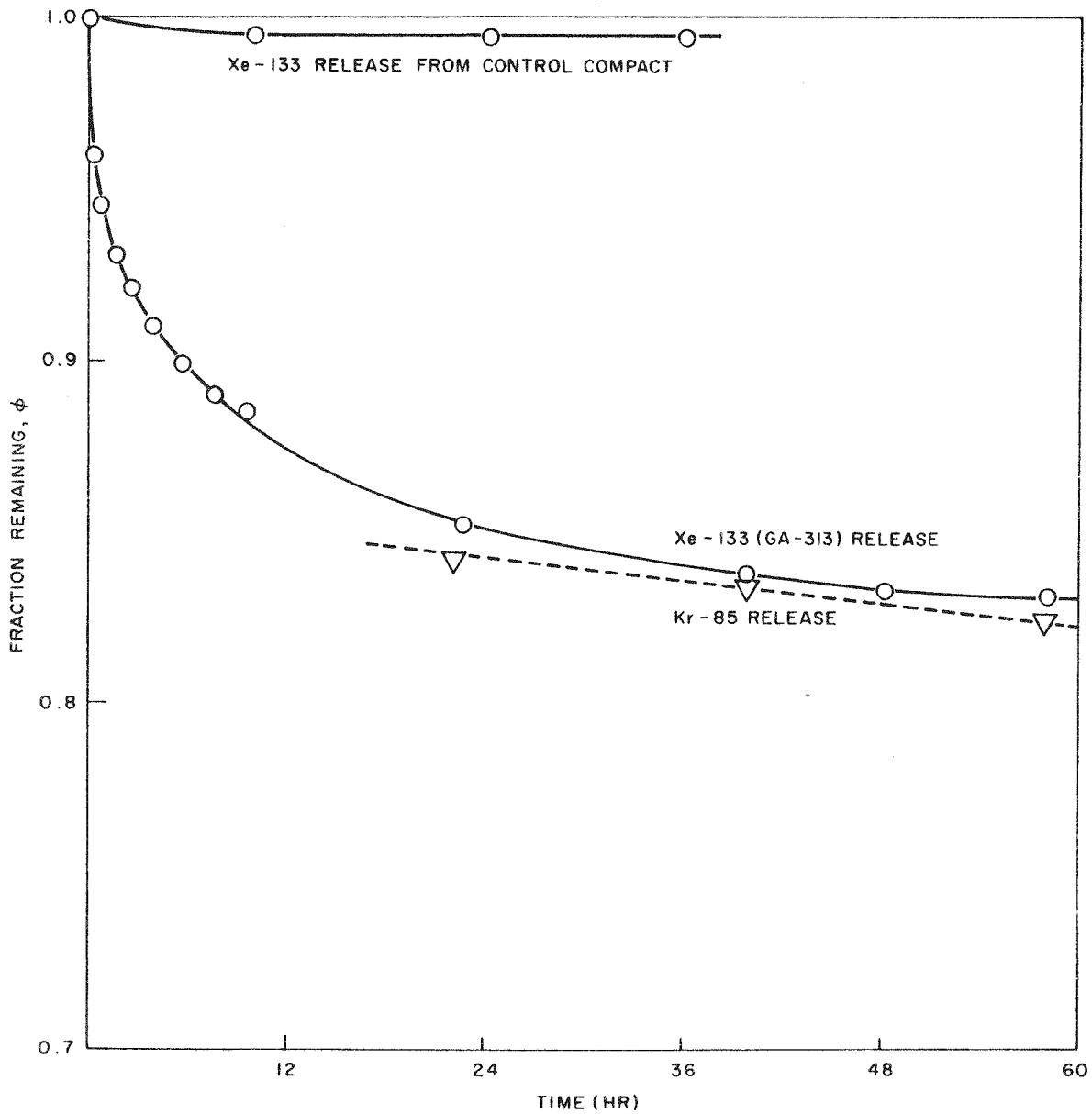

Figure 9 -- Fission Product Release at 1700°C
from Compact GA-313 (High Burnup)

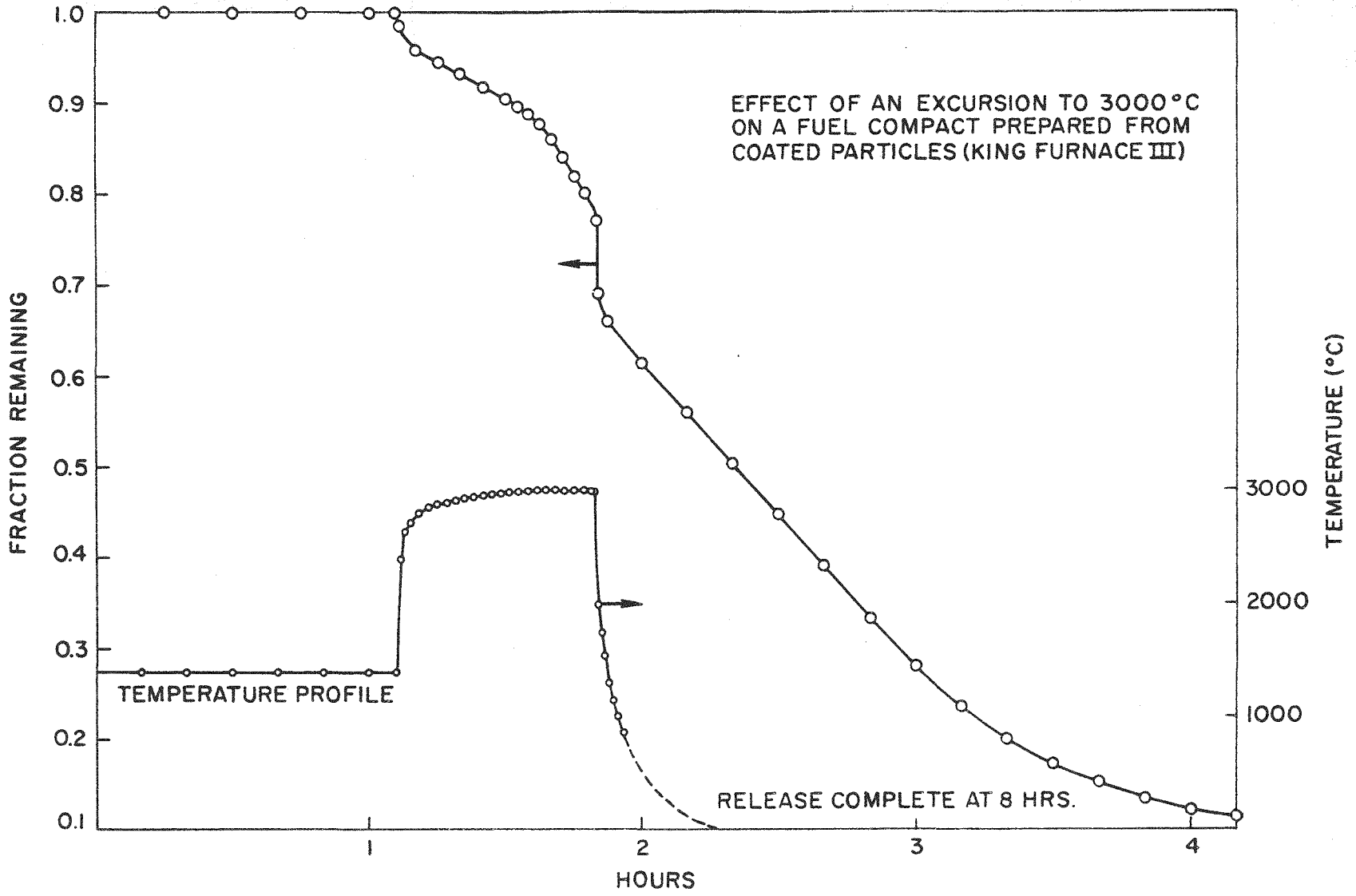

Figure 10 -- Effect of an Excursion to 3000°C on a Fuel Compact Prepared from Coated Particles (King Furnace III).

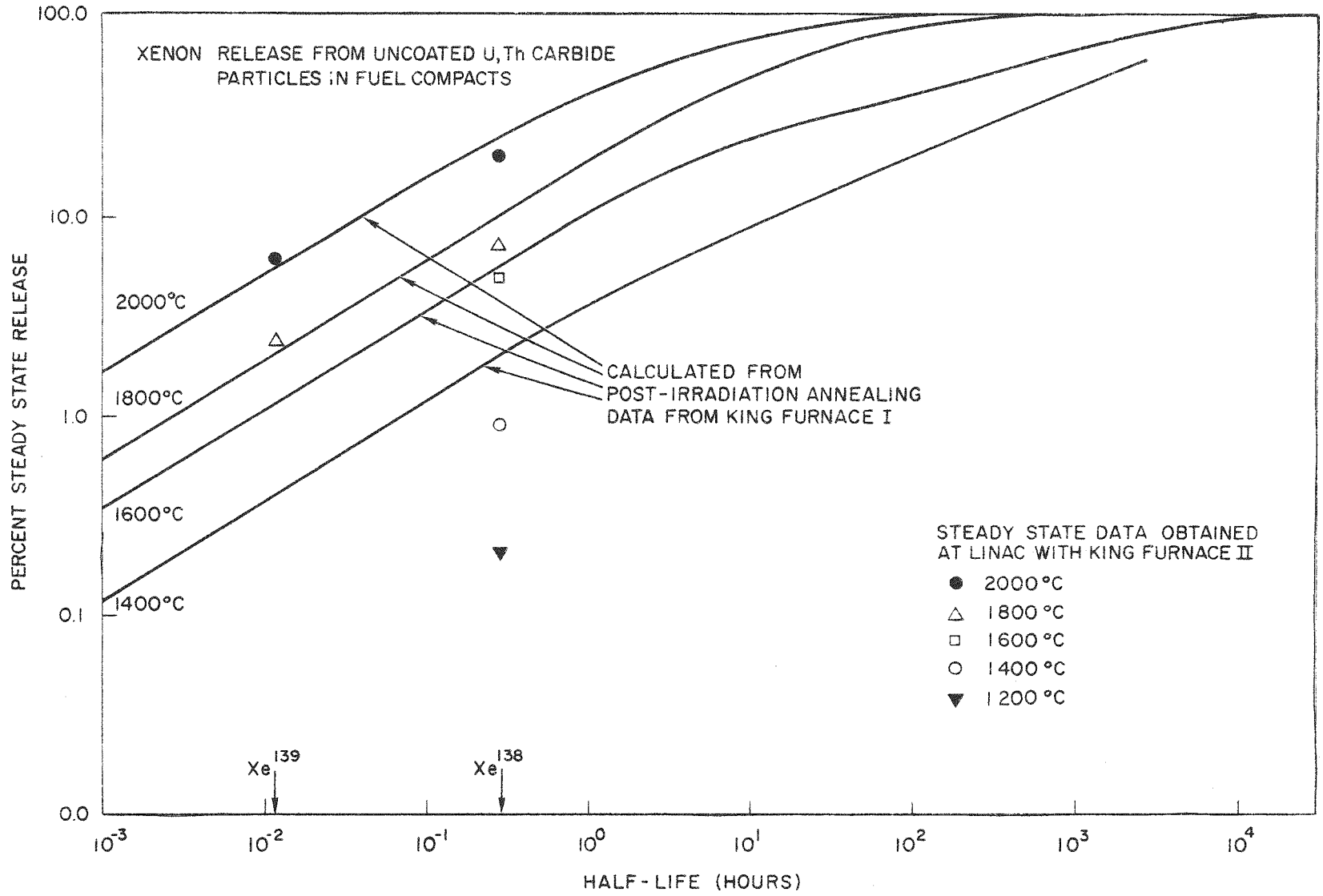

Figure 11 -- Xe Release from Uncoated U, Th Carbide Particles in Fuel Compacts.

crystallites or grains plus diffusion of a small percent of the recoiled fission products from graphite grains are the rate limiting processes for release. In accordance with this it has been assumed that release can be approximately represented as diffusion from a number of kinds of grains (differing in size and/or material). Then the fractions ϕ (t) of a volatile fission product retained at time, t, can be represented by

$$\phi(t) = \sum_{i=1}^{n} c_1 \mathcal{F}(t/\tau_i) \tag{1}$$

where

$$\sum c_i = 1$$

and

$$\mathcal{F}(t/\tau_i) = \frac{6}{\pi^2} \sum_{m=1}^{\infty} \frac{1}{m^2} e^{-\frac{m^2\pi^2}{\tau_i} t}$$

Corresponding to this information under the condition of a constant fission rate, the steady state activity release fraction of nuclide j from the fuel body is given by

$$F_j = \frac{\text{Activity outside of fuel body}}{\text{Total activity}}$$

$$= \sum_{i=1}^{n} c_i \frac{3}{A_{ij}} \left(\coth A_{ij} - \frac{1}{A_{ij}}\right) \tag{2}$$

where

$$A_{ij} = \sqrt{\tau_i \lambda_j}$$

and

λ_j = radioactive decay constant of j

The above formulation corresponds to considering the fuel particle-graphite matrix system as comprising an assemblage of n types of "equivalent spheres"[7] (each with a weighting factor, c_i) in which fission products are uniformly deposited and from which the fission products diffuse. Then,

$$\tau_i = \frac{a_i^2}{D_i} \tag{3}$$

where

a_i = the radius of the equivalent sphere of type i

D_i = diffusion coefficient for sphere of type i

This formulation is useful, although only an empirical approximation, in that the characteristic diffusion times τ_i and the coefficients c_i may be extracted from annealing data (ϕ vs t) curves by graphical analysis and values

of F_j calculated. The curves shown in Figure 11, which show fair agreement with the experimentally determined points, were calculated in this manner.

The values of c_i and τ_i used in the calculations were obtained from an analysis of the ϕ vs t curves of Figure 8. Two components were found to give an adequate fit - the values follow.

Release Data from Runs on Uncoated-Particle Compacts

Temp. (°C)	c_i Fraction Released		Characteristic Diffusion Time (hr), τ_i/π^2	
	Fast	Slow	Fast	Slow
2000	0.304	0.696	1.15	16
1800	0.133	0.867	9.1	47.1
1600	0.243	0.757	8.8	2400
1400	0.055	0.954	7.1	5830

ACKNOWLEDGEMENTS

Thanks are due to Professor Leo Brewer, University of California, Berkeley, who brought the many advantages of the King furnace to our attention, and to Dr. J. S. Kane, Lawrence Radiation Laboratory, Livermore, who showed us their King furnace and discussed the characteristics and design problem of this type of apparatus. Credit is due to Mr.W. J. Dougherty for his contributions to the design and construction of the several King furnaces and their ancillary equipment.

REFERENCES

1. HTGR Quarterly Progress Reports, 40-MW(e) Prototype High-Temperature Gas-Cooled Reactor Research and Development Program: Reports GA-1378, March 1960; GA-1640, June 1960; GA-1774, September 1960; GA-1982, December 1960; and GA-2204, March 1961, General Atomic Division of General Dynamics.

2. A. S. King, An Electric Furnace for Spectroscopic Investigations with Results for the Spectra of Titanium and Vanadium, Astrophysical Journal, 28: 335 (1908).

3. P. Fortescue, D. Nicoll, C. Rickard, and D. Rose, HTGR-Underlying Principles and Design, Nucleonics, 18: 86 (1960).

4. W. V. Goeddel, The Development and Evaluation of Graphite-Matrix Fuel Compacts for the HTGR, Report GA-2289, General Atomic Division of General Dynamics, August 1961.

5. A. C. Wahl, Nuclear Charge Distribution in Fission; Cumulative Yields of Short-lived Krypton and Xenon Isotopes from Thermal-Neutron Fission of U^{235}, J. Inorg. Nucl. Chem., 6,: 263 (1958).

6. W. B. Lewis, The Return of Escaped Fission Product Gases to UO_2, Canadian Report DM-58, January 1961.

7. A. H. Booth and G. T. Rymer, Determinations of the Diffusion Constant of Fission Xenon in UO_2 Crystals and Sinter·Compacts, Canadian Report CRDC-720, August 1958.

8. A. H. Booth, A Suggested Method for Calculating the Diffusion of Radioactive Rare Gas Fission Products from UO_2 Fuel Elements, Canadian Report DCI-27, September 1957.

STUDIES OF FISSION GAS RELEASE FROM IN-PILE TESTS:

I. RECOIL LOSS FROM CERAMIC FUEL ELEMENTS

By E. A. Aitken, P. K. Conn, E. S. Collins, and R. E. Honnell

Nuclear Materials and Propulsion Operation
General Electric Company, Evandale, Ohio

INTRODUCTION

Fission fragments and products can escape from the fueled portion of a fuel element via several different modes:

1. Any fission fragments ejected from a point within one fission fragment range of an exterior unclad surface can escape directly as a consequence of the fission process. This mode is called recoil loss.

2. Fission products can diffuse from any point in the interior of the fuel element to its surface.

3. Fission products are contained within a substrate or host material, but corrosion or erosion of the host material results in loss of fission products.

Release by a recoil mechanism would be expected to be time and temperature independent. Release by a diffusion mechanism would be expected to be both temperature and time dependent with a time dependency related to the half-life of the fission product. Release due to corrosion or erosion would also be time and temperature dependent but would be expected to have a different time and temperature relationship than that due to diffusion.

As a part of a high temperature fuel element development program, methods were developed for in situ measurement of fission product release[1]; experiments were performed under a variety of conditions and data were obtained which verified all three release mechanisms. This paper on recoil release is intended as the first of a series in which in situ fission product data covering the three aforementioned modes of release will be presented.

EXPERIMENTAL PROCEDURES

The ceramic fueled body selected for this study was a homogeneous dispersion of chemically stabilized UO_2 in BeO. The UO_2 was chemically

stabilized to prevent the volume increase on oxidation to U_3O_8 and also to drastically reduce high temperature fuel loss; the body contained less than 30 v/o UO_2. The as-fabricated bodies were dense flat plates (> 98% of theoretical density) 40 mils thick, and dense tubes (> 98% of theoretical density), relatively thin walled and less than one-half inch outside diameter. A fueled body of BeO-UO_2-MgO, in which the fuel was not chemically stabilized, also was tested. A small amount of the MgO was added as a sintering aid.

Recoil release studies were made, using a catcher foil technique, on the flat plate specimens. The specimens were wrapped tightly in 10 mil thick Al foil and irradiated in the Low Intensity Test Reactor (LITR) at temperatures of ~ 80°C. The nuclear heat generated was removed by passing cooling air over the wrapped specimen. The catcher foils and the accompanying fission dosimeter foils were analyzed radiochemically for several fission products by Nuclear Science and Engineering Corporation, Pittsburgh, Pennsylvania.

The tubular specimens were used in two types of tests to study the fission product release at elevated temperatures during irradiation at temperature. In one type of test the tubular specimens were stacked into hexagonal-shaped bundles for the in-pile tests as shown in Figure 1. Six fueled tubes were stacked in a hexagonal configuration and the seventh tube was placed in the center of the hexagon. The test temperature was measured with Pt; Pt-10% Rh thermocouples located in the interstices around the middle tube and also on the outside of the bundle. The tubes were assembled into the test rig in such a manner that most of the cooling air passed through the bores. The tubes were tested under self-heat generating conditions in dry air of -40°F dew point. The designated maximum temperature conditions were established and maintained by counterbalancing the nuclear heat with a flow of cooling air through the bore of the tubes. Since the nuclear heat was generated almost uniformly along the tube, cooling air passing through the bore set up a longitudinal temperature differential of 270°-450°C as shown in Figure 2. For a maximum test temperature of 1370°C, approximately one-third of the total tube surface was at that temperature. As the maximum temperature decreased, the amount of tube surface at that temperature increased. All test temperatures quoted are the maximum indicated fuel tube temperature; the precision of the temperature readings was ± 15°C.

In order to minimize the longitudinal temperature variation a second type of test was performed on a single tube using electrical heaters surrounding the tube to supplement the nuclear heat. Three tests were conducted at maximum temperatures of 430, 470, and 1400°C and much improved longitudinal temperature profiles, as shown in Figure 2 for the 430 and 1400°C tests, were obtained.

The fission product release from the tubes was monitored with chilled charcoal traps which sampled about 1% of the total effluent. During normal test operation traps were taken twice a day, and the traps usually were in use for six hours. The traps were determined to have retention efficiencies for I^{131}, Kr^{89}, and Xe^{140} of over 99%[1]. The traps were subsequently leached chemically and the leach solution analyzed for I^{131}, I^{133}, Sr^{89} and Ba^{140}. After each test, the exhaust gas ducting also was removed, leached chemically for deposited fission products, and the leach solution analyzed. The chemical procedures used were developed by Oak Ridge National Laboratory personnel; removal efficiencies of 95% or better were determined for these chemical procedures[1].

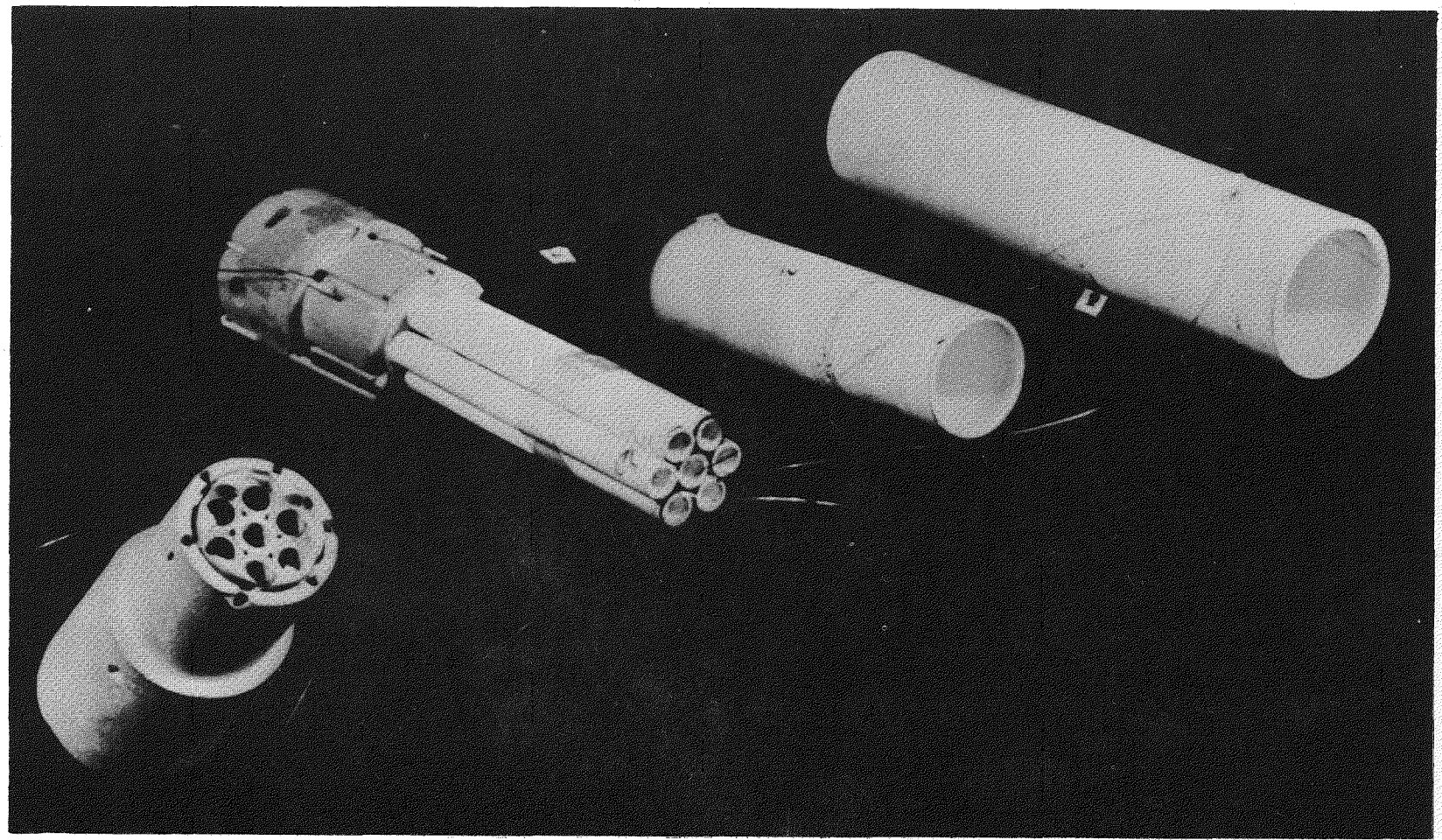

FIGURE 1

IN-PILE TEST CAPSULE ASSEMBLY

FIGURE 2

TEMPERATURE PROFILE OF LITR TEST SPECIMENS

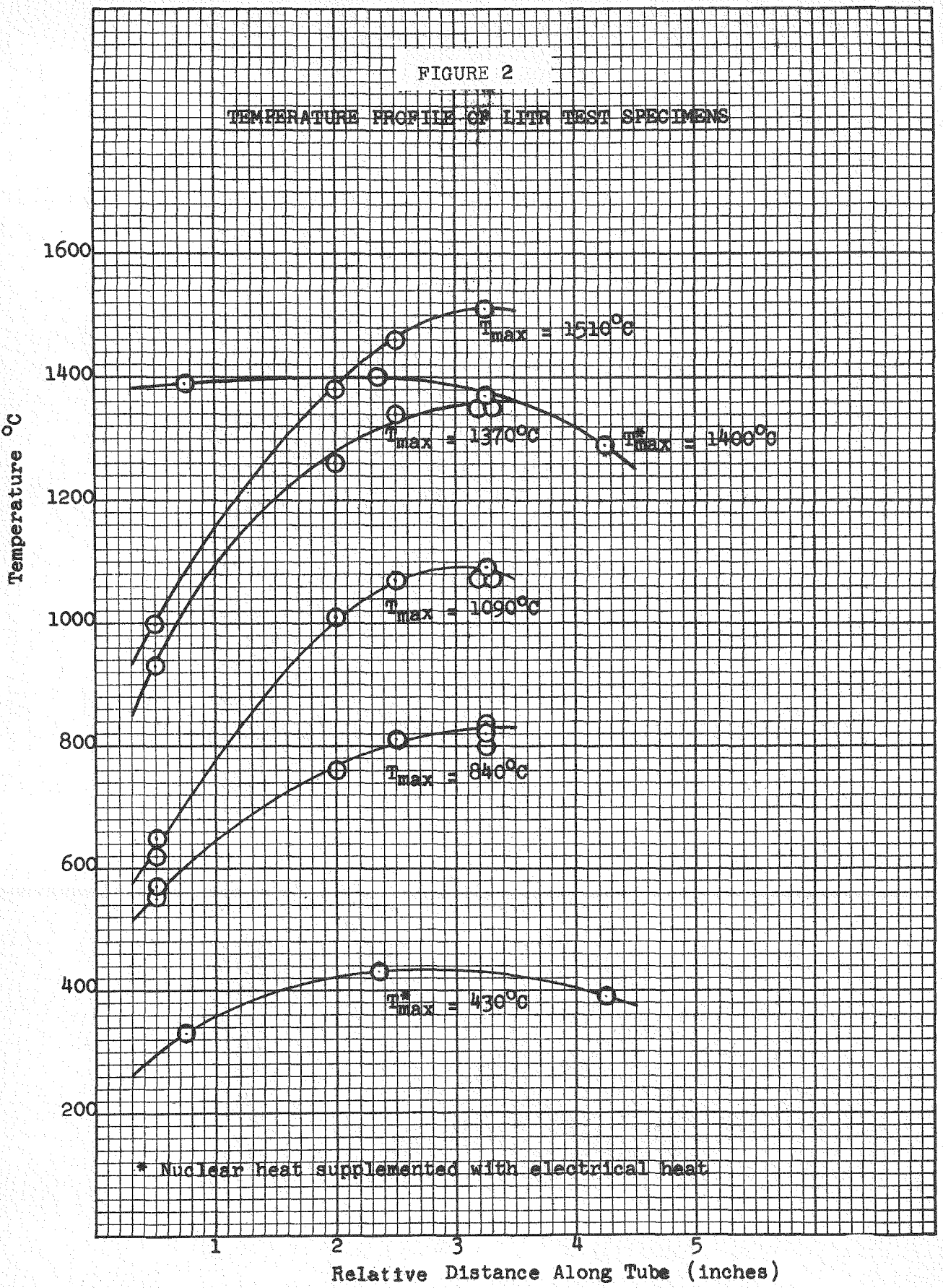

The radiochemical data from the traps were converted to a fractional release defined as the ratio of the average appearance rate on the trap to the production rate in the specimens. The ratio was corrected to total flow and converted to percent. As the traps were used for several hours, the activity found on the trap was corrected for decay during the trapping interval in order to calculate the average appearance rate. To get the total fractional release for I^{131}, i. e., the ratio of the release rate to the production rate, the trap data were corrected for fission product deposition which occurred between the test specimens and the traps. Past experience has shown that the fraction of isotope depositing did not change drastically whether short or long time tests were run. The deposition fraction was also found to not vary drastically with magnitude of the release. Consequently, it was assumed that deposition was a constant fraction of the total release at all times, thereby preserving any rate effects shown by successive traps. A correction factor, normalized to the total deposition found experimentally, was calculated for the trap data based on the fact that the deposition underwent simultaneous accumulation and decay during the test. Both the trap calculation and the deposition correction calculation were programmed for the IBM 704 and 7090 computers to expedite data handling. Correction factors for Sr^{89} and Ba^{140} deposition were not computed as they did not exceed respectively 10 and 25% of the trap values.

DISCUSSION OF DATA

The recoil release data obtained from the flat plate specimens are shown in Table I. From a solid angle type calculation, it can be shown that the recoil fraction from one side of a thin slab is, $F_r = 0.25\ R_r/W$ where W = slab thickness and R_r = the recoil range. Using a range of 10μ in BeO, the recoil release from both sides of a slab equals 0.5% in excellent agreement with the experimental measurements.

Typical data from the tube tests are shown in Figures 3, 4, 5, and 6 for maximum indicated test temperatures of 820, 1090, 1370, and 1400°C, respectively, as a function of time at temperature. The data shown in the figures are the trap measured fission product release for I^{131}, Ba^{140}, and Sr^{89}, and the deposition corrected trap release for I^{131}. Reactor shutdowns which occurred during test operation are shown in the figures also. The first three figures contain data obtained from three of the seven tube tests; the last figure contains data from a single tube test run with a near isothermal longitudinal temperature profile. As can be seen from the figures, the release for I^{131} was 0.02-0.03%, for Kr^{89} (measured as Sr^{89}) 0.02-0.05%, and for Xe^{140} (measured as Ba^{140}) 0.01-0.02%. These values for barium and strontium include the deposition found experimentally. The wider range in the krypton data is believed to be caused by leakage of air on the backsides of the tubes in some tests. The figures indicate that the release is independent of time and temperature indicating that release is due to recoil.

A Monte Carlo type recoil calculation for small bore tubes was programmed for the IBM 704 computer[2]. The program was based on the assumptions that re-entry into the opposite wall occurred for those fission fragments which did not expend their kinetic energy in egressing from the matrix and traversing the cooling air column, and that the fuel was distributed homogeneously throughout the body. A value of 0.02-0.04% was obtained from the computer program for the recoil release from tubes comparable in dimensions to those used in the experiments, and under the same conditions of temperature and pressure. The

TABLE I

RECOIL RELEASE FROM THIN SLABS

Isotope	Percent Escaped[a]	Recoil Range[b] (mg/cm^2)
I^{131}	0.57	3.3
Ce^{137}	0.54	3.1
Te^{129}	0.50	2.9
Y^{91}	0.75	4.4

[a] Escape measured from both sides.

[b] Maximum recoil range of 10μ was assumed.

FIGURE 3

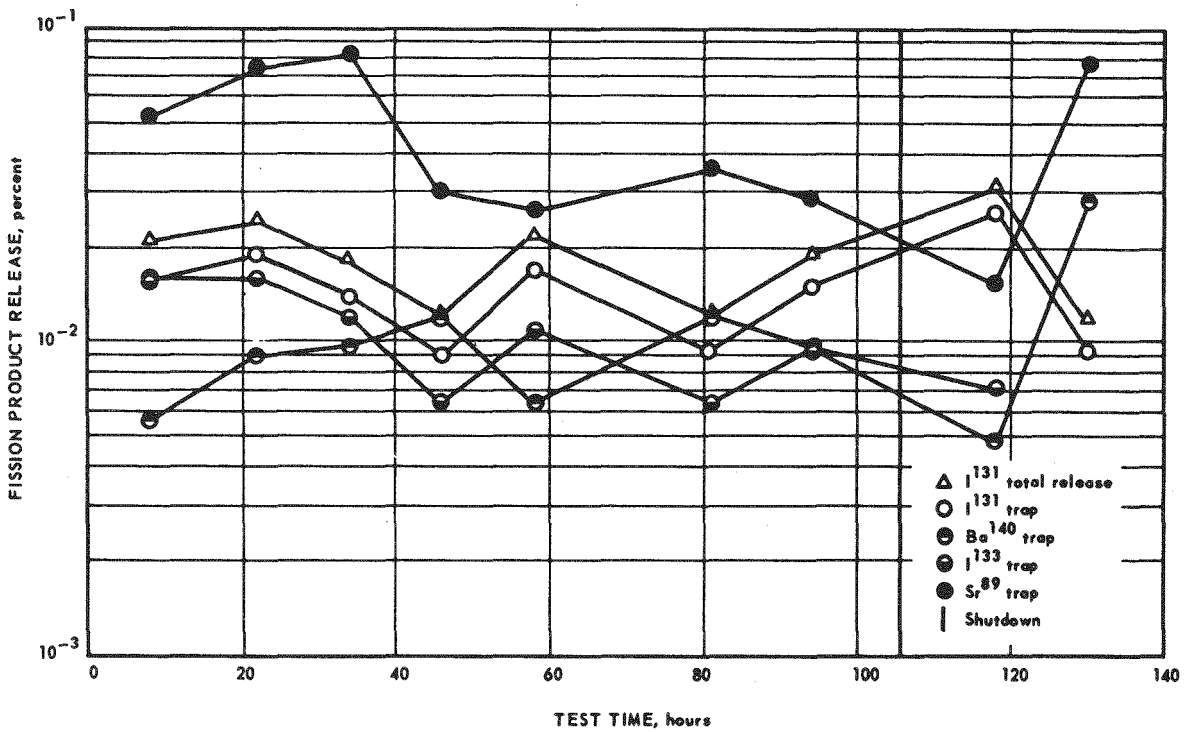

FISSION PRODUCT RELEASE FROM BeO TUBES
CONTAINING STABILIZED UO_2 at 820°C

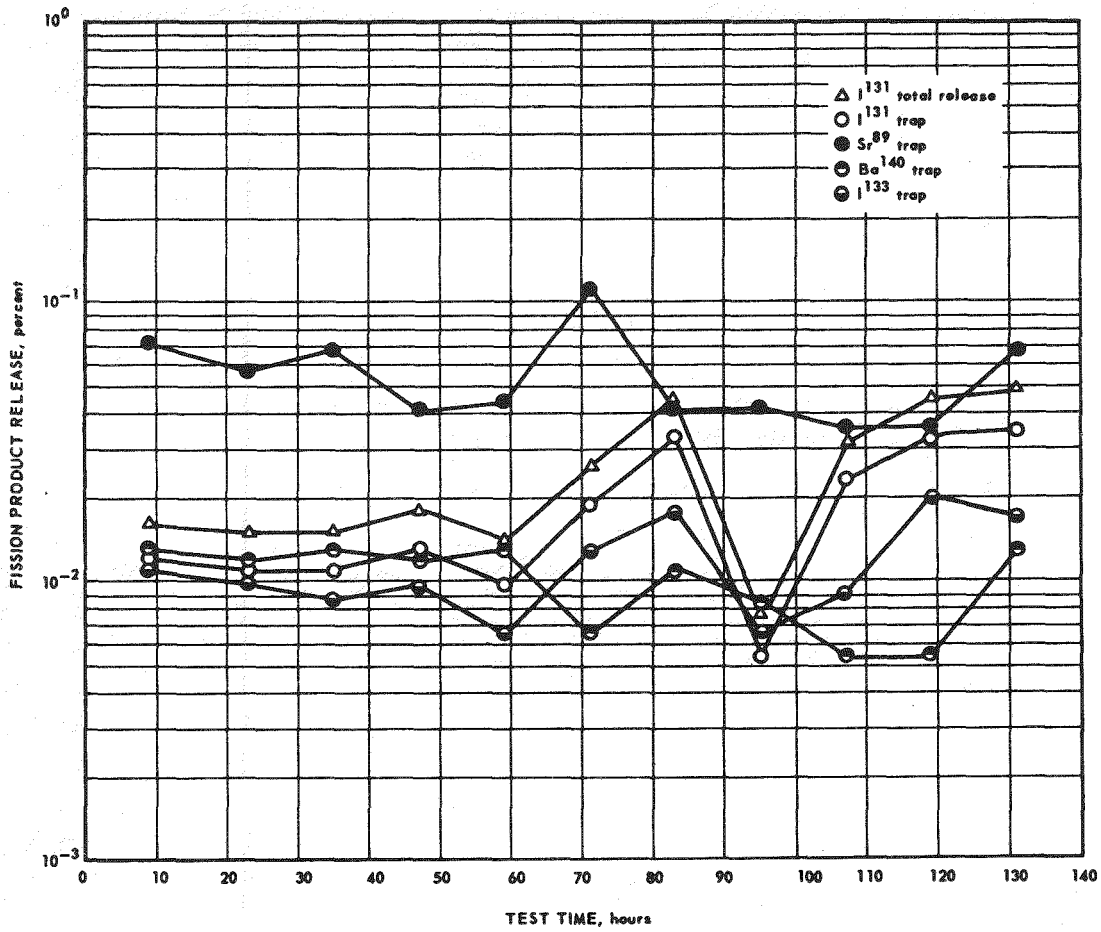

FIGURE 4

FISSION PRODUCT RELEASE FROM BeO TUBES
CONTAINING STABILIZED UO_2 AT 1090°C

FIGURE 5

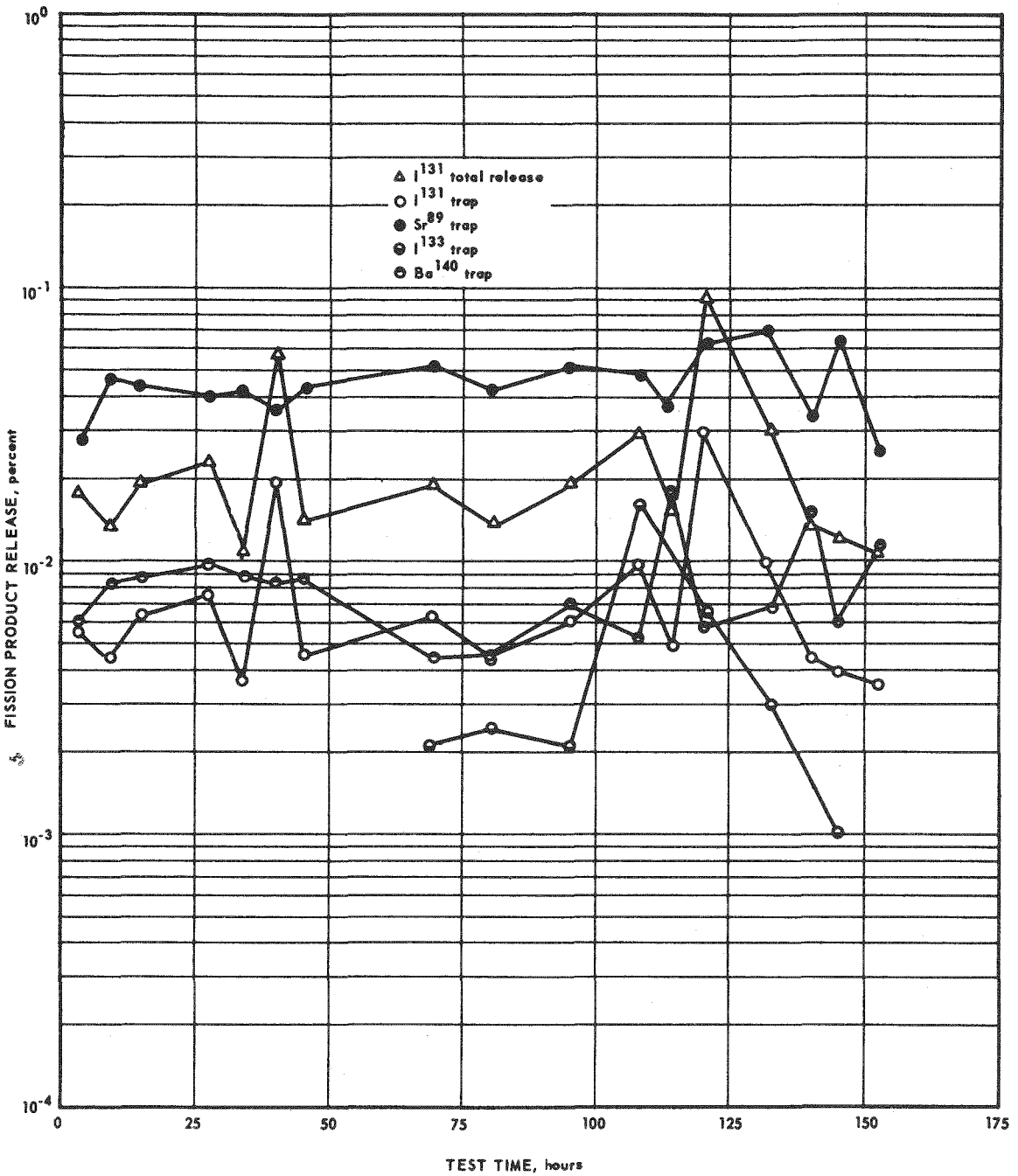

FISSION PRODUCT RELEASE FROM BeO TUBES CONTAINING STABILIZED UO_2 AT 1370°C

FIGURE 6

FISSION PRODUCT RELEASE FROM BeO TUBES CONTAINING STABILIZED UO_2 AT 1400°C

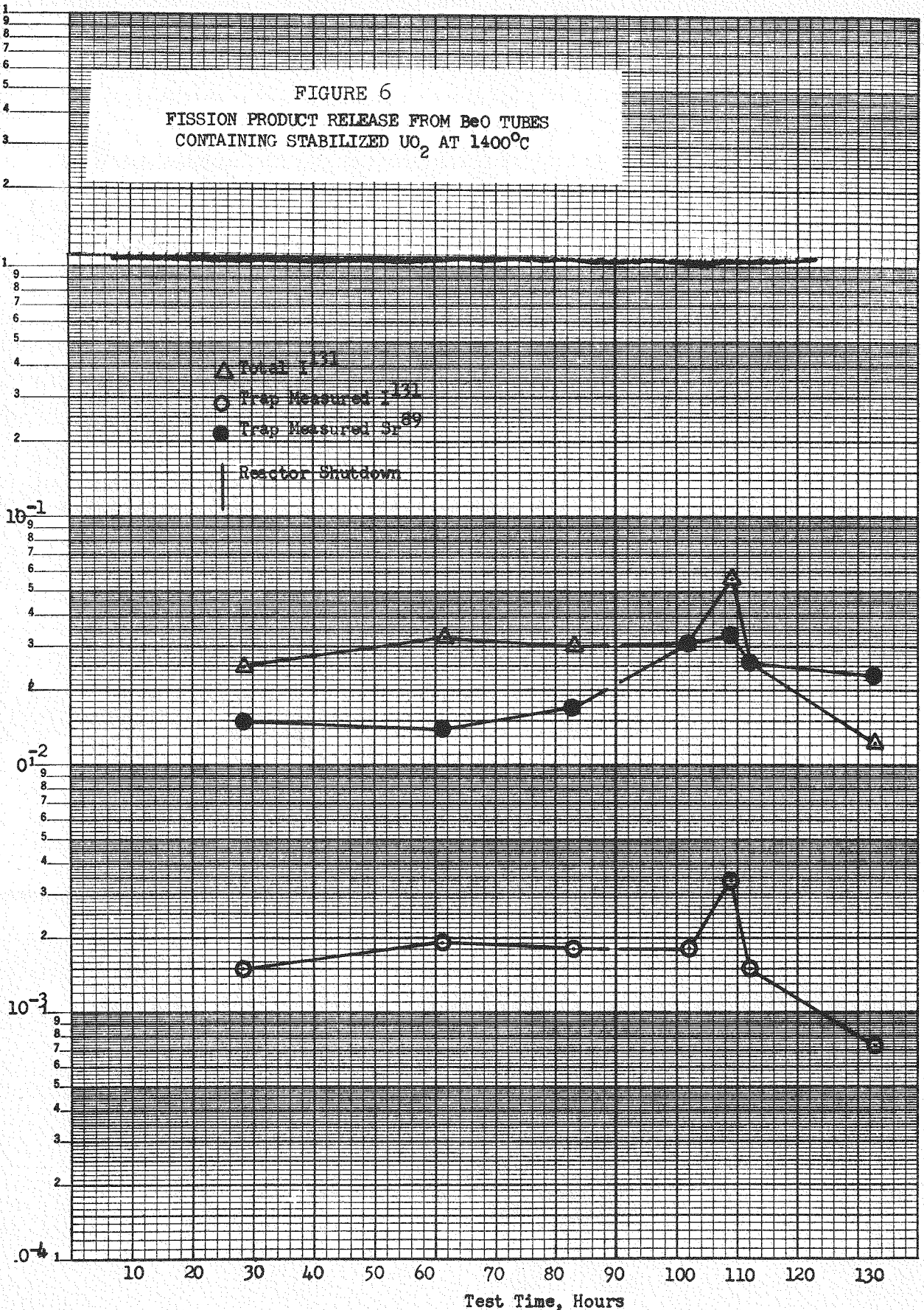

experimental data were in excellent agreement with the calculated results indicating that the dominant release mechanism was direct recoil.

Because of the data scatter obtained from the in-pile measurements, rate changes expected for diffusional behavior could be masked. This is certainly true for diffusion processes with small diffusion coefficients ($< 10^{-14}$ cm^2/sec) in which the diffusion current egressing from the specimen is a factor of 5-10 less than the recoil current. However, I^{131} behavior typical of diffusion has been observed from in-pile measurements as shown by the data in Figure 7. The data shown in the figure were obtained from a reactor test on seven tubes tested at a maximum indicated temperature of 1090°C in dry air for 270 hours. The tubes did not contain fuel which had been chemically stabilized; the composition was BeO-UO_2-MgO and the bodies were in excess of 98% theoretical density. In contrast to the previous figures, the data in Figure 7 clearly show a time dependency for I^{131} release higher than the recoil contribution. Kr^{89} and Xe^{140} release are also higher than the recoil contribution but are time-independent after the first twenty hours.

Fifteen tests were run on the chemically stabilized BeO-UO_2 dispersed oxide type body at maximum temperatures ranging from 450 to 1650°C and for test times from seven to 236 hours. An average I^{131} release rate was obtained for the deposition corrected release data from each reactor test and are presented as a function of maximum test temperature in Figure 8. The time each test ran at temperature is shown beside the average release for the test. The correction for iodine deposition was estimated for those tests in which it was not obtained experimentally. The data from all of these tests appeared to be time independent. The average I^{131} release rates obtained from the tests at 1400°C and less were 0.015-0.03% and were in excellent agreement except for one test performed very early in the test series. The higher releases measured for I^{131} at temperatures greater than 1400°C as shown in the figure is not understood. The figure indicates that recoil is the dominant release mechanism up to ~ 1400°C and test times to 236 hours for dispersed oxide type fuel elements containing chemically stabilized UO_2. Apparently the addition of the stabilizing additive to the fuel phase greatly improves the fission product retention over that of the BeO-UO_2 system. A test on the BeO-UO_2 composition without the stabilizing additive showed diffusion of fission products, higher than the recoil contribution, at a temperature as low as 1090°C. For tubes containing the additive, the diffusion current did not exceed the recoil current until temperatures exceeded 1400°C.

CONCLUSIONS

1. The measured recoil release fraction for several fission products from a dense thin slab of BeO containing chemically stabilized UO_2 was in excellent agreement with the recoil release predicted from a theoretical calculation made for the same geometry.

2. The measured fission product release fraction from dense tubes of BeO containing chemically stabilized UO_2 indicated that recoil was the dominant release mechanism; the data appeared to be independent of time to 236 hours. The measured release fraction also was in excellent agreement with a recoil release fraction predicted from theoretical calculations made for the same sample geometry and test

FIGURE 7

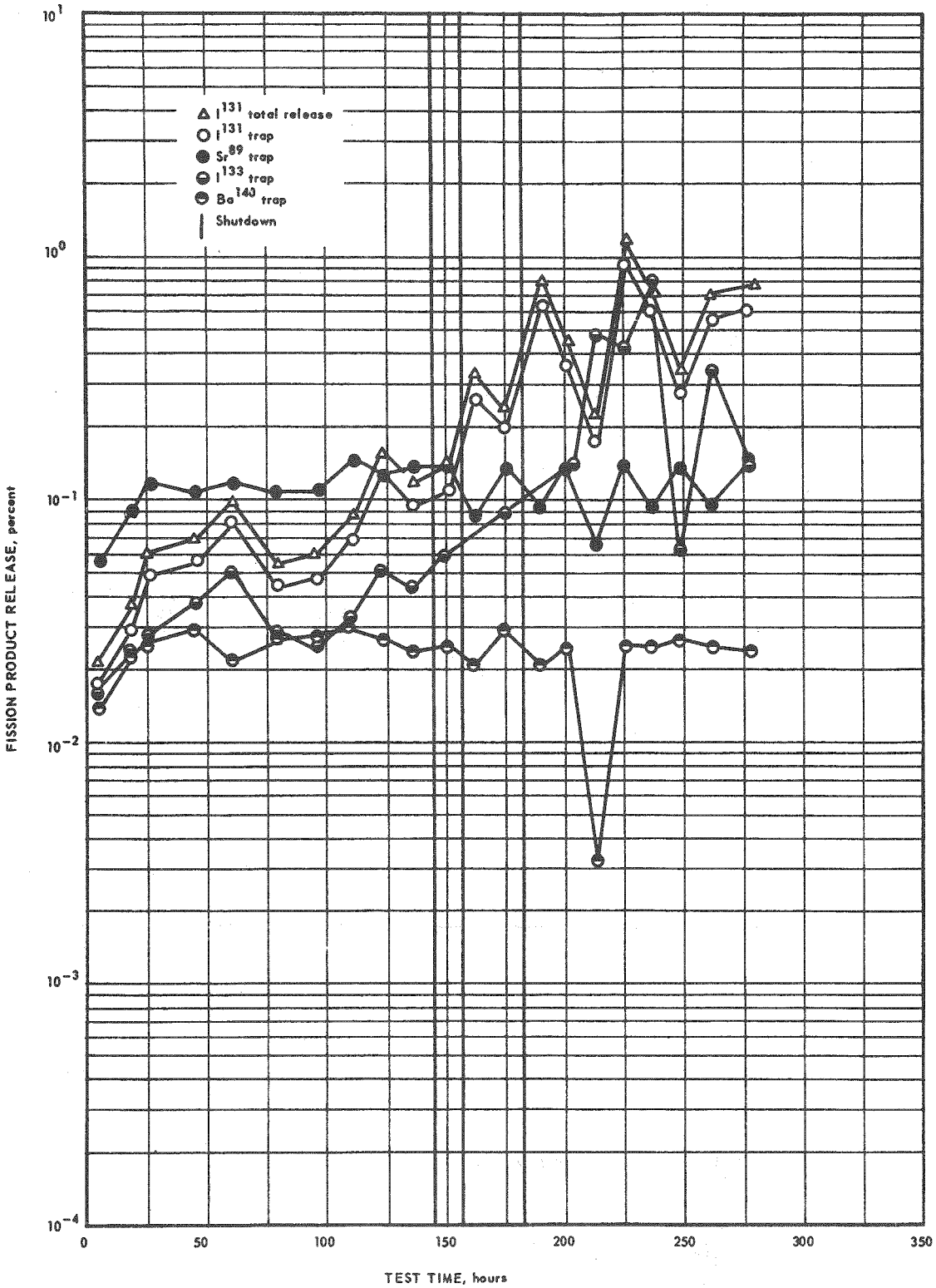

FISSION PRODUCT RELEASE FROM BeO TUBES CONTAINING UNSTABILIZED UO_2 AT 1090°C

FIGURE 8

I^{131} RELEASE FROM BeO TUBES CONTAINING STABILIZED UO_2 VERSUS TEMPERATURE

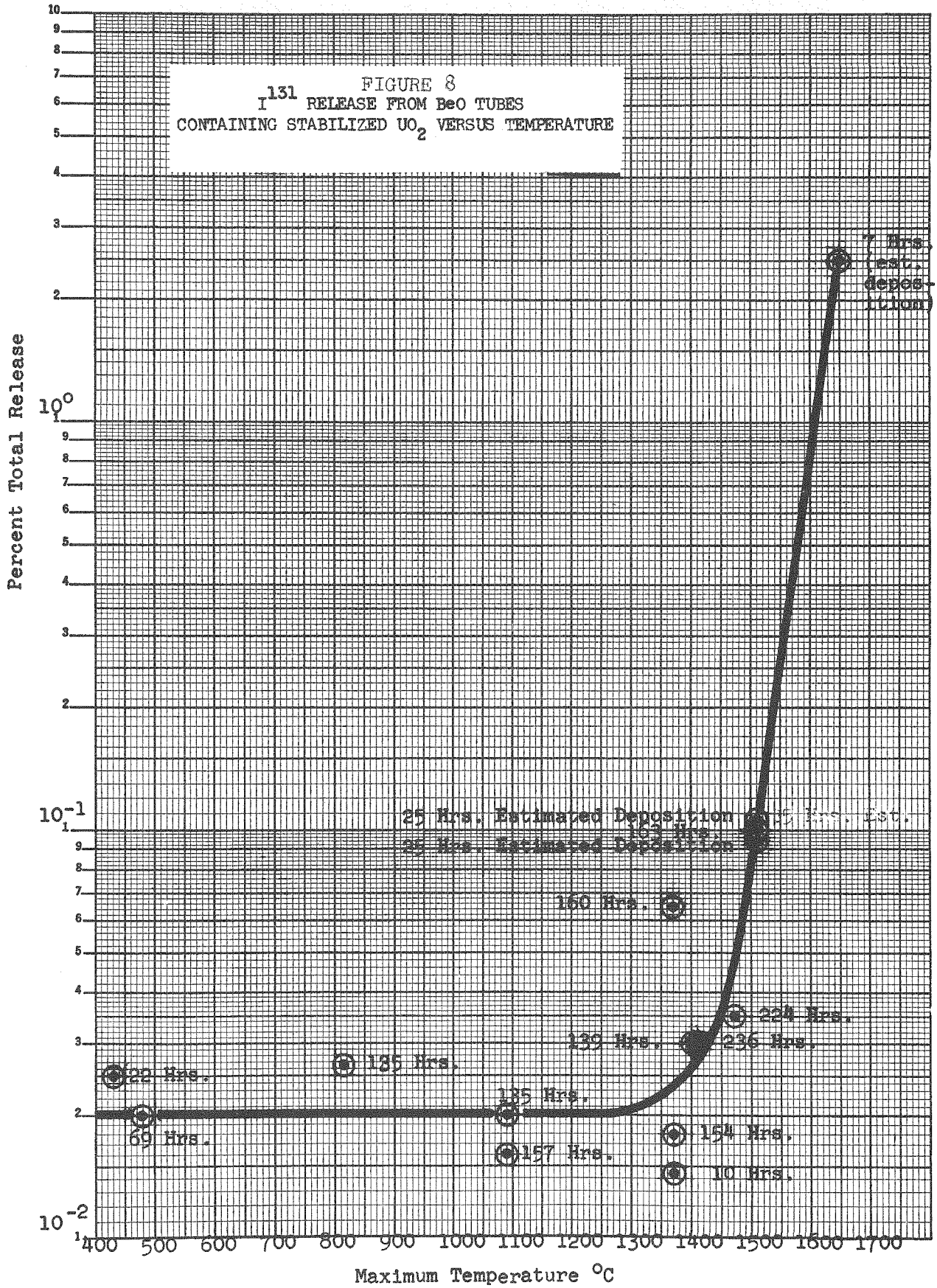

conditions. Above 1400°C the fractional release increased with increasing temperature.

3. Use of a stabilizing additive with UO_2 in the fuel phase greatly improved the fission product retention of the BeO dispersed oxide type samples over that of the BeO-UO_2 samples without the stabilizing additive.

REFERENCES

1. P. K. Conn, E. S. Collins, J. B. Trice, General Electric Company, Isotope Deposition Hazards in Gas Cycle Reactors, American Nuclear Society Meeting, Gatlinburg, Tennessee, June 17, 1959.

2. J. R. Beeler and J. M. McGurn, Fission Fragment Absorption in the Coolant Channels of Fueled Gas-Cooled Samples, Trans. of A.N.S., Vol. 4, No. 1, pp. 67-68, June 1961.

RELEASE OF FISSION PRODUCTS ON THE IN-PILE MELTING OF REACTOR FUELS

By R. P. Shields, C. E. Miller, Jr., R. A. Lorenz, and W. E. Browning, Jr.

Oak Ridge National Laboratory[a], Oak Ridge, Tennessee

Reactor safety studies being sponsored by the Atomic Energy Commission include determination of the release of fission products when reactor fuels melt. The objective of the In-Pile Meltdown Program is to determine the fission product release characteristics of various fuels under conditions which simulate as closely as possible those which may exist at the time of a reactor incident. Such information is essential to a realistic evaluation of the probable hazards of operating a power reactor. This becomes increasingly important with the increased use of large power reactors. The lack of such information has made it necessary in some cases to assume 100% release of fission products during a reactor fuel meltdown incident. This assumption has made power reactor site selection difficult and imposed severe and costly specifications upon reactor containment. Therefore, reliable fission product release information is needed in order to deal effectively with these major problems of operating nuclear power reactors.

Fission product release studies have been carried out by G. W. Parker and co-workers by melting irradiated fuel specimens outside the reactor (See Paper No. 13). This paper will deal with the release of fission products when fuel materials are melted in a reactor by fission heat. In a reactor, power is applied to all parts of a fuel, and consequently, the center temperature is always higher than the outside. A loss of coolant or a power surge can cause the fuel temperature to rise quickly and the material in the center to become molten before the outside. This difference between out-of-pile and in-pile melting may very well affect the mechanisms by which fission products separate themselves from the mass and thus to be carried away from the site of the melting fuel and possibly away from the immediate environment of the reactor.

Several parameters can be listed which may influence the mechanism and extent of fission product release. The size of the specimen may have some bearing on release. Temperature history before melting, i. e., how hot the fuel was during the formation of the fission products, can affect their movement and

---

[a]Operated for the U. S. Atomic Energy Commission by Union Carbide Corporation.

final release at time of melting. Once the fuel is melted, volatile products will continue to be released as long as the mass remains molten and chemical reactions will also be taking place which may convert some of the non-volatile fission products to volatile compounds which can escape. Therefore, the time the fuel is molten is an important parameter.

In the study of the release of fission products, a sweep gas is used to remove the fission products from the site of melting. The composition of this gas may be important. For example, other investigators have shown that oxygen will oxidize UO_2 to change its structure and thus enhance the release of fission products.

The extent to which the fuel in a reactor has undergone fissioning can affect the release by what might be termed a flushing action by the greater quantities of volatile fission products and also by the radiation damage to the crystal structure which may allow a more rapid rate of diffusion and coalescing of gases. Burnup may, therefore, prove to be an important parameter for the in-pile studies, as indicated by previous out-of-pile studies.

The plan for studying the effects of these various parameters on fission product release calls for the production of fission products in the specimen and the subsequent melting of the specimen by fission heat to determine the fission product release. In the initial experiments, unirradiated specimens will be mounted in the experimental apparatus and lowered into the reactor to a point where the temperature of the stainless steel cladding does not exceed its melting point and allowed to remain there until a trace inventory of fission products is produced. After this, the specimen will be further lowered to a point where fission and gamma heat will be sufficient to melt the specimen. In later experiments, the desired degree of burnup will be provided by exposing specimens in a separate reactor facility prior to introducing them into in-pile meltdown apparatus.

A schematic diagram of the reactor facility which is located in the Oak Ridge Research Reactor is shown in Figure 1. As was mentioned before, the specimen position in the reactor can be remotely controlled. This is accomplished by means of the hydraulic cylinder which has a hollow piston shaft with a three-inch inside diameter. This allows the experimental unit to pass through into the entry tube. The entry tube receives a flow of cooling water by diverting some of the reactor water from the top of the pressure vessel. When the reactor furnace is withdrawn from the lattice the cooling water can be shut and simultaneously the water is diverted through a pipe beside the entry tube to a plunger valve at the bottom which prevents loss of reactor water during the insertion and removal of experiments. The ability to insert or remove experiments while the reactor continues to operate is a great advantage since the Oak Ridge Research Reactor operates on an eight-week cycle and since each experiment requires not more than five or six days in the reactor.

The reactor furnace is shown in more detail in the schematic drawing in Figure 2. This consists essentially of a stainless steel can containing ceramic insulators. In the center is shown the stainless steel clad UO_2 specimen with overall dimensions of about 1/4-inch diameter by one-inch high. This is fitted into a pedestal made of porous thoria which in turn is mounted on a porous zirconia block. A thoria cylinder surrounds the specimen and is closed by a thoria plug on top. The thoria plug and cylinder are surrounded by

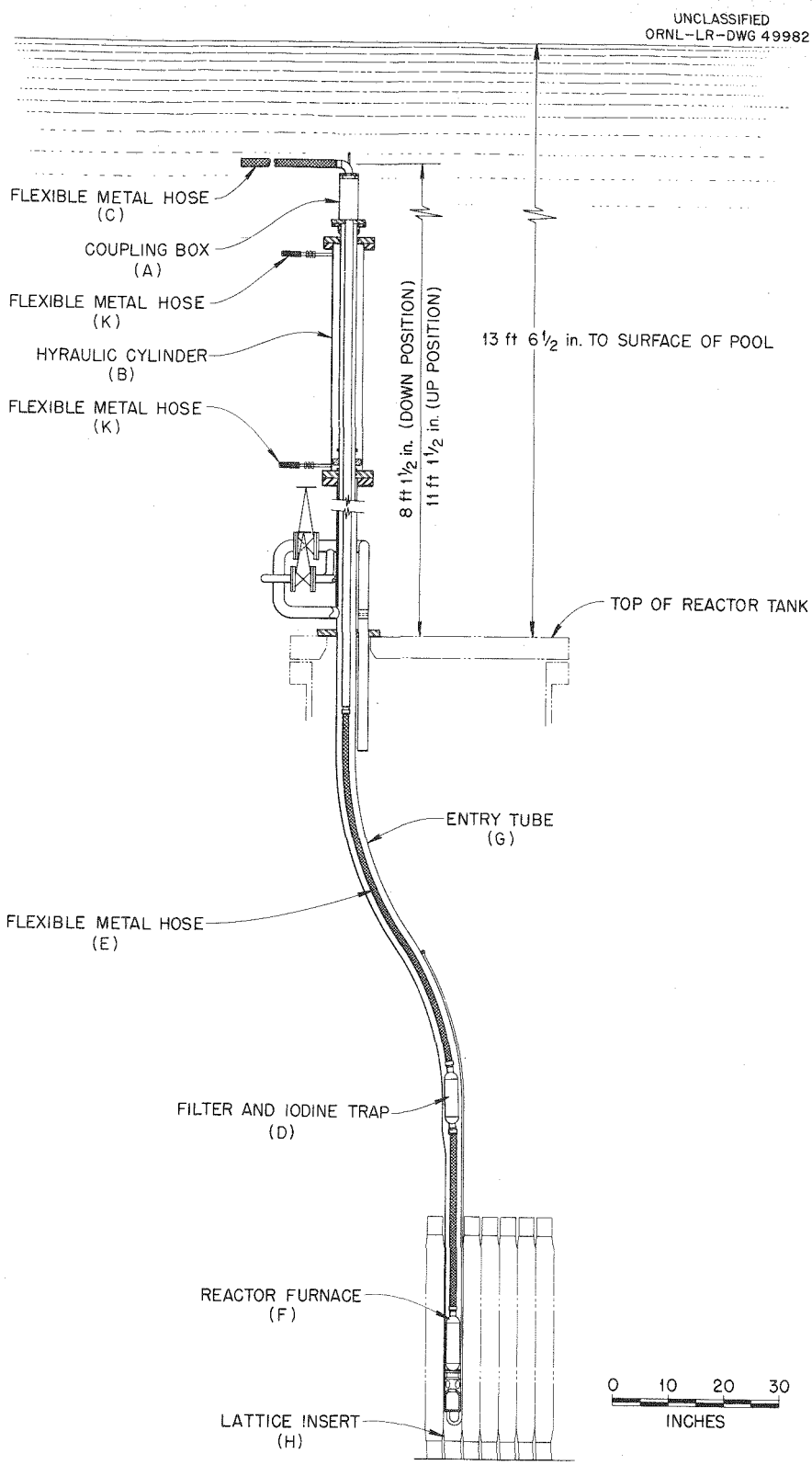

Figure 1. Fuel Meltdown Experiment Assembly in Reactor.

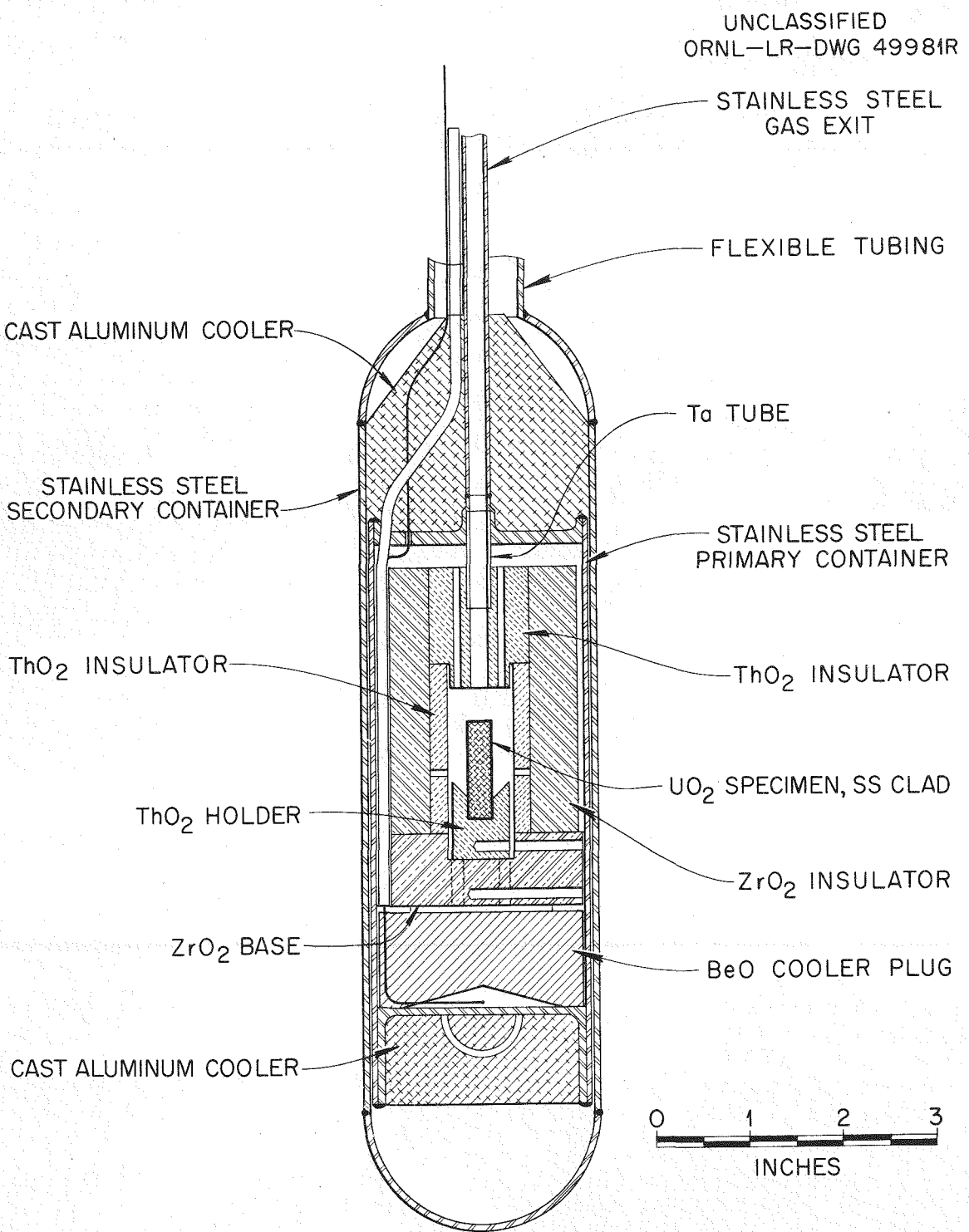

Figure 2. Reactor Furnace; for Fuel Element Meltdown Experiments.

a cylinder of zirconia which rests on the same base as the pedestal. The whole assembly is supported on a beryllia block which has good thermal conductivity to help divert heat to the side where heat transfer to the water is efficient. The aluminum blocks at the ends are to aid heat dissipation from the end caps. A photograph of the capsule mounting and ceramic insulators is shown in Figure 3. Helium enters the furnace through the tube on the side of the primary container and sweeps over the specimen and then through the exit line which leads to a series of graded filters to remove particulate matter and thence to a charcoal trap at reactor water temperature (119°F). Only the rare gases are left in the sweep gas after passing through the charcoal trap and these are held in a liquid nitrogen-cooled charcoal trap outside of the reactor pool.

The first and only experiment completed to date had a 3% enriched UO_2 specimen. The reactor furnace shown in Figure 2 was lowered into the reactor until the stainless steel cladding reached about 1170°C. It was left in this position long enough to build up trace quantities of fission products. The next step was to lower the furnace about half the remaining distance to the center line of the reactor and to allow temperature equilibrium to be established. At this point, the steel cladding on the UO_2 had melted and the thermocouples inside the thoria cylinder and had failed. This step was made to check the heat calculations on which the furnace design was based. The tungsten-tungsten-26% rhenium thermocouple outside the thoria registered 1190°C while the pedestal temperature was 1170°C and that of the primary walls was 100°C.

After the furnace reached the center line of the reactor the following temperatures existed at equilibrium; between thoria and zirconia 1900°C, pedestal 1900°C, center of zirconia 1425°C, and primary wall 175°C. After about 10 minutes at the center line the furnace was retracted to the halfway position and finally moved to the point of maximum retraction.

Post-irradiation examination of the experiment in the hot cells showed that all the ceramic parts were in place and in good shape except for a few cracks. The condition of the pellet of UO_2 is shown in Figure 4. The outside surface is covered with small black crystals. About 1/4 of the lower end of the specimen was broken from this piece and is shown in Figure 5. The hole in the UO_2 which is visible in this photo is also present in the large piece and extended for about 2/3 of the length of the piece. Note the globular steel and black material in the depression around the pellet. Figure 6 is an enlarged section of the crystal surface of the specimen. The pyramid shaped crystals have a spiral step arrangement shown on the surface of many of the crystals. This is said to be characteristic of crystals built up by vapor deposition of UO_2. Figure 7 is a metallographic section of the UO_2 which was broken from the specimen. The rim is about 1.7 to 1.8 millimeters thick and about 1/3 of this is outside the original boundary of the specimen. The inside curve represents part of the 1/8-inch diameter hole in the center.

The above-mentioned examinations indicated that a large part of the UO_2 has undergone a change of state, either by being molten or by transfer as vapor. This would seem to favor release of a large fraction of the fission products. Analysis of the UO_2 has been performed, but data on fission products from sections of the apparatus such as the gas exit line, filter papers, and charcoal trap are not available at the present time; therefore, fractional release values cannot be computed now. It appears, however, that most of the rare gases were

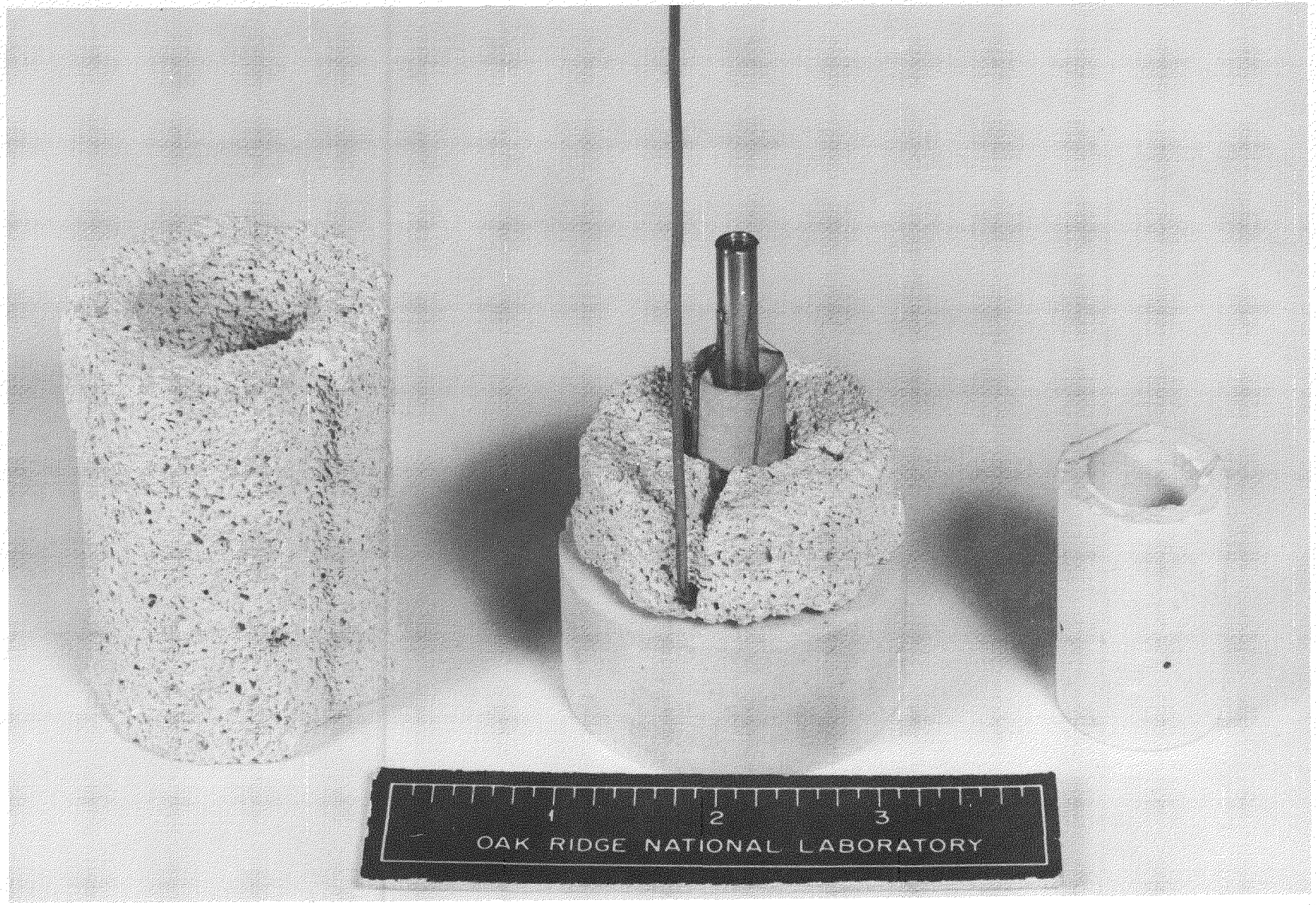

Reactor Furnace; for Fuel Element Meltdown Experiments.

Fig. 3

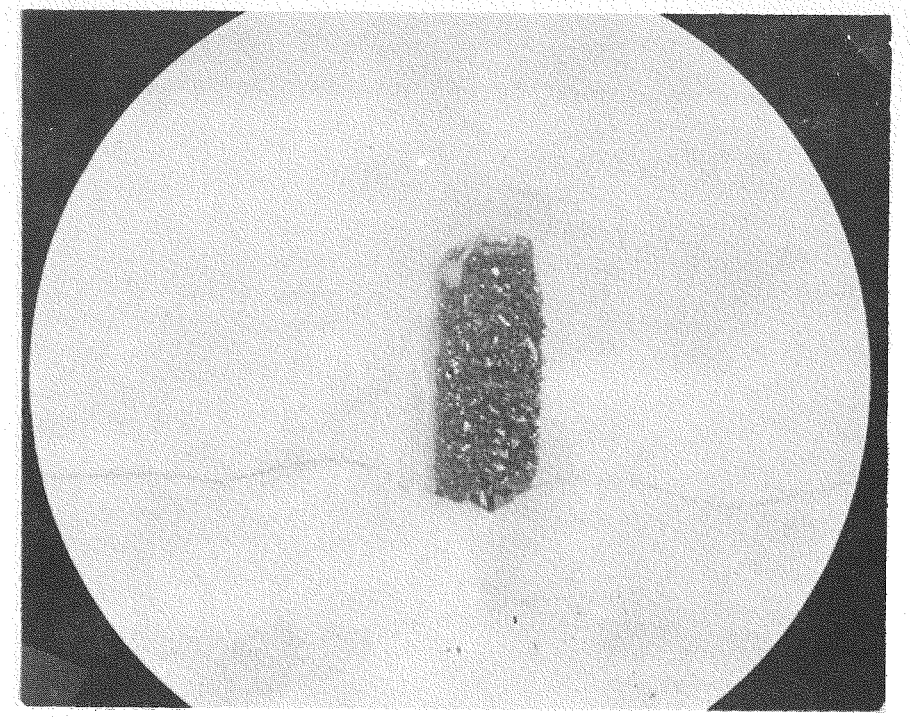

Fig. 4. Outside Surface of Irradiated UO_2 Pellet.

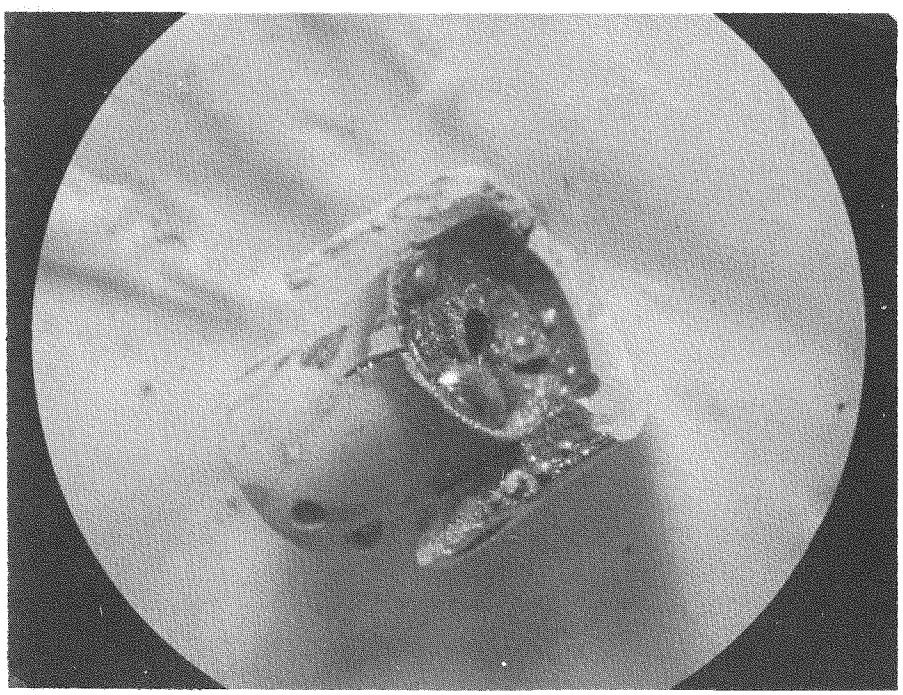

Fig. 5. Thoria Holder with Part of UO_2 Pellet.

Fig. 6. Enlarged Section of Crystal Surface of Specimen.

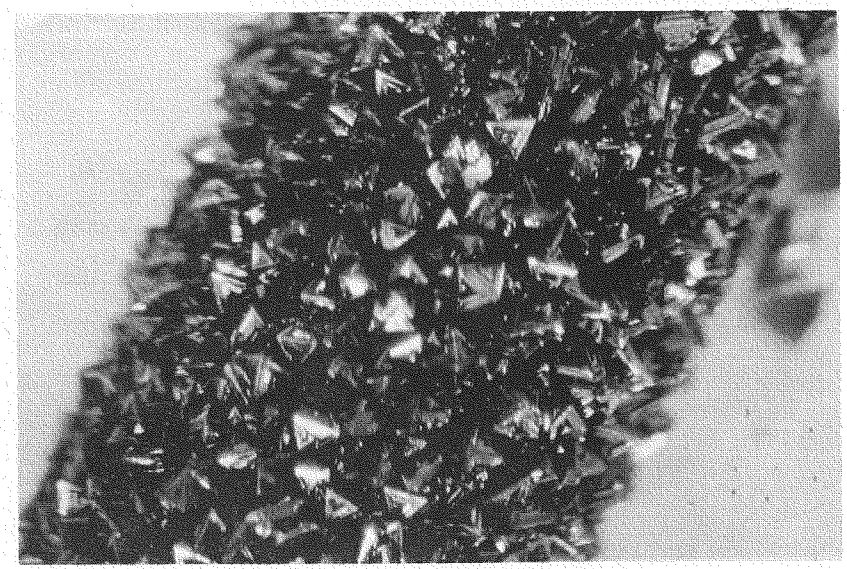

Fig. 7. Metallographic Section of UO_2 Specimen.

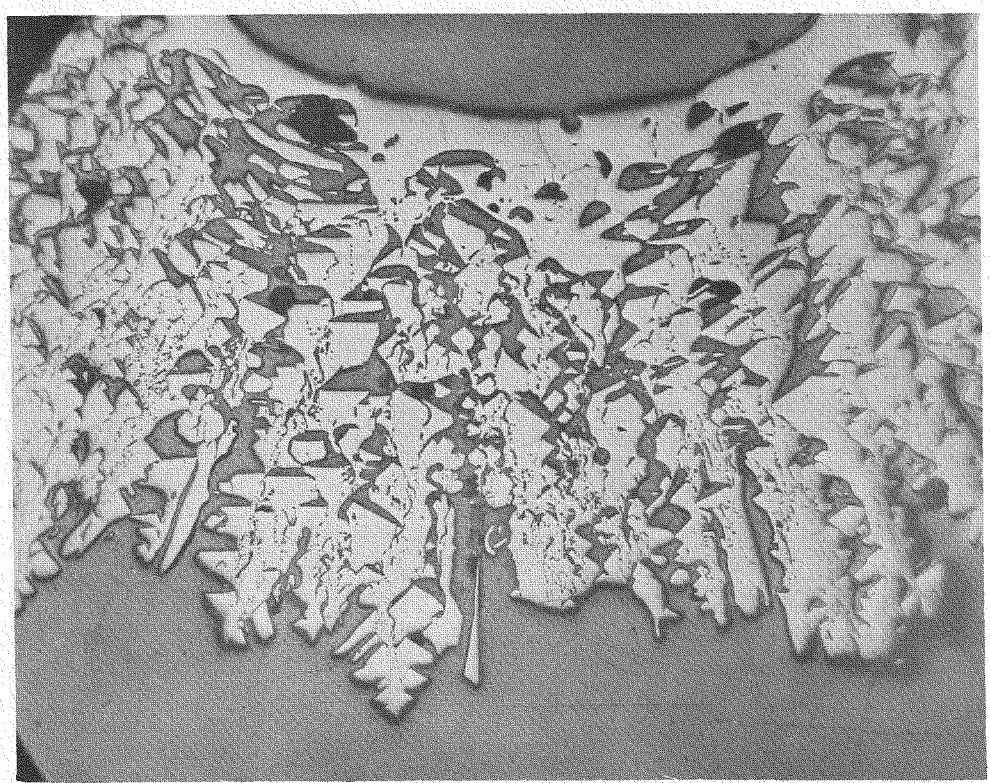

in the liquid nitrogen-cooled charcoal trap. Analysis of the UO_2 showed a large fraction of many of the isotopes still present. These generalizations are based on calculations of the relative amounts of isotopes produced which were, in turn, based on preliminary estimates of the neutron flux intensity.

This brief description of the first in-pile experiment indicates that the equipment as designed will be satisfactory for studying in an operating reactor some of the parameters influencing release of fission products when reactor fuels are melted. In the next experiment we will employ a 25% enriched specimen of the same dimensions as the one used in the first experiment. Following this, other trace level meltdown experiments will be performed and then a study of various parameters will be made with at least 1% burnup. Future experiments will also include other non-metallic fuel elements which are important in power reactors.

FISSION PRODUCT BEHAVIOR IN DIRECT-CONTACT CORE LIQUID-METAL-FUELED REACTORS[a]

By R. M. Bidwell

Los Alamos Scientific Laboratory, Los Alamos, New Mexico

ABSTRACT

Enough experimental evidence is at hand to predict the behavior of fission products in continuously extracted liquid-metal-fueled reactors. Particular attention is given to the "dynamic-core" concept, where fuel is circulated by a stream of sodium, which acts concurrently as heat transfer medium and extractant.

Fission products are classified as elements more soluble or more stable in sodium, elements soluble in plutonium, metals sparingly soluble in both, and rare gases. The behavior of each class in a reactor is predicted on the basis of well-established thermodynamic and phase data, and the evidence from out-of-pile and reactor observations on actual fuel alloys is shown to be consistent with this information.

The speeds of extraction of fission products from liquid plutonium alloys are estimated for different modes of operation and compared with direct experimental data. Fission product extraction is found to be very efficient and may even lead to a serious control problem due to the removal of delayed-neutron precursors.

The volume of each element building up in the fuel phase is estimated, and it is shown that whereas only about 40% of the atoms produced are extracted by the sodium, these correspond to 70% of the potential volume increase in the fuel, ignoring additional expansion due to the formation of rare-gas bubbles. The fission products remaining are nearly equal to the plutonium burned.

If an amount of plutonium equal to the initial inventory were burned up, the resulting poisoning would be about 6%, calculated at 100 kev average neutron energy, while the summed concentration of the slightly soluble Zr, Nb, and Mo might have reached 1%. Provided that plutonium is added to maintain criticality, it seems quite feasible, therefore, to operate a dynamic core reactor to "100% burnup," using such a dilute fuel as Pu-Co-Ce(7.5-25-67.5 at. %). The final concentration of plutonium would be 8 at. %, while smaller relative changes would occur with the other components. In comparison, the

change in the composition of the much larger sodium phase would be negligible, and purification of the sodium would be desirable for reasons of safety rather than of operation.

In summary, it is shown that a dynamic-core reactor can be operated as a continuous chemical system. Its economic feasibility is not limited by the usual considerations of poisoning, radiation damage, and burnup.

---

[a]The information in this paper has been submitted for publication in Nuclear Science and Engineering.

THE REMOVAL OF RADIOACTIVE KRYPTON AND XENON FROM A FLOWING HELIUM STREAM BY FIXED-BED ADSORPTION[a]

By R. D. Burnette, W. W. Graham III, and D. C. Morse

General Atomic Division of General Dynamics,
San Diego, California

INTRODUCTION

In the High-temperature Gas-Cooled Reactor (HTGR), appreciable release of volatile fission products from the fuel bodies may occur because of the high operating temperature of the fuel. Removal of radioactive fission products from the reactor's helium coolant is desirable in order to improve the operational and safety characteristics of the reactor system. Of the various fission products, the noble gases krypton and xenon are the most difficult to remove because they are chemically inert and highly volatile (See Table I for a list of the krypton and xenon isotopes produced by fission). This problem is not peculiar to high-temperature gas-cooled reactors, but is encountered in the off-gas stream from liquid-fueled reactors and in reactors with metal-clad fuel where cladding failure has occurred.

Fixed-bed adsorption is one of the few satisfactory methods for removing krypton and xenon from helium or air streams; the relative simplicity and reliability which can be obtained with an adsorption process are significant advantages when the process stream contains high levels of radioactivity. The removal of radioactive krypton and xenon impurities differs in several ways from the more conventional applications of adsorption:

1. The impurities are radioactive, and the radioactive decay process is in itself one method of removal.

2. The mass quantities of krypton and xenon produced in a nuclear reactor are small by conventional standards. If the krypton and xenon enter a flowing gas stream, their concentrations will be very low (generally in the parts per million to parts per billion range).

3. Very high removal efficiencies are often required because of stringent tolerances on radiation dose rates and on concentrations of radioactive materials in air. Allowable concentrations of the radioactive isotopes in the effluent from the adsorber may be as low as 10^{-6} of the inlet concentrations.

[a]Work performed under USAEC Contract AT(04-3)-314.

TABLE I

RADIOACTIVE Kr AND Xe FISSION PRODUCTS[a]

Isotope	Half-life	Total U^{235} Fission Yield (%)
Kr^{83m}	112 min	0.54
Kr^{85m}	4.4 hr	1.30
Kr^{85}	10.3 yr	0.29
Kr^{87}	78 min	2.49
Kr^{88}	2.8 hr	3.57
Kr^{89}	3.2 min	4.39
Xe^{131m}	12 days	0.023
Xe^{133m}	2.3 days	0.16
Xe^{133}	5.27 days	6.59
Xe^{135m}	15.3 min	1.83
Xe^{135}	9.13 hr	6.41
Xe^{137}	3.9 min	6.00
Xe^{138}	17 min	5.45

[a]Isotopes having half lives of less than 1 min are omitted.

4. The fact that the impurities are radioactive makes even very low concentrations readily detectable by radiation monitors.

5. If sufficient radioactivity is present in the adsorbate, appreciable radiation heating of the adsorbent may result.

In using an adsorption system for the removal of radioactive krypton and xenon, two alternative modes of operation can be considered. The first method is the conventional one, in which the process gas stream is passed through an adsorber bed until "breakthrough" occurs, i. e., until the concentration in the effluent from the adsorber has reached a specified level. The adsorbent is then either regenerated or removed. A liquid-nitrogen-cooled charcoal adsorber has been used in this manner to remove radioactive krypton from the dissolver off-gas stream at the Chemical Processing Plant, National Reactor Testing Station, Arco, Idaho.[1] Equilibrium data for the adsorption of krypton and xenon on charcoal and silica gel are reported by Burdick[2] for the temperature range from -20° to -183°C. General relationships describing the penetration of adsorbate through an adsorber have been developed by Hougen and Marshall[3], who used the "height of a mass-transfer unit" to define the rate of exchange between the gas stream and the adsorbent.

The alternative mode of operation is to use the adsorber as a "delay bed". In this case, the adsorber is run at saturation (i. e., breakthrough is allowed to occur), but the adsorber bed is sized to provide an adequate chromatographic delay of the radioactive krypton and xenon isotopes. In other words, krypton and xenon are delayed in passage through the adsorber by a continuous process of adsorption and desorption, and the radioactive isotopes are allowed to decay before they penetrate through the adsorber. A delay bed can operate continuously for very long periods of time, since there is no net accumulation of krypton or xenon in the bed once steady-state conditions have been obtained; the only materials which do accumulate in the bed are the stable nonvolatile daughter products of the radioactive krypton and xenon isotopes. The effectiveness of a delay bed in holding up radioactive krypton and xenon is independent of krypton or xenon concentration in the carrier gas as long as the concentration falls under the linear portion of the adsorption isotherm (the isotherm is a plot of the amount adsorbed versus gas-phase concentration). If the concentration becomes sufficiently high, or the temperature sufficiently low, the adsorption isotherm will become appreciably nonlinear and the effectiveness of the delay bed will start to decrease with increasing concentration. This loss of effectiveness occurs because the adsorbate occupies an appreciable fraction of the adsorbent surface, and thus interferes with further adsorption.

A water-cooled charcoal delay bed has been used to remove radioactive krypton and xenon from the off-gas stream of the Homogeneous Reactor Test at Oak Ridge National Laboratory.[4] A number of experiments on delay-bed performance have been conducted by W. E. Browning and his associates at Oak Ridge;[5,6] their work has been directed primarily at removal of krypton from air or oxygen streams by room-temperature activated charcoal. Adsorption of krypton and xenon on charcoal has also been measured at Harwell in Great Britain.[7,8]

The studies reported here were initiated in order to provide the necessary information for the design of a fission-product trapping system for the HTGR. The first step was to derive general relationships describing the behavior of

radioactive gases in an adsorber. An experimental program was then carried out to obtain the basic physical data required. The experiments were directed at the holdup of krypton and xenon on charcoal delay beds in the temperature range from -78 to 93°C, with helium as the carrier gas.

THEORY

Both equilibrium and rate relationships are required to fully describe a mass-transfer process. In the case of adsorption, the equilibrium relationship is expressed by the adsorption isotherm. For pure physical adsorption, as described by the Langmuir equation, the isotherm becomes linear when the concentration of adsorbate on the adsorbing surface is sufficiently low. In this range, the equilibrium relationship is

$$a = kc^*$$

where a = amount of adsorbate adsorbed per unit mass of adsorbent (moles/g),

k = slope of adsorption isotherm (cm^2/g) (the isotherm slope, k, is also referred to as the "dynamic adsorption coefficient").

c^* = gas-phase concentration of adsorbate in equilibrium with adsorbent loading a ($moles/cm^2$).

We have chosen to describe the rate of transfer of adsorbate between the gas stream and the adsorbent in terms of the "height of a mass-transfer unit," a concept originated by Chilton and Colburn[9] and later applied to adsorption by Hougen and Marshall[3]. The rate equation is as follows:

$$R = \frac{V}{H}(c - c^*) = \frac{V}{H}\left(c - \frac{a}{k}\right), \qquad (2)$$

where

R = rate of adsorption per unit length of adsorber bed (moles/sec-cm),

V = volume flow rate of gas (cm^3/sec),

H = height of mass-transfer unit (cm),

c = concentration of adsorbate in gas stream ($moles/cm^2$).

Equation (2) in effect defines the height of a mass-transfer unit as a rate constant for this process.

Using Eqs. (1) and (2) as a basic description of the adsorption process, general equations for fixed-bed, isothermal adsorption of a radioactive gas from a nonadsorbing gas stream can be derived. A material balance on the adsorbate in gas phase within an increment of adsorber bed length dx during an increment of time $d\tau$ gives

$$Vc\,d\tau - V\left(c + \frac{\partial c}{\partial x}dx\right)d\tau = \frac{V}{H}\left(c - \frac{a}{k}\right)dx\,d\tau + \frac{MF}{L\rho}\left(\frac{\partial a}{\partial \tau}\right)dx\,d\tau + \frac{MF}{L\rho}\lambda c\,dx\,d\tau \qquad (3)$$

where

τ = time (sec)

x = distance along adsorber bed (cm)

M = total mass of adsorbent in bed (g)

F = void fraction in adsorber bed

L = total length of bed (cm)

ρ = bulk density of adsorbent, (g/cm^3)

λ = radioactive decay constant (sec^{-1})

A similar balance on the adsorbed material within increment dx gives

$$\frac{V}{H}\left(c - \frac{a}{k}\right) dx\, d\tau = \frac{M}{L} dx \left(\frac{\partial a}{\partial \tau}\right) d\tau + \frac{M}{L} \lambda a\, dx\, d\tau \qquad (4)$$

Using the identities

$$\alpha = \frac{1}{H} \qquad \beta = \frac{LV}{kHM} \qquad \gamma = \frac{MF}{LV\rho}$$

Eqs. (3) and (4) may be rewritten as follows:

$$-\frac{\partial c}{\partial x} = -(\alpha + \gamma\lambda)c - \frac{\alpha}{k} a + \gamma \frac{\partial c}{\partial \tau} \qquad (5)$$

$$\frac{\partial a}{\partial \tau} = \beta k c - (\beta + \lambda)a \qquad (6)$$

In most practical situations, where the amount of adsorbate in gas phase is small compared with the amount on the adsorbent, the terms in Eq. (5) involving γ become insignificant, and Eq. (5) becomes

$$-\frac{\partial c}{\partial x} = \alpha c - \frac{\alpha}{k} a \qquad (7)$$

Using the boundary conditions $a = 0$ at $\tau = 0$ for all values of x and $c = c_o$ at $x = 0$ for all values of τ, the solution to the set of partial differential equations, (6) and (7), is

$$\frac{c}{c_o} = e^{-\alpha x r/(1+r)}\left[1 - \frac{1}{1+r} e^{-\beta\tau(1+r)} \int_0^{\alpha x} e^{-t/(1+r)} I_o\left(2\sqrt{\beta\tau\, t}\right) dt\right] \qquad (8)$$

$$\frac{a}{a_o} = e^{-\alpha x} \int_0^{\beta\tau} e^{-t(1+r)} I_o\left(2\sqrt{\alpha x t}\right) dt \qquad (9)$$

where c_o = concentration in gas stream entering bed ($moles/cm^3$),

$a_o = kc_o$ $\qquad$ $r = \lambda/\beta$

and I_o is the modified Bessel function of the first kind and zero order.

Equations (8) and (9) may be simplified for several restricted cases. If r approaches zero (for a long-lived or stable adsorbate), the equations become

$$\frac{c}{c_o} = 1 - e^{-\beta\tau} \int_0^{\alpha x} e^{-t} I_o \left(2\sqrt{\beta\tau\, t}\right) dt \tag{10}$$

$$\frac{a}{a_o} = e^{-\alpha x} \int_0^{\beta\tau} e^{-t} I_o \left(2\sqrt{\alpha x t}\right) dt \tag{11}$$

These expressions are identical to those given by Hougen and Marshall.[3] Because of our interest in low values of c/c_o, we have used a digital-computer to extend the graphs of c/c_o and a/a_o given by Hougen and Marshall (which were in turn based on the Schumann-Furnas[10] charts); the results are shown in Figs. 1 and 2. Similar graphs could be computed from Eqs. (8) and (9), for a particular value of the decay constant, λ.

Another case of special interest is the equilibrium situation, where concentrations are no longer changing with time; this case represents the operation of a delay bed. Letting time τ approach infinity, Eqs. (8) and (9) become

$$\frac{c}{c_o} = e^{-\alpha x r/(1+r)} \tag{12}$$

$$\frac{a}{a_o} = \frac{1}{1+r}\, e^{-\alpha x r/(1+r)} \tag{13}$$

Recalling the definitions of r and β, the concentration of adsorbate leaving the bed (i. e., at x = L) can be expressed as

$$\left(\frac{c}{c_o}\right)_{exit} = \exp\left[-\frac{\lambda\tau_m}{1 + (\lambda\tau_m/\alpha L)}\right] \tag{14}$$

where τ_m is the mean holdup time (kM/V). The denominator in the exponent may be thought of as a correction term reflecting the statistical distribution of holdup times experienced by individual atoms about the mean holdup time. As the number of transfer units in the bed (αL) becomes large, the statistics become very good and the exit concentration assumes a simple exponential dependence on the mean holdup time.

EXPERIMENTAL APPARATUS AND PROCEDURE

The apparatus used in this work, depicted schematically in Figure 3,was designed to operate under conditions of helium pressure, helium velocity, and adsorbate concentration which might be expected in the HTGR system. Experiments were performed at pressures of 1 to 25 atm, velocities of 0.5 to 15 cm/sec, and krypton and xenon concentrations in the vicinity of 1 ppm.

The experimental system consists of a small gas loop in which helium and Kr^{85} or Xe^{133} tracer are circulated through a test trap containing the adsorbent of interest. The effluent gas passes through a flow ionization chamber

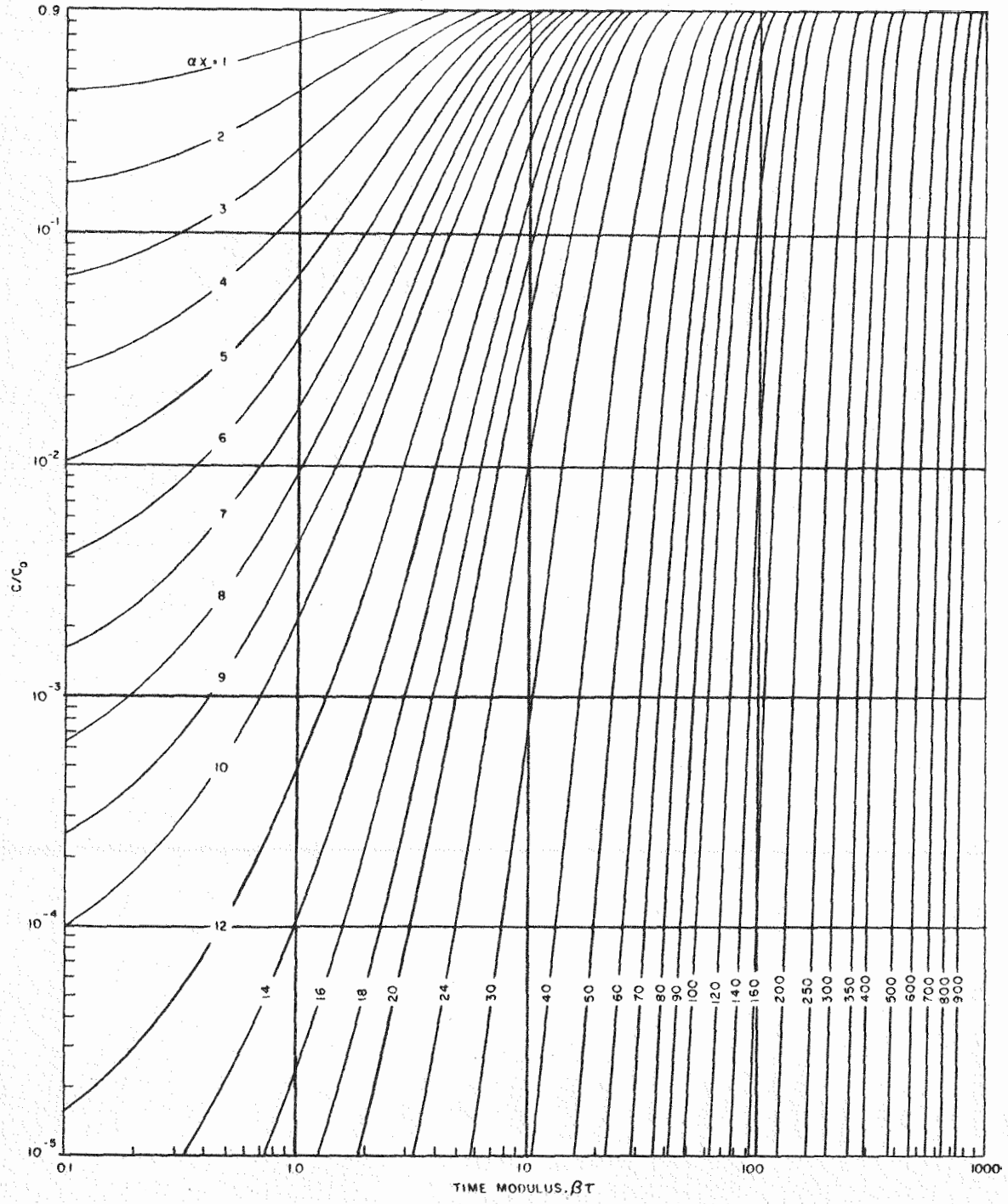

Fig. 1--Concentration profile in adsorber (gas phase)

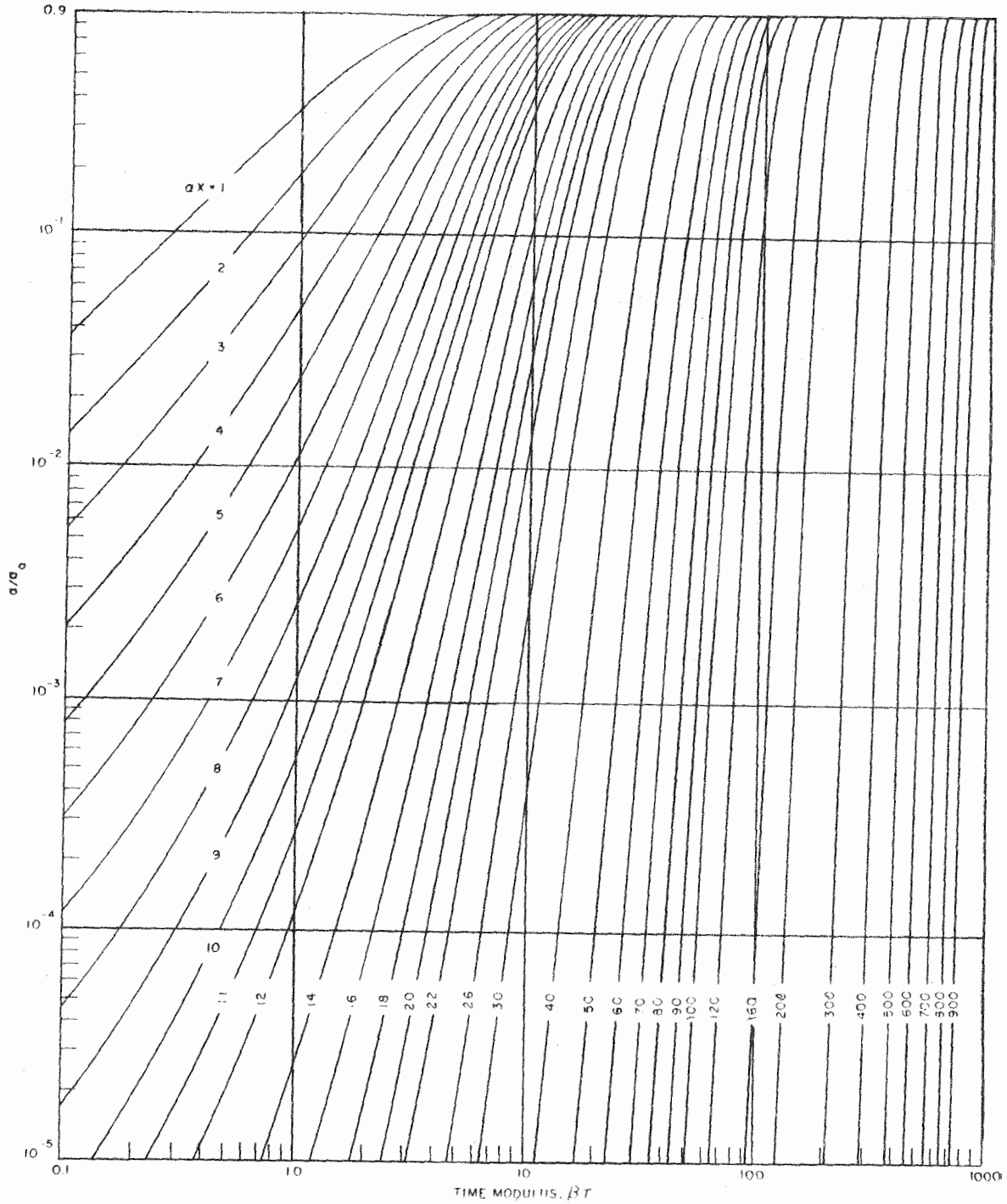

Fig. 2--Concentration profile in adsorber (adsorbed phase)

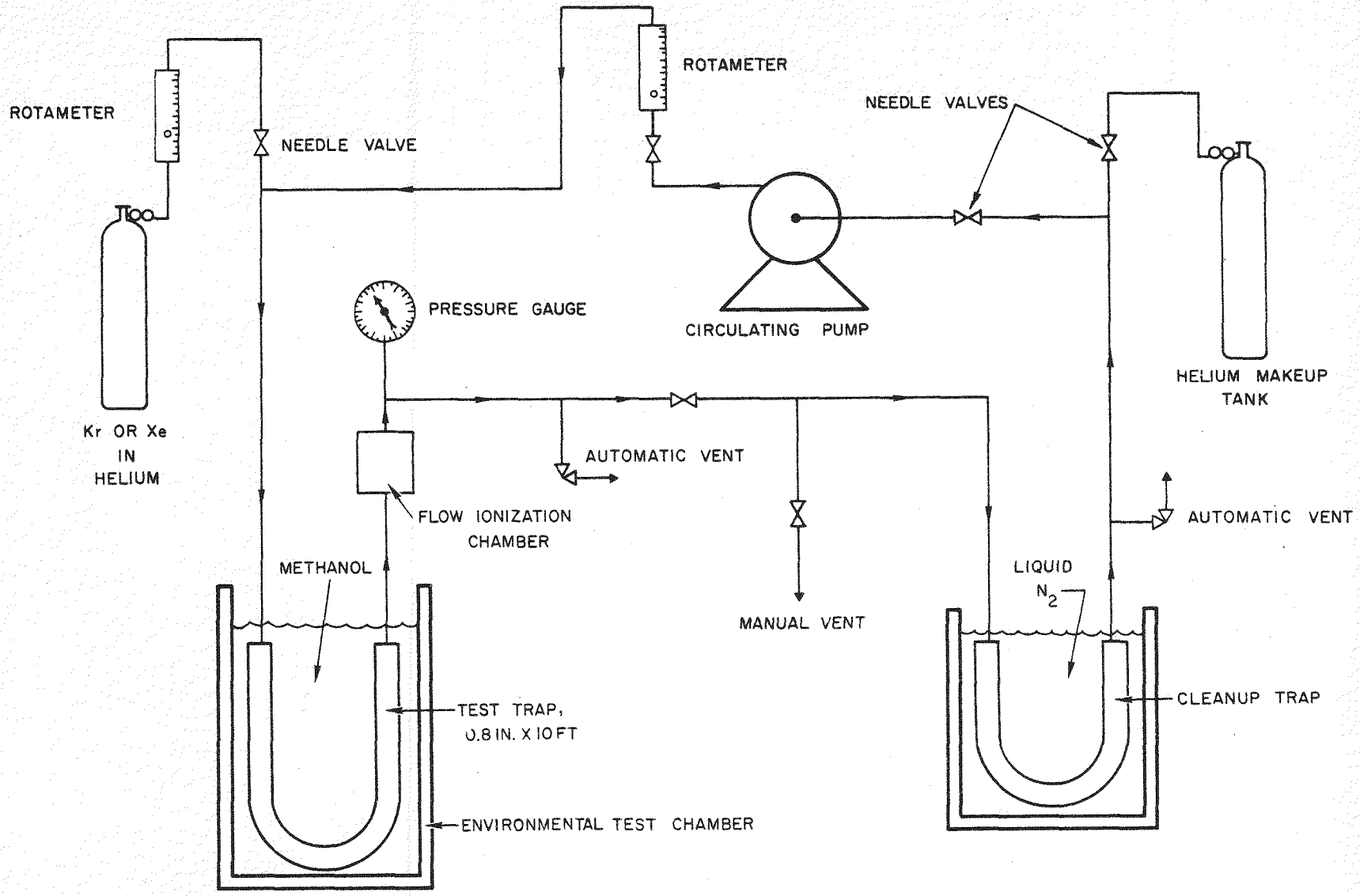

Fig. 3--Experimental apparatus

whose ion current is measured by a Dynacon Electrometer. A continuous plot of the ion current, and hence of the effluent-gas activity level, is obtained by using a 10-mv strip chart recorder with the electrometer. A Lapp Pulsafeeder diaphragm pump is used to circulate the gas at flow rates up to 11 cm^3/sec. Flow rates as high as 50 cm^3/sec were attained by discharging gas from a high-pressure bottle directly through the system.

Krypton or xenon adsorbate is supplied to the system from a separate helium tank of relatively high specific activity (10 to 20 μc/std cm^3). This adsorbate rich helium is bled into the circulating helium at a point upstream of the test trap, the system pressure being held constant by a sensitive back-pressure regulator. A liquid-nitrogen-cooled charcoal trap is placed after the ionization chamber to remove the activity and other impurities prior to recirculation of the helium through the test trap.

The choice of adsorbents to be tested was limited to various grades of activated charcoal, since previous work[5] had indicated that charcoal was superior to other adsorbents in this application. For room-temperature runs, the test trap consisted of a 10-ft section of straight steel pipe with an inside diameter of either 0.875 in. or 2 in. Low-temperature runs were performed with 10-ft-long, 0.82-in. pipe looped in a configuration which permitted its insertion in a refrigeration chamber capable of producing temperatures as low as -60°C. A lower temperature, -78°C, was obtained by using a dry ice-methanol cold bath. Temperatures up to 93°C were achieved with a constant-temperature water bath. Before entering the test trap, the helium stream was adjusted to adsorber temperature by passing it through a 12-in. coil in the bath. The charcoals were normally outgassed at about 250°C for 16 hr prior to testing. More extensive outgassing did not affect the results of the tests.

Two types of experiments were performed. In the first type, which was developed by Browning[5], a short burst of Kr^{85} or Xe^{133} is injected into the flowing helium. This pulse of activity passes through the test trap, and the strip-chart-recorder traces out the shape of the pulse as it leaves the trap and passes through the ionization chamber. For the relatively long test traps used in our experiments, the pulse is reasonably symmetrical, and the time elapsed between injection of the activity and appearance of maximum activity in the trap effluent is equal to the mean holdup time of activity in the test trap. The dynamic adsorption coefficient, k, which is in fact equal to the slope of the linear adsorption isotherm, can then be derived from the following expression:

$$k = \frac{V\tau}{\frac{m}{M}} .$$

In the second type of experiment, the Kr^{85} or Xe^{133} is injected into the flowing helium continuously at a constant rate. After some time, the activity "breaks through" the test trap, and the activity concentration in the trap effluent increases until it equals the inlet concentration (decay of the tracer was not significant in these tests). The shape of the effluent-activity curve can then be analyzed, using the procedures outlined by Hougen and Marshall[3] to determine both the dynamic adsorption coefficient and the height of a mass-transfer unit, H.

EXPERIMENTAL RESULTS

In order to compare the adsorptive capacity of various grades of activated charcoal, a series of krypton pulse-injection tests were run. All the tests were performed with the test trap at 25°C. Dynamic adsorption coefficients for the different grades of charcoal are given in Table II. The variation between grades is generally small, but it is probably significant that the highest adsorption coefficients measured were for coconut-shell-base charcoals.

In Figure 4, the dynamic adsorption coefficients for both krypton and xenon are plotted against inverse temperature, for Barnebey-Cheney Grade 107 charcoal (6/10 mesh) with helium at 350 psia as the carrier gas. The data have been fitted by a straight line on semilog paper, but a theoretical curve based on constant heat of adsorption would actually have a slight curvature. For the range of temperatures covered here, however, the theoretical curve would deviate from a straight line by only a few percent, which is well within experimental uncertainty. The heats of adsorption indicated by these data are 4.8 kcal/g-mole for krypton and 7.6 kcal/g-mole for xenon.

Values of the height of a mass-transfer unit were obtained from a number of steady-krypton-injection runs. These runs were carried out over a wide range of helium flow rates, with trap temperatures of 25 and 93°C and trap diameters of 7/8 and 2 in. In Figure 5, experimental values of outlet concentration divided by inlet concentration, taken from a typical run, are plotted against time after the start of krypton injection; the experimental data are fitted quite well by a theoretical curve based on a particular number of transfer units.

In Figure 6 the transfer-unit height for Barnebey-Cheney Grade 107 6/10-mesh charcoal is plotted against particle Reynolds number. The method of data analysis used here yields several values of the transfer-unit height for each run. In Figure 6, data points represent the average of these values, and vertical lines represent the spread of values about each point. Transfer-unit heights for the 2-in. diameter trap are lower than those of the 7/8-in. diameter trap, indicating a significant wall effect. The data for the 7/8-in. trap are correlated by the following empirical equation;

$$h = 0.038\left(\frac{D_P G}{\mu}\right)^{0.4}$$

where h = height of a mass-transfer unit (ft),

D_P = diameter of adsorbent particle (ft),

G = mass velocity of carrier gas (lb/ft^2-hr),

μ = viscosity of carrier gas (lb/ft-hr).

Our correlation is similar in form to the ones given by Gamson, Thodos, and Hougen[11] and by Wilke and Hougen[12], which are based on mass transfer between the gas stream and the particle surface. We would not expect quantitative agreement with these mass-transfer correlations, however, since wall effects are appreciable in our experiments and since other steps in the adsorption process (diffusion through the pores of the adsorbent and adsorption at the adsorbing surface) could contribute significant rate limitations.

TABLE II

DYNAMIC ADSORPTION COEFFICIENTS OF VARIOUS GRADES OF CHARCOAL AT 25°C

Supplier	Grade	Mesh	Type	k(cm^3/g)
National Carbon	CXC	6/8	Petroleum base	54.7
National Carbon	NXC	6/8	Petroleum base	58.5
National Carbon	G	8/14	Coconut	61.4
Pittsburgh	PCB	6/16	Coconut	62.0
Barnebey-Cheney	L5578-2	6/14	Coconut	58.7
Barnebey-Cheney	107	6/10	Coconut	61.0
Barnebey-Cheney	AC4	6/10	Coconut	57.5
Barnebey-Cheney	HH1	6/10	Coconut	48.0

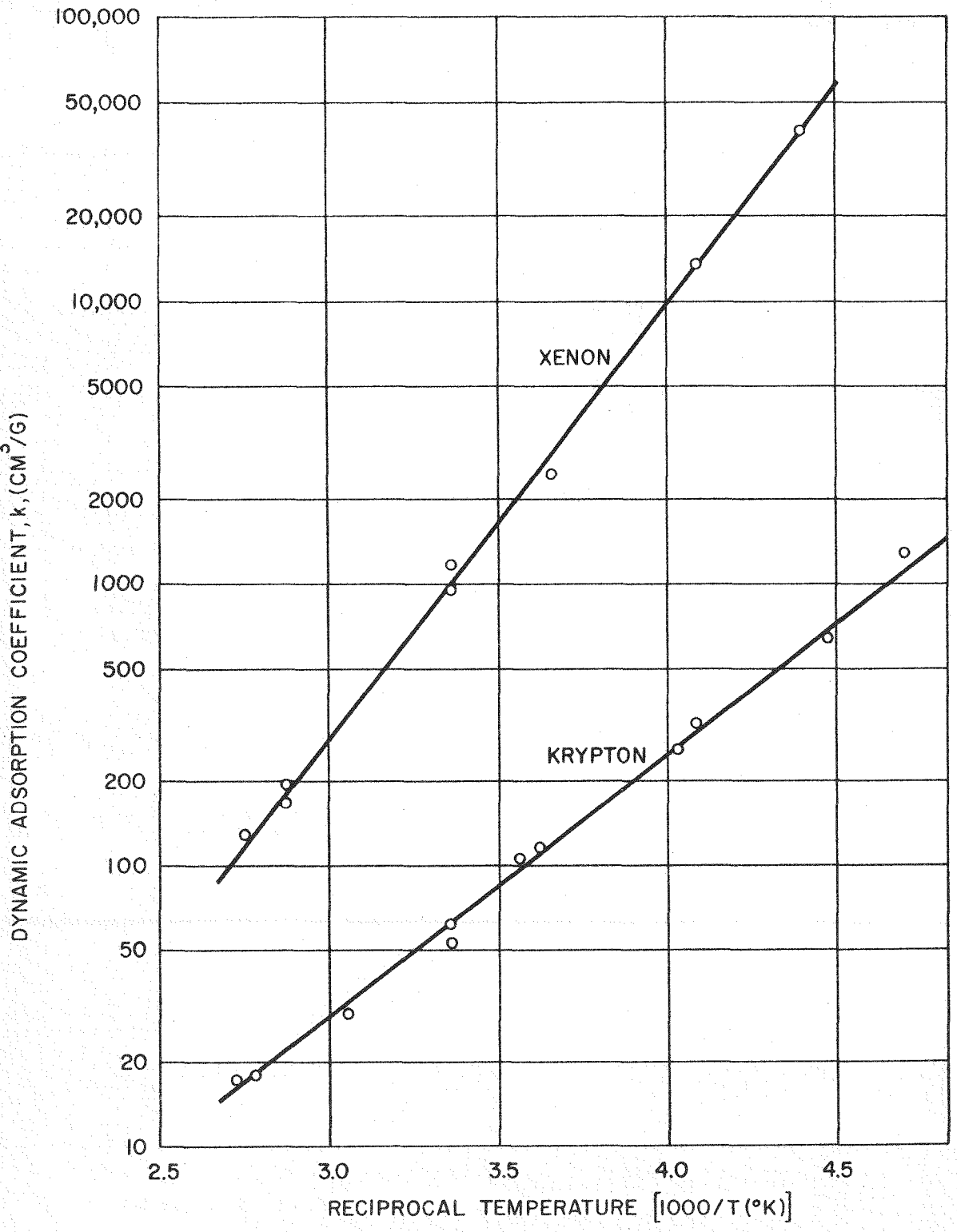

Fig. 4--Dynamic adsorption coefficient

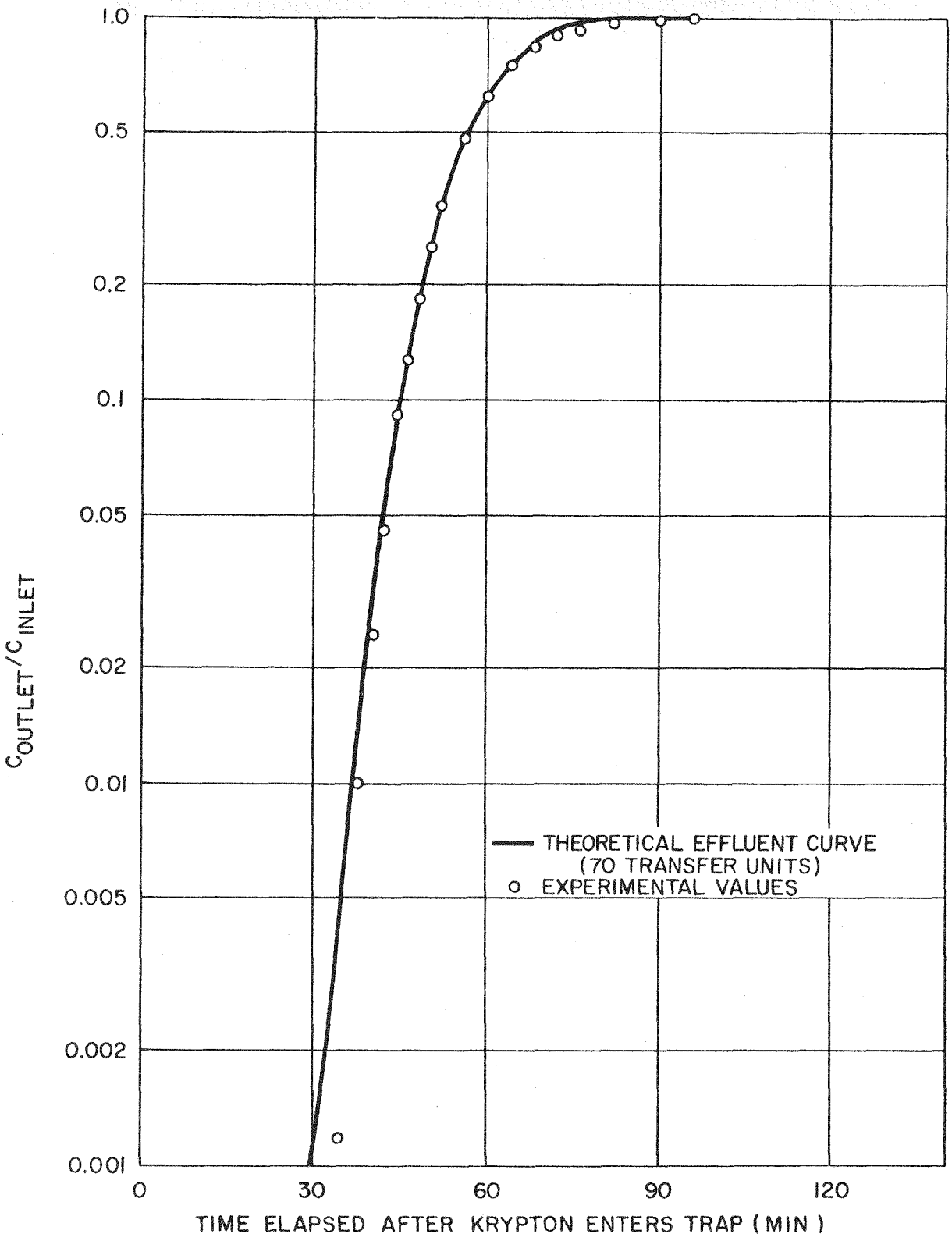

Fig. 5--Adsorption trap effluent

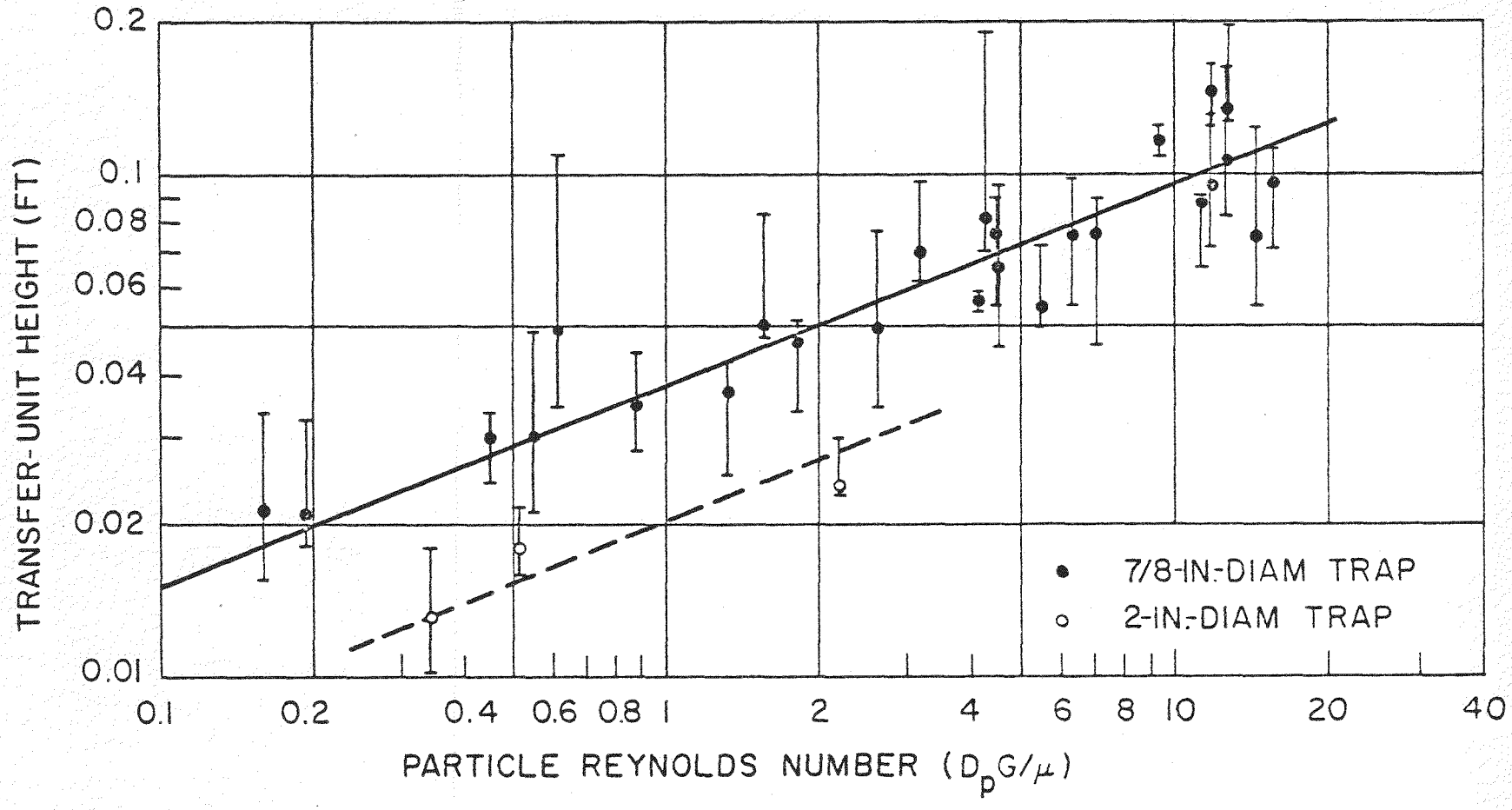

Fig. 6--Height of a mass-transfer unit

DESIGN OF ADSORBERS

Although the detailed design of an adsorption system is outside the scope of this report, it is appropriate to comment briefly on several of the problems which may arise when one seeks to apply data of the type reported here to the design of a fission-product trapping system. In particular, the limitations of the data should be understood.

Whenever the quantity of adsorbed gas on the surface of the adsorbent occupies an appreciable fraction of the total surface available, the effectiveness of the adsorbent for further adsorption will be diminished by interference effects. These interference effects may be due to adsorption of the carrier gas, adsorption of impurities in the carrier gas, or self-interference of the adsorbed krypton and/or xenon. Our experiments have indicated only a slight effect of helium pressure on room-temperature krypton and xenon adsorption, but the effect would be more pronounced with other carrier gases. The effect of solids deposited on the adsorbing surface (in particular, the solid daughter products of radioactive krypton and xenon) should be relatively small.

In a reactor system in which appreciable fractions of the volatile radioactive fission products produced are transported to the fission-product trapping system, the high levels of radioactivity contained in the trapping system will give rise to a number of serious problems. Obviously, the system must be leaktight and must be adequately shielded. Maintenance or removal of system components may be difficult. Furthermore, the radioactive fission products may give rise to significant decay-heat generation in the adsorbent, in which case the adsorbent must be cooled.

Because of the sharp variation of adsorption capacity with temperature, there is considerable incentive to operate the adsorber at temperatures as low as $-320^{\circ}F$. At liquid-nitrogen temperature, however, the cost of decay-heat removal may be prohibitive. The choice of coolants may be limited by the susceptibility of many liquids to radiation damage.

NOMENCLATURE

For convenience in our laboratory work, we have used cgs units everywhere except in the empirical equations for the height of a transfer unit.

a = amount of adsorbate adsorbed per unit mass of adsorbent (moles/g)

a_o = value of a in equilibrium with inlet gas concentration, c_o (moles/g)

c = concentration of adsorbate in gas stream ($moles/cm^3$)

c^* = gas-phase concentration in equilibrium with adsorbent loading a ($moles/cm^3$)

c_o = gas-phase concentration at inlet to adsorber bed ($moles/cm^3$)

D_p = diameter of adsorbent particle (ft)

F = void fraction in adsorber bed

G = mass velocity of carrier gas (lb/ft^2-hr)

H = height of mass-transfer unit (cm or ft)

k = slope of adsorption isotherm, or dynamic adsorption coefficient (cm^3/g)

L = total length of adsorber bed (cm)

M = total mass of adsorbent in bed (g)

r = λ/β

V = volume flow rate of gas (cm^2/sec)

x = distance along adsorber bed (cm)

α = $1/H$

β = LV/kHM

γ = $MF/LV\rho$

λ = radioactive decay constant (sec^{-1})

μ = viscosity of carrier gas(lb/ft-hr)

ρ = bulk density of adsorbent (g/cm^3)

τ = time (sec)

τ_m = mean holdup time kM/V (sec)

R = rate of adsorption per unit length of adsorbed bed(moles/sec-cm)

REFERENCES

1. J. M. Holmes, Design of the Dissolver Off-gas System for the Idaho Chemical Processing Plant, USAEC Report CF-52-11-39, Oak Ridge National Laboratory, November 1952.

2. J. N. Burdick, Adsorption of Krypton and Xenon, USAEC Report ORO-118, Oak Ridge Operations Office, November 1951.

3. O. Hougen and W. R. Marshall, Jr., Adsorption from a Fluid Stream Flowing Through a Stationary Granular Bed, Chem. Eng. Prog., 43: 197 (1947).

4. R. E. Adams and W. E. Browning, Fission Gas Holdup Tests on HRT Charcoal Beds, USAEC Report CF-58-4-14, Oak Ridge National Laboratory, April 1958.

5. W. E. Browning, R. E. Adams, and R. D. Ackley, Removal of Fission Product Gases from Reactor Off-gas Streams by Adsorption, USAEC Report CF-59-6-47, Oak Ridge National Laboratory, June 1959.

6. W. E. Browning and C. C. Bolta, Measurement and Analysis of the Holdup of Gas Mixtures by Charcoal Adsorption Traps, USAEC Report ORNL-2116, Oak Ridge National Laboratory, August 1958.

7. D. F. Sangster, The Isotherm for the Adsorption of Krypton on Charcoal, British Report AERE-C/M-280, June 1956.

8. C. B. Amphlett and B. F. Greenfield, Krypton and Xenon Adsorption Isotherms on Charcoal Irradiated with 1 Mev Electrons, British Report AERE-C/R-2632, July 1958.

9. T. H. Chilton and A. P. Colburn, Distillation and Absorption in Packed Columns, Ind. Eng. Chem., 27: 255 (1935).

10. C. C. Furnas, Trans. Am. Inst. Chem. Engrs., 24: 142 (1930).

11. B. W. Gamson, G. Thodos, and O. A. Hougen, Heat, Mass and Momentum Transfer in the Flow of Gases Through Granular Solids, Trans. Am. Inst. Chem. Engrs., 39: 1 (1943).

12. C. R. Wilke and O. A. Hougen, Mass Transfer in the Flow of Gases Through Granular Solids Extended to Low Modified Reynolds Numbers, Trans. Am. Inst. Chem. Engrs., 41: 445 (1945).

FISSION PRODUCT LEVELS IN THE SM-1 COOLANT

By C. A. Bergmann and J. F. Cox

Alco Products, Inc.
Schenectady, N. Y.

INTRODUCTION

This paper presents data on fission product activities found in the SM-1 coolant during nearly 4 years of operation. The SM-1 is a small (2 MWe) pressurized water reactor with an all stainless steel primary system. The reactor is used primarily for training and development purposes and its operation has been intermittent. As a result, data interpretation becomes complex. The level of fission product activity has been measured frequently since one year after start-up as part of a research and development program to establish the identity, level, and origins of fission products in the coolant.

RADIOACTIVITY LEVELS

The out-of-core activity in a pressurized water reactor primary loop exists either in the primary coolant or is deposited on primary system piping and components. Knowledge of the activity in the coolant is important for short-lived radiation levels, health physics, and waste disposal considerations. The long-lived activity deposited on the surfaces is important when considering access and maintenance aspects. In the SM-1, experimental work has shown that the major source of activity in the coolant is due to fission products, while the activity deposited on system surfaces is due primarily to long-lived induced nuclides formed from corrosion products.

Periodic analyses were performed on SM-1 primary coolant in order to determine the specific activities (dpm/ml) of approximately sixteen fission product nuclides and nine induced nuclides.

Several analyses were also done on circulating and deposited crud. The analytical procedures used were standard radiochemical methods for analysis. A description of sampling and analytical procedures and complete listing of the data obtained is reported in references 1, 2, and 3.

The nuclides identified and their concentrations in the coolant during December, 1958 are listed in Table I. The data include the contribution of activity in the circulating crud since the crud was filtered from the sample, taken into solution and recombined with the sample. The values for radioactive

TABLE I

FISSION PRODUCTS AND INDUCED NUCLIDES IDENTIFIED IN SM-1 COOLANT

Nuclide		Concentration
Fission Products	Half-life	dpm/ml
Sr^{89}	51d	8.7×10^{2}
Sr^{90}	28y	2.7×10^{1}
Sr^{91}	9.7h	4.2×10^{4}
Y^{92}	3.5h	4.0×10^{4}
Y^{93}	10.3h	4.4×10^{2}
I^{131}	8.1d	2.1×10^{4}
I^{132}*	2.3h	2.0×10^{5}
I^{133}	21h	1.3×10^{5}
I^{134}	53m	4.0×10^{5}
Cs^{137}	30y	9.3×10^{1}
Cs^{138}	32m	2.2×10^{5}
Ba^{139}	85m	1.5×10^{5}
Ba^{140}	12.8d	4.5×10^{3}
Kr^{88}	2.8h	1.3×10^{5}
Kr^{85m}	4.4h	6.5×10^{4}
Xe^{135}	9.2h	6.5×10^{4}
Induced Nuclides		
Mn^{54}	280d	5.0×10^{3}
Co^{58}	71d	7.0×10^{3}
Co^{60}	5.3y	4.0×10^{3}
Cr^{51}	27.8d	7.0×10^{3}
Fe^{59}	45d	1.0×10^{3}
Mn^{56}	2.6h	1.4×10^{6}
Ni^{65}	2.6h	1.4×10^{3}
W^{185}	74d	1.6×10^{1}
W^{187}	24.0h	1.3×10^{5}

*Calculated from I^{131} equilibrium level.

xenon and krypton are averages of two analyses on separate days. Isotopes of zirconium, niobium, cerium, and molybdenum were also found several months earlier. However, their concentrations were so low that their contribution to coolant activity is insignificant. The concentrations are corrected to time of sampling, and thus represent the levels in the coolant when the reactor is operating.

Short-lived (half-life 2.5 hours and less) radiation levels around the primary coolant piping 1.7 hours after shutdown were about 100 mr/hr. Calculations were made to determine which of the gamma-emitting nuclides of Table I would contribute significantly to the short-lived radiation level[4]. It was calculated that two short-lived nuclides, Mn^{56} and W^{137}, which originate from induced reactions, contributed about 20 percent of the total short-lived radiation level. The remaining 80 percent consisted primarily of iodine, cesium, and krypton radioisotopes. However, only about one-half of the short-lived dose rate could be accounted for. The discrepancy between the observed and calculated values appears to be due to the exclusion of nuclides not identified. Nuclides not identified which could contribute to significant dose rates are probably the gaseous isotopes, since it will be shown later that the sum of the activity levels of the nuclides found in the coolant (excluding the gaseous isotopes) agrees well with that found during health physics tests.

At shutdown, the contribution of long-lived (half-life greater than 2.5 hours) fission product activity in the coolant to total long-lived coolant activity was found to be about 70 percent.[5] Five days after shutdown, fission product activities account for about 30 percent of the total coolant gamma activity. Although the long-lived fission product activity is over two times the induced activity in the coolant, the contribution of this activity to radiation levels on the external side of the primary piping and components is negligible when compared to deposited activity. Radiation levels external to the primary system of the SM-1 have been shown to be due almost solely to deposited material.[4] To compare the amount of deposited fission product activity to deposited induced nuclide activity, data obtained from deposits removed from a Croloy 16-1 coupon were investigated. Croloy 16-1 deposits were used since Type 340 SS deposits are not sufficiently large to perform a large number of radiochemical analyses. The data showed that the gamma activities of the long-lived fission products analyzed account for about 1 percent of the total gamma activities found. Thus, it appears that deposited long-lived fission products do not significantly contribute to after-shutdown radiation levels observed at the SM-1. In the circulating crud, the isotopes Sr^{90}, Y^{91}, Sr^{91}, Ba^{140}, Cs^{134}, and Cs^{137} were found. In general, their concentrations in the crud, on a volume basis, were negligible when compared to their concentrations in the coolant.

The total activity of the coolant was calculated in terms of μc/cc to compare it with health physics data. Health physics samples of the primary coolant are evaporated to dryness and counted on a G-M tube 30 minutes after sampling. To compare the experimental data with health physics data, it was assumed that the gaseous nuclides (krypton, xenon, and iodine isotopes) would be lost when the sample is evaporated. The total coolant activity, based on the experimental values, was calculated at approximately 0.7 μc/cc. Health physics data during the same time of sampling showed the coolant activity was between 0.6-0.8 μc/cc. Thus, it appears that the significant nuclides in the coolant (excluding the gases) were accounted for.

DISCUSSION OF FISSION PRODUCT DATA

Fission products can arise in a reactor coolant from three sources: (1) surface contamination, (2) bulk cladding contamination, and (3) cladding defects [1]. In order to evaluate which of the above sources contributed significantly to the observed fission product levels, the ratios of fission products in the coolant, the behavior of I^{131} during startup and shutdown tests, and the change of equilibrium fission product levels with time were studied.

Some surface contamination was known to be present on the SM-1 elements. Spare elements were wipe tested and some alpha activity was found, but it was not possible to quantitatively measure the alpha contamination. It was calculated that a surface contamination of 74 μg U^{235} /ft^2 would be required to support the observed equilibrium I^{131} level of 2.1×10^4 dpm/ml. While this amount of contamination is not inconceivable, it is felt to be rather unlikely, since the average range of contamination found on SM-1 Core II elements was 0.0-0.11 μg U^{235} /ft^2.

In the case of bulk cladding contamination of the stainless steel, it was calculated that an impurity concentration of 6300 ppm of natural uranium in the cladding is required to support the observed I^{131} level. This degree of contamination is considerably higher than could be expected. Therefore, it appeared that a cladding defect best accounted for the presence of fission products. This tentative conclusion was further checked by examination of the fission product ratios. Calculations were made for certain nuclide ratios assuming the fission products were due to cladding and/or surface contamination. The calculated ratios based on equilibrium concentrations are compared to the observed equilibrium ratios in Table II. If experimentally determined ratios exceed calculated ratios for surface and cladding contamination, a defect may be assumed to be present [11]. The first four ratios indicate clearly that fission products must be due to a source other than surface or cladding contamination. However, the last two ratios do not bear out this conclusion. Thus, the behavior of $I^{131,133}$ during startup and shutdown tests was studied.

The buildup of iodine in the coolant was expressed by an equation which assumed a constant release rate, such as would be the case if the activity were due to a surface or cladding contamination. It was calculated that 5.5 days would be required for I^{131} to reach an equilibrium level. Actually, it took 7 days for I^{131} to reach an equilibrium concentration. Thus, it was concluded that the release rate was not constant but increased with time to some equilibrium value of its own. This case is consistent with the assumption of a cladding defect, in which there would be a buildup of fission products within and behind the defect. The buildup would continue until the rate of decay plus escape of a given nuclide became equal to the rate of accumulation of the nuclide. The mechanism of accumulation could be recoil from the uranium or, less likely, by diffusion of the fission product out of the matrix. Equations were derived assuming a void defect behind the core cladding and the calculated results were found to agree well with the experimental data.

The behavior of radioiodine during shutdown tests showed that in some cases the I^{131} level in the coolant increased about 50 percent above the equilibrium level about 17 hours after shutdown. This is not consistent with a recoil mechanism for entry of fission products into the coolant, since the addition of a significant amount of fission products would cease when the reactor is

TABLE II

FISSION PRODUCT RATIOS (ATOMS/ML)

Ratio	For Bulk Cladding Contamination	For Surface Contamination	Experimental Results
$\frac{Sr^{90}}{Sr^{91}}$	3.16	3.16	15.8
$\frac{Cs^{137}}{Cs^{138}}$	43.7	43.7	208
$\frac{Ba^{140}}{Sr^{91}}$	3.1	1.4	3.3
$\frac{I^{131}}{I^{133}}$	0.8	0.86	1.5
$\frac{Ba^{140}}{Ba^{139}}$	14.8	14.8	6.7
$\frac{I^{133}}{Cs^{138}}$	23.2	23.2	22.8

scrammed. An increase of 3 percent of I^{131} activity would be expected from tellurium deposited on the system surfaces. Calculations showed that the observed increase in the iodine level could be explained if a void defect were assumed. Thus, the results of the iodine startup and shutdown tests indicated strongly that a great portion of fission product activity originated from cladding defects.

Additional evidence that defects are responsible for the fission products is seen in Fig. 1, which shows the increase in concentration in the coolant of Cs^{137} and Sr^{90} during nearly all of Core I lifetime. If the source of Cs^{137} and Sr^{90} is due to cladding or surface contamination, then the activity of these long-lived nuclides is dependent on the "half-life" of the purification system, assuming that they remain in the coolant and do not deposit on system surfaces. Since the half-life of the SM-1 purification system is about 17 hours, these fission products should reach equilibrium in about 5 days. This equilibrium level should decrease with time because of depletion of the source. Most of the data points were taken during tests in which the reactor had run more than 5 days. Thus, the levels were at equilibrium. However, the fact that these levels keep increasing with time definitely show that defects in the elements had occurred.

As further evidence of cladding defects, it was noted that the gross fission product iodine levels decreased from 20,000 cpm before the end of Core I life to about 7000 cpm after the start-up of Core II operation. These levels were measured by passing a coolant sample through a cation resin column and counting the effluent in a well scintillation detector. The equipment was biased so as to detect only those gamma photons emitted from iodine nuclides.

In summary, SM-1 Core I definitely had defects in the cladding. However, the level of fission product activity was not sufficient to cause any major operational or health physics problems.

REFERENCES

1. W. S. Brown and R. A. Hasse, SM-1 Research and Development Program, Final Report on Short-lived and Fission Product Activity in SM-1 Primary Coolant, Task III, Report APAE No. 44, Alco Products, Inc., March 10, 1959.

2. R. A. Hasse, SM-1 Research and Development Program, Final Report on Fission Product Activity in the SM-1 Primary Coolant, Task XIII, Report APAE No. 50, Alco Products, Inc., June 30, 1959.

3. R. A. Hasse and J. L. Zegger, Fission Product Activity in SM-1 Core I Primary System and Surface Contamination on SM-1 Type Fuel Elements, Report APAE No. 76, Alco Products, Inc., Feburary 28, 1961.

4. W. S. Brown, et al, SM-1 Research and Development Program Activity Buildup Program, Task I, Report APAE No. 51, Alco Products, Inc., August, 1959.

5. C. A. Bergmann, SM-1 Research and Development Program, Long-Lived Induced Activity Buildup During SM-1 Core I Lifetime, Report APAE No. 77, Alco Products, Inc., November 30, 1960.

FIGURE 1

BUILDUP OF TWO LONG-LIVED FISSION PRODUCTS IN SM-1 PRIMARY COOLANT

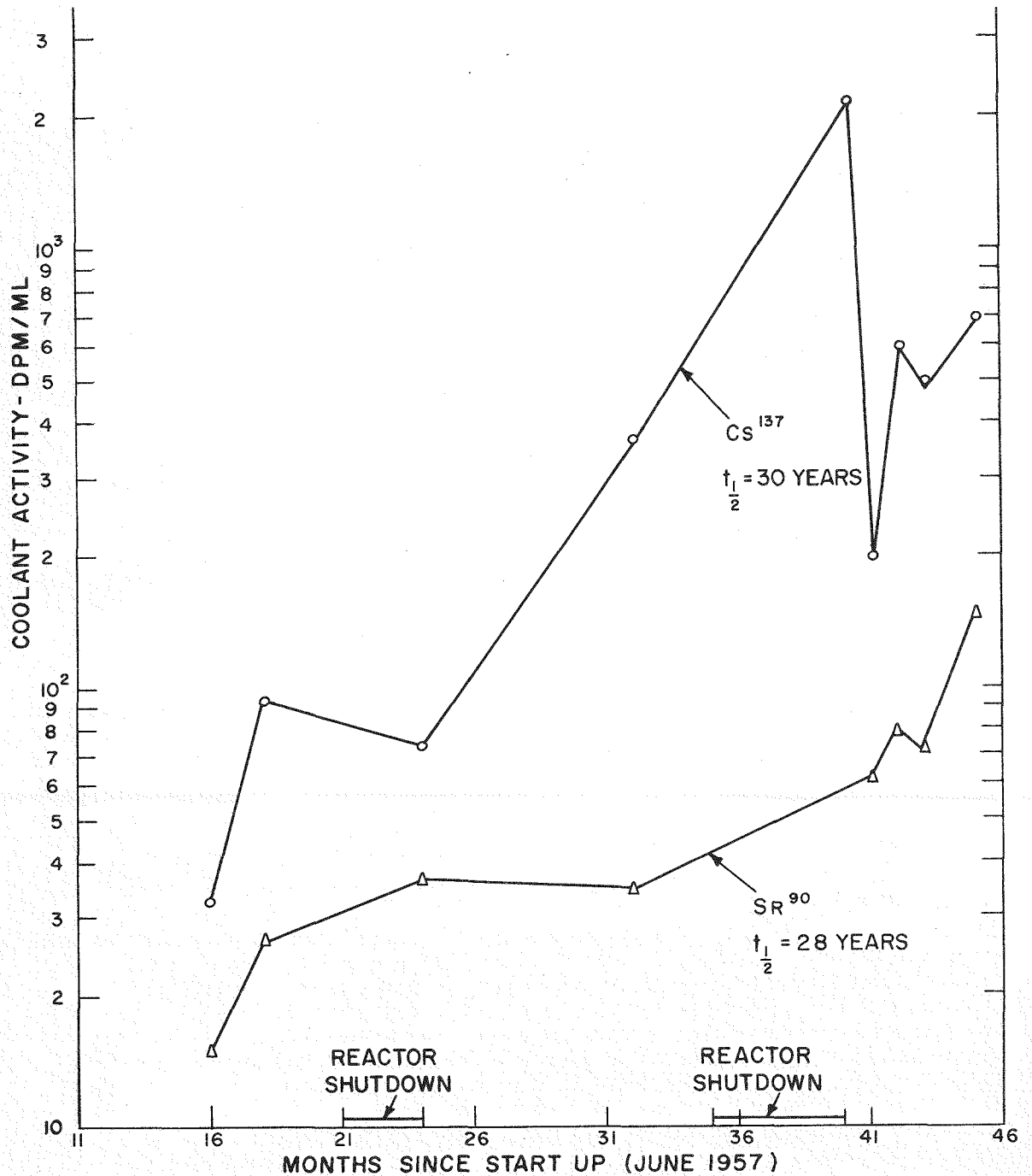

A DIFFUSION MODEL FOR THE TRANSPORT OF GASES IN POROUS MEDIA[b]

By G. M. Watson, R. B. Evans III, and J. Truitt

Oak Ridge National Laboratory[a], Oak Ridge, Tennessee

ABSTRACT

Pore-diffusion phenomena in porous media are customarily discussed in terms of two basic concepts: Knudsen (or molecular flow) and normal diffusion. Treatment of diffusion in terms of these two concepts restricts the discussion to either of the corresponding limiting cases - gas-gas collisions only (normal diffusion) or gas-wall collisions only (Knudsen) - and is not applicable to the situation in which both collision mechanisms are significant. The primary objective of this investigation was the development of a generalized diffusion model applicable to the more realistic case where both collision mechanisms are superimposed.

The model is based on (1) the results of a series of uniform pressure experiments involving the interdiffusion of two gases in four different graphites, and (2) a theoretical postulation that a portion of the porous medium immediately involved in surface collisions behaves as a collection of uniformly distributed "dust" particles. When these particles are treated as large molecules and as the third gas component of the mixture, all the desired results can be obtained from classical multicomponent formulations. These theoretical equations yield the experimentally observed flux ratio,

$$(m_2/m_1)^{1/2},$$

for binary gas mixtures, the Bosanquet interpolation formula, and a differential equation for diffusion applicable over the entire pressure range. Application of the model to earlier studies with permeable graphites[1,2] reveals that all conclusions made and equations used previously regarding uniform-pressure measurements remain valid. Fluxes determined experimentally for low-permeability graphites are in agreement with calculated values, based on the model parameters, since the model is applicable to all porous media and over all pressures ranging from the Knudsen to the normal region. The model does not characterize the porous medium, but if the interdiffusive rates of a particular binary gas mixture are measured in a certain medium, then the

---

[a]Operated for the U. S. Atomic Energy Commission by Union Carbide Corporation.

diffusive rates for the other gas mixtures through this same medium can be predicted. Only two parameters are required to define a given binary gas-porous medium system in terms of the model. These are an effective normal diffusion coefficient (characteristic of both gases and the medium) and an effective Knudsen coefficient for one of the gases in the same medium.

REFERENCES

1. R. B. Evans III, J. Truitt, and G. M. Watson, Superposition of Forced and Diffusive Flow in a Large Pore Graphite, USAEC Report ORNL-3067, Oak Ridge National Laboratory, February 1961.

2. J. Truitt, Interdiffusion of Helium and Argon in Speer Moderator No. 1 Graphite (A Terminal Report on Large-Pore Graphites - Experimental Phases), USAEC Report ORNL-3117, Oak Ridge National Laboratory, June 1961.

---

[b] The information in this paper has been submitted for publication in the Journal of Chemical Physics.

XENON-133 DIFFUSION IN ALUMINA

by R. H. Barnes, T. S. Elleman, and D. N. Sunderman

Battelle Memorial Institute
Columbus, Ohio

INTRODUCTION

One of the coated fuel-particle systems currently being developed at Battelle for high-temperature gas-cooled reactor applications is alumina-coated UO_2. In order to provide information needed to assess the effectiveness of alumina coatings in preventing escape of fission products from fuel particles, an investigation is in progress to obtain data on fission-product diffusion in alumina. As part of this investigation, diffusion coefficients have been determined for Xe^{133} in single-crystal α-alumina at temperatures ranging from 700 to 1550°C.

EXPERIMENTAL PROCEDURE

To determine diffusion coefficients, small spheres of single-crystal α-alumina were dispersed in UO_2 powder containing natural uranium and irradiated at low temperatures, where diffusion is negligible. These spheres, which then contained fission products that recoiled into them from the surrounding UO_2 powder during irradiation, were separated from the powder and heated at constant temperature. Xe^{133} released from the alumina was measured as a function of time and the results of the release measurements were then used to determine diffusion coefficients. In general, diffusion measurements were conducted at several temperatures with a given group of spheres. The duration of the measurement at each temperature was usually about 6 hours.

The single-crystal α-alumina used for the Xe^{133} diffusion measurements was obtained from the Linde Company in the form of highly polished 1-mm diameter sapphire spheres which weighed 0.0021 g each. Tolerance on the diameter of the spheres was less than $\pm$ 1 micron. The spheres, which were transparent, had been prepared from 99.95 percent pure α-alumina.

For irradiation, the alumina spheres were packed in 1-micron UO_2 powder inside quartz tubes which were then sealed under helium. The tubes containing the alumina spheres were irradiated in aluminum capsules in thermal-neutron fluxes of about 1×10^{13} nv for periods between 10 and 14 hours. Integrated thermal-neutron exposures were monitored with cobalt dosimeters which were irradiated

a. This work performed under AEC Contract W-7405-eng-92.

with the spheres. The maximum temperature experienced by the alumina during irradiation is estimated to have been less than 400°C.

Following irradiation, the alumina spheres were separated from the UO_2 and cleaned with distilled water in an ultrasonic bath. Satisfactory removal of the UO_2 was confirmed by assaying the spheres for alpha contamination with a windowless proportional counter.

The amount of Xe^{133} and other fission products contained in the irradiated spheres was determined using a gamma-ray spectrometer to assay the 1.6-Mev photopeak associated with La^{140}. These results were found to be in favorable agreement with calculations based on thermal-neutron dosimetry.

The apparatus employed for the Xe^{133} release measurements is described in detail in an earlier report.[1] Another report[2] covers results of other diffusion experiments with this apparatus which involved fission-gas release from UO_2. Heating of the alumina spheres was performed inside a gas-tight ceramic tube. To eliminate prolonged effects due to changing temperature, the alumina was taken to the desired temperature in 15 sec. Fission gas evolved from the alumina was conveyed in a flowing helium stream to charcoal adsorption traps where the fission gas was collected from the helium for radioassay. The helium employed for these measurements contained less than 10 ppm each of oxygen and water vapor. To follow the variation of release with time, the fission gas was collected in a series of consecutive samples by changing charcoal traps at different intervals during the course of a diffusion measurement. A gamma-ray spectrometer was used to analyze the Xe^{133} collected in the charcoal adsorption traps.

ANALYSIS OF DATA

Analysis of the Xe^{133} release data in terms of diffusion coefficients is based on a solution of Fick's diffusion equation for the appropriate boundary conditions.[a] For the case where a sphere is surrounded by a medium in which recoiling atoms are generated, the concentration of recoil atoms which come to rest in the sphere as a function of sphere radius can be expressed as:

$$C = \frac{B\zeta}{4\delta^2 r}\left(r^2 + 2r\delta + \delta^2 - a^2\right),$$

for $(a - \delta) \leq r \leq a$,

where

C = concentration of recoil atoms in sphere, atoms per cm^3
B = number of recoil atoms generated in fuel, atom per cm^3
r = radial distance in sphere, cm
a = sphere radius, cm
ζ = recoil range in fuel, cm (4.9×10^{-4} cm for Xe^{133} in UO_2)
δ = recoil range in sphere, cm (8.5×10^{-4} for Xe^{133} in Al_2O_3).

Assuming an initial concentration of the diffusing species represented by the preceding equation, the fraction of atoms released from the sphere by diffusion is given by:

---

a. The mathematical derivations were performed at Battelle by S. D. Beck.

$$f = 1 \frac{24}{\upsilon^2(12-\upsilon^2)} \sum_{n=1}^{\infty} \left[\frac{\upsilon(\upsilon+2)}{(n\pi)^2} - \frac{2 \operatorname{Sin} n\pi\upsilon}{(n\pi)^3} - \frac{2(1-\operatorname{Cos} n\pi\upsilon)}{(n\pi)^4} \right] \exp(-n^2\pi^2\tau^2),$$

where

f = accumulative fraction of diffusing species released from sphere
$\upsilon = \delta/a$
$\tau = Dt/a^2$
D = diffusion coefficient, cm^2 per sec
t = diffusion time, sec.

For intermediate diffusion times ($0.1\ \upsilon^2 \leq \tau \leq 0.1$) the following approximation is valid:

$$f = \frac{24}{\upsilon^2(12-\upsilon^2)} \left[\frac{\upsilon(\upsilon+2)\sqrt{\tau}}{\sqrt{\pi}} - (1+\upsilon)\tau + \frac{4\tau^{3/2}}{3\sqrt{\pi}} - \frac{4\tau^{3/2}+\upsilon(\upsilon+3)\sqrt{\tau}}{3\sqrt{\pi}} e^{-\frac{\upsilon^2}{4\tau}} \right.$$

$$\left. + \frac{\upsilon^2(\upsilon+3)+6(1+\upsilon)\tau}{6} \operatorname{erfc} \frac{\upsilon}{2\sqrt{\tau}} \right].$$

Further simplification of this approximation is possible for the case of short diffusion times ($\tau/\upsilon^2 \leq 0.1$), resulting in the equation:

$$f = \frac{24}{\upsilon^2(12-\upsilon^2)} \left[\frac{\upsilon(\upsilon+2)\sqrt{\tau}}{\sqrt{\pi}} - (1+\upsilon)\tau + \frac{4\tau^{3/2}}{3\sqrt{\pi}} \right].$$

For very short diffusion times ($\tau < 0.01$), the equation reduces to the familiar square root of time relationship given by the equation:

$$f = \frac{12(\upsilon+2)}{\upsilon(12-\upsilon^2)\sqrt{\pi}} \sqrt{\tau} \quad .$$

Interpretation of the release data was complicated, however, by a difference between the slopes followed by the experimental results and the theoretical curve. This anomaly is best illustrated by Figure 1 which shows accumulative fractional release as a function of the square root of heating time. On the basis of simple diffusion kinetics, fractional release would be expected to be linear with the square root of time and pass through the origin, however, actual release was observed to be quite rapid initially and it was only after prolonged heating that Xe^{133} evolution became linear with respect to the square root of heating time. This initial release anomaly appears to be similar to the initial burst observed by various investigators during postirradiation heating measurements of fission-gas release from UO_2. In order to fit the release data to the theoretical curve, the data was adjusted by subtracting a constant value, which was determined by trial and error, to make the data points conform to the theoretical slope. This constant has been interpreted as representing the magnitude of the initial burst.

In calculating a diffusion coefficient for cases where the same specimens were used at a series of different temperatures, it was necessary to consider prior diffusion which had occurred. This was accomplished by correlating the release data through use of a logarithmic plot of f as a function of a corrected τ, which is just τ as defined by the diffusion equation minus the sum of the τ

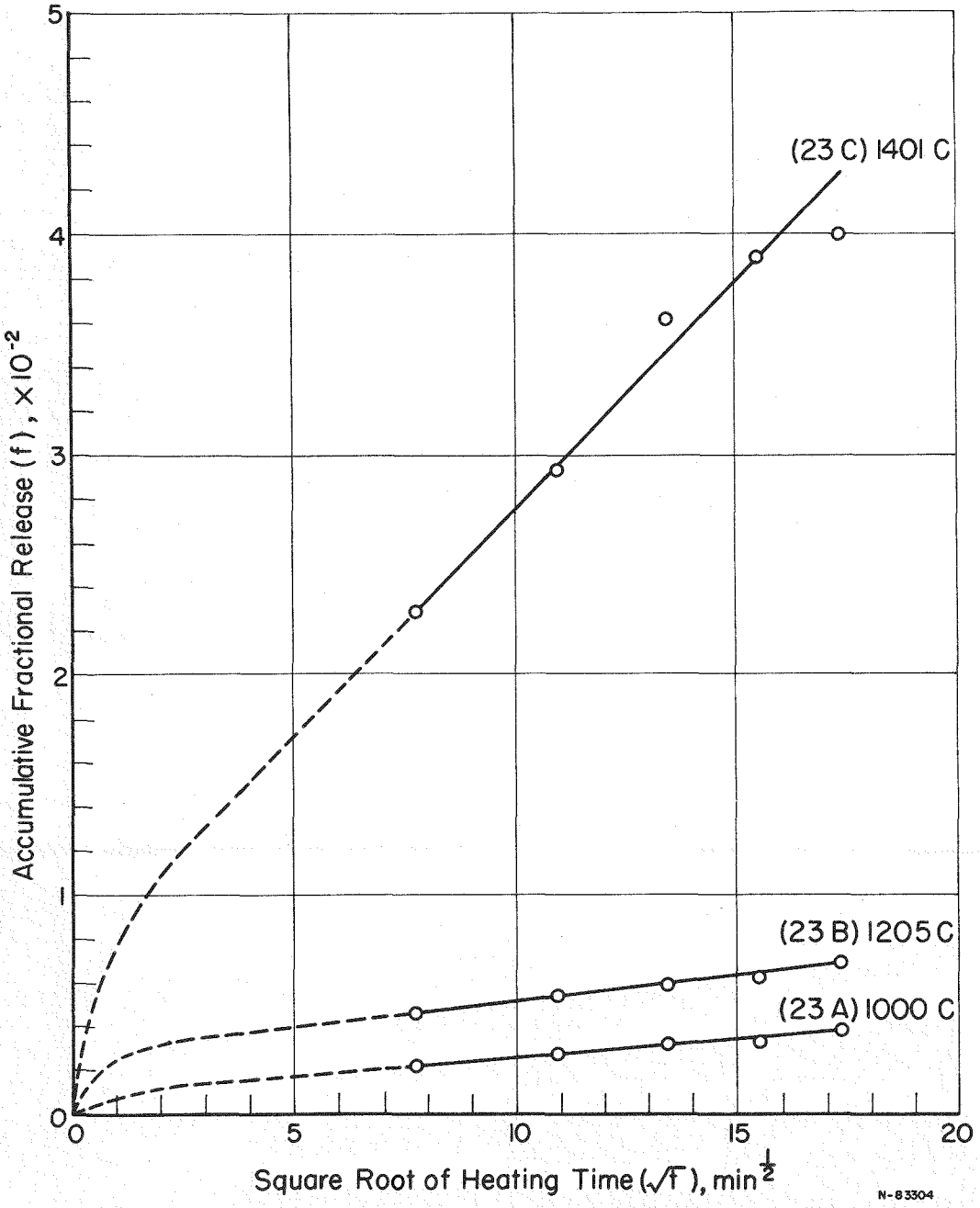

FIGURE 1. TYPICAL RELEASE MEASUREMENTS OF XENON-133 EVOLUTION FROM SINGLE-CRYSTAL ALPHA ALUMINA

values for previous diffusion release.

SUMMARY OF RESULTS

The results of the measurements of Xe^{133} diffusion in single-crystal α-alumina are summarized in Table I. Figure 2 presents the diffusion coefficients as a function of temperature. The letters following the run numbers designate the sequence in which multi-temperature measurements were performed; A being the first measurement, B the second, and so on. Xe^{133} diffusion in single-crystal α-alumina was found to follow the equation $D = 1.57 \times 10^{-5} \exp(-71{,}700/RT)$ cm^2 per sec from about 1040° to 1550°C. Below 1040°C, diffusion followed the expression $D = 7.15 \times 10^{-16} \exp(-9{,}190/RT)$ cm^2 per sec.

Figure 3 shows the fraction of Xe^{133} released in the burst. Generally, the size of the initial burst is temperature dependent. As temperature increases the burst increases. The temperature dependency of the burst can be represented by an activation energy of approximately 30 kcal per g-mole.

CONCLUSIONS

For purpose of comparison, the Xe^{133} diffusion coefficients are shown in Figure 4 along with data for diffusion of other species in alumina. In general, Xe^{133} diffusion was about two orders of magnitude more rapid than oxygen self-diffusion in single-crystal α-alumina. Rn^{222} diffusion was almost a factor of 10,000 faster in polycrystalline α-alumina than xenon diffusion in single-crystal material. However, in this case activation energies were about the same for both gases, and the breaks in the diffusion curves occur at about 1000°C.

In conclusion, the diffusion coefficient values obtained in this investigation seem reasonable; however, the meaning of the initial burst and its implications are still obscure. Further work to explore the burst effect is currently in progress, and further results will be reported as they become available.

REFERENCES

1. R. H. Barnes and D. N. Sunderman, Apparatus for the Study of Fission-Gas Release from Fuels During Postirradiation Heating at Temperatures up to 1600°C, AEC Report BMI-1453, Battelle Memorial Institute, July 1960.

2. R. H. Barnes, M. Kangilaski, J. B. Melehan, and F. A. Rough, Xenon Diffusion in Single-Crystal and Sintered UO_2, AEC Report BMI-1533, Battelle Memorial Institute, August 1961.

3. Y. Oishi and W. D. Kingery, Self Diffusion in Single Crystal and Polycrystalline Aluminum Oxide, J. Chem. Phys. 33, p. 480 (Aug. 1960).

4. J. N. Gregory and S. Moorbath, The Diffusion of Thoron in Solids, Trans. Faraday Society 47, p. 844 (1951).

TABLE I. SUMMARY OF DIFFUSION COEFFICIENT MEASUREMENTS FOR Xe^{133} IN SINGLE-CRYSTAL α-ALUMINA

Run	Temp, C	Irradiation Details: Thermal-Neutron Flux, nv	Irradiation Details: Time, hr	Number of Spheres Heated	Alpha Contamination on Spheres, counts per minute per sphere[a]	Maximum Concentration of Oxygen in Helium Carrier Gas, ppm	Time Between End of Irradiation and Beginning of Diffusion Measurement, min	Number of Xe^{133} Atoms in Spheres[b]	Heating Time, min	Fraction of Xe^{133} Released in Initial Burst	Total Fraction of Xe^{133} Released	Diffusion Coefficient, cm^2 per sec
21A	1300	1.7×10^{13}	10	3	0.5	4.9	7,771	1.12×10^{10}	240	8.0×10^{-3}	1.95×10^{-2}	1.30×10^{-15}
21B	1495					4.1	9,120	9.96×10^{9}	300	4.0×10^{-2}	7.00×10^{-2}	6.95×10^{-15}
22A	807	"	"	8	20	3.9	16,215	1.18×10^{10}	240	5.0×10^{-4}	6.42×10^{-4}	1.39×10^{-19}
22B	1001					3.6	17,615	1.15×10^{10}	265	3.8×10^{-3}	5.33×10^{-3}	2.45×10^{-17}
22C	1195					3.9	19,020	1.11×10^{10}	300	3.0×10^{-3}	9.13×10^{-3}	3.21×10^{-16}
22D	1398					4.3	20,450	9.52×10^{9}	300	4.0×10^{-2}	4.10×10^{-2}	1.19×10^{-14}
23A	1000	"	"	6	11	4.3	24,915	3.67×10^{9}	300	7.3×10^{-4}	3.94×10^{-3}	6.95×10^{-17}
23B	1205					3.9	26,370	4.88×10^{9}	300	1.0×10^{-3}	6.92×10^{-3}	2.10×10^{-16}
23C	1401					3.9	28,775	3.99×10^{9}	300	6.0×10^{-3}	4.00×10^{-2}	1.03×10^{-14}
24A	1210	"	"	4	6	3.9	29,235	1.98×10^{9}	300	6.0×10^{-3}	1.03×10^{-2}	1.49×10^{-16}
24B	1398					4.1	30,675	1.84×10^{9}	300	5.0×10^{-3}	3.90×10^{-2}	9.05×10^{-15}
24C	1547					4.1	35,010	1.43×10^{9}	300	7.0×10^{-3}	4.73×10^{-2}	3.60×10^{-14} (c)
25A	1400	"	"	4	2.5	3.9	36,435	1.17×10^{9}	300	2.5×10^{-2}	4.67×10^{-2}	3.94×10^{-15}
25B	1555					3.9	37,890	1.00×10^{9}	304	5.0×10^{-3}	4.85×10^{-2}	1.53×10^{-14} (c)
30A	699	6.0×10^{12}	13.5	7	0	4.3	12,485	7.25×10^{9}	180	0	6.48×10^{-4}	7.90×10^{-18}
30B	905					4.5	13,915	7.45×10^{9}	180	5.0×10^{-4}	1.20×10^{-3}	1.17×10^{-17}
30C	1108					4.5	15,370	6.41×10^{9}	303	5.0×10^{-4}	4.04×10^{-3}	1.46×10^{-16}
31	1507	"	"	5	0	4.3	16,805	4.13×10^{9}	360	5.0×10^{-2}	6.05×10^{-2}	7.58×10^{-15}
40A	703	6.6×10^{12}	12.5	12	< 8	7.6	8,302	3.80×10^{10}	325	3.4×10^{-3}	4.36×10^{-3}	6.31×10^{-18}
40B	898					10.1	9,607	3.50×10^{10}	325	6.0×10^{-4}	2.25×10^{-3}	1.39×10^{-17}
40C	1101					9.9	11,082	2.74×10^{10}	325	4.0×10^{-3}	8.55×10^{-3}	1.18×10^{-16}

(a) Counting efficiency is probably about 30 per cent.

(b) Determined by analysis of 1.6-Mev La^{140} photopeak.

(c) Estimated from f vs $\sqrt{t}$ plot of data.

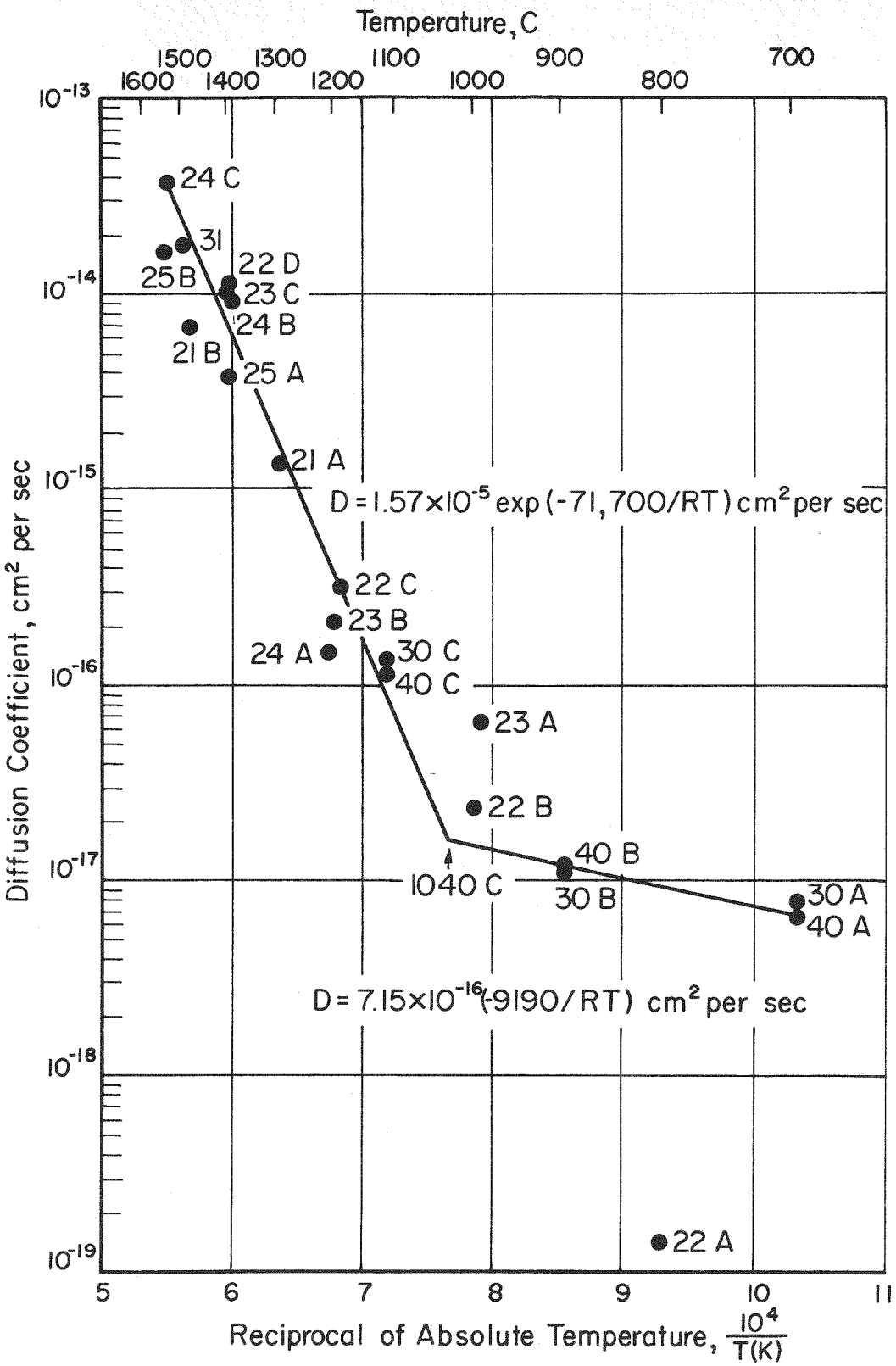

FIGURE 2. DIFFUSION COEFFICIENTS FOR XERON-133 IN SINGLE-CRYSTAL ALPHA ALUMINA

N-83305

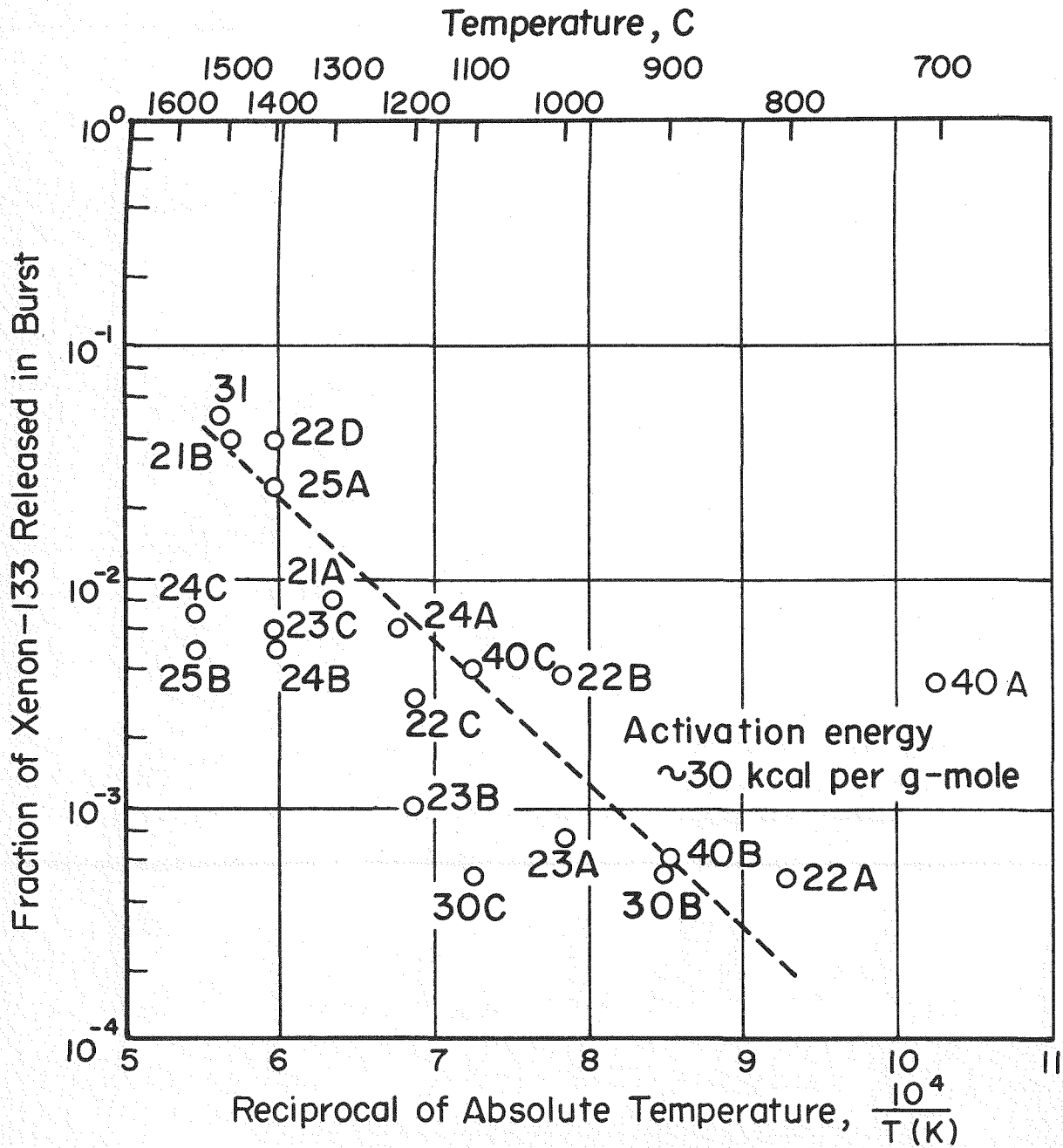

FIGURE 3. INITIAL BURST AS A FUNCTION OF TEMPERATURE

N-83306

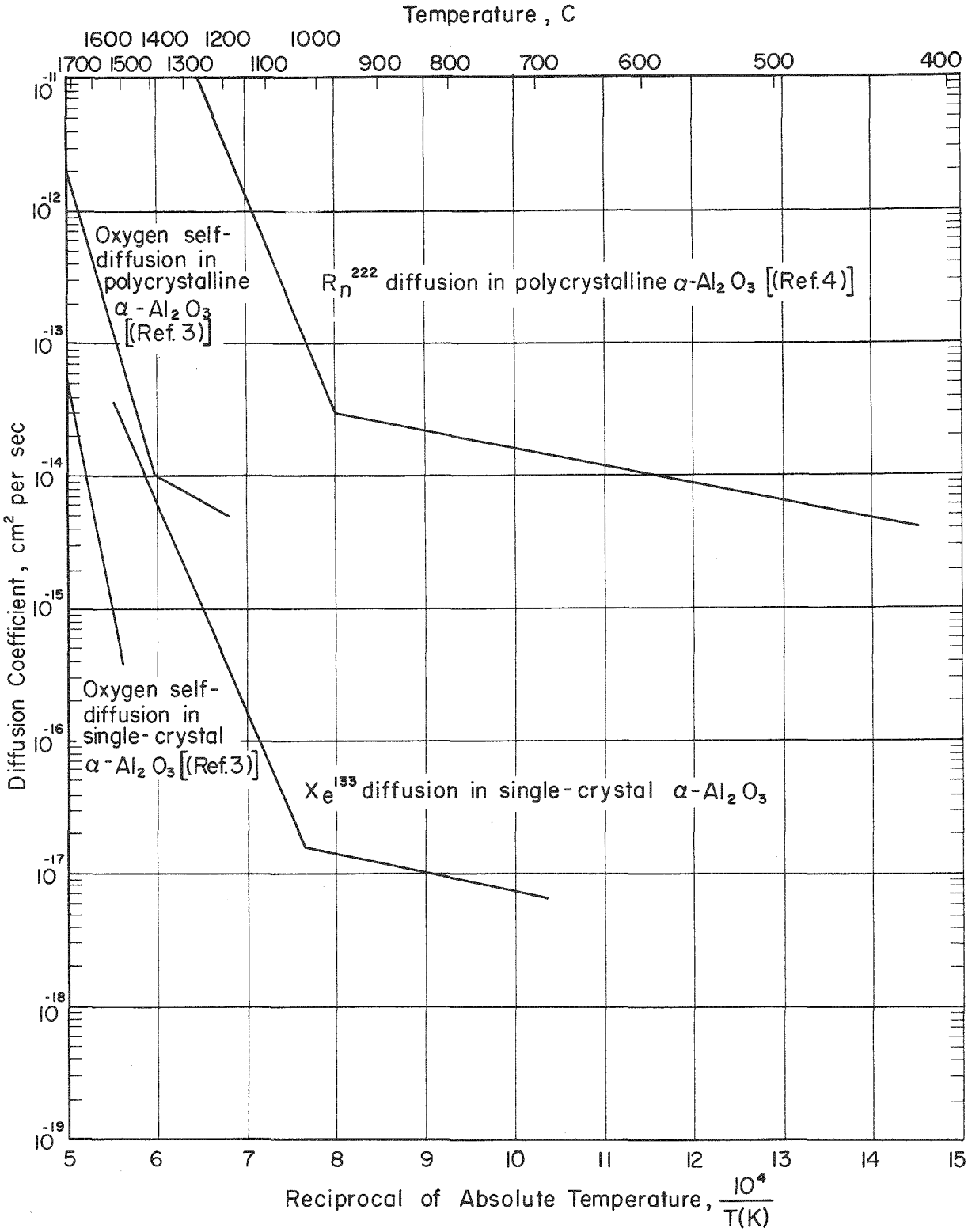

FIGURE 4. DIFFUSION OF VARIOUS SPECIES IN ALPHA ALUMINA α-Al_2O_3

N-83307

MEASUREMENT OF HELIUM GENERATION AND RELEASE IN IRRADIATED BeO[a]

Frank F. Felber, Jr.

Pratt and Whitney Aircraft Hot Cell Facility
Middletown, Connecticut

INTRODUCTION

Much has been written about the production and release of fission gases from irradiated fuel materials. However, measurements of helium generation and release from a variety of fuel, control, moderator, and structural material have not been very extensive. Determination of the quantity of helium released from a test sample may readily be accomplished by mass spectrometer analysis of the gas evolved when the specimen is irradiated in a gas tight container. The total helium production may sometimes be determined by calculation, with a knowledge of the neutron flux and the nuclear constants involved. In boron-containing materials, the helium generation may be related to a measured burn-up. In general, however, the neutron spectrum or the nuclear constants are not well known enough to permit even a reasonably accurate calculation. It is then necessary to make the determination analytically by destroying the sample and recovering the gas quantitatively. Samples which have low enough melting temperatures can usually be handled by vacuum fusion techniques. However, refractory materials such as BeO, which have very high melting points, cannot easily be analyzed by a fusion method. One must then resort to estimating the amount of gas remaining in the sample by extrapolating a diffusion anneal curve to infinite time.

Another technique which, to the author's knowledge, has not been used extensively is that of total sample dissolution in a closed system. Although the method was developed for remote measurement of helium generation in irradiated BeO, it may be applied to a great variety of materials, including irradiated fuels. This paper, therefore, describes the apparatus, techniques, and results of measurements of the fractional helium release from pressed and sintered BeO pellets. A discussion of the extension of the measurement technique to other systems is also included.

---

[a]Work performed under AEC Contract AT(30-1)-2789.

EXPERIMENTAL PROCEDURE

A bundle consisting of nineteen specimens of BeO, each nominally one inch long and one-eighth inch in diameter, was irradiated in the Engineering Testing Reactor. The specimens, which were encapsulated in an argon atmosphere in sealed tubes, were among a group of others tested in a Pratt and Whitney Aircraft In-Pile Forced Convection Loop. The irradiation lasted 728 hours at 175 Megawatts, during which time the tubes were immersed in NaK at a bulk temperature of about 1575°F.

After disassembling the loop, the specimens were recovered and vented in the apparatus shown schematically in Figure 1. The venting apparatus is an improved version of one which has been described elsewhere.[1] The tubes were held in a specially designed vise which positioned them under the drill in the evacuated vent rig. The drill entered the rig through a Wilson Seal. A leak rate of less than two micron-liters per 1000 seconds was attained while venting. The venting operation was timed so that the appropriate leakage correction could be made. The net amount of gas released from the specimen was usually greater than 30 micron-liters, making the leak rate correction small compared with the sample size.

A Todd McLeod type gauge connected directly to the calibrated vent rig volume served as the pressure measuring device. After making the measurement, the gas was transferred quantitatively to a 100 cc sample bulb using the diffusion pump and the Toepler pump. Mass spectrometer analysis of the sample served to identify the contents and indicate the amounts present. A typical analysis showed the presence of variable but low concentrations of hydrogen, methane, air, carbon dioxide, and higher molecular weight compounds, thought to be pump fluids or stopcock grease decomposition products. Periodic simulated vents using pure argon and helium revealed the above constituents to be inherent background in the venting system. Helium was not found in simulated vents with argon, although the reverse was true. A Consolidated Electrodynamics Corporation Model 21-620A Mass Spectrometer was used for the analysis. The instrument was provided with a D.C. preamplifier to maximize the sensitivity, and was also modified to handle low pressure samples. The modification consisted of the following:

1. The three liter expansion tank was valved off to minimize the pressure reduction when the sample was introduced into the spectrometer. This reduced the inlet volume to about 450 cc.

2. A small tilting McLeod gauge was connected in place of the manometer to measure the low (10-1000 microns) input pressures. The tilting McLeod gauge has since been replaced with a CEC micromanometer attachment which provides a more accurate pressure measurement.

The determination of the amount of gas remaining in the BeO was made by dissolving a weighed sample in the closed system apparatus shown schematically in Figure 2. A 1:1 mixture of concentrated sulfuric and phosphoric acids was used as the solvent. Figure 3 shows the dissolver system as installed in the hot cell. The operation of the system was as follows. The dissolver flask was pumped out up to stopcock 3 and flushed several times with argon. This

SCHEMATIC OF VENT RIG AND GAS COLLECTION APPARATUS

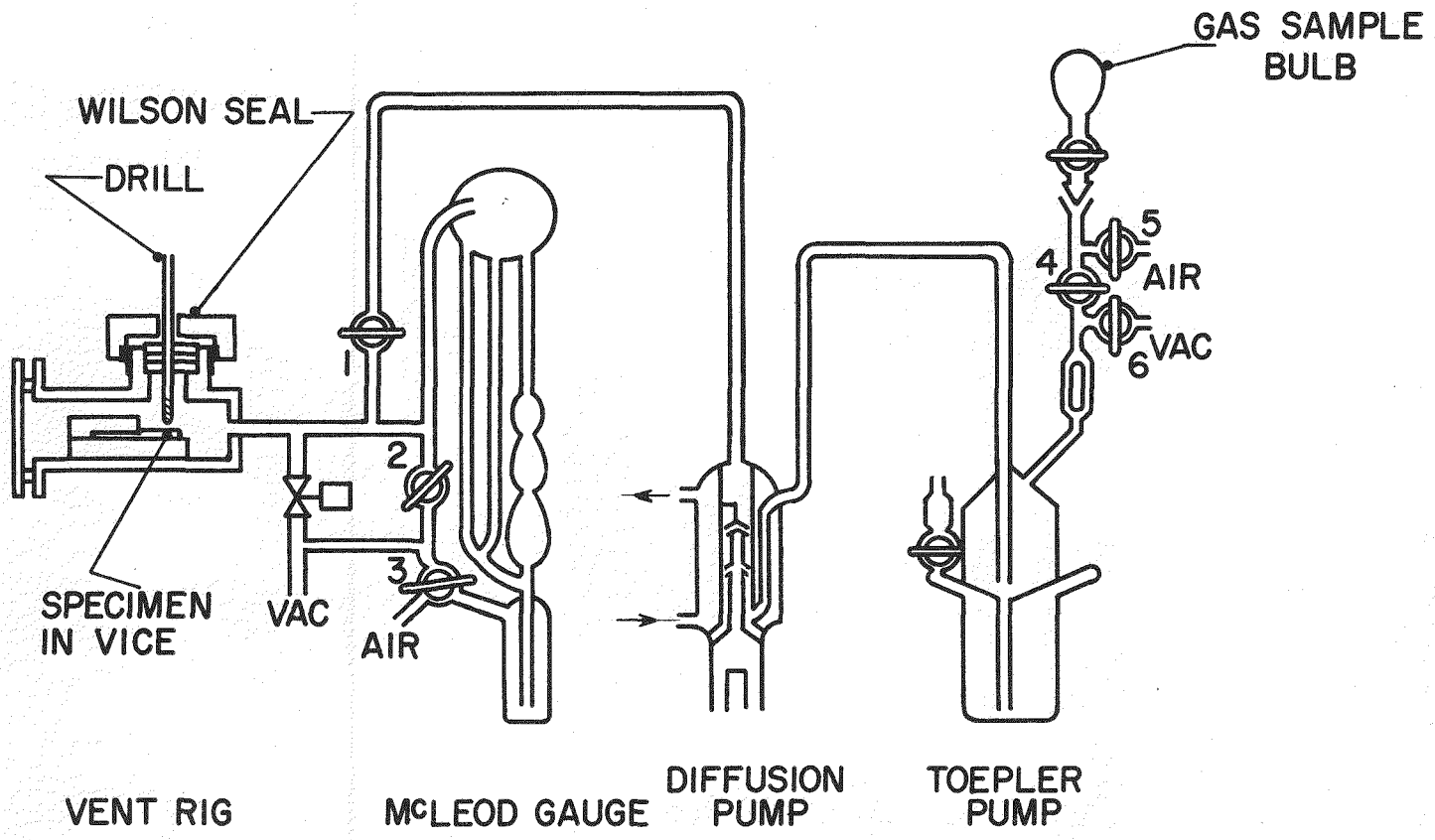

FIGURE I

SCHEMATIC OF CLOSED SYSTEM DISSOLUTION APPARATUS

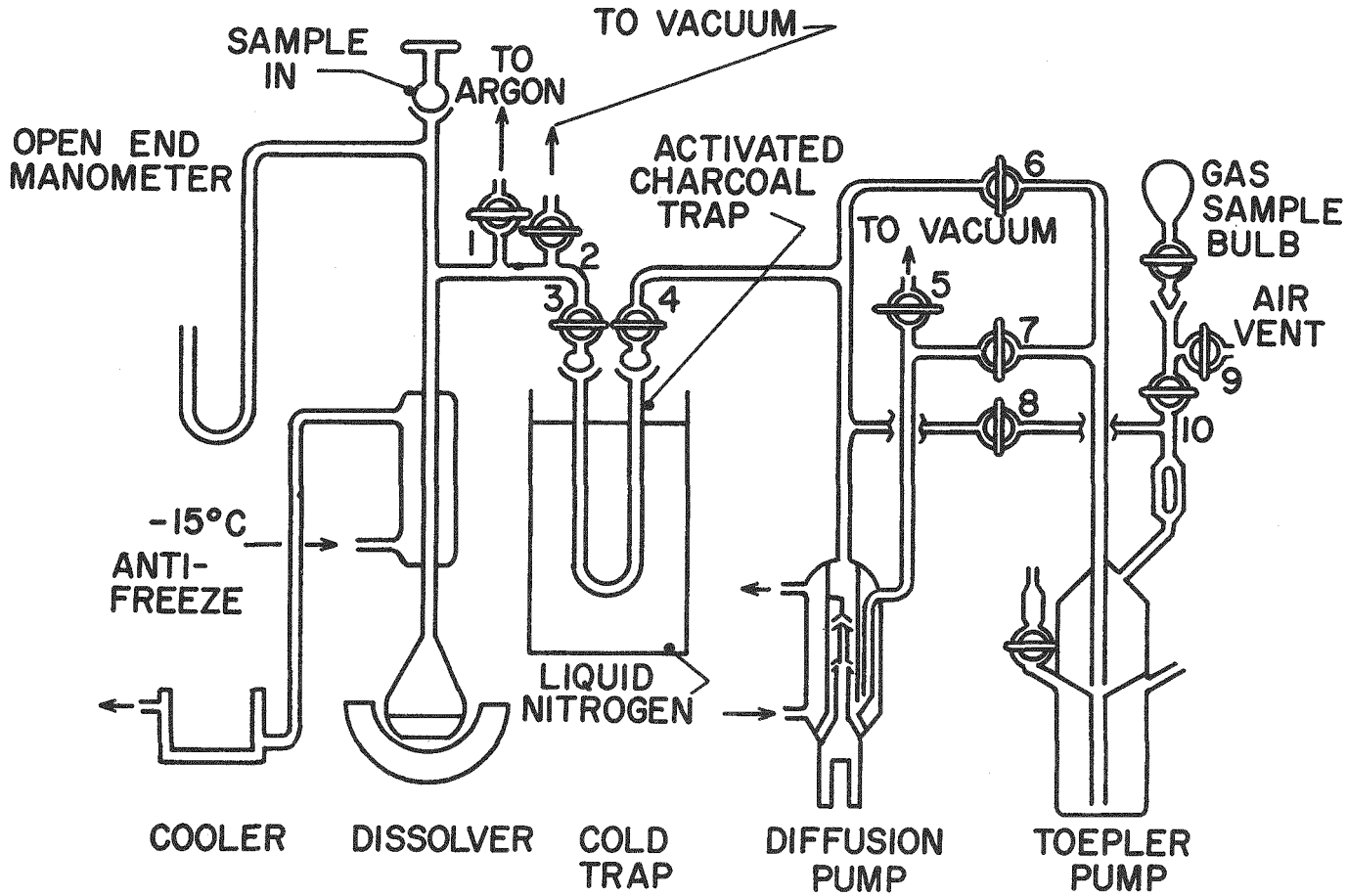

FIGURE 2

DISSOLUTION APPARATUS SHOWN IN HOT CELL

FIGURE 3

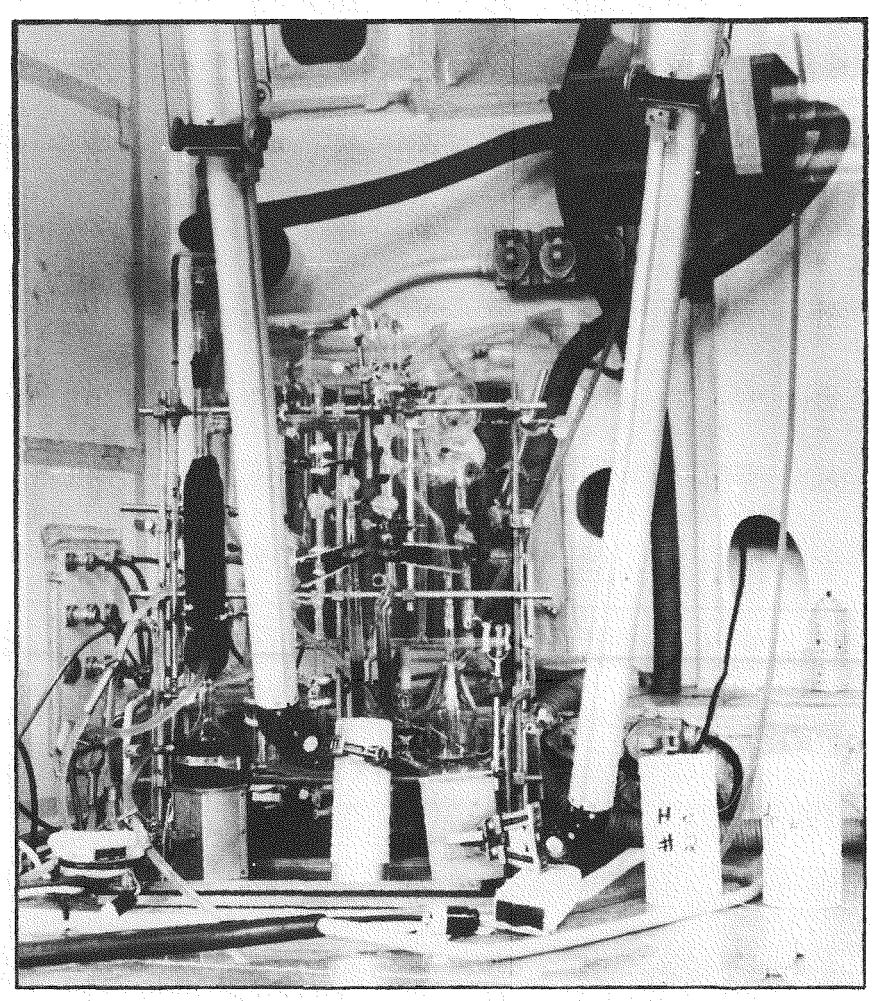

was necessary since the air system contained enough helium to seriously alter the results. The ball-and-socket joint at the top of the dissolver flask was removed and argon flow maintained while the solvent was added. The sample was dropped in, the argon flow cut off, and the ball-and-socket joint closed. This method of sample introduction was acceptable because of the slow rate of dissolution of the BeO. After pumping out the system to about 0.5 atmosphere, the acid was heated to boiling, bringing the total pressure to about one atmosphere. If the pressure was too low, it could be increased by bleeding in argon through stopcock 1. Excessive pressure was bled through stopcock 3 into the charcoal trap, which had previously been baked out and evacuated.

Refluxing for 4-12 hours was required to dissolve a typical BeO pellet. Although it was not necessary to maintain the condenser at -15°C for the BeO dissolution, the system was designed for low temperature operation to permit utilization of nitric acid in the solvent mixture. The nitric acid would be needed for oxidizable fuel samples or for metallic beryllium samples.

When the sample was dissolved, the heating mantle was removed and the solution cooled to room temperature. The cooler, filled with anti-freeze, was put in the place of the heating mantle. After a few minutes the acid was below 0°C and the charcoal trap (precooled in a liquid nitrogen bath) was opened to pump out the dissolver. Cooling was necessary to prevent pumping the acid vapors into the charcoal. The downstream side of the trap was opened and the helium (plus any hydrogen formed) was selectively and quantitatively transferred with the diffusion pump and Toepler pump into the sample bulb. The bulb was then removed from the cell to the analytical laboratory and analyzed in the mass spectrometer. The analysis usually showed the argon content to be two or three orders of magnitude less than the helium. Initially there was 10^4 times more argon than helium. This corresponds to a helium-argon separation factor of about 10^6 to 10^7, certainly adequate for the determination.

To ready the system for the next run, the acid was siphoned out of the dissolver flask and the flask rinsed first with water and then with the solvent acid mixture.

RESULTS

The results of the venting and dissolution experiments are shown in Table I. The first three columns give, respectively, the sample number, percent purity, and percent of theoretical density. The fourth column indicates the number of gram atoms of helium released per gram of BeO. Analysis of as-fabricated control samples vented in the same system as the irradiated ones verified that the specimen cover gas was pure argon. Six of the samples were analyzed before modifying the mass spectrometer to handle low pressure samples, and were lost as a result.

Column five shows, for the three samples analyzed, the measured amount of helium generated in the BeO per gram of the material. The samples, which were chosen at random, gave identical results, within about a five percent precision. Since the samples were irradiated in a bundle and since the total volume of of reactor space occupied by the specimens was small, it was concluded that the helium generation was constant throughout the bundle. This conclusion is consistent with the assumption that the ETR fast flux could be considered constant over the one inch diameter by one inch high volume of the bundle. Two

TABLE I

HELIUM PRODUCTION AND RELEASE IN BeO

Sample Number	Percent Purity	Percent Density	He Released[a]	He Produced[a]	Percent He Released
NB 4	94	93	10.8×10^{-8}		2.5
NB 5	94	93	Lost		
NB 6	94	93	5.4×10^{-8}	4.4×10^{-6}	1.2
NB 7	94	93	3.3×10^{-8}		0.8
NB 1	92	94	9.4×10^{-8}		2.1
NB 2	92	94	8.7×10^{-8}		2.0
NB 3	92	94	5.5×10^{-8}	4.4×10^{-6}	1.2
B 8	99	96	6.1×10^{-8}		1.4
B 9	99	96	Lost		
B 10	99	96	6.4×10^{-8}		1.5
B 11	99	96	Lost		
B 12	99	96	9.1×10^{-8}		2.1
B 17	99	97	5.6×10^{-8}		1.3
B 18	99	97	2.5×10^{-8}		0.6
B 19	99	97	6.3×10^{-8}		1.4
C 13	99	98	Lost		
C 14	99	98	1.1×10^{-8}		0.3
C 15	99	98	Lost		
C 16	99	98	Lost	4.4×10^{-6}	

[a]Helium produced and released is expressed in gram atoms per gram of BeO.

control samples were dissolved and analyzed to determine whether any helium was present prior to irradiation. The results showed that the control specimens contained less than 5×10^{-10} gram atoms of helium per gram of unirradiated BeO. This is equivalent to about 0.01 percent of the total helium produced, and represents a negligible error.

The last column of Table I shows the percent helium released from the samples. There is no indication in the table of any clear correlation of percent release with either density or purity. However, the high density, high purity samples do exhibit a slightly lower gas release, as is expected. In any case, the results show that, for temperatures up to 1600°F and irradiation times of the order of 700 hours, it is necessary to allow for about one to two percent helium release from BeO of greater than 92 percent purity and 93 percent density. Furthermore, the lack of a definite correlation between release and density or purity indicates that somewhat poorer grades of BeO might also have a 98 percent helium retention factor.

APPLICATION TO OTHER TYPES OF SAMPLES

The closed system dissolution process described above covered only the technique of dissolving samples which do not react with the solvent and liberate gaseous products. It is fortuitous that the reaction products of nitric and sulfuric acids, the two most common solvent acids, are liquid at -15°C. Because of this, excessive pressure buildup due to the liberation of NO_2 or SO_2 can be virtually eliminated. To test this hypothesis, approximately one gram of copper metal was dissolved in nitric acid in a closed system of about 250 cc volume. The total increase in pressure if the NO_2 were not condensable if the reaction proceded to completion would have been about three atmospheres(45 psi). The actual increase, as measured with the open end mercury manometer connected to the system, was in the range of 1 to 1.5 psi, well within the capability of the glass apparatus. During the test, the condenser coolant temperature was maintained at -15°C. The weight of copper used in the test liberated an amount of NO_2 equivalent to about 8 grams of an average fuel sample, a much larger size sample than would ordinarily be used. The experiment was repeated with a HNO_3-H_2SO_4 mixture, with essentially the same results.

The principal difficulty with the method arises when the gas in the dissolver flask is pumped through the cryogenic charcoal trap. Large amounts of condensable gases can cause plugging in the trap. However, if the trap is sized so that the amount of charcoal is great compared with the amount of gas to be trapped, and if the openings are kept sufficiently large, this difficulty will be overcome. A 22 millimeter OD U-tube filled with a total length of about 10 inches of 6-14 mesh charcoal was found to be adequate for the equivalent of about 0.25 gram of an average fuel sample.

Another important aspect to be considered when trapping NO_2 and SO_2 is that of removing these gases after the experiment is over. Pumping can cause trouble because of the difficulty of outgassing the charcoal, and because these vapors will corrode the pump parts. For this reason, it is necessary to design the trap so it can be removed from the system and replaced with fresh charcoal after each run. The gases are then carried away in the hot cell ventilation system, in which they are diluted considerably.

Several samples of irradiated fuels having fission burnups in excess of five percent have been analysed by use of the apparatus. It has been demonstrated by these runs that the system will work with irradiated fuel samples with a sensitivity of about 10^{-7} gram atoms of helium per sample. It is believed that this sensitivity can be increased by at least an order of magnitude with some minor adjustments in the ionization current of the mass spectrometer.

Thus, the method described herein is generally applicable if the following criteria are met:

1. A suitable solvent can be found for the sample.

2. The dissolution reaction products are condensable at reflux column operating temperatures.

ACKNOWLEDGEMENTS

The author wishes to express his gratitude to Mr. Vernon Van Sickel and Mr. Donald Farmelo for developing and performing, respectively, the procedures for the mass spectrometer analysis and the closed system dissolution. Thanks are also due to the Hot Laboratory Engineering Staff for design, construction, and operation of the vent rigs.

REFERENCES

1. C. E. Cunniff, Jr., Hot Machine Shop Cell at Pratt and Whitney Aircraft Hot Cell Facility, Sixth Hot Laboratories and Equipment Conference, Chicago, Illinois, 1958.

IRRADIATION EXPERIMENTS WITH AQUEOUS SUSPENSIONS OF PuO_2 and $ThO_2.UO_2$

By H. S. G. Slooten

N. V. KEMA, Arnhem, The Netherlands

and

R. G. Sowden, B. R. Harder, and A. E. Truswell

U. K. Atomic Energy Authority, Harwell, England

INTRODUCTION

Fissile and fertile oxides in aqueous suspension have been important to several concepts of the homogeneous aqueous reactor. The Oak Ridge National Laboratory's Homogeneous Reactor Project has concentrated its effort on the development of a thoria slurry for use as a fertile blanket surrounding the uranyl sulphate solution core; workers in the KEMA project in the Netherlands are developing a single zone $ThO_2.UO_2$ slurry reactor; general slurry work at Harwell has included studies directed towards the development of a PuO_2 suspension reactor. Other studies in the United States, Canada, and England have been devoted to the complex UO_3 hydrate system as a suspension fuel.

It has been established that the particle size of the solid is of paramount importance: the presence of submicron particles can promote the caking of a slurry, while the presence of large particles (> 10μ) tends to enhance the erosion of container surfaces[1]. These findings led to the development at ORNL of a carefully controlled process which would yield thoria having a narrow range of particle size[2]. Similarly, workers at KEMA have devoted considerable effort to the control of particle size distribution of their UO_2 and $ThO_2.UO_2$ fuel spheres[3,4], the chief motive in their case being to ensure the removal of a large fraction of the fission products by recoil separation from the bulk solid[5]. Studies have been made of the effect of pumping on particle size distribution, and experience has shown, at least for ThO_2, that mechanical degradation is minimized if the solid fuel has been fired to a high temperature, so that each individual particle contains only a few large crystals[6].

The problem of particle integrity in the presence of ionizing radiation, however, has received much less attention, though as long ago as 1944, Hiskey[7] considered that radiation-induced fragmentation might be a major difficulty in the development of an oxide slurry reactor.[a] The tacit optimum which has accompanied the general attitude regarding radiation stability was in part

justified by limited tests with oxide slurries, and by radiation work in other fields. Thus it was found by Krohn and McBride at ORNL[8] that the viscosity of a concentrated ThO_2 slurry underwent no detectable change during in-pile irradiation while, at Harwell, Dawson, et al[9] found that a negligible change was produced in the agglomerate size distribution of a flocculated ThO_2 slurry irradiated under boiling conditions. Furthermore, the experiments of Wait[10] established that single crystals of UO_2 irradiated at a nominal temperature of 65°C to a burnup of 1000 MWD/ton suffered no crystal fragmentation; the only effect was a small lattice dilation, which could be annealed out at higher temperatures.

The work described in this paper originated with experiments at Harwell on the irradiation of dilute suspensions of PuO_2, designed primarily to study the distribution of fission products between the solid surface and the aqueous phase. The production of a green colloidal solution after quite short periods of irradiation revealed that radiation-induced fragmentation of the particles was taking place. An extension of the work then established that this effect persisted with high-fired material, and with $ThO_2.PuO_2$ solid solutions in which the power density was reduced by a factor of thirty[11]. At this stage the work became a collaborative venture between AERE, Harwell and the Reactor Development Group of N. V. KEMA, Arnhem. This paper will present the progress made in attempting to define the factors which control radiation-induced fragmentation. It must be strongly emphasized that most of the work is still at an exploratory stage; the opinions advanced are of a tentative nature only and may well be modified in the light of further experience.

EXPERIMENTAL METHODS

Pile irradiations were carried out in the belt-stringer of the experimental reactor BEPO. The temperature during irradiation was about 80°C and the thermal neutron flux was between 1.1×10^{11} and 1.4×10^{12} n $cm^{-2}sec^{-1}$. The evacuated, sealed silica ampoules (~ 4 ml) containing the slurries were encased in aluminum cans along with a neutron flux monitor of pure cobalt wire. The dose-limiting factor in this type of experiment is the buildup of radiolytic gas within the ampoule: conditions were selected to ensure that this pressure did not exceed 5 atmospheres.

---

[a] "When fission occurs, products of heavy mass are formed, which recoil away from each other in nearly opposite directions. In their path through the crystal . . they will break a large number of U-O bonds, and the particles will be continually tunnelled by their action. Gradually the entire structure may be weakened, and the solid may disintegrate into smaller and smaller fragments."

Some evidence to support Hiskey's pessimism was in fact obtained by Blomeke[17], who found that UO_3 hydrate slurries irradiated at 250° in unstirred autoclaves suffered degradation, and severe caking took place. However, the process was accompanied by transformation of orthorhombic-I rodlets to orthorhombic-II platelets, and comparison with a slurry of a simple unhydrated cubic oxide is not possible.

After a cooling period of a few days (except in selected cases) the ampoules were broken open, and the slurry was centrifuged for 1 min at a nominal maximum of 1000G using an MSE laboratory centrifuge. Aliquots of the supernatant liquid containing the colloidal fragments were then transferred to aluminum traps which were dried and counted using an α-scintillation counter. Plateau determinations showed that it was possible to make an accurate assessment of the α-activity ($\pm$ 5%) despite the fairly high β-γ background due to fission products. Blank experiments were performed to assess the amount of α-activity leached from the solid in the absence of radiation.

In some cases, particularly those where the irradiation was carried out under flocculating conditions, a further test for the presence of dispersible colloidal material was necessary. This was carried out by shaking the dried powder for 2-3 days with a stabilizing solution, after which sampling and counting were performed as before.

Samples of colloid for examination by electron microscopy were removed from an irradiated, centrifuged, suspension by dipping a carbon film supported on a copper grid into the liquid. The oxide samples used in the experiments were as follows:

Ref. No.	Oxide	Surface Area (m^2g^{-1})	Mean Particle Size (micron)	Calcination Temp. in Air (^oC)
1	PuO_2	29	1-2	500
2	PuO_2	3	1-2	900
3	PuO_2	0.3	1-2	1600 (Pellet crushed after sintering)
4	ThO_2.20%UO_2(4% U^{235})	3	5.5 (spheres)	950
5	"	0.2	6 "	1150
6	"	0.2	6 "	1300
7	ThO_2.20%UO_2(20% U^{235})	3	5.5 "	950
8	"	0.2	6 "	1150

The PuO_2 was prepared from the oxalate[12] and $ThO_2.UO_2$ by the 'emulsion-gelation' technique[4].

RESULTS

The results of the irradiation experiments are summarized in Tables I-IV and Figures 1-6. Particular attention has been paid to the effects of surface area of solid, irradiation time (within the limits imposed by radiolytic gas production), power density, and dispersion characteristics of the solid.

At higher levels of breakup, the appearance of the supernate after centrifugation at 1000G was that of a clear solution, colored bright green in the case of the PuO_2 experiments and yellow-brown in the case of the $ThO_2.UO_2$ experiments. The colloidal nature of these solutions was first established by experiments with a high speed centrifuge (Baird and Tatlock, Ltd.) at a nominal

TABLE I
FRAGMENTATION OF PuO_2

Expt. No.	Medium	Weight of Oxide Irradiated (mg)	Irradiation Time (min)	No. of Fissions x 10^{-12}	No. of Atoms in Super-natant liquid x 10^{-15}	No. of Atoms Ejected per Fission = N x 10^{-3}	% Material in Colloidal Form
A.	29 m^2 g^{-1}, Oxide No. 1.						
1	H_2O	3.9	15	7.1	1540	220	18
2	H_2O	4.6	15	8.4	2030	240	20
3	H_2O	5.2	15	9.3	1850	200	16
4	10^{-2} M HNO_3	4.0	15	7.3	1490	200	17
5	H_2O	5.5	15	10.0	2150	220	18
6	H_2O	5.4	30	19.7	4070	210	34
7	H_2O	6.2	30	22.6	6690	290	49
8	H_2O	5.1	30	18.6	4150	220	37
9	10^{-2} M HNO_3	4.6	30	16.8	5280	310	52
10	10^{-1} M HNO_3	6.1	30	22.3	610	27	4.5
11	H_2O	4.9	75	44.5	3800	85	35
12	H_2O	4.0	115	56.0	3450	62	40
13	H_2O	5.0	120	73.0	4780	65	56
B.	3 m^2g^{-1}; Oxide No. 2						
14	H_2O	4.0	15	7.3	15	2	0.17
15	H_2O	6.2	15	11.3	32	3	0.24
16	H_2O	4.9	30	17.9	12	0.7	0.11
17	H_2O	5.0	30	18.2	257	14	2.4
18	10^{-2} M HNO_3	6.3	30	23.0	602	26	4.4
19	H_2O	5.0	76	46.3	137	3	12.5
20	H_2O	4.8	120	70.0	235	33	22
21	H_2O	5.2	120	76.0	241	32	21
22	H_2O	2.6	240	76.0	209	28	37
C.	0.3 m^2g^{-1}; Oxide No. 3.						
23	H_2O	5.8	15	10.6	1.3	0.12	0
24	H_2O	4.8	120	70.0	355	5.1	3.2
25	H_2O	4.5	120	66.0	550	9.2	5.6
26	H_2O	3.1	120	45.0	325	7.2	4.8
27	H_2O	3.6	240	10.5	730	6.9	9.2
D.	3 m^2g^{-1}; Oxide No. 2a. (In H_2O).						
28	ThO_2.30W/O PuO_2	3.6	600	36.5	970	27	60
29	ThO_2.3 W/O PuO_2	10.0	4320	236	330	1.4	50

TABLE II

FRAGMENTATION OF ThO_2-20% UO_2 CONTAINING 4% U^{235}

Expt. No.	Medium	Weight of Oxide Irradiated (mg)	Irradiation Time (hr.)	No. of Fissions x 10^{-12}	No. of Atoms in Supernatant Liquid x 10^{-15}	No. of Atoms Ejected per Fission = N x 10^{-3}	% Material in Colloidal Form
A. ~ $3 m^2 g^{-1}$; Oxide No. 4.							
411	10^{-2} M KOH	25	1	4.5	145	32	0.26
434	10^{-2} M KOH	25	1.2	5.4	149	27	0.27
431	10^{-2} M KOH	25	2.5	11.2	395	35	0.7
432	10^{-2} M KOH	25	3.8	17.1	930	54	1.7
402	10^{-2} M KOH	25	4	18.0	1440	80	2.6
404	10^{-2} M KOH	25	4	18.0	1360	75	2.4
428	10^{-2} M KOH	10	12	21.6	1130	52	5.0
424	10^{-2} M KOH	5	36	32.4	2820	87	25
418	10^{-2} M KOH	2.5	96	43.1	690	16	12
419	10^{-2} M KOH	2.5	200	90.0	435	5	7.8
B. ~ 0.2 $m^2 g^{-1}$; Oxide No. 5.							
408	10^{-2} M KOH	25	4	18.0	0	0	0
413	10^{-2} M KOH	25	4	18.0	32	1.8	0.06
429	10^{-2} M KOH	10	12	21.6	30	1.4	0.1
436	10^{-2} M KOH	10	12	21.6	32	1.5	0.2
438	10^{-2} M KOH	10	24	43.2	108	2.5	0.5
425	10^{-3} M KOH	5	36	32.3	55	1.7	0.5
420	10^{-2} M KOH	2.5	96	43.1	158	3.7	2.8
440	10^{-2} M KOH	2.5	96	43.1	191	4.4	3.4
421	10^{-2} M KOH	2.5	200	90.0	280	3.1	5.0
C. ~ 0.2 m^2 g^{-1}; Oxide No. 6.							
406	10^{-2} KOH	25	4	18.0	30	1.7	0.05
415	10^{-2} KOH	25	4	18.0	0	0	0
430	10^{-2} KOH	10	12	21.6	37	1.7	0.17
437	10^{-2} KOH	10	12	21.6	44	2.0	0.20
439	10^{-2} KOH	10	24	43.2	124	2.9	0.55
426	10^{-3} KOH	5	36	32.3	0	0	0
422	10^{-2} KOH	2.5	96	43.1	145	3.4	2.6
441	10^{-2} KOH	2.5	96	43.1	170	4.0	3.0
423	10^{-2} KOH	2.5	200	90.0	415	4.6	7.5

TABLE III

FRAGMENTATION OF ThO_2-20% UO_2 CONTAINING 20% U^{235} (OXIDE NO. 7) ~ $3m^2g^{-1}$

Expt. No.	Medium (pH)	Weight of Oxide Irradiated (mg)		Irradiation Time (min)	No. of Fissions x 10^{-12}	No. of Atoms in Supernatant Liquid = N x 10^{-15}	No. of Atoms Ejected per Fission = N x 10^{-3}	% Material in Colloidal Form
101	10^{-2} M KOH;	12.5	25	1	22.5	315	14	0.6
121	10^{-2} M KOH;	12.5	25	1	22.5	520	23	0.9
104	10^{-2} M KOH;	12.5	10	4	36.0	1400	39	6.2
151	10^{-2} M KOH;	12.5	10	6	54.0	1040	19	4.6
103	10^{-2} M KOH;	12.5	5	8	36.0	1640	45	14.5
105	10^{-2} M KOH;	12.5	4	12	43.2	3170	73	35.0
102	10^{-2} M KOH;	12.5	2	30	54.0	1355	25	30.0
170	10^{-3} M KOH;	11.2	6	10	54.0	4140	77	18.0
152	10^{-4} M KOH;	10.2	6	10	54.0	4580	85	20.0
113	H_2O;	8.1	4	10	36.0	500	1.4	2.2
152	H_2O;	8.1	6	10	54.0	2370	4.4	10.6
155	10^{-5} HNO_3	7.9	6	10	54.0	3650	6.7	16.1
169	$1.2x10^{-5}$ HNO_3;	7.0	6	10	54.0	770	1.4	3.4
154	10^{-4} HNO_3;	5.5	6	10	54.0	3	0	0
168	10^{-4} HNO_3;	5.5	6	10	54.0	330	0.7	1.5
167	$5x10^{-4}$ HNO_3;	4.0	6	10	54.0	3260	6.0	14.5
118	10^{-2} HNO_3;	2.5	10	10	90.0	1110	1.2	5.0

TABLE IV. FRAGMENTATION OF ThO_2-20% UO_2 CONTAINING 20% U^{235} (OXIDE NO. 8) 0.2 m^2/g

Expt. No.	Medium (pH)		Wt. (mg)	Time hrs.	No. of Fissions x 10^{-12}	No. of Atoms in Super-natant x 10^{-15}	No. of Atoms Ejected per Fission N x 10^{-3}	% Material in Colloidal Form	No. of Atoms in Super-natant after leaching x 10^{-15}	N Calculated from Previous Column
106	10^{-2} M KOH	12.5	25	1	22.5	126	5.5	0.2		
122	10^{-2} M KOH	12.5	25	1	22.5	32	1.4	0	33	1.5
131	10^{-2} M KOH	12.5	25	1	22.5	74	3.3	0.1		
107	10^{-2} M KOH	12.5	10	4	36.0	200	5.5	0.9		
143	10^{-2} M KOH	12.5	10	6	54.0	395	7.3	1.8		
108	10^{-2} M KOH	12.5	5	8	36.0	136	3.8	1.2		
109	10^{-2} M KOH	12.5	4	12	43.2	300	6.9	3.3		
110	10^{-2} M KOH	12.5	2	30	54.0	550	10.1	12.0		
142	10^{-3} M KOH	11.2	10	6	54.0	500	9.3	2.2	620	11.4
166	10^{-3} M KOH	11.2	10	6	54.0	545	10.1	2.4		
141	10^{-4} M KOH	10.2	10	6	54.0	42	0.8	0.2	35	0.7
140	10^{-5} M KOH	9.5	10	6	54.0	10	0.2	0.05	34	0.6
117	H_2O	8.1	10	4	36.0	23	0.6	0.1		
124	H_2O	8.1	5	8	36.0	0	0	0	8	0
123	H_2O	8.1	4	16	57.7	0	0	0	8	0
150	10^{-5} HNO_3	7.9	10	6	54.0	40	0.7	0.2	150	2.8
165	10^{-5} HNO_3	7.9	10	6	54.0	0	0	0	15	0.3
164	1.2×10^{-5} HNO_3	7.0	10	6	54.0	0	0	0		
149	10^{-4} HNO_3	5.5	10	6	54.0	0	0	0	72	1.3
163	5×10^{-4} HNO_3	4.0	10	6	54.0	350	6.5	1.6		
114	10^{-2} HNO_3	2.5	10	4	36.0	280	7.8	1.3		
144	10^{-3} M $Th(NO_3)_4$		10	6	54.0	395	7.3	1.8		
145	10^{-4} M $Th(NO_3)_4$		10	6	54.0	164	3.0	0.7		
157	10^{-1} NaCl		10	6	54.0	0	0	0		
158	10^{-2} NaCl		10	6	54.0	0	0	0		
161	10^{-2} KOH + 10^{-1} NaCl		10	6	54.0	0	0	0		
162	10^{-2} KOH + 10^{-2} NaCl		10	6	54.0	25	0.5	0.1		

TABLE IV, continued

Expt. No.	Medium (pH)	Wt. (mg)	Time hrs.	No. of Fissions x 10^{-12}	No. of Atoms in Supernatant x 10^{-15}	No. of Atoms Ejected per Fission N x 10^{-3}	% Material in Colloidal Form	No. of Atoms in Supernatant after leaching x 10^{-15}	N Calculated from Previous Column
159	10^{-2} KOH	12.5	10	6	92.0	811	8.8	3.6	Flux: 1.7 x 10^{11} n $cm^{-2}sec^{-1}$
160	10^{-2} KOH	12.5	10	6	72.0	447	6.2	2.0	Flux: 1.3 x 10^{11} n $cm^{-2}sec^{-1}$

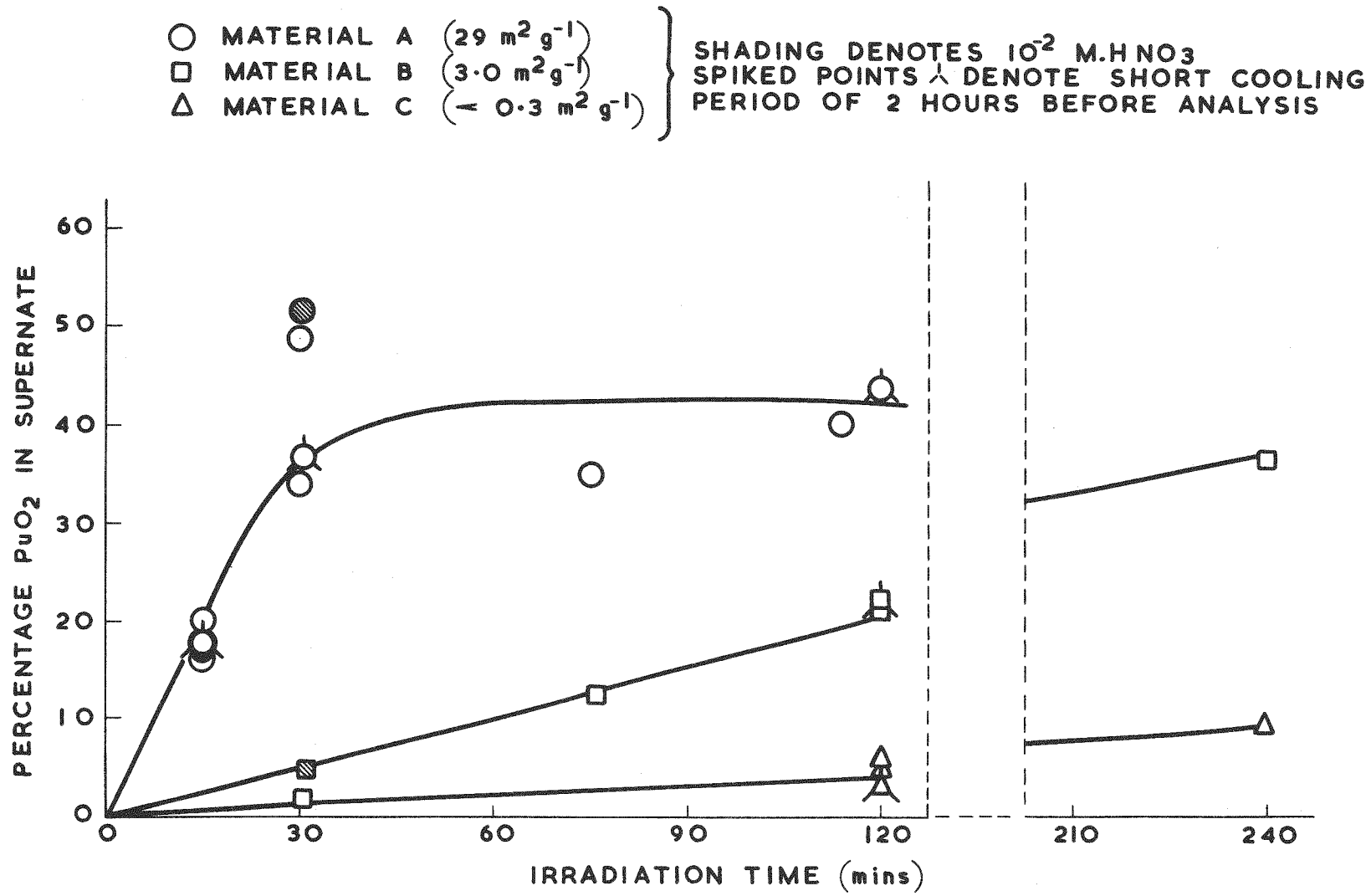

FIG. 1. VARIATION OF PERCENTAGE PuO_2 IN COLLOIDAL FORM WITH IRRADIATION TIME AND SOLID SURFACE AREA.

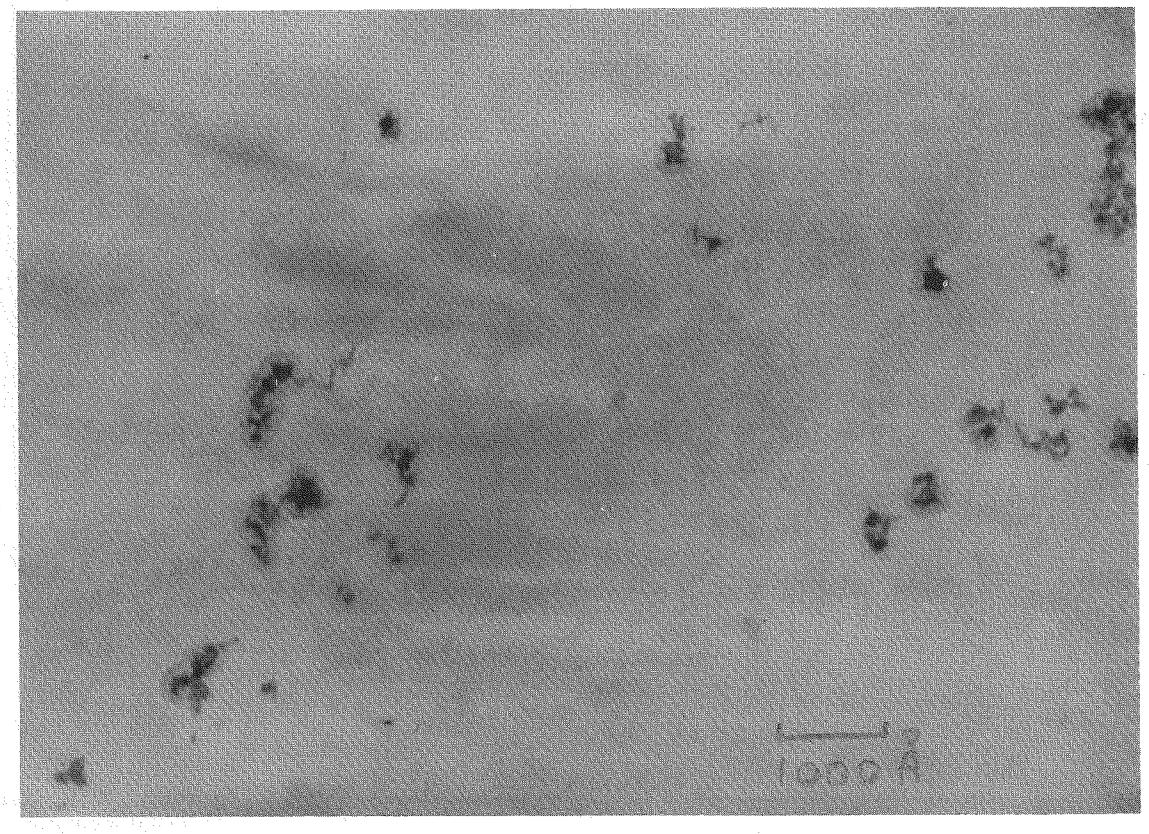

Figure 2.

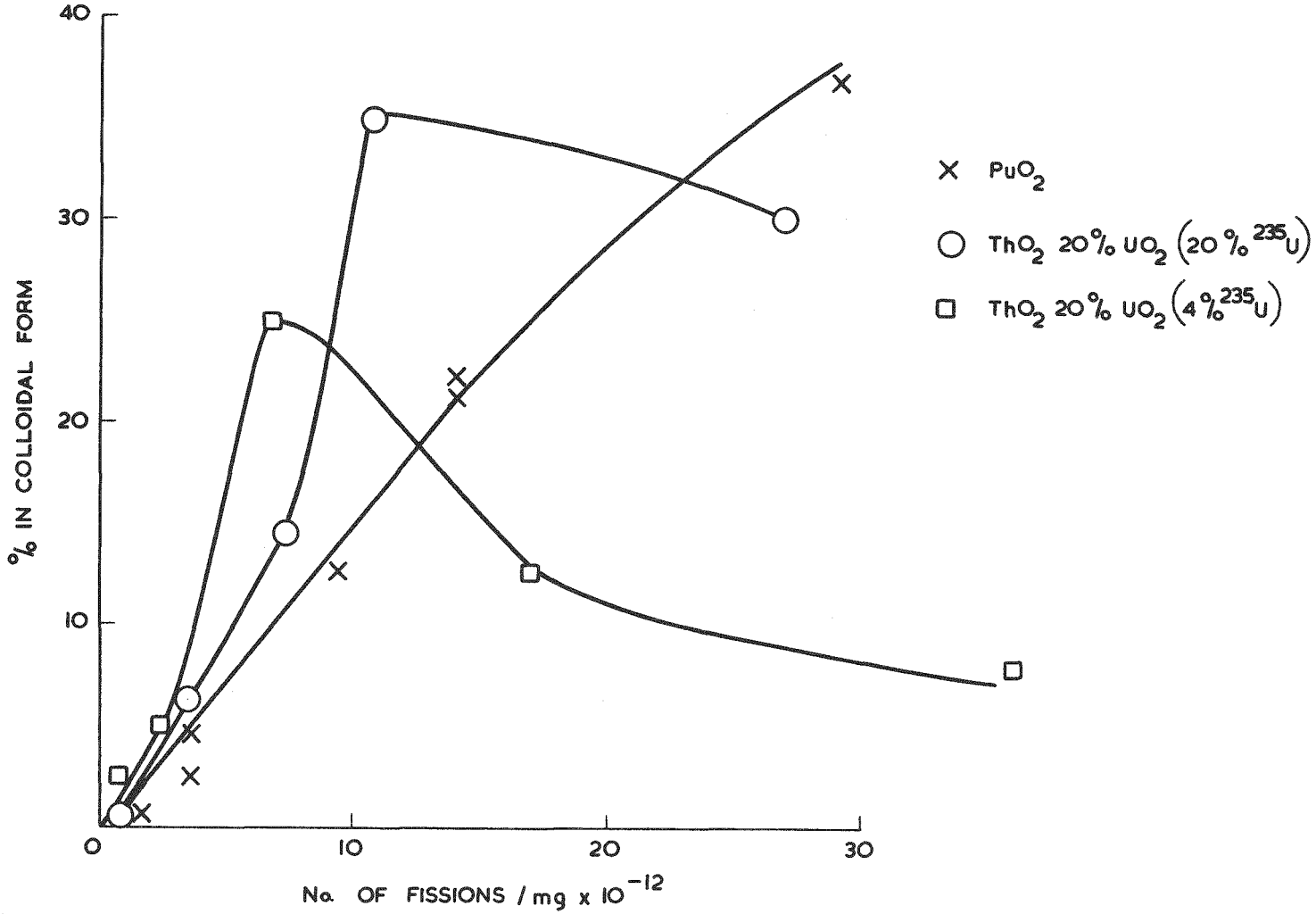

FIG. 3. VARIATION OF PERCENTAGE OF METAL ATOMS IN COLLOIDAL FORM WITH TOTAL DOSE (ALL SOLIDS 3 m^2/g)

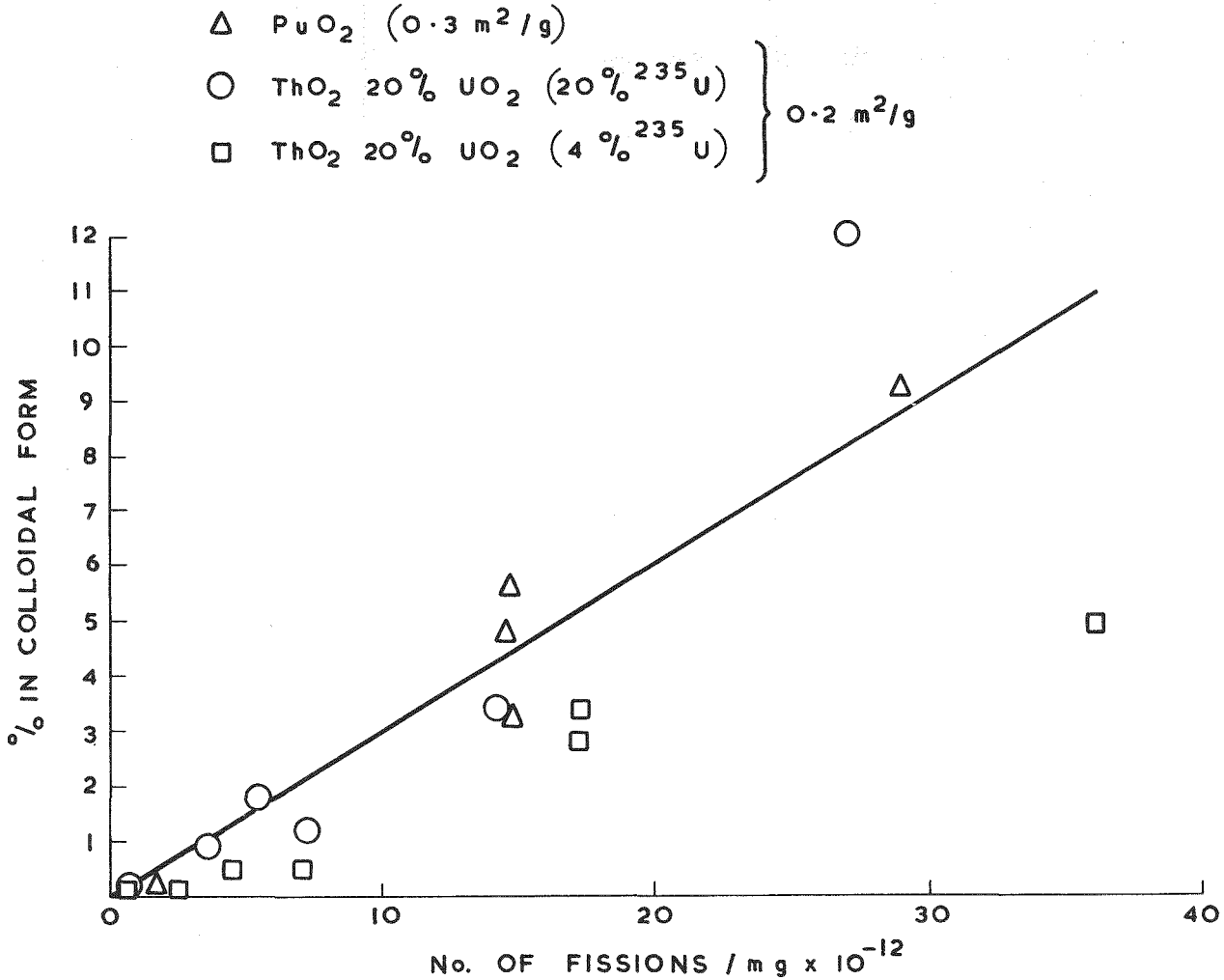

FIG. 4. VARIATION OF PERCENTAGE METAL ATOMS IN COLLOIDAL FORM. WITH TOTAL DOSE (ALL SOLIDS LOW SURFACE AREA.)

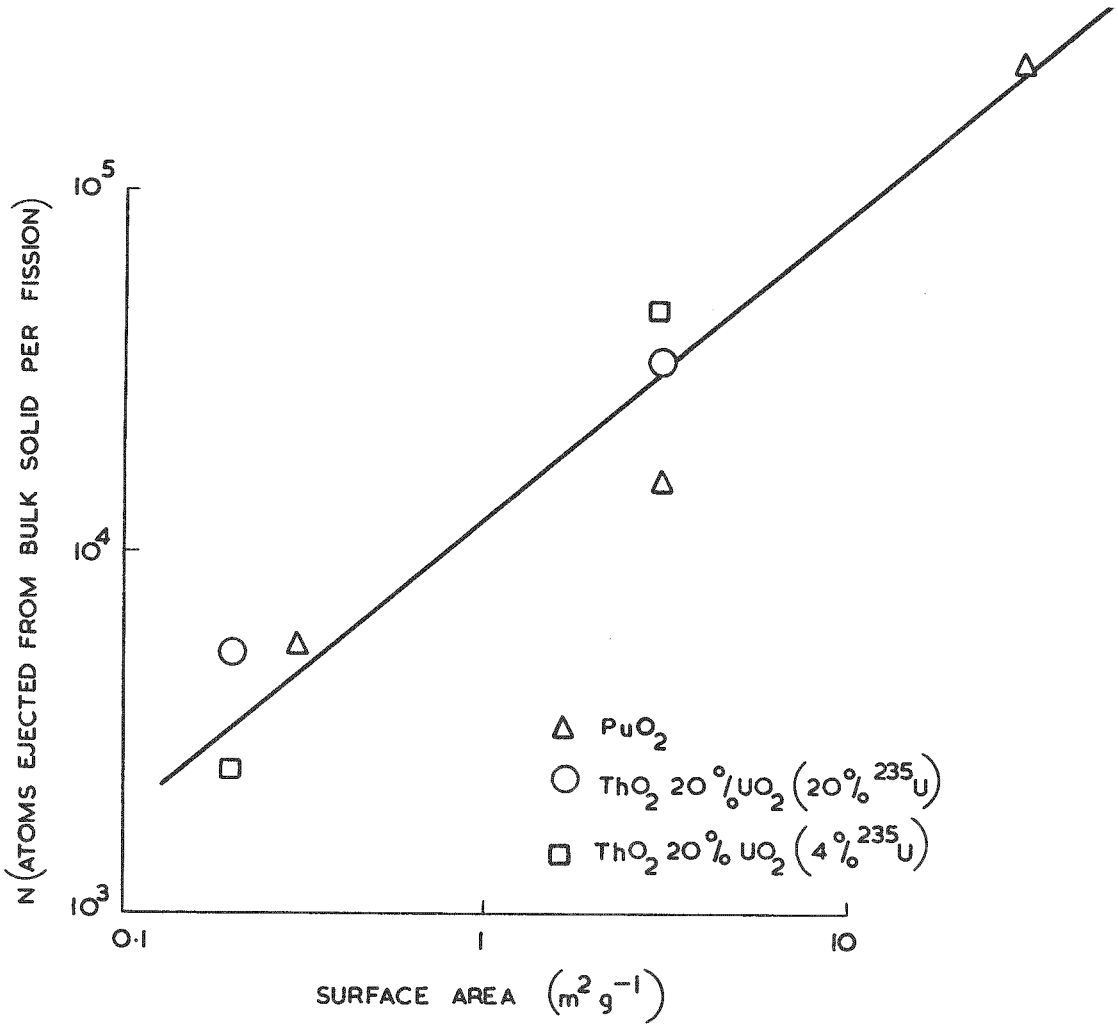

FIG. 5. VARIATION OF INITIAL RATE OF FRAGMENTATION WITH SURFACE AREA OF SOLID.

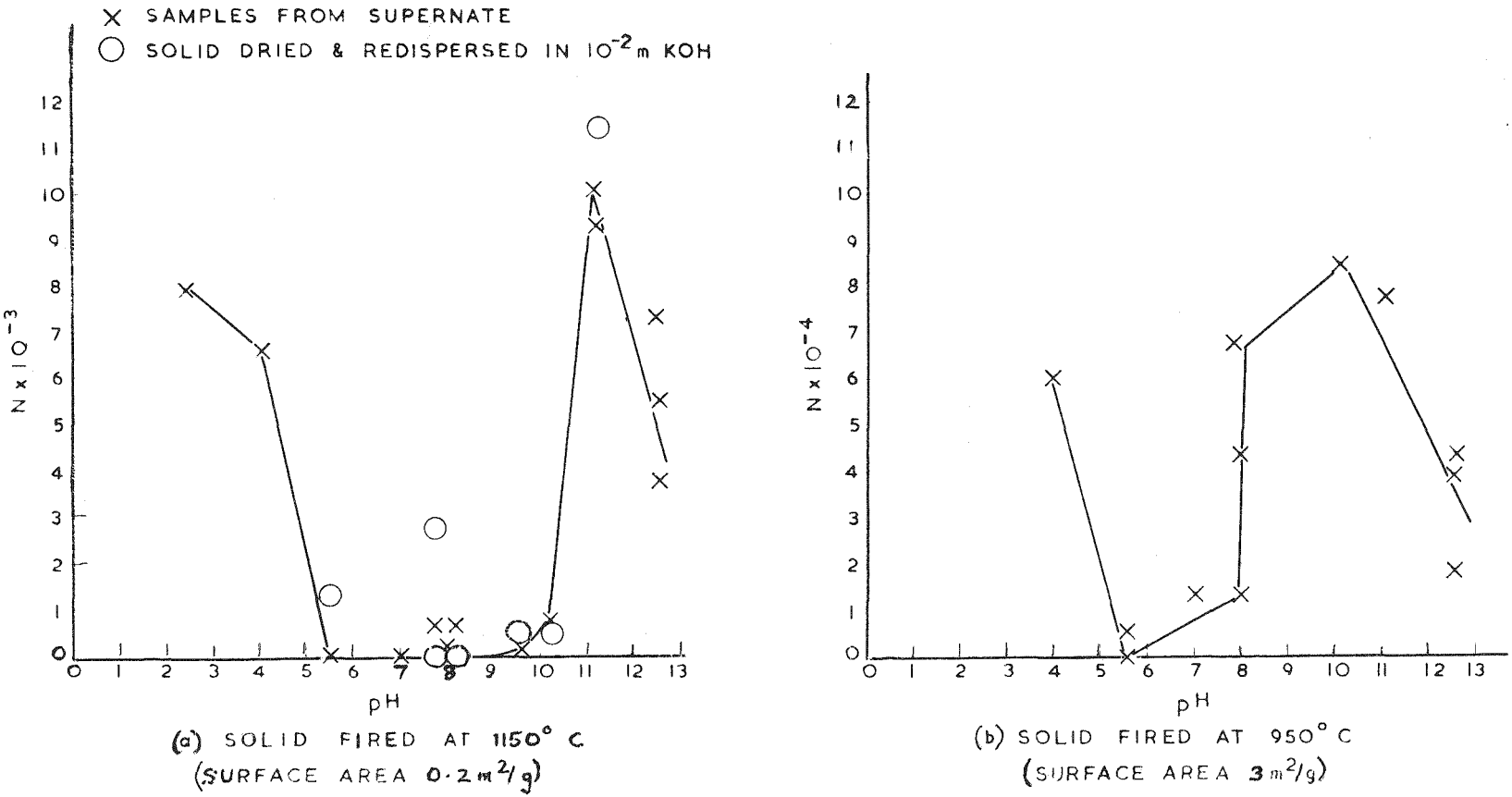

FIG. 6. EFFECT OF pH OF SUPERNATE ON THE FRAGMENTATION OF ThO_2 20% UO_2 (20% ^{235}U)

maximum of 7000G. After centrifuging for 1 hr under these conditions, the supernatant liquid had separated into a colorless aqueous layer and a thixotropic solid deposit. From centrifuging times with the PuO_2 colloid, the size of the colloidal fragments was estimated to be not greater than 400Å. During later experiments with $ThO_2.UO_2$ suspensions, it was possible to take electron photomicrographs of colloidal samples. An example is reproduced in Figure 2; the mean diameter is in fact about 50Å, and the fragments appear to be joined in a chain-like structure.

The variation of the fragmentation as a function of irradiation dose is graphically represented in Figures 1, 3, and 4. In the case of material of higher surface area (29 m^2g^{-1} PuO_2 and $3m^2g^{-1}ThO_2.UO_2$)the effect appears to reach a maximum and then suffers a decline. Whether this is due to a real decrease in the rate of fragmentation or to a partial flocculation of the colloidal material is not yet clear. No such saturation is evident for the low surface area oxides (0.2-0.3 m^2g^{-1}) or for the PuO_2 of surface area 3 m^2g^{-1}.

The number of metal atoms N ejected from the bulk solid per fission event, calculated from the initial rate of fragmentation in all cases, is plotted against the surface area of the solid in Figure 5; this shows clearly that the degree of fragmentation is essentially unaffected by a 100-fold change in power density, but is essentially in direct proportion to the surface area of the unirradiated solid.

All of the data presented in Figures 1-5 refer to results obtained when the oxides were irradiated in dispersing media (PuO_2 in H_2O or 10^{-2} M HNO_3; $ThO_2.UO_2$ in 10^{-2} or 10^{-3} M KOH and in 10^{-3} or 10^{-4} M $Th(NO_3)_4$ solution). The effect of dispersion was examined by carrying out similar experiments in flocculating media (PuO_2 in 10^{-1} M HNO_3; $ThO_2.UO_2$ in H_2O, NaCl, and NaCl-KOH solutions).

The results provide clear evidence that when irradiation is carried out under flocculating conditions, the degree of fragmentation is markedly reduced. The irradiation runs were supplemented by a large number of unirradiated control experiments; in cases where the α-activity in the supernates of the control runs was comparable with that after irradiation, the degree of fragmentation is recorded as zero.

The variation of fragmentation as a function of pH is shown on the graphs of Figure 6 for two kinds of oxide irradiated in pure water and in solutions of HNO_3 and KOH.[a] It is interesting to note that the center of the region of low breakup for the 0.2 m^2/g material coincides with the point of zero charge for ThO_2 (pH 8.5[13]), whereas the pH at which minimum breakup occurs in the case of the 3 m^2/g material corresponds with the point of zero charge for UO_2[4]. This may be related to the fact that the UO_2 in the lower fired material is not completely in solid solution and can exert an overriding effect on the surface properties of the mixed oxide.

---

[a] Data obtained at < pH 3 may be affected by leaching of uranium into true solution. This was indicated by the fact that unusually high amounts of α-activity remained after prolonged centrifuging at 7000G.

In order to determine if any fragmentation was still taking place under flocculating conditions, but was being masked by loose adhesion of colloidal fragments to the surface of the bulk solid, post-irradiation dispersing experiments were carried out. The irradiated solid was separated from the flocculating medium, dried, and subjected to several days agitation in 10^{-2} M KOH solution. The increase in α-activity of the supernate was in most cases no greater than that obtained with unirradiated samples, and the situation was unaffected when drying of the sample prior to adding the dispersing solution was omitted. A similar failure to disperse colloidal material was encountered with samples irradiated in the dry state. By contrast a colloid-bulk solid mixture obtained after irradiation in 10^{-2} M KOH could be separated, dried, and the colloid quantitatively redispersed (Figure 6a). We conclude from these experiments that a dispersing medium is an essential requirement for a high degree of radiation-induced fragmentation to take place. This contention was supported by preliminary data obtained on irradiation in the non-dispersing medium benzene, but these experiments were abandoned because of considerable radiation-induced polymerization of the organic phase.

Some attempt has been made to monitor the radiation damage in terms of changes in surface area as well as in terms of production of colloidal fragments. Surface area measurements (performed by the BET method using krypton) have of necessity been carried out on small samples, and the inaccuracy is rather large. Nevertheless we have obtained firm evidence that fragmentation is accompanied by a substantial increase (a factor of $\sim$ 10 after 5×10^{12} fissions/mg) in the surface area of the residual bulk solid. In contrast, no significant change in surface area is produced when solids are irradiated in the dry state or under flocculating conditions.

CONCLUSIONS AND DISCUSSION

This investigation of radiation-induced fragmentation is still in progress at the time of writing; conclusions must therefore be tentative and discussion highly speculative. Above all it must be emphasized that our experiments relate to extremely low values of burnup (20 MWD/ton) and it is premature to assume that the trends we have discussed will extend to the much higher burnups which will prevail in a suspension reactor. With these provisions in mind, the following generalizations can be made:

1. Radiation-induced fragmentation is appreciable only if the bulk solid is irradiated in a dispersing medium.

2. The fragmentation of a number of the solids examined tends to a maximum and even suffers a decline at increasing doses. However, it has been possible to induce breakup of at least 10 w/o of the original solid in all cases studied.

3. The fragmentation per fission at the early stages of breakup is roughly proportional to the surface area of the unirradiated solid.

4. The fragmentation per fission is essentially independent of dose rate (power density) over a wide range - from 2×10^{9} fissions/mg-sec to 3×10^{7} fissions/mg-sec. (PuO_2 in flux 1.2×10^{12}; $ThO_2.UO_2$ (20% U^{235}) in flux 1.2×10^{11}).

On the basis of the results so far obtained, it is possible to make some suggestions regarding the mechanism of the breakup. In particular, some possibilities can be eliminated. Thus it seems unlikely that fragmentation is brought about solely by intercrystalline weakening followed by dispersion of the crystallites; electronmicrographs show that colloidal particles from oxides having surface areas of 3 and 0.3 m^2g^{-1} have the same mean diameter (50 Å), which is several powers of ten lower than the crystallite size (equivalent spherical diameter) estimated from the surface areas;moreover, work carried out by E. Wait on single crystals[10] and by J. Bloch[14] on polycrystalline UO_2 has established that no decrease in crystallite size takes place after burnups two powers of ten higher than those of the present investigation; it is most unlikely that a different situation will obtain for PuO_2 and $ThO_2.UO_2$, and crystal fragmentation occurring in the bulk of the solid must therefore be ruled out.

From this we are forced to conclude that the formation of colloidal fragments of sub-crystallite size takes place by a surface mechanism. This hypothesis is qualitatively supported by the large influence of both the surface area of the solid and the nature of the liquid medium surrounding the particles.

The following mechanisms could play an important part in this type of process:

1. The passage of a fission fragment through the surface layers creates a short-lived region of amorphous material. This could become electrically charged by interaction with the solvent, and so be dispersed to form a stable colloid.

2. It is known that the passage of a fission fragment through the surface causes a considerable number of atoms to be "evaporated". If ejected into an aqueous medium, the atoms would be hydrated and (at a relatively high pH) hydrolyzed, the product eventually condensing to particles of colloidal dimensions. Under non-dispersing conditions the fragments would return to the surface, and could become permanently sintered there under the influence of the localized high temperatures in subsequent fission tracks.

On the basis of mechanism (2), the number of atoms evaporated per fission in our experiments is at least two powers of ten higher than the value observed by Ershler and Lapteva[15] for the fission fragment-induced evaporation of U atoms from oxide-coated U^{233} metal. However, it would be premature to reject (2) in favor of (1) on the basis of this discrepancy alone. A distinction might be made between the two mechanisms by the application of tracer techniques; thus if $M^{18}O_2$ were irradiated in $H_2{}^{16}O$, the isotopic composition of the colloid oxygen could distinguish whether the fragments were part of the original surface or were formed by hydrolysis in the aqueous phase.

Experiments are now in progress to test the effects of irradiation on single crystals of $UO_2.ThO_2$ prepared by crystallization from a borax melt[16]. Attention is also being paid to possible effects due to non-stoichiometric oxygen; the $ThO_2.UO_2$ samples employed so far were calcined in air, and the average uranium valency is therefore considerably greater than four. We are unable at present to advance any reasonable interpretation of the variable 'saturation' effect illustrated in Figures 1 and 3.

The effects of reactor conditions, particularly high temperature and agitation of the slurry, on radiation-induced fragmentation are difficult to predict at this stage, and an assessment of the technological magnitude of the effect must await further experiments. The main value of our work so far has been to show that conditions exist under which severe radiation damage to suspended oxide particles can take place.

The fact that fragmentation is greatly reduced under flocculating conditions gives some grounds for optimism, for flocculation is the most readily obtainable state at elevated temperatures. Furthermore, although a stable suspension might undergo a rather fast breakdown of the fuel (with the production of ~ 5 Kg of fines per MWD of heat (N = 5000), caking under stable conditions may not be serious. The colloid (which has been shown to be a good scavenger for fission products)[11] might be processed in a by-pass circuit, but the feasibility of this would depend upon the actual value of N.

ACKNOWLEDGEMENTS

We wish to thank Dr. J. K. Dawson of Harwell and Mr. M. E. A. Hermans of KEMA for stimulating discussions. The surface area measurements were carried out by Mr. J. Butterfield.

REFERENCES

1. E. L. Compere, et al., in USAEC Report ORNL-2493, Oak Ridge National Laboratory, August 1958.

2. R. L. Pearson, F. H. McCorkle, C. U. Ellison, and P. A. Haas, Preparation of Thoria for Homogeneous Blanket Use, USAEC Report ORNL-2509, June 1958.

3. M. E. A. Hermans, The Preparation of Uranium Dioxide Fuel for a Suspension Reactor, Proc. Second U. N. Conf. on the Peaceful Uses of Atomic Energy, Vol. 7, p. 39, 1958.

4. M. E. A. Hermans and H. S. G. Slooten, Preparation of UO_2 and ThO_2 Powders with Specific Properties, E.A.E.S. Symposium on Reactor Materials, Sweden, 1959.

5. M. E. A. Hermans and Th. van der Plas, Fission Product Recoil Separation in Suspension Reactors, Nucl. Sci. Eng. 2: 224 (1957).

6. E. L. Compere, Corrosion by Slurries, USAEC Report TID-7540, p. 249 (1957).

7. C. F. Hiskey, The Heavy Water Homogeneous Pile. A Review of Chemical Researches and Problems, Report CC-1383, Feburary, 1944.

8. N. A. Krohn and J. P. McBride, Reactor Irradiation of Thorium and Uranium Oxide Slurries, USAEC Report ORNL-CF-57-1-119, Oak Ridge National Laboratory, January 1957.

9. N. A. Dawson, K. Alcock, D. R. Chilton, and T. Johnson, AERE, Harwell, unpublished work, 1956.

10. E. Wait, AERE, Harwell, unpublished work, 1959.

11. B. R. Harder and R. G. Sowden, Irradiation Experiments with Aqueous Suspensions of Plutonium Dioxide, British Report AERE-R-3537, Atomic Energy Research Establishment, Harwell, March 1960.

12. K. E. Francis and R. G. Sowden, The Microstructure of Plutonium Dioxide Prepared by Various Methods, British Report AERE-R-2939, Atomic Energy Research Establishment, Harwell, June 1959.

13. J. Kalshoven and Th. van der Plas, KEMA, Arnhem, unpublished work, 1960.

14. J. Bloch, Restauration Thermique du Parametre d'UO_2 Faiblement Irradie, J. Nucl. Materials, 3: 237 (1961).

15. B. V. Ershler and F. S. Iapteva, The Evaporation of Metals by Fission Fragments, J. Nucl. Energy II, 4: 471 (1957).

16. J. Garton, Clarendon Laboratory, University of Oxford, personal communication, 1961.

17. J. O. Blomeke, Aqueous Uranium Slurries, USAEC Report ORNL-1904, Oak Ridge National Laboratory, October 1955.

IRRADIATION EFFECTS ON THORIA-URANIA SLURRIES

by E. L. Compere, A. J. Shor, L. F. Woo, and H. C. Savage

Oak Ridge National Laboratory[a]
Oak Ridge, Tennessee

It will be useful for the reader to keep in mind the restrictions imposed by the objective of developing a thorium breeder power reactor in connection with this paper. Thorium must be converted to U-233 at a high enough neutron economy to manufacture more uranium than the amount burned. One of the most efficient ways of doing this is to put a high concentration of thorium (500-1000 g/liter) in a heavy water blanket. Since appreciable power is to be produced as an additional objective, the blanket must operate at a high temperature, for example, 280°C. This might be done with pellets or with a slurry of thorium oxide. When all the engineering and fuel cycle problems are considered, the slurry-type blanket appears to offer the simplest and most efficient system.

The purpose of this paper is to describe what we have observed in the way of irradiation effects in aqueous slurries of thoria-urania powders. Our studies were aimed at examining the corrosion and irradiation effects on such high-temperature slurries, using in-pile autoclaves and an in-pile loop as research devices.

It is sufficient, with respect to the corrosion studies, to point out that no serious corrosive effects have been discovered at the fission power densities that we have examined, either in loops or in autoclaves. A temporary increase in corrosion rate has generally been observed when irradiation commenced, but appreciable corrosion levels were not reached and the corrosion rate diminished as exposure continued.

Thoria and thoria-urania powders were prepared by oxalate precipitation as shown in Table I. Uranium could be incorporated in the slurry in two ways. In one method, it was adsorbed on high surface area, low-fired thoria particles from an ammonium uranyl carbonate solution, and incorporated into the solid by calcination. In the other technique, uranium (IV) oxalate was dissolved in a mixture of ammonium oxalate and oxalic acid. Addition of this solution to a solution of thorium nitrate co-precipitated the thorium and uranium as oxalates, which were subsequently calcined to produce an oxide having the desired surface

---

[a] Operated by Union Carbide Corporation for the U.S. Atomic Energy Commission.

area. No differences in irradiation behavior of materials prepared by the two techniques have been observed. Both kinds of preparation have been used in autoclave experiments; co-precipitated thoria - 0.5% urania was used in the in-pile loop experiment.

Unless otherwise mentioned all studies were carried out using heavy water slurries of oxalate-precipitated thoria or thoria-urania, calcined to surface areas of 1-3 m^2/g. In general, the average particle size of most preparations was about 2 μ, with very little material smaller than 0.6 μ or larger than 5 μ. Concentrations were in the range of 400-1000 g (Th + U)/liter, at 280°C. In most experiments, an oxygen atmosphere was maintained over the slurry.

Since the loop experiment was the most extensive study of this type performed to date, it will be discussed first. Figure 1 shows the loop which is a modification of earlier solution loops described by Savage et al.[1]

The loop consisted primarily of a 5-gpm canned rotor pump connected by several feet of 3/8-in. stainless steel piping (Sch. 40, type 347) to a coiled pipe core and connected through a sintered stainless steel filter to a pressurizer system. Filtered water was heated, passed into the pressurizer where a steam-gas space was maintained and then, after cooling, into the rear of the pump, where it served to keep solids flushed out of the pump cavity. Corrosion specimens were placed in forward and rear regions of the core and in loop piping well away from the reactor lattice.

The loop was operated in horizontal beam hole HB-2 of the ORNL Low Intensity Test Reactor. Operating conditions for the experiment are given in Table II. The loop was loaded to an original concentration of 980 g Th/liter with 90% of the thorium being present in the form of $(Th,U)O_2$ containing 0.5% enriched urania, and the other 10% in the form of thoria having a large surface area and containing adsorbed palladium to serve as a catalyst for the recombination of D_2 and O_2 formed by radiolysis. After 895 hr of out-of-pile operation, the loop was operated in-pile for a period of 2220 hr, over 7/8 of which were under irradiation. No particular operating difficulties were encountered. There is evidence that the filter had cracked before the loop was inserted in the reactor beam hole, and possibly one-third of the solids originally in circulation had left the main circulating stream. Since these materials did not circulate further, their loss had no effect, aside from concentration changes, on the properties of the irradiated circulating slurry.

Radiolytic gas buildup had been anticipated, and palladium catalyst had been put in the slurry to effect recombination of the gases, but no pressure increase was observed. Subsequent calculations (based on a gamma recombination G-value of 5 molecules H_2 per 100 ev absorbed, as given by Hochanadel[2]) indicated that the radiolytic gases generated at rates determined by our uranium concentration could be recombined by the reactor gamma radiation absorbed in the water.

It should be noted before proceeding that no evidence of unsatisfactory or unusual slurry behavior was observed during the experiment and circulation of the slurry was uneventful. A dozen samples of the circulating slurry were taken as desired without difficulty. Slurry was easily added to the loop on one occasion. Drainage of slurry from the main circulating loop at the conclusion of the experiment was straightforward and left essentially clean piping surfaces. No caked residues have been found. After including the slurry found in the pressurizer and filter systems, an excellent material balance was achieved.

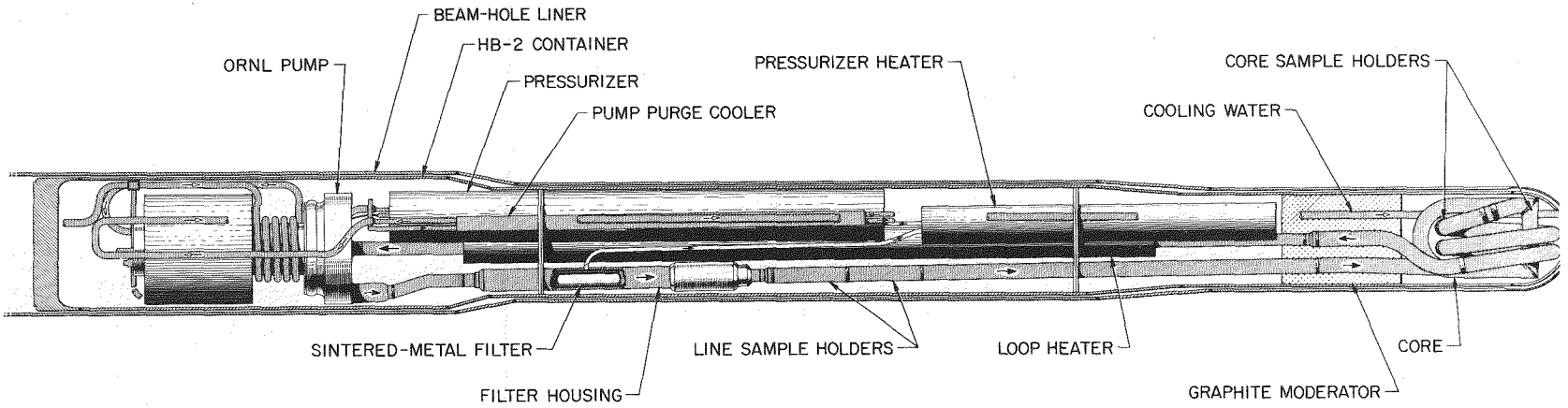

Slurry In-Pile Loop.

Figure 1. Slurry In-Pile Loop.

Table I

METHODS USED TO PREPARE Th-U OXIDES

1. Adsorption

   a. ThO_2 (650°C-Calcined) + $2(NH_4)_2CO_3 \cdot UO_2CO_3 \cdot 2\ H_2O$ (Boil to decompose).

   b. Calcine to incorporate U in the solid.

   Final mixed oxide has particulate properties of the ThO_2 used; hence control of particle size and shape.

2. Coprecipitation

   a. $U^{+4}(C_2O_4)_2$ in $(NH_4)_2C_2O_4 + H_2C_2O_4 + Th(NO_3)_4 \rightarrow Th\text{-}U(C_2O_4)_x$ (Mixed crystal).

   b. Calcine to Th-U Oxide.

   Particulate properties controlled by rate of addition of reagents, solution temperature, rate of mixing, etc.

Table II

IN-PILE SLURRY LOOP OPERATING CONDITIONS

Slurry: $(Th\text{-}U^*)O_2$ in D_2O, Oxalate-Co-Pptd, 1225°C Air Calcined.

Conc., g/liter: Th 980; U* 3.8; Pd 1.5.

Time, hrs: 3115 Total; 2220 In-Pile; 1839 Irradiated.

Temp., °C: Main Loop 280, Pressurizer 295, Pump 60.

Pressure, psi: Steam 1200; Oxygen 100.

Volume, ml: Main Loop 900; Pressurizer 520; Total 1640.

Flow, fps: Main Loop 9; Core 6; Specimens 8, 22.

Pressurizer Purge: 4 cc/sec.

Radiochemical data, shown in Table III, indicated a fission dose of 7×10^{16} fissions/gram solids (7×10^{17} fissions/cc of solids), with a U-235 burnup of 0.003% of the total fertile (Th) and fissionable (U) atoms. The mean average perturbed neutron flux was 2.4×10^{12}. A maximum perturbed flux of 1.9×10^{13} has been estimated for the slurry in the core nose. Fission and neutron absorption products were distributed about as expected, with only alkali metals (e.g., Cs-137) being found associated with the slurry liquid rather than with the slurry solids.

Table III

RADIOCHEMICAL DATA

(Irradiated 1839 hr)

In-Pile Slurry Loop L-2-27S

Fissions/g Solids	7×10^{16}
Burnup	0.9% of orig. U-235 or 0.003 a/o of metal atoms
Average Flux	2.4×10^{12}
nvt	1.6×10^{19}

Distribution of Fission Products

	Cs-137	Zr-95	Ce-144	Pa-233
K, Solids/Liq.	~1	$>10^5$	10^4	10^4

One of the most striking of the irradiation effects is illustrated in Figure 2. The particle size distribution in samples taken at various periods before and during irradiation is shown, with weight percentage smaller than a given size being plotted for relevant sizes against time. During the pre-irradiation period, little appeared to happen, although the analytical results were rather erratic in the middle part of the period. The average particle size was somewhat above 1.5μ, perhaps 1.7μ, and practically no material was found to be smaller than 0.7μ. Centrifugal sedimentation techniques indicated that the average particle size decreased until at the end of the experiment it was about 0.3μ, with 20-30% of the material being smaller than 0.087μ (870 Å) in size.

At the same time, the surface area (as measured by N_2 adsorption) which had shown no particular change before in-pile operation, began steadily to increase as irradiation continued, from 1-2 m^2/g to values exceeding 40 m^2/g. These effects occurred under the simultaneous actions of irradiation and circulation.

Figure 3 shows electron microscope photographs of a number of samples. The scale in the photo of the original material is probably a bit in error, as it should show particles of the same size as its right hand neighbor. The particles appear to have been somewhat cubic and fairly regular in size. It will be noted that, as irradiation time increased, particle edges became progressively more irregular, and the proportion of fines steadily increased. Thus a

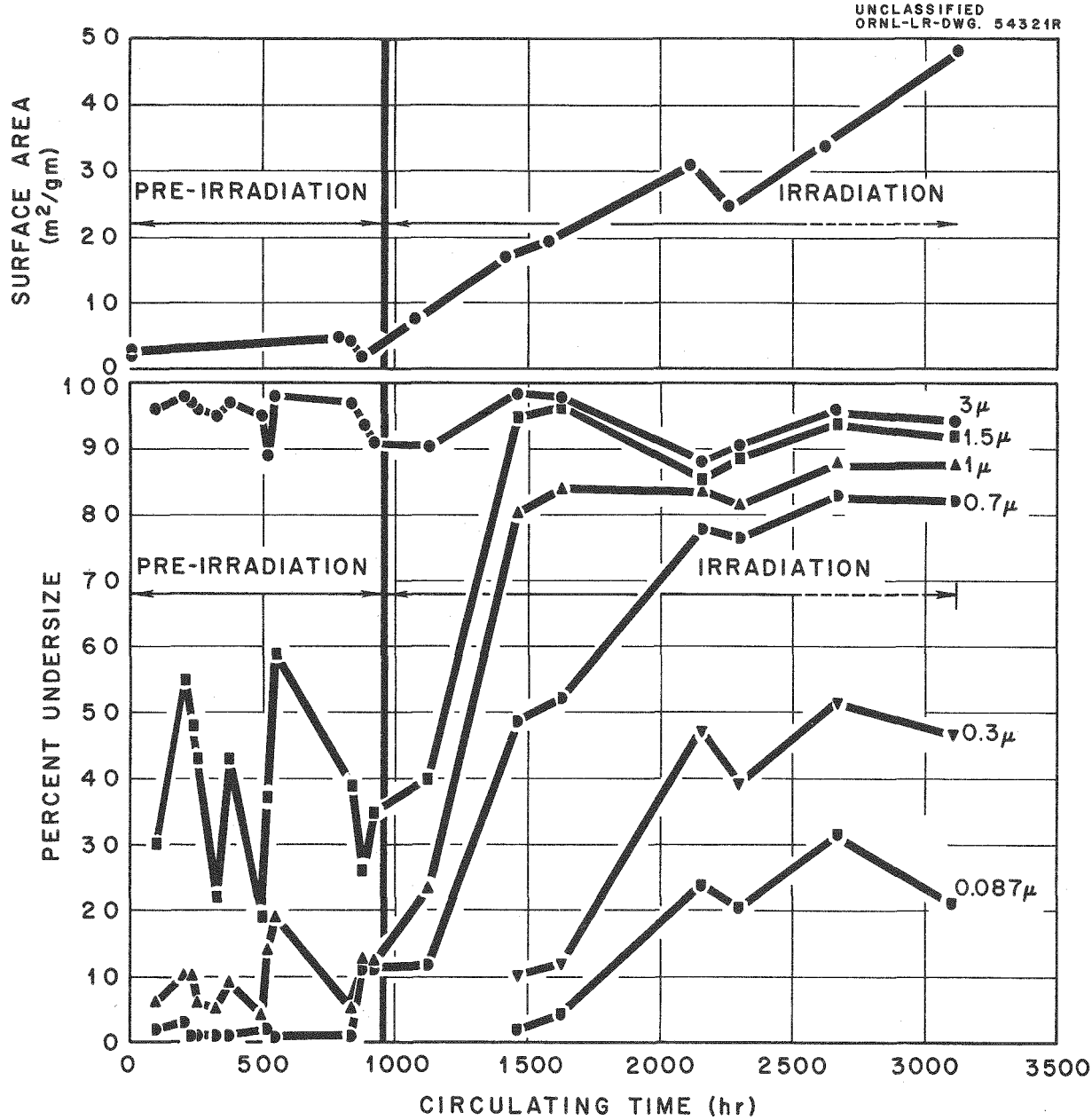

Figure 2. Effect of Irradiation and Circulation on Slurry Particle Size Distribution and Surface Area.

UNCLASSIFIED
ORNL-LR-DWG. 58164

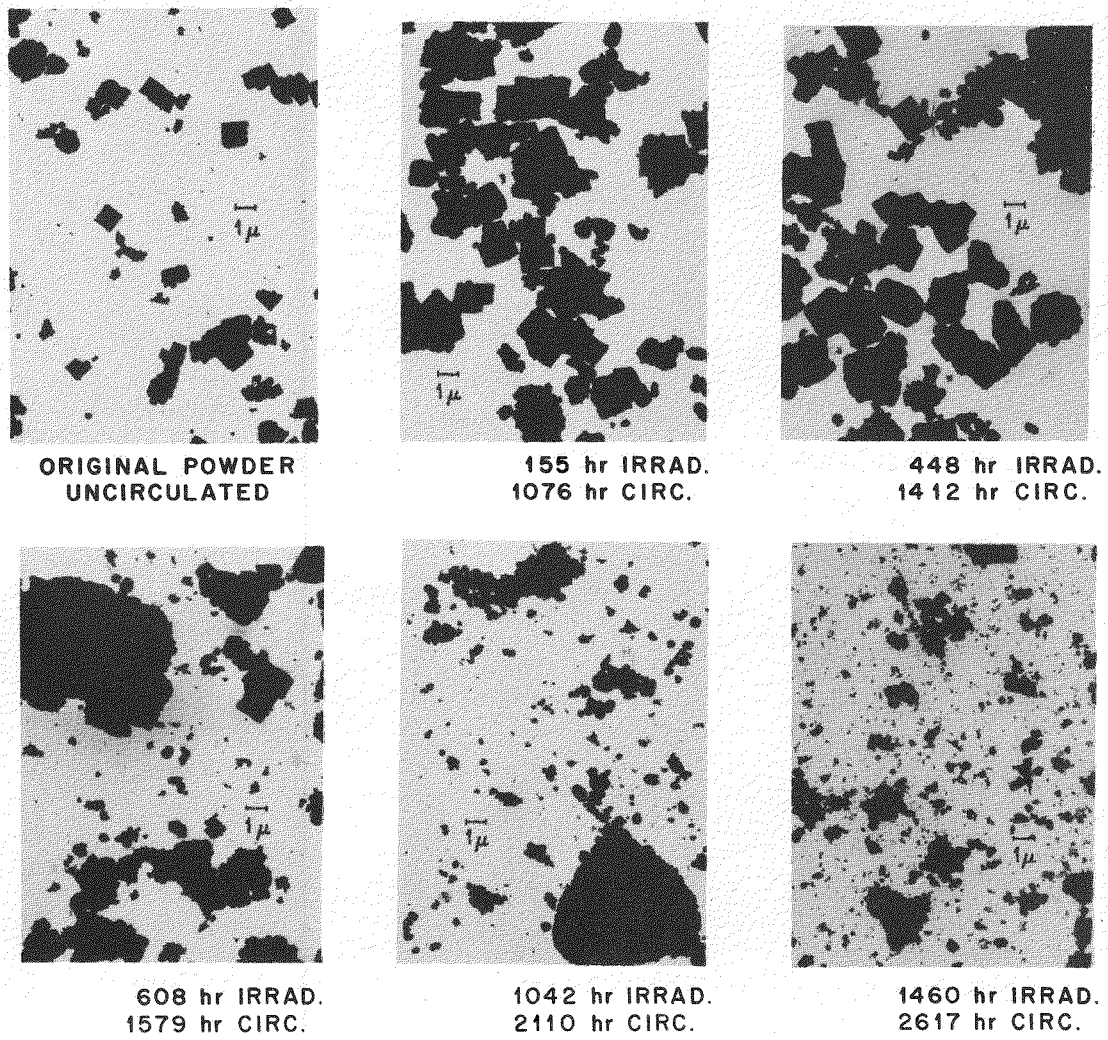

Figure 3. Electron Photographs of Slurry from In-Pile Loop L-2-27S.

progressive degradation of particles by circulation and irradiation was indicated.

A few larger masses were also noted and are shown in Figure 3. It is possible that these masses are agglomerates, the formation of which was prompted by the presence of fines and more irregular shapes under the action of pumped circulation and, of course, irradiation.

A question arises as to whether pumping affected the breakup of particles. To help answer this question, an irradiation experiment was conducted in a gently rocked autoclave, under the same conditions, and with the same materials as the loop experiment. Approximately the same fission dose was achieved. Some results of this experiment are shown in Figure 4, where particle size distribution is shown for the original and for the irradiated material. Loop data, the same as were presented earlier, are shown in the chart at the left while data from the autoclave experiment are on the right side. It is easily seen that no change in particle size was produced by irradiation except that the fines associated with the thoria-palladium catalyst were agglomerated.

However, surface area and crystallite size of the oxide particles employed in the autoclave experiment were affected by radiation. Surface area, originally 8 m^2/g, increased to 30 m^2/g and crystallite size decreased from 1795 Å to 220 Å. At a corresponding irradiation dose in the loop experiment, the surface area was 25 m^2/g and the crystallite size was about 300 Å.

Thus, similar radiation damage effects to crystallite size and surface area were found in the autoclave and loop experiments, but the particle size degradation, which occurred only in the loop, must be attributed to the combined action of pumping and irradiation.

Crystallite size results from a number of autoclave irradiations of thoria-urania slurries are shown in Figure 5. The size of the original material is indicated by a dot while the change that occurred on irradiation is shown by a dash. In all cases a substantial reduction in crystallite size developed. A slight reduction in crystallite size was encountered in two unirradiated control experiments. Although no simple correlation of reduction in crystallite size with fission dose is evident, it is clear that irradiation of high-temperature aqueous thoria-urania slurries to levels of 10^{17} fissions/gram of solids will result in crystallite sizes of 100-200 Å. No noteworthy changes in particle size occurred in the experiments.

Changes in crystallite size and surface area are compared for the loop experiment in Figure 6. Both are plotted on logarithmic scales; the scale for surface area is inverted. The two properties, in general, changed in similar manner as circulation and irradiation proceeded.

An automatic B.E.T. apparatus has been developed by Dake[3] for the determination of pore volume using nitrogen adsorption and desorption isotherms. It was shielded to permit handling the nine-months cooled samples from the in-pile loop experiment. Data from the isotherms obtained were used according to the method of Barrett, et al.,[4] to compute incremental pore volume as a function of pore radius. Pore volume distributions of three samples are shown in Figure 7. The distribution for the original thoria-urania particles before catalyst addition is shown in the lower curve. The material shown by the intermediate distribution curve had been pumped but not irradiated and contained about 10% of thoria-palladium catalyst. The thoria catalyst support had a high surface area and a small crystallite size material and would, consequently, be expected to exhibit

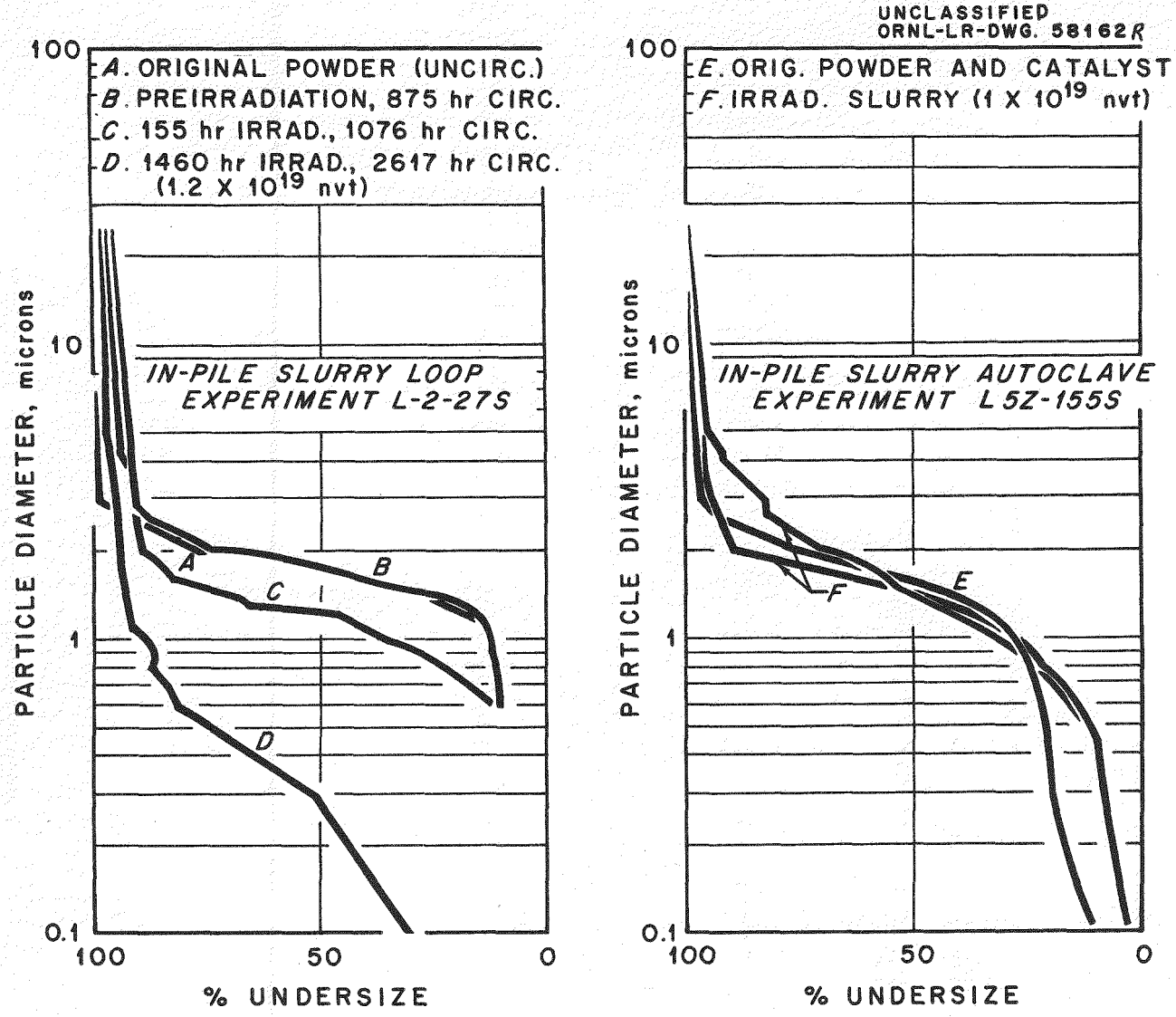

Figure 4. Effect of Irradiation on Particle Size Destruction in Loop and Autoclave Experiments.

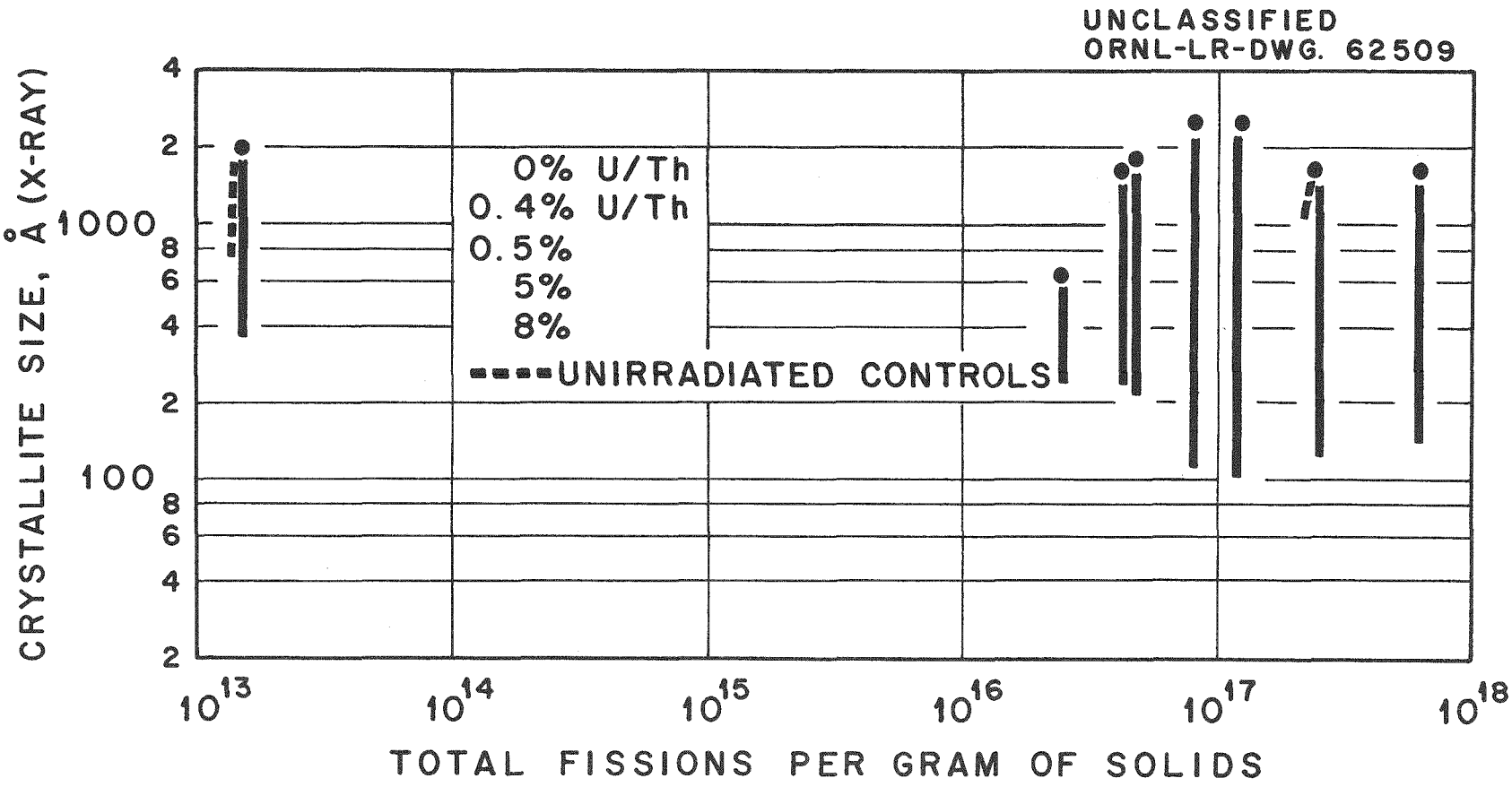

Figure 5. Effect of Fissions in Solids on Crystallite Size Degradation (Autoclave Experiments).

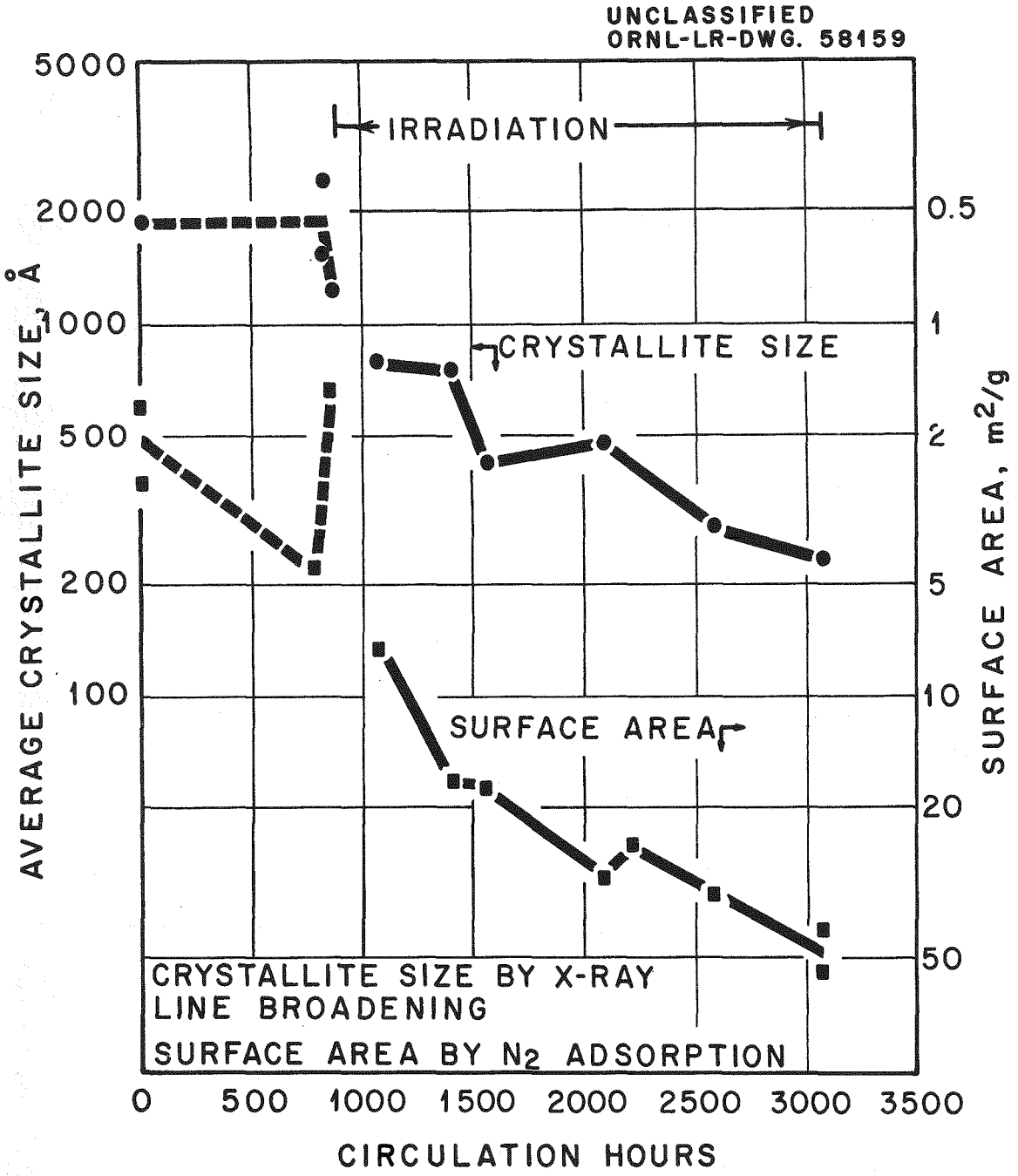

Figure 6. Changes in Properties of Solids In-Pile Loop L-2-27S.

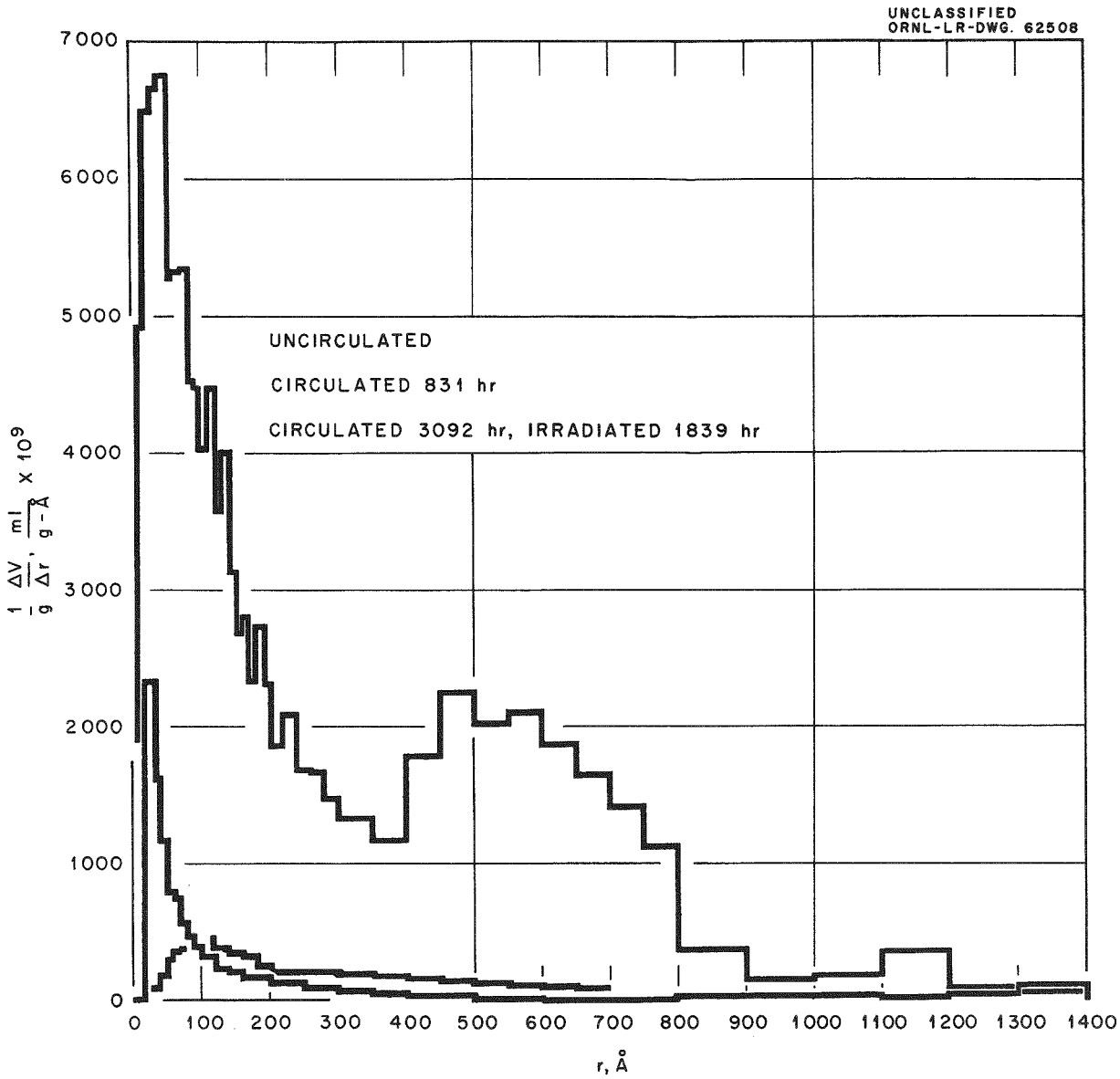

Figure 7. Distribution of Pore Volume as a Function of Pore Radius.

porosity of the observed magnitude.

Material recovered after termination of irradiation of the in-pile loop experiment gave the upper curve. It is evident that a very substantial increase in porosity of the solids occurred as a result of irradiation. It has been pointed out by Emmett[5] that the minor peak in pore volume of the irradiated material in the region 400-800 Å radius is larger than would be expected from particles of about 3000 Å average diameter.

The superficial and internal surface areas may be deduced from these data. The relationship of pore area to pore radius was computed from the pore volume data using a cylinder model for the pores. Results of this calculation are shown in Figure 8. First of all, the total pore surface as integrated from this model may be compared with that given by the usual B.E.T. monolayer. Agreement for the various samples is good and indicates that the cylindrical model is a useful approximation in this case.

Over half of the surface area of the irradiated material was associated with pores of radius below 45 Å and a substantial amount with those smaller than 10 Å. It will be recalled that crystallite thicknesses of 220 Å were reported on this sample.

The contribution to surface area of the particle exterior surface was calculated from particle diameter distributions determined by sedimentation of a portion of the irradiated sample, reported earlier (Figure 2), and this amounted to about 4 m^2/gram. Thus, the major part of the surface area was internal.

It is of interest to return once more to the surface area-crystallite size data, this time for the purpose of attempting correlation of the two as shown in Figure 9 in the manner suggested originally by Allred et al.,[6] for thorium oxide particles fired to different temperatures.

The heavy lines are theoretical lines for different limiting geometries. It will be noted that, in all observations before irradiation began, the points were found to the left of and below the limiting sphere-cube line, as would be expected. However, as irradiation continued surface areas were generally above the line (or X-ray line broadening crystallite sizes to the right). Since any strains in the crystal should result in greater line broadening and smaller apparent crystallite sizes (i.e., to the left), it is concluded that such strains are not the dominant effect. Surface areas of about 25 m^2/g might have been expected at a crystallite size of 220 Å; areas of 35~50 m^2/g were observed. It would appear that some material might be contributing about 10 m^2/g to the surface area without being observed in the crystallite size data.

It is possible that this material could be either corrosion products or material resulting from the fission process. There was present at the end of irradiation about 0.01 grams of corrosion products per gram of slurry; in order to achieve the indicated surface area increment of 10 m^2/g, the specific surface area of the corrosion product material would have to be of the order of 1000 m^2/g (maximum crystallite size, 6 Å).

The other possibility is that some amorphous thoria of high specific surface area may have been produced. The loss of material by "evaporation" as a result of fission fragment bombardment was described by Sowden et al., (see Paper No. 26) as occurring in stagnant dispersing systems at a low temperature with yields of 10^5 evaporated atoms per fission. The evaporation of uranium or plutonium in a vacuum

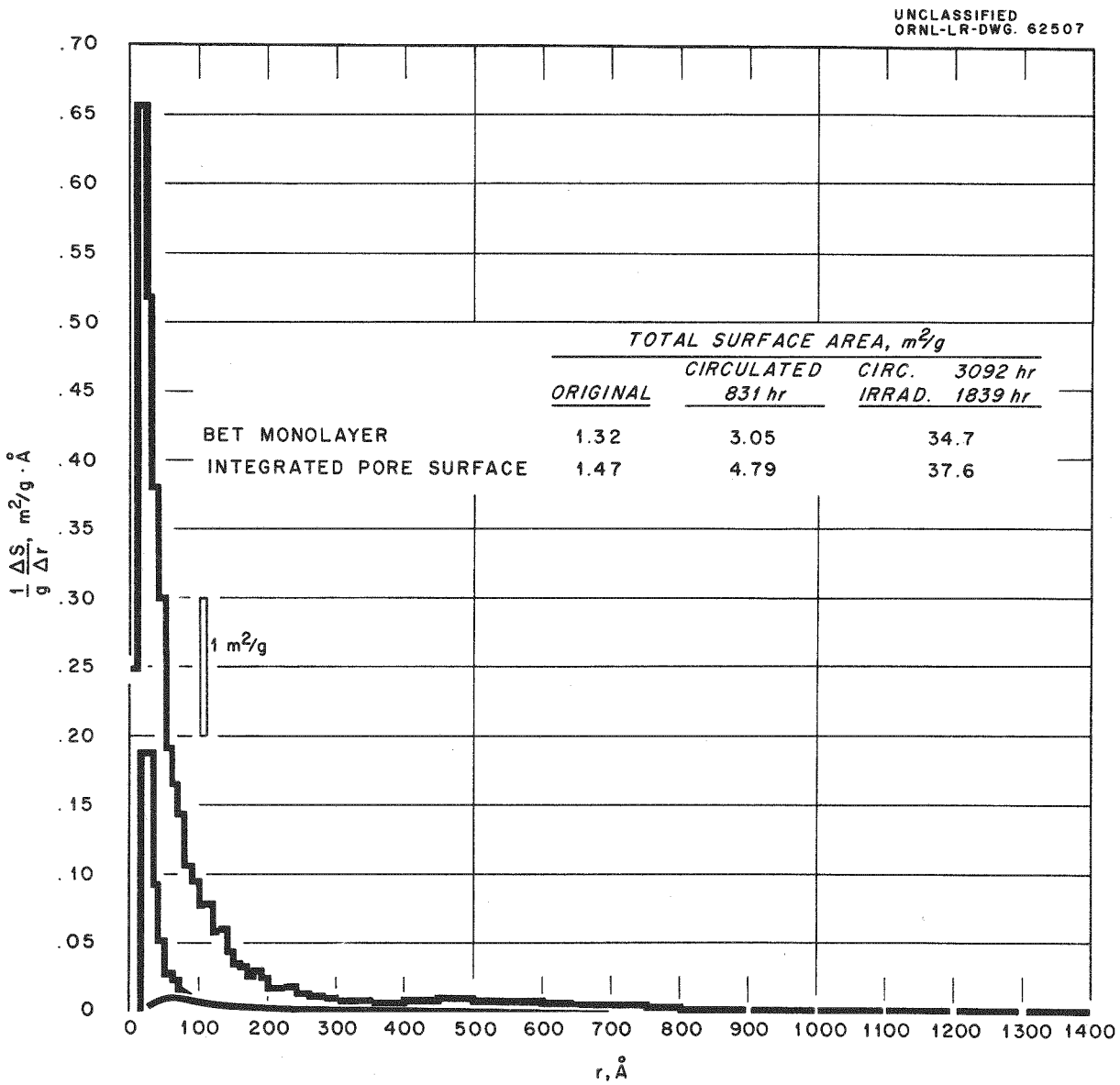

Figure 8. Distribution of Surface Area as a Function of Pore Radius.

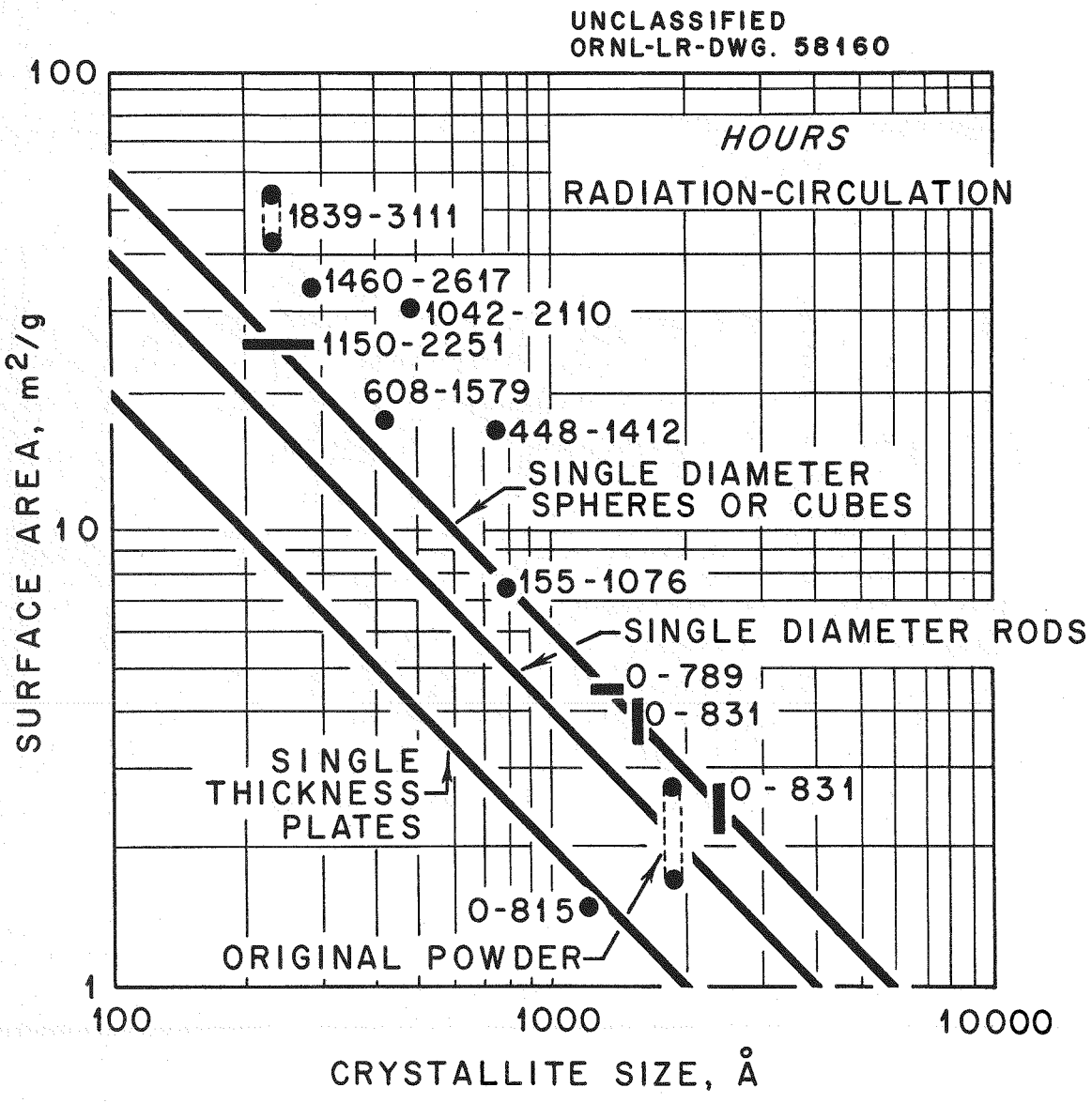

Figure 9. Effect of Irradiation on Properties of Slurry Particles in In-Pile Loop Experiment.

by fission fragment energy has been described by Lapteva and Ershler.[7]

An estimate can be made of the amount of thoria which might be evaporated by fragments from one fission. Let us assume that all energy below 116 kev directly results in knock-ons and that most knock-ons occur in this region. Noting that the energy of evaporation of thoria is 6.9 e.v., if we assume that about 10% of the fission fragments are captured by re-entry into slurry particles, then about 3500 thorium atoms per fission would be evaporated as a minimum. If these all coalesced into cubic particles, they would be about 50 to 60 Å on edge.

The new surface area generated by such particles after a fission dose of 7×10^{16} fissions/g would amount to approximately 10 m^2/g, without accounting for additional surface created by the loss of evaporated material. This is of the right order of magnitude if the particles did not much affect x-ray line broadening. Since thoria contains 2.3×10^{21} Th atoms/g, the fission dose developed in the loop experiment would involve the evaporation of 2.5×10^{20} Th atoms/g, and would thus include about 10% of the metal atoms in the slurry.

It appears likely that such fragments in an agitated or pumped flocculated system would be gathered to the remaining slurry particles in the manner that corrosion products, catalyst-thoria preparations, and fission product oxides have been observed to do. This would result in a more flocculated slurry.

Table IV presents some settling data obtained on irradiated loop samples that indicate the flocculation qualities of these materials. As the irradiation time increased, the settling rate decreased, and at high irradiation time the settled bed was well flocculated, containing only 7 v/o solids. It was observed that this material exhibited no handling problems.

Table IV

SETTLING CHARACTERISTICS OF IRRADIATED SLURRIES

Radiation Hours	0[a]	155	1460
Circulating Hours	0-810	1076	2712
Original Vol. % Solids	11.2	9.4	5.4
Settling Rate, cm/min x 10^3	52	33	0.8
Subsidence Halflife, min	19	28	120
Final Settled Bed, v/o solids	20	21	7

[a] Mixed Y-12 Samples.

What do all the above observations mean concerning the use of slurries as reactor blanket or fuel materials? A reactor slurry should at least meet the requirement of inventory control, so that it is feasible to handle the material and control the amount of material at any point as desired. There should be no segregation, caking, or dropout. In the loop experiment, none was observed; with the exception of loss through the cracked filter, inventory control was maintained. Furthermore, a reactor slurry should not be unduly erosive, and should exhibit good heat transfer. These conditions presumably existed in the loop slurry experiment. In addition, a reactor slurry should have reasonably stable properties. In this case, it is difficult without further experimentation to be certain what substantially greater irradiation would do to the slurry.

Was the breakup of particles an artifact of the particular thoria-urania preparation used? Evidence on different thoria-urania preparations in autoclaves implies that a general phenomenon has been observed and the evaporation hypothesis assumes that this is true.

Another in-pile loop experiment which will start with pure thoria (and inbreed U-233) is currently being prepared. It is hoped that it will be possible to operate this loop to greater fission doses than those of the in-pile slurry loop experiment described in this paper; it is also hoped that this experiment may provide answers to some of the questions raised by the present experiment.

In summary, a number of thoria-urania aqueous slurry preparations have been exposed to reactor irradiation at elevated temperatures in autoclaves and in an in-pile slurry loop. Fissioning in the particles resulted in substantial reductions in crystallite size and increases in surface area. In the pumped loop experiment, particle size degradation was also noted. A substantial number of very small diameter internal voids was revealed in the irradiated material. The successful, trouble free operation of the loop demonstrated an effective tool for the examination of irradiation effects on slurries of interest to thorium power breeder reactors. The lack of handling problems with the irradiated slurry in the loop experiment indicates that irradiation damage effects reported in this paper may not necessarily preclude the utilization of thorium oxide slurries in breeder reactors.

REFERENCES

1. H. C. Savage, G. H. Jenks, and E. G. Bohlmann, In-Pile Corrosion Test Loops for Aqueous Homogeneous Reactor Solutions, USAEC Report ORNL-2977, Oak Ridge National Laboratory, Nov. 1960.

2. C. J. Hochanadel, Oak Ridge National Laboratory, The Radiation Induced Reaction of Hydrogen and Oxygen in Water at 25°C to 250°C, International Conference on the Peaceful Uses of Atomic Energy, Geneva, 1955, P/739.

3. P. G. Dake, E. A. Woy, and H. A. Kermicle, Oak Ridge Gaseous Diffusion Plant, Routine Automatic N Adsorption-Desorption Measurements, Paper 48, Fifth Conference on Analytical Chemistry in Nuclear Reactor Technology, Gatlinburg, Tennessee, October 10-12, 1961.

4. E. P. Barrett, L. G. Joyner, and P. P. Halenda, The Determination of Pore Volume and Area Distributions in Porous Substances. I. Computations from Nitrogen Isotherms, J. Am. Chem. Soc. 73, 373 (1951). A computer code developed by Barton Roberts of the ORNL Reactor Chemistry Division was used.

5. P. H. Emmett, Oak Ridge National Laboratory Cónsultant, private communication with E. L. Compere.

6. V. D. Allred, S. R. Buxton, and J. P. McBridge, Characteristic Properties of Thorium Oxide Particles, J. Phys. Chem. 61, 117 (1957).

7. F. C. Lapteva and B. V. Ershler, Evaporation of Metals by Fission Fragments, Atomnya Energia 4, 63-66 (1956).

ETUDE DE LA FORMATION ET DE LA REPARTITION DES GAZ DISSOUS ET DE L'EAU OXYGENEE DANS L'EAU D'UN REACTEUR PISCINE (TRITON)

par J. Chenouard, J. Rozenberg, L. Dolle, and G. Dirian

Commissariat a l'Énergie Atomique
Saclay, France

INTRODUCTION

En vue de faire des prévisions valables du taux de radiolyse (volume d'hydrogène produit par kWh de puissance nominale) de l'eau dans une pile piscine, des mesures de la concentration des gaz de radiolyse et de l'eau oxygénée dissous dans l'eau de sortie du coeur ont été faites dans le réacteur Triton avant son démarrage, pendant la montée en puissance et en régime de puissance stable. La répartition des concentrations de gaz et d'eau oxygénée dissous dans le compartiment coeur et dans la piscine avant le démarrage du réacteur et pendant son fonctionnement en puissance a été également étudiée.

La détermination du taux de radiolyse dans le réacteur consiste à étudier la variation, en fonction du temps, des quantités de gaz en solution dans l'eau sortant du coeur – plus particulièrement celle de l'hydrogène, qui provient presqu'exclusivement de la radiolyse[a] – et d'eau oxygénée. Suivant l'importance relative des vitesses de formation (radiolyse) et de disparition (par dégazage de l'eau dans le circuit ou dans la piscine) de l'hydrogène, deux cas peuvent se présenter:

1. l'établissement d'une concentration stationnaire d'hydrogène correspondant à l'égalité des vitesses d'apparition et de disparition en régime de puissance stable du réacteur. La vitesse de disparition serait difficile à déterminer directement, alors que la vitesse de formation peut être déduite des mesures de la concentration d'hydrogène à l'entrée et à la sortie du coeur, les deux valeurs étant significativement différentes.
2. un accroissement régulier de la concentration d'hydrogène dans l'eau jusqu'à la limite de solubilité de ce gaz au delà de laquelle il se dégagerait en bulles.[b] Ce phénomène se produirait si la vitesse de disparition de l'hydrogène était beaucoup plus faible que sa vitesse de formation. L'accroissement relatif de la concentration d'hydrogène dans l'eau lors de son passage par le coeur serait alors faible et sa mesure ne donnerait qu'une idée grossière du taux de radiolyse. La meilleure détermination de celui-ci serait alors de suivre l'évolution de la concentration de gaz dissous dès la mise en puissance du réacteur, après avoir pris la précaution d'amener initialement cette concentration à une valeur voisine de zéro. La pente à l'origine de la courbe représentant l'évolution de cette concentration d'hydrogène serait alors une mesure du taux de radiolyse.

Cette façon d'envisager les mesures du taux de radiolyse exclut naturellement l'hypothèse de l'existence d'un équilibre radiolytique qui aurait pour effet de produire une concentration stationnaire d'hydrogène pendant la courte durée (quelques secondes) du passage de l'eau dans le coeur du réacteur; le taux de radiolyse serait alors nul.

---

a. Une partie de l'hydrogène peut provenir de la corrosion des pièces métalliques.
b. Ce cas est peu probable à priori, car la formation de bulles n'est généralement pas observée.

MODE OPERATOIRE[a]

Le réacteur Triton est une pile piscine dont le circuit primaire de réfrigération est entièrement logé dans la piscine. La circulation forcée de l'eau est assurée par une turbopompe d'un débit nominal de 220 m^3/h. L'eau est aspirée vers le bas et séjourne pendant environ 5 minutes, grâce à une série de chicanes, dans un réservoir de désactivation situé à 1,25 m en dessous du coeur et dont le volume est d'environ 16 m^3, avant de circuler dans l'échangeur de température. La figure 1 représente la disposition du coeur et du circuit de réfrigération dans la piscine.[1] Un batardeau sépare le compartiment coeur du reste de la piscine.

Chaque expérience comporte deux parties: (1) le prélèvement des échantillons d'eau, (2) l'analyse en laboratoire.

Prélèvement des échantillons d'eau

Le coeur étant placé an position de circulation forcée, les prélèvements ne peuvent pas être effectués directement à la sortie. L'eau est recueillie dans le puits de réfrigération entre la maçonnerie et l'échangeur de chaleur, après traversée du bac de désactivation. De ce fait, les temps de prélèvement sont décalés de quelques minutes par rapport à la sortie du coeur. L'eau est aspirée par une pompe à travers un tuyau dont l'extrêmité est lestée pour en permettre la localisation au point de prélèvement choisi, dans des ampoules à deux robinets. Un échantillon supplémentaire peut être recueilli dans un flacon pour le dosage de l'eau oxygénée. Une succession rapide des prélèvements a été obtenue à l'aide d'une batterie d'ampoules telle qu'elle est représentée sur la fig. 2.

L'analyse en laboratoire

L'analyse en laboratoire consiste à dégazer les échantillons d'eau et à déterminer la composition des gaz par chromatographie d'adsorption. La précision sur la quantité d'hydrogène ainsi mesurée atteint 0,05 ml par litre d'eau. L'eau oxygénée est dosée par la méthode iodométrique suivie d'une colorimétrie au moyen d'un spectrophotometre de type classique.[b] La précision atteint $2 \cdot 10^{-6}$ mol.g par litre d'eau.

Des fluctuations importantes de la concentration d'oxygène dans des prélèvements rapprochés pourraient provenir de la décomposition de l'eau oxygénée. Des précautions sont donc prises en vue de limiter celle-ci.

RESULTATS

Mesure des concentrations de gaz et d'eau oxygénée dissous dans l'eau de sortie du coeur

Trois expériences similaires ont été entreprises dont les résultats sont reportés sur les fig. 3 et 4. L'instant où le palier de puissance du réacteur est atteint a été arbitrairement choisi comme origine des temps.

Hydrogène. – Pile arrêtée et circulation en marche, l'eau contient de l'hydrogène dissous en quantités variables non négligeables, de l'ordre de 2 ml par litre. Pile en marche, une concentration stationnaire de 2,85 à 3 ml par litre d'eau est obtenue après environ 10 minutes de fonctionnement du réacteur en palier de puissance. Ce retard est vraisemblablement le résultat du séjour de l'eau dans le bac de désactivation où les premières portions passées par le coeur se diluent.

Oxygène et azote. – Pile arrêtée et circulation en marche, on observe des concentrations variables d'oxygène (6 à 6,5 ml par litre d'eau) et d'azote (9 à 11,5 ml par litre d'eau). Lorsque la puissance du réacteur augmente, il se produit de fortes variations, comme s'il y avait d'abord dégazage avec baisse brutale de la concentration de ces deux gaz, suivie d'une augmentation rapide, puis d'une fluctuation régulière dans de larges limites. Les concentrations d'oxygène et d'azote ne correspondent pas exactement à la saturation sous 1 atmosphère aux températures de l'eau. L'oxygène est en excès, ce qui résulte probablement de la radiolyse. Le fait qu'il ne se dégage pas dans ces conditions pourrait être aisément expliqué par l'existence de pressions hydrostatiques importantes au niveau du coeur. Les différences de pression hydrostatique et de température, ainsi que les remélanges d'eau pourraient, par ailleurs, probablement expliquer les fluctuations observées des concentrations d'oxygène et d'azote.

---

a. La partie expérimentale a été exécutée avec la collaboration de J. Leconte.

b. Fournisseur: Jobin et Yvon – Paris.

Installation de réfrigération de Triton.

[1]

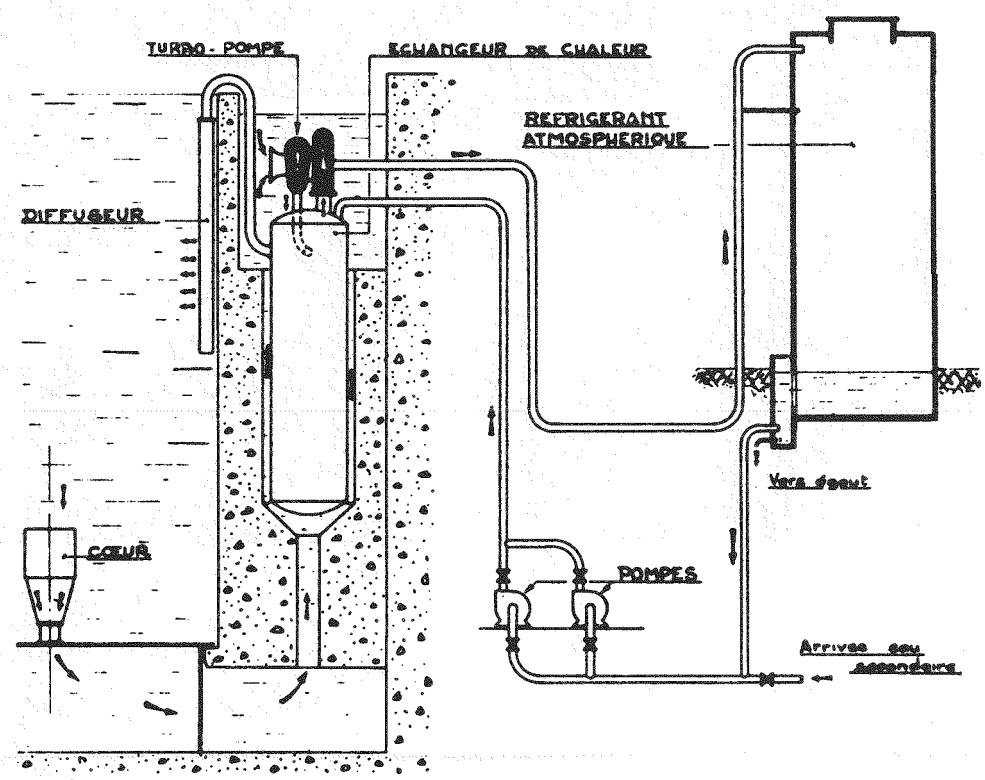

FIG. 1

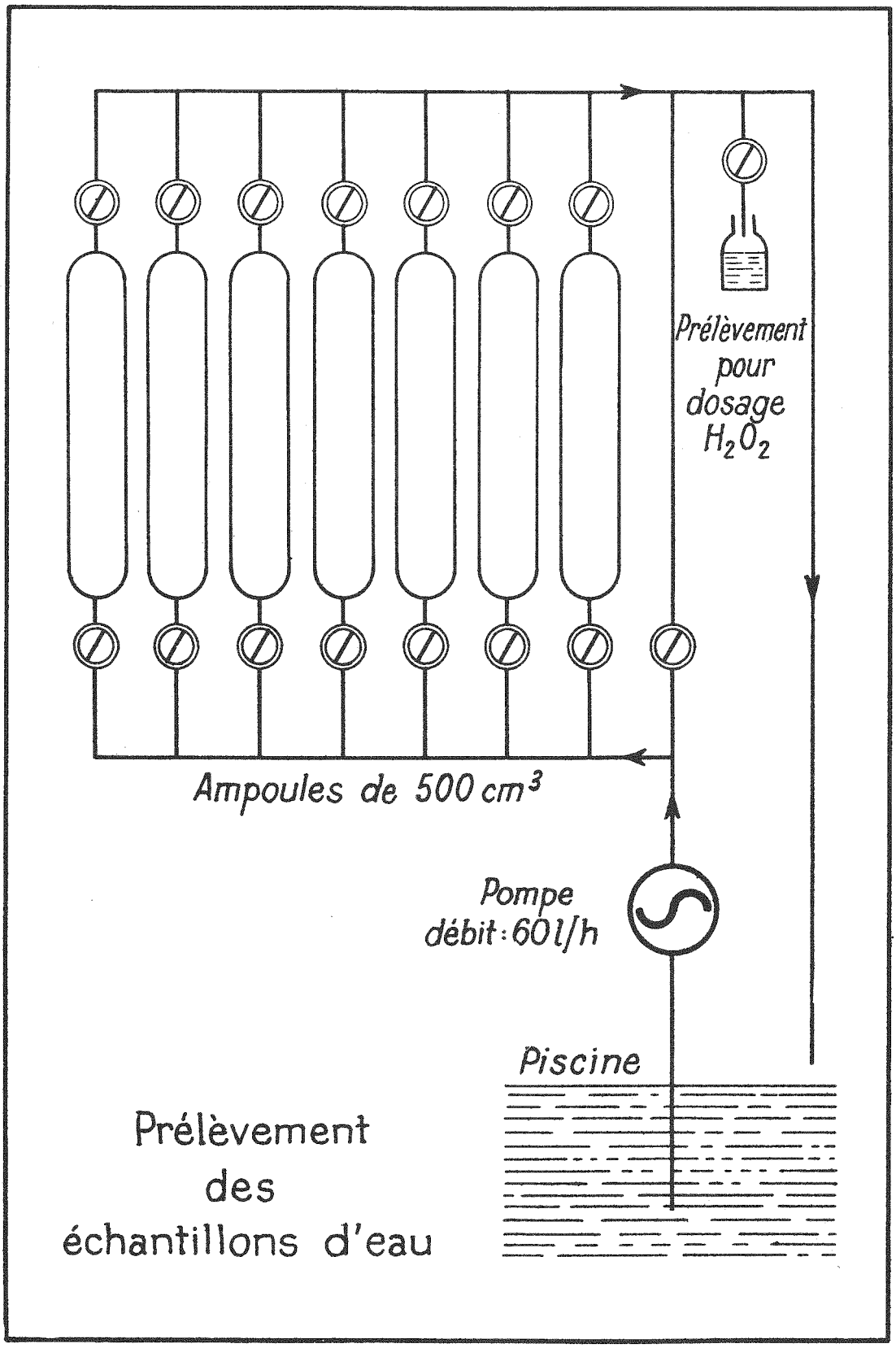
Prélèvement pour dosage H_2O_2
Ampoules de 500 cm³
Pompe débit : 60 l/h
Piscine
Prélèvement des échantillons d'eau

Figure 2.

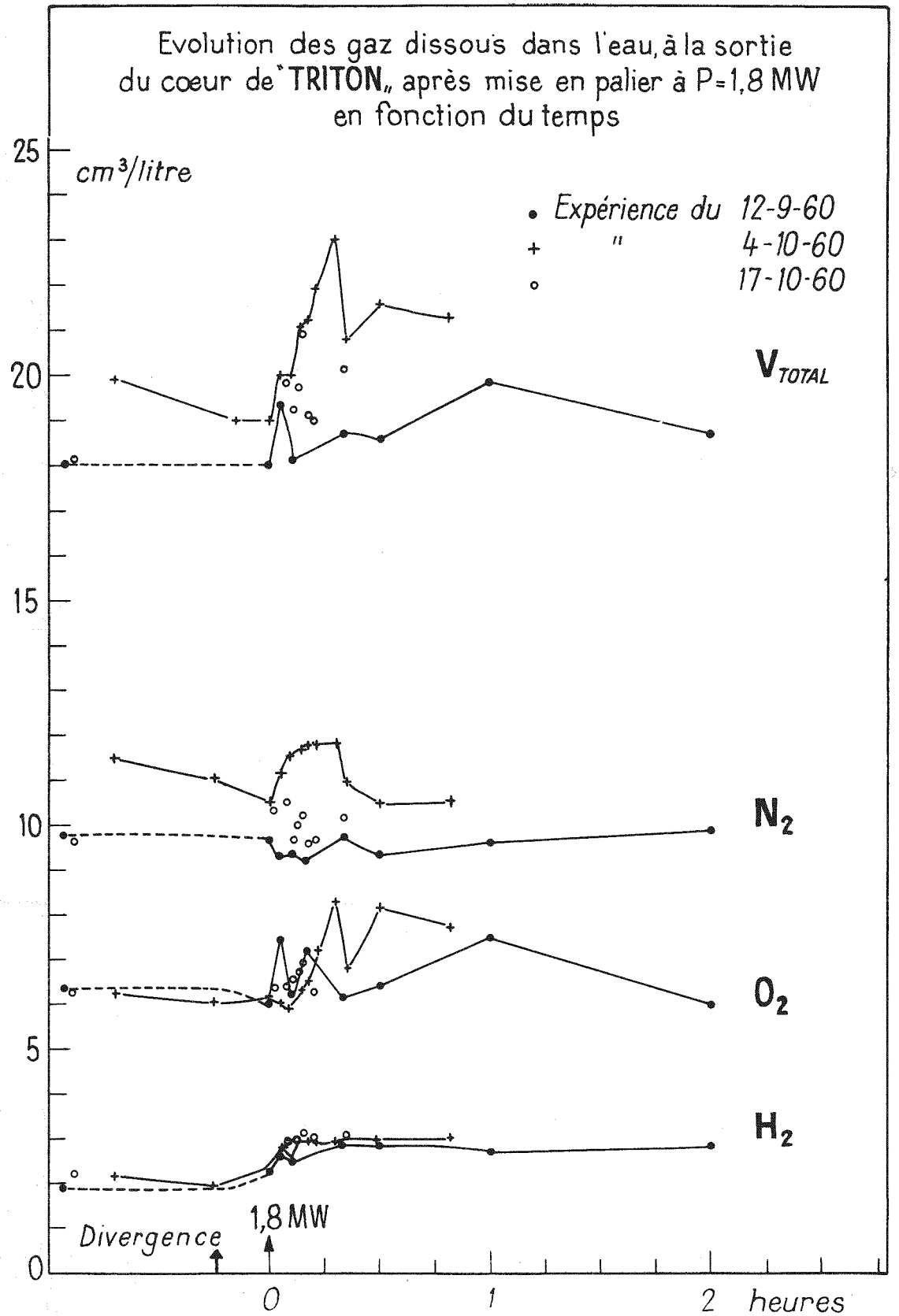
Evolution des gaz dissous dans l'eau, à la sortie
du cœur de "TRITON" après mise en palier à P=1,8 MW
en fonction du temps
cm³/litre
• Expérience du 12-9-60
+ " 4-10-60
○ 17-10-60
V TOTAL
N2
O2
H2
Divergence
1,8 MW
25
20
15
10
5
0
0
1
2
heures

Figure 3.

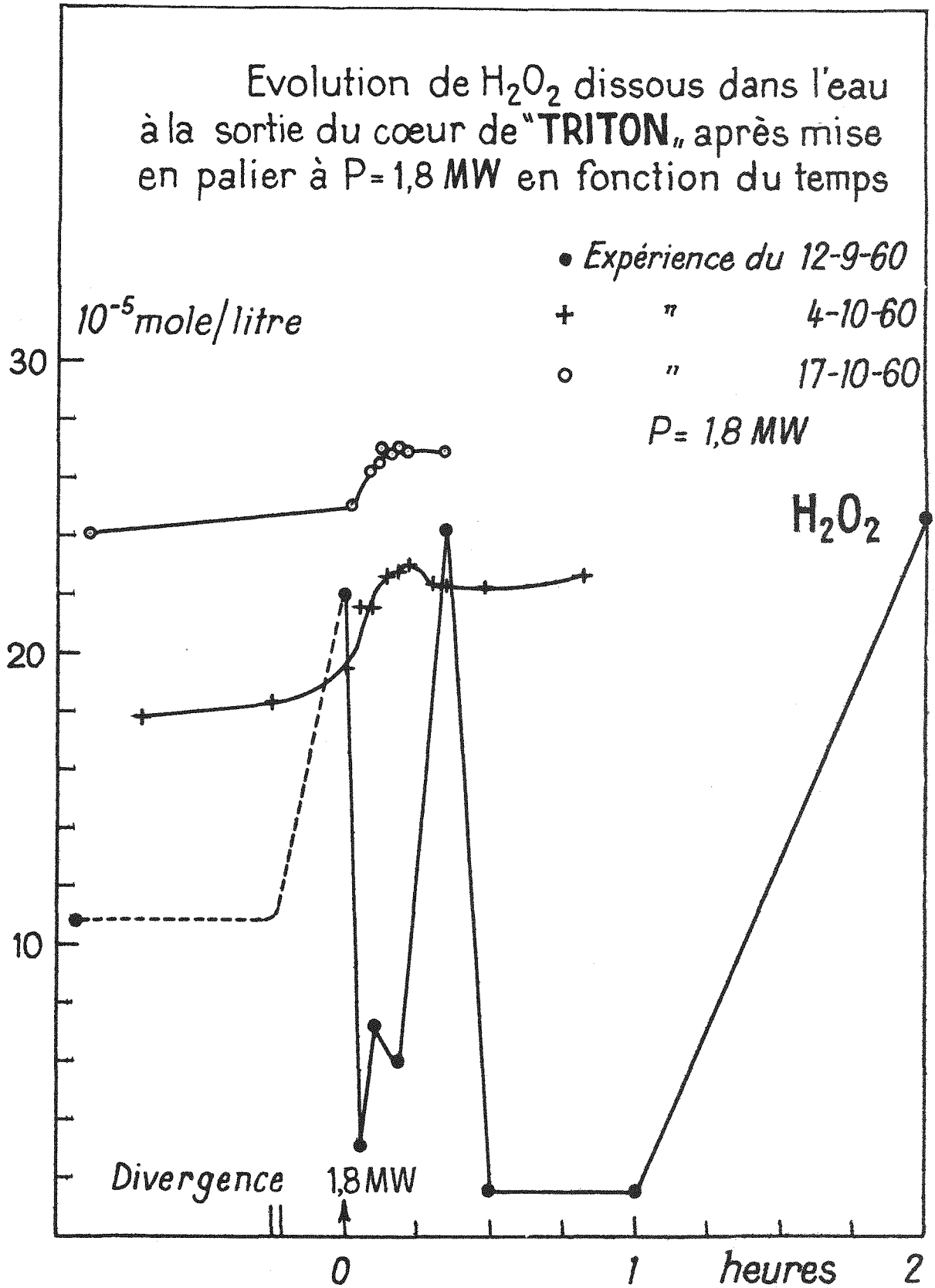
Evolution de H_2O_2 dissous dans l'eau à la sortie du cœur de "TRITON" après mise en palier à P = 1,8 MW en fonction du temps
• Expérience du 12-9-60
+ " 4-10-60
o " 17-10-60
P = 1,8 MW
10^{-5} mole/litre
30
20
10
H_2O_2
Divergence
1,8 MW
0
1
heures
2

Figure 4.

Eau oxygénée. – On observe que la concentration de l'eau oxygénée augmente régulièrement avant d'atteindre une valeur stationnaire au bout d'une dizaine de minutes en palier de puissance. L'existence d'un temps de montée à l'équilibre est probablement due encore à la dilution de l'eau dans le bac de désactivation. Mais alors que le palier de concentration de l'hydrogène semble s'établir à une valeur constante, celui de l'eau oxygénée varie d'une expérience à l'autre – parallèlement d'ailleurs, à sa concentration initiale –.

Etude de la répartition des concentrations de gaz et d'eau oxygénée en solution dans l'eau de la pile à l'arrêt et en puissance

Les échantillons sont prélevés, le réacteur étant arrêté et l'eau immobile, puis circulant à raison de 190 m^3/h, à diverses profondeurs et en divers endroits de la piscine. Ensuite, des prélèvements sont faits dans les mêmes conditions pendant le fonctionnement du réacteur en régime de puissance. Le tableau I montre les résultats obtenus et la fig. 5 une carte des concentrations d'hydrogène dans la piscine.

DISCUSSION

L'hydrogène est toujours présent dans l'eau de la piscine en quantités considérables même après un arrêt prolongé du réacteur et avec circulation de l'eau. La circulation de l'eau ne produit par conséquent aucun dégazage appréciable. Il est donc impossible, de ce fait, de mesurer le taux de radiolyse d'après la pente à l'origine de la courbe d'enrichissement de l'eau en hydrogène. D'autre part, en raison même de la lenteur d'un tel dégazage, il serait peu logique d'admettre que le palier de concentration observé résulte d'un état de régime où tout l'hydrogène formé serait extrait de l'eau. Il pourrait, par conséquent, résulter d'un équilibre radiolytique correspondant à l'égalité des vitesses des deux réactions antagonistes de décomposition en produit moléculaires,

$$2\,H_2O \longrightarrow H_2 + H_2O_2\,,$$

et de rétrogradation par formation de radicaux,

$$H_2O \longrightarrow H + OH\,.$$

Cette hypothèse est en accord avec l'existence d'un palier analogue de la concentration d'eau oxygénée.

La carte des concentrations d'hydrogène confirme bien la lenteur extrême du dégazage. La concentration d'hydrogène devient pratiquement homogène dans l'eau de toute la piscine après 1 ou 2 jours de circulation forcée après arrêt du réacteur. Toutefois, à proximité immédiate du coeur, on observe une teneur légèrement mais significativement plus faible. Les mesures faites pile arrêtée et circulation en marche montrent que la concentration d'hydrogène mesurée au puits de réfrigération est suffisamment représentative de celle dans l'eau à la sortie du coeur. L'eau s'enrichit donc considérablement en hydrogène lors de son passage dans le coeur du réacteur, semble s'appauvrir très légèrement pendant son séjour dans le bac de désactivation, et se trouve très appauvrie au moment de son aspiration dans le coeur.

Une explication possible de la répartition observée des concentrations d'hydrogène serait la suivante: pendant son passage dans le coeur du réacteur, l'eau est soumise à un champ de rayonnements avec forte prédominance des neutrons rapides et subit une dissociation radiolytique importante, s'enrichissant ainsi en hydrogène. La reprise de cette eau par la pompe centrifuge pourrait être responsable d'un léger dégagement d'hydrogène, mais ce point reste douteux, car la différence de concentration observée est trop insignifiante. Par contre, lors de son séjour au voisinage du coeur, après réinjection dans la piscine, la prédominance de rayonnement γ par rapport aux neutrons pourrait être responsable d'une recombinaison radiolytique intense. Cette recombinaison sous l'effet du rayonnement γ expliquerait aussi la baisse légère de la teneur d'hydrogène au voisinage immédiat du coeur quand le réacteur est arrêté.

Ainsi, il est possible de concevoir qu'aucun dégagement de gaz de radiolyse se produise dans les conditions de fonctionnement habituelles dans les piles piscines du C.E.A. Pour qu'un tel dégagement puisse se produire il faudrait que l'intensité de la radiolyse soit telle qu'à la sortie du coeur, la concentration des gaz soit supérieure à leur limite de solubilité, compte tenu, le cas échéant, de la pression hydrostatique et des dépressions ou surpressions dynamiques. La radiolyse globale est pratiquement nulle, malgré un taux de

TABLEAU I

Emplacements des prélèvements	Pile à l'arrêt						Pile à 1,3 MW					
	t°C	H_2 cm^3/l	O_2 cm^3/l	N_2 cm^3/l	Gaz total cm^3/l	H_2O_2 mol. gr/l $\times 10^{-5}$	t°C	H_2 cm^3/l	O_2 cm^3/l	N_2 cm^3/l	Gaz total cm^3/l	H_2O_2 mol. gr/l $\times 10^{-5}$
Verticale du coeur												
–0,02 m*	27.5	1.63	6.3	10.25	18.2	10.15	27.5	3.09	7.0	10.2	20.3	22.5
–2,85 m	28.5	1.52	5.95	9.55	17	10.35	28	3.09	6.15	9.85	19.1	21.9
–5 m	28.7	1.55	6.0	9.9	17.45	6.80						
entrée du coeur												
(–6,40 m)	28	1.37	5.65	8.8	15.8	8.50						
sortie du coeur												
(puits)	29.2	1.75	6.35	9.75	17.85	0.35						
Circulation en marche:												
entrée du coeur												
(–6,40 m)	>26.6	1.38	6.1	9.65	17.2	9.50	28.5	2.40	7.15	10.2	19.75	22.6
30′ après	27.5	1.37	6.45	10.1	17.4		28.5	2.22	7.25	9.85	19.30	22.0
sortie du coeur												
(puits)	28	1.58	6.5	9.8	17.9	7.20	31.3	3.36	5.7	10.65	19.7	21.9
30′ après	28	1.2	6.2	9.4	16.8		32.3	3.25	8.0	10.2	21.45	23.25
Verticale piscine												
(loin du coeur) – 0,02 m	27.5	1.57	5.85	9.65	17.1	10.45						
– 6,60 m	27.5	1.60	6.05	9.75	17.4	9.45	27	2.94	7.45	9.65	19.30	20.5

*Distances comptées à partir de la surface libre de l'eau.

TRITON - Carte des concentrations d'hydrogène dissous

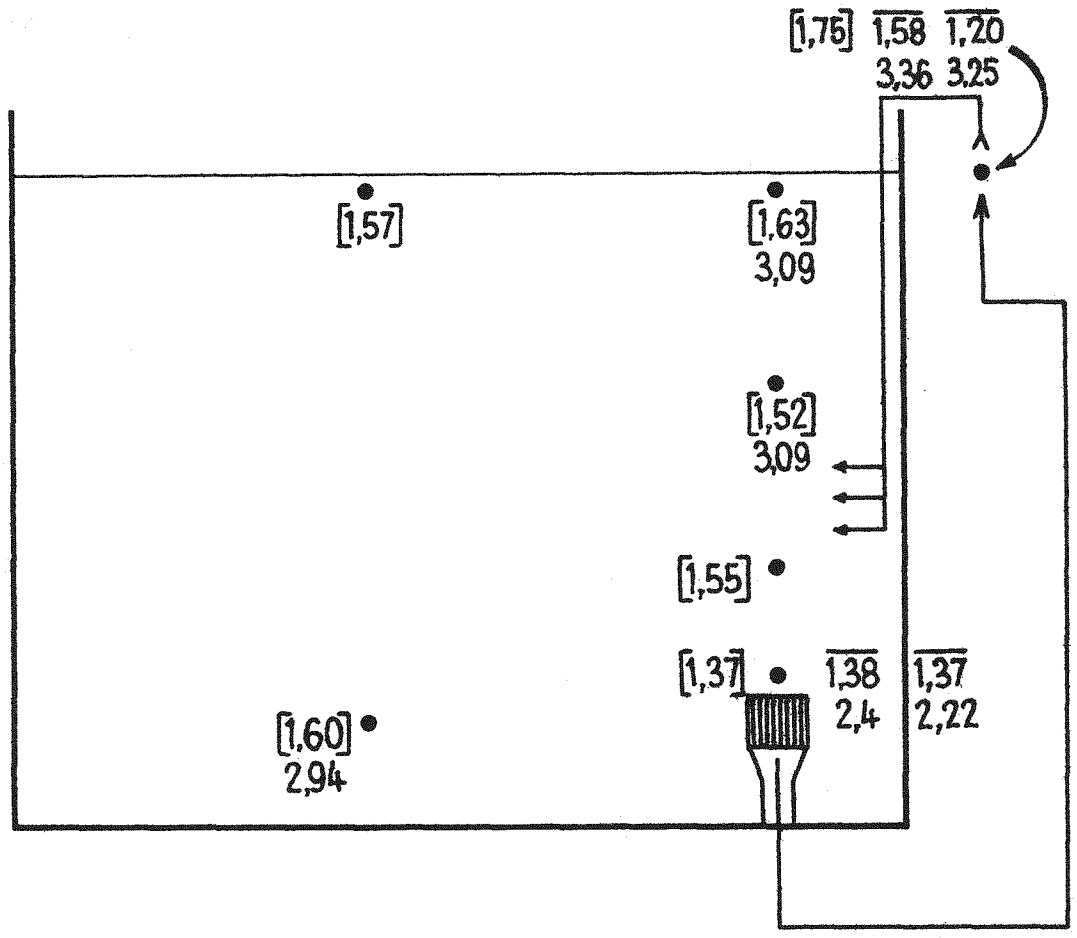

[1,57] *Réacteur arrêté, sans circulation d'eau* } 21.11.60

1,20 " " *avec circulation* " }

3,09 *Réacteur à 1,3 MW* 23.11.60

Figure 5.

radiolyse important dans le coeur, à cause de l'équilibre dû aux conditions de circulation et de géométrie qui en permet la compensation par recombinaison dans la piscine.

Dans un réacteur dont le circuit de refroidissement du coeur serait separé de la piscine, les phénomènes pourraient être différents. Si la recombinaison hors du coeur était inexistante, on observerait dans Triton un dégagement gazeux calculable à l'aide des concentrations d'hydrogène à l'entrée (2,22 à 2,4 ml par litre d'eau) et à la sortie du coeur (3,25 à 3,36 ml par litre d'eau) pour le débit d'eau normal de 215 m^3 par heure. Il serait de 215 litres d'hydrogène par heure, avec une imprécision de ±20. Le taux de radiolyse correspondant serait alors de 165 ml par Kwh.

Cependant, un taux de radiolyse ainsi calculé reste probablement supérieur au taux réel que l'on serait en droit d'attendre dans un réacteur dont le circuit de refroidissement serait indépendant de la piscine, car la recombinaison radiolytique au voisinage du coeur ne serait jamais complètement exclue.

CONCLUSION

Les résultats obtenus permettent de décrire l'allure probable des phénomènes de radiolyse de l'eau dans les piles piscines. Les prévisions quantitatives dans les réacteurs de différentes constructions restent cependant hypothétiques. Pour préciser davantage l'aspect quantitatif des phénomènes, il serait nécessaire de mesurer avec une précision suffisante la répartition spatiale des concentrations d'hydrogène autour du coeur, et de connaître davantage le parcours de l'eau entre le point de réinjection dans la piscine et son entrée dans le coeur. Mais le taux de radiolyse ainsi déterminé dans le réacteur Triton concorde de façon satisfaisante avec ceux que l'on peut calculer à l'aide de certains résultats observés par ailleurs. C'est ainsi que la quantité et la composition des gaz résultant du dégazage de l'eau de refroidissement du MTR[2] permet de calculer un taux de radiolyse voisin de 178 ml par Kwh, tandis que la mesure de la concentration des gaz de radiolyse dans l'eau du même réacteur à l'entrée et à la sortie du coeur conduirait, avec une imprécision appréciable, à trouver un taux de radiolyse de l'ordre de 220 ml par Kwh; ces taux de radiolyse se comparent eux-mêmes assez bien avec les taux de radiolyse probables du réacteur ETR.[3] Par ailleurs, le taux de radiolyse dans Triton s'accorde avec certains résultats de mesures dans le réacteur EWA.[4] De ce fait meme, les taux de radiolyse effectifs qu'il est possible de prévoir dans une pile piscine sont suffisamment justifiés.

BIBLIOGRAPHIE

1. G. Halbronn and A. Peuchnaur, Bull. Inf. Sci. Tech. C.E.A. 35, pp. 66–70, (1959).
2. J. H. Rainwater, Maintenance of Primary Coolant Water Quality in the Materials Testing Reactor, USAEC Report IDO-16322, February 1957.
3. F. C. Haas, Maintenance of ETR Coolant, USAEC Report IDO-16463, August 1958.
4. A. Kostyrko, Nukleonika V 3, pp. 133–142, (1960).

FORMATION AND DISTRIBUTION OF DISSOLVED GASES AND HYDROGEN PEROXIDE IN THE WATER OF A SWIMMING-POOL REACTOR (TRITON)[a]

by J. Chenouard, J. Rozenberg, L. Dolle, and G. Dirian

Commissariat a l'Energie Atomique
Saclay, France

INTRODUCTION

With the object of making useful predictions of the radiolysis rate (hydrogen volume produced per kw-hr of nominal power) of the water in a swimming-pool reactor, studies were made of the concentration of the radiolysis gas and hydrogen peroxide dissolved in the water of the Triton reactor. Measurements were taken before start-up, during start-up, and during steady-state operation, from the pool proper, from the core compartment, and from the core exit.

The radiolysis rate was determined by studying the variation with time of the amounts of hydrogen peroxide and of gas in solution in the water leaving the core (especially the variation of hydrogen, which was produced almost exclusively by radiolysis).[b] With respect to the relative magnitude of the rate of formation (radiolysis) and rate of disappearance (by degassing of the water during circulation or in the swimming pool) of hydrogen, two possibilities were presented.

1. Establishment of a constant hydrogen concentration corresponding to equal rates of formation and disappearance during steady-state reactor power operation. The rate of disappearance would be difficult to determine directly, while the rate of formation could be derived by measuring the hydrogen concentration at the entrance and exit of the core, since the two values were appreciably different.

2. A uniform increase in hydrogen concentration up to the limit of its solubility in water, beyond which it would be liberated in the form of bubbles.[c] This phenomenon would occur if the disappearance rate of hydrogen were much less than the rate of formation. The relative increase in hydrogen concentration in water during its passage through the core would then be slight, and a measurement of it would give only a rough

---

a. Translated from the original French by A. L. Monks, ORNL.
b. A portion of the hydrogen could be produced from the corrosion of the metallic parts.
c. This is quite improbable a priori, because the formation of bubbles is not generally observed.

idea of the radiolysis rate. The best method for determining the latter would then be to trace the development of dissolved gas at reactor start-up after taking the precaution of setting the initial concentration at a value near zero. The initial slope of the curve representing the change in rate of formation of hydrogen would then be a measure of the radiolysis rate.

This second method of determining the radiolysis rate naturally precludes consideration of a radiolytic equilibrium which would produce a constant concentration of hydrogen during the short time (several seconds) it takes the water to pass through the core of the reactor; the radiolysis rate would then be zero.

OPERATION[a]

The Triton is a swimming-pool reactor in which the primary cooling circuit is located entirely within the pool. Forced circulation of water is provided by a turbopump with a nominal discharge of 220 m^3/h. The water is pumped downward and is held for approximately five minutes by a series of plates in a deactivation tank (volume about 16 m^3) situated 1.25 m below the core; it then circulates into the heat exchanger. Fig. 1 shows the location of the core and the cooling citcuit in the swimming pool.[1] A dike separates the core compartment from the rest of the pool.

Each experiment consisted of two parts: (1) water sampling, and (2) laboratory analysis.

Water Sampling

Since the core is located in a forced circulation system, water samples could not be taken directly at the exit. After passing through the deactivation tank, the water was collected in the cooling well between the wall and the heat exchanger. Thus several minutes elapsed from the time the water left the core until the samples could be taken. The water was pumped through a weighted tube which could be lowered to the selected sample point, and into bulbs which were equipped with two stopcocks. An additional sample could be collected in a flask for the determination of hydrogen peroxide. A rapid series of samples has been obtained using bulbs arranged as shown in Fig. 2.

Laboratory Analysis

The water samples were degassed and the composition of the gases was determined by adsorption chromatography. Hydrogen peroxide was determined by a colorimetric-iodometric method using a conventional spectrophotometer.[b] The precision thus obtained was 2×10^{-6} gm mol per liter of water.

The significant variations found in the oxygen concentrations of comparable samples could result from decomposition of hydrogen peroxide. Precautions were taken to limit this phenomenon.

---

a. The experimental part was carried out in collaboration with J. Lecomte.

b. Supplier - Jobin and Yvon, Paris.

RESULTS

Concentration of Dissolved Gas and Hydrogen Peroxide in the Water at the Core Exit

Three identical experiments were carried out with results given in Figs. 3 and 4. Time 0 was arbitrarily defined as the moment the reactor reached power level.

Hydrogen. - With the reactor off and water circulating, the dissolved hydrogen content, of the order of 2 ml per liter, showed considerable variation. With the reactor in operation, a steady concentration of 2.85-3.0 ml of H_2 per liter of water was obtained only after about 10 minutes of operation at power. This delay was probably due to the hold-up of the water in the deactivation tank where the first portions which passed through the core were diluted.

Oxygen and Nitrogen. - With the reactor off and water circulating, varying concentrations of oxygen (6-6.5 ml per liter of water) and of nitrogen (9-11.5 ml per liter of water) were observed. When the reactor power level increased marked variations were produced, as if there had first been a sharp drop in the concentration of these two gases, followed by a rapid increase and then a uniform fluctuation within wide limits. The oxygen and nitrogen concentration did not correspond exactly to the saturation values at one atmosphere pressure at the pertinent water temperatures. There was an excess of oxygen, presumably resulting from radiolysis. The fact that the excess was not released under these conditions might well have been due to the existence of significant hydrostatic pressures at the core level. Variations in the hydrostatic pressures and in the temperature, as well as the recycling of water, could probably explain the observed fluctuations in the concentration of oxygen and of nitrogen.

Hydrogen Peroxide. - Fig. 4 shows that the concentration of hydrogen peroxide increased uniformly before reaching a constant value after about 10 minutes at power level. The time required to reach equilibrium was, again, presumably due to the dilution effect in the deactivation tank; but while the hydrogen concentration apparently came to a constant value in all three experiments, that of hydrogen peroxide varied from one experiment to another in a manner related to its initial concentration.

Distribution of Gas and Hydrogen Peroxide Dissolved in the Water

With the reactor shut down and with the water first not circulating, and then circulating at 190 m^3/h, samples were taken at various depths and locations in the pool. Samples were then taken under the same conditions with the reactor at power. Table I presents the results obtained and Fig. 5 shows a chart of the hydrogen concentration in the swimming pool.

DISCUSSION

Hydrogen was always present in the pool water in considerable amounts even after a prolonged shutdown of the reactor and with the water circulating. Water circulation, therefore, did not produce appreciable degasification. Thus, it was impossible to measure the radiolysis rate from the slope at the beginning of the hydrogen-in-water enrichment curve. Moreover, because of such slow degasification, it would be quite illogical to assume that the constant concentration value observed results from a state where all the hydrogen formed would be lost from the water. Consequently, it could result from a radiolytic equilibrium due to equal rates of the two competing reactions: decomposition into the molecular products,

TABLE I

ANALYSES OF SAMPLES TAKEN FROM VARIOUS LOCATIONS IN THE TRITON UNDER VARIOUS OPERATING CONDITIONS

Location of the Samples	Reactor Shut Down						Reactor at 1.3 MW					
	Temp. °C	H_2 cm^3/l	O_2 cm^3/l	N_2 cm^3/l	Total Gas cm^3/l	H_2O_2 g mol/l x 10^{-5}	Temp. °C	H_2 cm^3/l	O_2 cm^3/l	N_2 cm^3/l	Total Gas cm^3/l	H_2O_2 g mol/l x 10^{-5}
Vertical Line Above the Core												
0.02 m*	27.5	1.63	6.3	10.25	18.2	10.15	27.5	3.09	7.0	10.2	20.3	22.5
2.85 m	28.5	1.52	5.95	9.55	17	10.35	28	3.09	6.15	9.85	19.1	21.9
5.0 m	28.7	1.55	6.0	9.9	17.45	6.80						
Core Entrance (6.4 m)	28	1.37	5.65	8.8	15.8	8.50						
Core Exit (cooling compartment)	29.2	1.75	6.35	9.75	17.85	0.35						
With Water Circulating:												
Core Entrance (6.4 m)	>26.6	1.38	6.1	9.65	17.2	9.50	28.5	2.40	7.15	10.2	19.75	22.6
30 min. later	27.5	1.37	6.45	10.1	17.4		28.5	2.22	7.25	9.85	19.30	22.0
Core Exit (cooling compartment)	28	1.58	6.5	9.8	17.9	7.20	31.3	3.36	5.7	10.65	19.7	21.9
30 min. later	28	1.2	6.2	9.4	16.8		32.3	3.25	8.0	10.2	21.45	23.25
Vertical Line Some Distance from the Core												
0.02 m	27.5	1.57	5.85	9.65	17.1	10.45						
6.60 m	27.5	1.60	6.05	9.75	17.4	9.45	27	2.94	7.45	9.65	19.30	20.5

* Distances measured from the pool surface.

$$2\ H_2O \rightarrow H_2 + H_2O_2,$$

and the formation of radicals,

$$H_2O \rightarrow H^+ + OH^-.$$

This hypothesis is in agreement with the existence of an analogous level of hydrogen peroxide concentration.

The chart showing the hydrogen concentration (Fig. 5) supplies an excellent confirmation of the extreme slowness of the degasification. The concentration of hydrogen became almost uniform in the water of the entire pool after one or two days of forced circulation following reactor shutdown. However, in the immediate vicinity of the core this value was slightly but significantly lower. The measurements made when the reactor was off and with the water circulating indicated that the hydrogen concentration measured in the cooling compartment was adequately representative of that of the water at the core exit. The hydrogen content of the water thus was significantly increased during its passage through the reactor core, appeared to be reduced very slightly during the time it remained in the deactivation tank, and was greatly reduced at the core intake.

The following is a possible explanation of the observed hydrogen distribution. During the time it passed through the reactor core, the water was exposed to radiation having a strong predominance of fast neutrons and underwent a significant degree of radiolytic dissociation, thus becoming enriched in hydrogen. The circulation of this water by the centrifugal pump could be responsible for a slight liberation of hydrogen, but this point remains doubtful because the difference in concentration observed was so slight. On the other hand, the predominance of gamma irradiation when the water came near the core, after its reentry into the pool, could cause marked radiolytic recombination. This recombination effect would also explain the slight decrease in the hydrogen concentration in the immediate vicinity of the core when the reactor was off.

Thus, it can be assumed that there was no liberation of radiolytic gas under normal operating conditions of swimming-pool C.E.A. reactors. In order to produce such a liberation, the degree of radiolysis would have to be such that at the exit of the core the concentration of the gases would be above their solubility limits, taking into account the hydrostatic and dynamic pressures. Overall radiolysis was practically zero, in spite of a significant rate in the core, because of the equilibrium due to conditions of circulation and geometry which permitted recombination of the radiolysis products in the swimming pool.

In a reactor which has a cooling circuit independent of the pool these phenomena could be different. If there were no recombination outside the core, liberation of gas would be observed in the Triton which could be calculated, using hydrogen concentrations at the entrance (2.22 to 2.4 ml per liter of water) and at the exit of the core (3.25 to 3.36 ml per liter of water) for a normal water discharge of 215 m^3 per hour. It would be 215 liters of hydrogen per hour, with an error of $\pm$ 20. The corresponding radiolysis rate would be 165 ml per kw-hr.

However, the radiolysis rate thus calculated is probably higher than the actual rate that would normally be expected in a reactor having a coolant circuit separate from the swimming pool, because radiolytic recombination in the vicinity of the core could never be completely excluded.

CONCLUSION

The results obtained make it possible to describe the probable course of radiolysis phenomena in the water of swimming-pool reactors. Quantitative predictions for reactors of differing characteristics, however, must remain hypothetical. In order to define beforehand the quantitative aspect of these phenomena, it would be necessary to measure with sufficient precision the spatial distribution of the hydrogen concentration around the core, and to know beforehand the path of the water between the point of reintroduction into the pool and its entrance into the core.

But the radiolysis rate in the Triton reactor, as determined above, appears to be in satisfactory agreement with that which would be calculated by using certain results observed elsewhere. Thus, by using the amount and composition of the gases produced from degasification of the cooling water of the MTR,[2] it is possible to calculate a radiolysis rate of about 178 ml per kw-hr; measurement of the concentration of radiolysis gases in the water of the same reactor at the entrance and exit of the core would result in finding, with a considerable amount of inaccuracy, a radiolysis rate of the order of 220 ml per kw-hr. These values are in quite good agreement with the probable radiolysis rate in the ETR reactor.[3] In addition, the radiolysis rate found in the Triton is in agreement with certain measurements obtained in the EWA reactor.[4] These results established the fact that it is possible to predict effective radiolysis rates for swimming-pool reactors.

REFERENCES

1. G. Halbronn and A. Peuchnaur, Bull. Inf. Sci. Tech. C.E.A. 35, pp. 66-70, (1959).

2. J. H. Rainwater, Maintenance of Primary Coolant Water Quality in the Materials Testing Reactor, USAEC Report IDO-16322, February 1957.

3. F. C. Haas, Maintenance of ETR Coolant, USAEC Report IDO-16463, August 1958.

4. A. Kostyrko, Nukleonika V 3, pp. 133-142, (1960).

THE NATURE OF HIGH BOILING RADIOLYSIS PRODUCTS OF POLYPHENYL COOLANTS[a]

By R. T. Keen, W. L. Orr, and R. C. Shepard

Atomics International Division of North American Aviation

Canoga Park, California

ABSTRACT

Commercially available polyphenyl materials, of interest as potential coolant-moderators for organic-moderated reactors, were irradiated in an in-pile loop in the Materials Testing Reactor. The materials studied were biphenyl, two isomeric terphenyl mixtures, and an isomeric mixture of isopropyl biphenyls. This paper discusses the changes in chemical composition of the coolant materials during irradiation and the characterization of the radiolysis products.

Decomposition products were classified into four groups of different volatility ranges: (1) gases, (2) low boilers, (3) intermediate boilers, and (4) high boilers. The high boilers accounted for 85 to 90% of the total decomposition products; therefore, this fraction was studied in detail.[1,2]

Investigation of the high-boiler fractions by low-voltage mass spectrometric analysis, high-temperature gas chromatography, molecular-weight determinations, and elemental analysis showed that high boilers change continually during irradiation; the molecular weight of this fraction continued to increase during irradiation, and the components with molecular weights above the detection limit of the mass spectrometer (mass 686) increased to as much as 30 to 40% of the total fraction. Interpretation of the mass spectral data showed that polyphenyls and triphenylenes (including alkylated derivatives) accounted for 92 to 97% of the high boilers "seen" in the mass spectrometer; hydrogenated polyphenyls and phenylphenanthrenes together amounted to less than 6% of the high boilers.

The radiolysis products formed can be explained in terms of four simple reactions:

1. Polymerization - Depolymerization. The major products are the result of reactions of the type $\phi_m + \phi_n \rightarrow \phi_m + n + H_2$, where ϕ_m and ϕ_n are any polyphenyls. The distribution of polyphenyls formed during an irradiation depends on the relative amounts of the various polyphenyls present in the system. For example, the abundant polyphenyls from irradiation of biphenyl (ϕ_2) and terphenyl (ϕ_3) are ϕ_{2n} and ϕ_{3n},

respectively, where n = 2, 3, . . .

2. Condensation of Ortho-Linked Phenyl Rings to Triphenylenes. Ring closure to form triphenylenes competes strongly with polymerization, since triphenylenes are the second most abundant group of compounds. Relationships are evident between the triphenylenes formed and the nature of the starting material. For example, triphenylene and triphenyltriphenylene were formed in the greatest amounts from the ortho-rich terphenyl mixture. In contrast, very little triphenylene was formed from biphenyl; in this case phenyltriphenylene and triphenyltriphenylene were the major triphenylenes formed.

3. Hydrogenation - Dehydrogenation. Addition of hydrogen to polyphenyls producing partially hydrogenated rings (olefins) and completely hydrogenated rings (cycloalkylpolyphenyls) was indicated. The amounts of these hydrogenation products were small in all cases.

4. Ring Rupture. Minor high-boiler constituents such as alkylpolyphenyls alkyltriphenylenes, and phenylphenanthrenes must result either from ring rupture or from reactions with fragments produced by ring rupture. Only very small amounts of products were produced by these reactions.

Detailed analyses of the high boilers produced from the various starting materials will be presented.

REFERENCES

1. An earlier paper describes lower-boiling radiolysis products: R. T. Keen, et al., Fourth Conference on Analytical Chemistry in Nuclear Reactor Technology, Gatlinburg, Tennessee, October 12-14, 1960, USAEC Report TID-7606, 1961.

2. Studies of OMRE high boilers (to be reported later) have shown that low and intermediate boilers reach a steady state; high boilers then account for nearly 100% of the total damage rate.

---

[a]The information in this paper appears in a topical report numbered NAA-SR-4355 available from the Office of Technical Services, Department of Commerce, Washington 25, D. C.

FAST NEUTRON DAMAGE TO POLYPHENYL COOLANTS[a]

By J. G. Burr, J. Yang, F. D. Goodspeed, J. F. Zack, Jr.
R. J. Mack, S. Berg, and N. M. Ewbank

Atomics International Division of North American Aviation
Canoga Park, California

ABSTRACT

The damaging effect of a fast neutron flux, relative to a gamma flux, on polyphenyl coolants has been re-evaluated by studying the effect of a flux of 1.6-Mev alpha particles (from Po^{210} through two 1/8-mil stainless steel windows) on o-terphenyl over the temperature range 60 to 300°C and by irradiating a mixture of terphenyls (Santowax OMP) at 330 to 340°C in the Curtiss-Wright Research Reactor. The fast neutron component in the CWRR flux was about 65%.

Use of alpha particles to study a fast neutron effect is warranted by demonstration that when a neutron is thermalized in polyphenyls the number of molecules damaged by knock-on collisions is a small fraction of the number of molecules damaged by ionization. The effect of fast neutron damage relative to gamma damage is thus an effect of changing linear energy transfer (LET) rather than a knock-on effect. The pertinent calculations are presented.

The values of G(-coolant) for irradiation of o-terphenyl with 1.6-Mev alpha particles are given for the range of temperature studied. The activation energy for terphenyl damage is shown to be about 1.0 to 1.5 kcal/mole. Total decomposition was about 1 to 3%. An improved micromethod for determining coolant loss is described. It is apparent that initially these alpha particles (LET = 150 ev/A) are about five times as effective in decomposing coolant as are electrons (LET = 0.028 ev/A). If a linear relationship between G(-coolant) and log LET is assumed (this assumption and its implications are discussed), and the normal effect of increasing the HB (high-boiling constituents) content upon G(-coolant) is used (a decrease factor of 2.60 in going from 0 to 30% HB), it can be calculated that the value of G_n(-coolant) for o-terphenyl would be about 0.22 at 30% HB content and 300°C. The initial value calculated for 0% HB is 0.58.

The corresponding value at 30% HB from OMRE data is 0.33. Data on Santowax OMP damage in the CWRR at 320 to 340°C are discussed. From the slope of the curve for these data, fitted by the method of least squares, the values of G(-coolant) can be obtained. The G(-coolant) at 30% HB is calculated to be 0.28; assuming $G_{electron}$ (-coolant) values of 0.10 and 0.08, the corresponding

values of $G_{neutron}$ (-coolant) are 0.32 and 0.38. At 0% HB, the initial value of $G_{neutron}$ (-coolant) is 0.65. When the extremely high value of LET for the alpha particles is considered, and the unproven validity of the G/log LET relationship is allowed for, the agreement between the alpha-particle data and the reactor data is good. A reliable scale of values for decomposition of polyphenyl coolants in mixed reactor fluxes at different temperatures and varying neutron/gamma ratios has been established.

---

[a] The information in this paper obtained by Dr. J. G. Burr and co-workers has been submitted for publication in the Journal of the American Chemical Society. The information in this paper obtained by Dr. J. F. Zack, Jr. and co-workers appears in a topical report numbered NAA-SR-6920, available from the Office of Technical Services, Department of Commerce, Washington 25, D. C.

A COMPARISON OF REACTOR NEUTRONS TO GAMMA RADIATION IN CROSS-LINKING POLYSTYRENE[b]

By J. E. White

Southern Illinois University, Alton, Illinois

and

W. W. Parkinson, Jr., D. Binder, and C. D. Bopp

Oak Ridge National Laboratory[a], Oak Ridge, Tennessee

ABSTRACT

Ionizing radiation, including both electromagnetic photons and energetic particles, produces valence bonds between molecules of polystyrene, along with a small amount of general decomposition. Electromagnetic radiation and energetic heavy particles such as fast neutrons, protons, and alpha particles give a decided difference in the distribution of excited and ionized species in irradiated substances. The rates of formation of intermolecular valence bonds (cross links) by Co^{60} gamma radiation and by the mixed gamma radiation and neutrons of a reactor have been measured in polystyrene.

Two grades of polystyrene were used to ascertain if trace impurities were undergoing neutron reactions which would vitiate the determination of doses with calorimeters and $Ce(SO_4)_2$. The polystyrene samples were also analyzed by various methods, and calculations of the maximum energy absorbed from neutron reactions showed that such reactions could not introduce an appreciable error in the determination of the energy absorbed by the specimens from the radiation field.

The doses of the specimens irradiated with gamma radiation were calculated from $Ce(SO_4)_2$ measurements of the Co^{60} source. The neutron and electromagnetic components of the reactor irradiation facility were measured by means of graphite and nylon calorimeters. A relation was established between the energy imparted to the calorimeters and to substances containing hydrogen and heavier elements in the carbon-oxygen range. Thereafter, $Ce(SO_4)_2$ solutions were used as relative monitors for individual exposures in the reactor.

The measurement of the yield of cross links was carried out by several methods. The number of cross links formed is equal to the reduction in the number of molecules per unit mass, which is inversely proportional to the

average molecular weight. The most convenient and reproducible method for determination of the molecular weight was the measurement of the viscosity of dilute solutions of the samples. The empirical relation between solution viscosity and molecular weight is dependent on molecular weight distribution and the degree of branching of the polymer. Since both of these may change during the irradiation of polystyrene, other measurements of cross-linking were performed.

The fraction of the polymer remaining soluble was measured as a function of radiation dose. This provided a qualitative indication of cross-link yield which was not sensitive to branching.

The insoluble portions of the solubility specimens were weighed wet, fully swollen with solvent, prior to drying. The ratio of wet to dry weight provided a measure of the degree of swelling, related to the average length of polymer chain between cross links in insoluble specimens. The degree of swelling measurements gave cross-linking yields which were not dependent on either molecular weight distribution or degree of branching.

The solution viscosity measurements indicated that the mixed gamma radiation and fast neutrons of the reactor produced about 3.3 times as many cross links as the gamma source, for a given amount of energy deposited in the specimen. The solubility measurements indicated that the reactor was about 2.5 times as efficient as a pure gamma source.

If the gamma component of the reactor radiation field is accounted for, then the fast neutrons alone produce about 4 times as many cross links as gamma radiation produces, per unit absorbed dose.

---

[a]Operated for the U. S. Atomic Energy Commission by Union Carbide Corporation.

[b]The information in this paper has been submitted for publication in the Journal of Physical Chemistry.

LIST OF AUTHORS (PAPER NUMBER)

SESSIONS CHAIRMEN

C. J. Barton, Oak Ridge National Laboratory
R. B. Briggs, Oak Ridge National Laboratory
W. H. Denton, U.K. Atomic Energy Research Authority
W. R. Grimes, Oak Ridge National Laboratory
L. R. Zumwalt, General Atomics Division of General Dynamics Corporation